MECHANISTIC AND KINETIC STUDIES OF THE SURFACE CHEMISTRY OF IRIDIUM AND RUTHENIUM

Thesis by

Dale Fredrick Johnson

In Partial Fulfillment of the Requirements

for the Degree of

Doctor of Philosophy

California Institute of Technology

Pasadena, California

1994

(Submitted 18 May 1994)

Dedicated to my loving parents,

Neil and Betty Johnson

ACKNOWLEDGEMENTS

Throughout my years as a graduate student, I have had the greatest fortune of being surrounded by a host of tremendously generous people. While some have helped me in overcoming the scientific challenges, others have offered the encouragement and support to keep me looking upward and beyond. I could not have achieved my goal without you, and I extend my warmest thanks to you.

My advisor, Henry Weinberg, allowed me the freedom to pursue many avenues in my research, and provided invaluable advice in how successfully to approach scientific investigations. John Parmeter and Malina Hills were my early year mentors in the Weinberg group, and their enthusiasm for surface chemistry was contagious. Tom Jachimowski was most gracious and unselfish in sharing his computer and in assisting me in keeping my experimental system operating. Wolf Widdra was an outstanding physicist and an irreplaceable asset in the lab, both because of his expertise and his kindness. Insightful discussions were shared with everyone in the group at one time or another; it was a great pleasure to have had the opportunity to work with all of the these talented people: Yong-Kui, Youqi, Bill, Jun, Randy, Roya, Buddie, Chuan, Kyle, I-Chun, Dan, Valerie, Chen, Xue-sen, Bao-qi, and Sang. Finally, the staff and shop personnel, at both Caltech and UCSB, with whom I had the chance to work were always helpful and they included: Chari McHale, Dian Buchness, Guy Duremberg, Tony Stark, Sandra Potter, Joy Dodds, Pat Kusman, Kathy Courtney, Laura Crownover, Rudi Stuber, Mickey Csuja, Bruce Thompson, and Joe Doyle.

During my seven months at Texas A & M, Wayne Goodman was truly gracious, and it was with him that I undertook my first kinetic studies. His take-charge style is perfectly balanced by a compassionate nature, and I am very thankful to him for the opportunity he gave me. There were numerous good relationships developed even in that short time with Rob Campbell, Jose Rodriguez, Jen-Wei Xue, Janos Szanyi, and Charles Truong, and, as a bonus, a lasting friendship with Lam Leung.

Ken Graham has been a true friend throughout these years of graduate school, and his loyalty to me has been unwavering. I expect that time and distance will attempt to separate us, but they will not succeed. My great roommates in Santa Barbara, Tom, Jason, Ken, Pepe, and Scott and in Pasadena, Bill and Mike (who lent me his computer for my thesis writing), have given me wonderful memories and kept the good times rolling. I have been blessed with numerous friendships from within my running club, and I collectively thank all of its members for their warmth and encouragement, especially Matt, Annie, Jim, Wes, Malcolm, and Dean. The completion of my graduate work would have been far more torturous without all of you.

Last, but far from being least, I would like to express my undying love and gratitude to my wife, my son, and my family. Your support and faith in me has indeed made the difference. Susan, you have been steadfast and unwavering in your love and belief in me, and you have supported me along each step of the way. Joe, your giving and generous spirit has boosted me in spite of the distance that keeps us apart. Mom, Dad, Karen, Kristi, Sheryl, and all of our extended family, your love has inspired me to attain the best possible for myself, and, believe me, I have heard your quiet cheering and have sensed your solemn prayers. With all that I am, I love you all.

ABSTRACT

Quantitative investigations of the mechanisms and the kinetics of the surface-catalyzed activation of C-H, N-H, C-C, and C-N bonds on the close-packed surfaces of Ir(111) and Ru(001) have been performed. The interaction of CH_3NH_2 with Ru(001) was investigated in ultrahigh vacuum with the techniques of high-resolution electron energy loss spectroscopy and thermal desorption mass spectrometry. Activation of the central C-N bond is observed, but it is less favored than the competing channel of complete dehydrogenation, by a ratio between 2:1 to 3:1. The decomposition mechanism has been characterized with several surface intermediates and gas-phase products identified. A pronounced preference for the activation of C-H over N-H and C-N bonds has been established. Additionally, the kinetics of the initial dissociation of short chain alkanes on Ir(111) has been examined, and the rate parameters of the activation of C-C bonds and primary, secondary, and tertiary C-H bonds have been determined. The formation of primary alkyl products is favored, over most of the experimental temperature range, despite the thermodynamic preference for the activation of individual secondary and tertiary C-H bonds in comparison to individual primary C-H bonds. At higher surface temperatures, the activation of C-C bonds occurs at competitive rates to the C-H reaction channel. The measured deuterium kinetic isotope effect implicates substantial deformation of the terminal methyl group in the transition state of C-C bond cleavage. Finally, the surface structure sensitivity of C-H bond cleavage has been quantified for smooth (111) and corrugated (110) surfaces of iridium and platinum, as well as for step edge defect sites on Ir(111).

TABLE OF CONTENTS

INTRODUCTION

The activation of individual bonds with the feedstreams of petroleum reforming processes, the conversion of coal and natural gas to value-added chemical products, and the catalytic removal of nitrogen and sulfur from these carbon-based energy sources represent three of the major fields of application for heterogeneous catalysis. Metal particles with effective diameters of between 10 and 100 Å are dispersed over high surface area support materials such as alumina and silica (**1**, **2**). In these commercial catalysts, a large fraction of the metal atoms may be considered as surface atoms. In order to characterize the role of the metal particles in these catalytic systems, oriented samples of the pure single-crystalline metal are studied under high and ultra-high vacuum conditions with techniques that are surface-sensitive. In this way, the experimentalist is able to probe the details of the chemistry operating on these model catalysts. By examining the mechanistic and kinetic details of the activation of C-H, N-H, C-C, and C-N bonds in such controlled studies, tremendous insight may be gained into the fundamental surface chemistry of the commercial applications cited above. Yet, there remains the fact that industrial catalytic processes operate at temperatures and pressures which preclude the *in situ* investigation of the catalyst surface. To bridge this pressure gap between the controlled studies and the commercial processes, the surface-sensitive analytical techniques are coupled with a higher pressure reaction chamber (**3**). The characterization of the system after having operated at the elevated pressures provides additional information regarding the chemical reactions on these single-crystalline surfaces.

The experimental systems used in the high and ultra-high vacuum studies are operated at base pressures of 1×10^{-8} to 2×10^{-10} Torr and at less than 2×10^{-10} Torr, respectively. The single-crystalline samples of the metal are cut, aligned, and polished to expose the desired crystallographic surface. X-ray diffraction techniques are used achieve the precise orientation of the crystal prior to its use in the vacuum chamber (**4**), while once inside the system electron diffraction techniques are used to verify the surface geometry. They are then mounted inside the vacuum systems, and when operated at these low pressures, interference from the adsorption of *background* contamination on the surface is minimized. The surface-sensitive analytical techniques employed at various times in the work described in this thesis include Auger electron spectroscopy (AES), thermal desorption mass spectrometry (TDMS), and high resolution electron energy loss spectroscopy (HREELS). These techniques are described below.

In AES, high energy electrons bombard the surface, causing the ejection of electrons from the core levels of the atom. A second electron in these now ionized atoms falls into the available core hole from a higher energy level. This event releases energy and induces the ejection of yet another electron, which for such interactions, have energies characteristic of the individual binding energies of the electrons in these core levels. These last electrons are called Auger electrons, and the scan of the emitted Auger electron spectrum for each element provides an element-specific "fingerprint." Thus, this technique is sensitive to the types of atoms that reside on the *surfaces* in our studies, and is used primarily as a means of insuring the cleanliness of the crystal prior to any experiments. In HREELS, the incident electron has much lower energy than in the case of AES, and the interaction of the elecron with the surface, and any species present on it, results in small

quantities of energy being transferred. In the loss spectrum, the incident electron has interacted with the electric fields of the various chemical species on the surface. The interaction is characterized by either scattering from the electron density of the surface, or exchanging energy with oscillating dipolar electric fields associated with the vibrating atoms in bonds. Thus, this technique yields information that may be compared to gas-phase vibrational infrared and Raman spectroscopies, and within the surface science community, is an extremely powerful analytical tool. In TDMS, the surface, with chemical reactants adsorbed upon it, is heated at a constant rate while the mass spectrometric signals assignable to the desorbing products are monitored. The identification of the desorption products is inferred from their mass spectra, which contain ionized fragments of the parent molecule which has desorbed. Surface coverages may be obtained from the integrated signal intensities, when compared relative to the signals from known, calibrated overlayers. Together with the HREELS technique, in particular, the progression of the mechanistic details of catalytic reactions may be followed. The mass spectrometer is a mass-specific instrument which may be used in kinetic studies to examine the temperature dependence of the rate of a selected reaction of interest.

The close-packed surfaces of Ru(001) and Ir(111) were selected for study in order to continue the ongoing research effort to characterize fully their fundamental surface chemical behaviors. Ruthenium is a very active metal for ammonia synthesis and for Fischer-Tropsch catalysis in the production of fuels and hydrocarbon feedstock chemicals. This latter process employs synthesis gas, H_2 + CO, which, in turn, is obtained from resources such as coal. Coal may be found in a wide variety of grades, each containing different, yet significant, amounts of sulfur and nitrogen. These constituents

must be removed, e.g., via hydrodenitrification and hydrodesulfurization methods, in order to optimize the Fischer-Tropsch process. Furthermore, the converted forms of the nitrogen and sulfur, generally as their oxides, SO_x and NO_x, must be prevented from entering the environment in uncontrolled and large quantities. This important commercial catalytic process, and the related issues that surround it, motivated the study of the surface chemistry of monomethylamine on ruthenium.

Chapter 2 is the detailed examination of the interaction and thermal decomposition of methylamine, CH_3CH_2, and its selectively deuterated isotopomers, CH_3ND_2 and CD_3ND_2, on the close-packed surface of ruthenium, Ru(001). Methylamine is introduced to the clean surface at liquid nitrogen temperatures, and bonds to the surface via the lone pair of the nitrogen atom. Upon annealing the overlayer, several reaction paths for the thermal decomposition begin to compete. From among these available reaction channels, preference toward the activation of C-H bonds over N-H and C-N bonds is observed. This is demonstrated by the HREELS vibrational spectra and the higher temperature production of D_2 relative to H_2 in TDMS experiments of the decomposition of CH_3ND_2. At an early step in the decomposition mechanism, the competing activation of C-N bonds is indicated by the production of NH_3. The majority path for the decompositon results in eventual complete dehydrogenation and the formation of adsorbed cyanide, CN(a). Numerous reaction intermediates have been proposed, and several identified, one of which is the aminocarbene, η^1-(C)- $HCNH_2$, formed in the majority path at 300 K. Its relevance to the commercial amination of aliphatic alcohols has been presented.

Chapter 3 is a communication of the discovery of the dehydrogenated product cyanide, CN(a), present on the surface between 400 K and 450 K.

The proposed structure of the cyano adsorbate results from the bonding interaction of both antibonding π^*-orbitals in the cyano species, with the carbon atom formally bonded via a σ-bond to a surface ruthenium atom. This structure is proposed from analogous isonitrile moieties found in organometallic compounds (**5**) and is formally indicated as μ_3-η^2-CN.

In the remaining chapters of the thesis, the kinetic investigations of the initial dissociation of small alkanes on the Ir(111) surface are presented. These kinetic studies were motivated by the technological importance of hydrocarbon activation in the fuels and chemical industries (**1, 2**), and by the desire to quantify the structure sensitivity of C-H bond activation in ethane, propane, and isobutane by comparing the results for activation on Ir(111) to those from other surfaces, including Pt(111), Pt(110)-(1x2), and Ir(110)-(1x2).

Chapters 3 and 4 are, respectively, the kinetics studies of the dissociative chemisorption of ethane on the smooth, close-packed Ir(111) surface, and on the defect sites which comprise ~2.5% of the Ir(111) surface. This investigation into the structure sensitivity of the cleavage of C-H bonds in ethane allowed an detailed quantitative comparison between the various systems to be made. In comparison to the smooth surface of Pt(111), the dissociation of ethane on Ir(111) is more active, and the difference in activation energies favors Ir(111) by 6300 cal/mol; however, in comparison to Ir(110)-(1x2), it is less active with a corresponding difference in activation energies of 5000 cal/mol. The intrinsic difference in activities of the two metals is effectively compensated for by the changes induced in the electronic structure of the surfaces associated with the corrugated (1x2) reconstruction of the open (110) surfaces. Thus, the activities of Ir(111) and Pt(110)-(1x2) are found to be the same and their activation energies differ by only 200 cal/mol. Quantification of the rate parameters for this same reaction on the

defect sites on the Ir(111) surface requires that surface diffusion be explicitly included in the description of the kinetic rate equation. By so doing, the defects on Ir(111) were found to be as active as the sites for C-H bond activation on Ir(110)-(1x2), and by comparison, several orders of magnitude more active than the sites on the smooth Ir(111) terraces.

Chapters 5 and 6 are the kinetics studies of the dissociative chemisorption of propane, n-butane, isobutane, and neopentane on the Ir(111) surface. These studies were motivatied by the desire to examine, and quantify, the selective activation of primary, secondary, and tertiary C-H bonds in these alkanes. The intrinsic differences in the bond strengths between primary, secondary, and tertiary C-H bonds would seem to indicate that their selective activation by transition metal surfaces would be possible. However, the corresponding products of the reaction bond to the surface with their own comparable differences in energy, which, it is seen experimentally, precludes the Ir(111) surface from demonstrating a marked selectivity for the activation of these individual C-H bonds. The unanticipated activation of C-C bonds in these alkanes was observed as well, and while the C-H bond activation energies on Ir(111) are all nearly 11 kcal/mol, the activation energy for the cleavage of C-C bonds is between 16 and 18 kcal/mol. The reaction of selectively deuterated isotopomers of these alkanes reveals that the terminal methyl group of the alkane chain experiences significant deformation during the C-C bond scission reaction, and, hence, these studies have cast new light on the mechanism of the activation of C-C bonds by transition metal surfaces.

References

1. Sinfelt, J. H. *Bimetallic Catalysts: Discoveries, Concepts, and Applications*; Wiley: New York, 1983.

2. Rasser, J. C. *Platinum-Iridium Reforming Catalysts;* Delft Univ. Press: Delft, Netherlands, 1977.

3. Goodman, D. W. *Acc. Chem. Res.* **1984**, *17*, 194.

4. Linke, U.; Poelsema, B. *J. Phys. E: Sci. Instrum.* **1985**, *18*, 26.

5. (a) Andrews, M. A.; Kaesz, H. D. *J. A. Chem. Soc.* **1979**, *101*, 7255. (b) Adams, R. D.; Katahira, D. A.; Yang, L.-W. *Organometallics* **1982**, *1*, 231.

CHAPTER 1

Chemisorption and Thermal Decomposition of Methylamine on the Ru(001) Surface

[The text of Chapter 1 consists of an article coauthored with Y. Wang, J. E. Parmeter, M. M. Hills, and W. H. Weinberg, which has appeared in *Journal of the American Chemical Society* **1992**, *114*, 4279.]

Abstract: The adsorption and decomposition of monomethylamine on Ru(001) have been studied using high-resolution electron energy loss spectroscopy and thermal desorption mass spectrometry. Molecular adsorption of CH_3NH_2 occurs via lone pair donation of the nitrogen atom, and the desorption of reversibly adsorbed methylamine from a saturated first layer is observed over the temperature range 200 to 340 k. Thermal decomposition of irreversibly adsorbed methylamine ($(\Theta)_{CH_3NH_2} = 0.15 \pm 0.01$ monolayer) produces H_2, N_2, NH_3 and surface carbon adatoms. Between 280 and 300 K cleavage of a C-H bond produces μ–η^2 –H_2CNH_2, and annealing above 300 K initiates competitive C–H and C–N bond cleavage reactions. The majority path (~70%) results in preferential cleavage of C–H bonds between 300 and 330 K to produce a mixture of η^1–(C)–$HCNH_2$ [ν(CN) = 1450 cm^{-1}] plus hydrogen adatoms. The minority path (~30%) gives rise to C–N bond cleavage between 300 and 320 K to yield short-lived CH_2 and NH_2 intermediates react to form CH, NH, NH_3 and hydrogen adatoms. The ammonia is stabilized by the presence of electron withdrawing intermediates and desrobs with a peak temperature of 365 K. Annealing betwen 330 and 360 K induces N–H bond cleavage in the majority path intermediates to form μ_3–η^2–HCNH [ν(CN) = 1450 cm^{-1}]. Cleavage of the final C–H bond between 370 and 380 K produces η^1–(C)–CNH [ν(CN) = 2275 cm^{-1}] and μ–CNH[ν(CN) = 1665 cm^{-1}], and this is followed by cleavage of the remaining N–H bond between 390 and 400 K to yield μ_3–η^2–CN[ν(CN) = 1660 cm^{-1}]. Rupture of the C–N bond over the temperature range 450-575 K forms carbon and nitrogen adatoms, the latter recombining to desorb as N_2 between 800 and 1000 K leaving only carbon on the surface.

I. *Introduction*

The study of the interaction of monomethylamine, CH_3NH_2, on the close-packed Ru(001) surface has been undertaken for a number of reasons. The selectivity of this surface toward activating CH, NH and CN bonds can be determined by studying the decomposition of CH_3NH_2 with thermal desorption mass spectrometry and high-resolution electron energy loss spectroscopy. Such an analysis will also allow for the identification of stable reactive intermediates, and hence, provide insight into the mechanistic details of related catalytic reactions. Finally, it is of interest to contrast the interaction and decomposition of this amine to that of ammonia on the Ru(001) surface, as well as to its chemical reactivity on other single-crystalline surfaces.

The commerical importance of amines, amides and isocyanates illustrates that there is much to be gained by the study and characterization of CN bond-containing molecules on single-crystalline transition metal surfaces. Heterogeneous catalytic applications found in practice include hydrodenitrification,[1] reductive amination of alcohols,[2,3] reduction of nitriles,[4] and production of HCN.[5,6] Homogeneous catalytic processes of related importance include hydrocyanation[7] and reductive carbonylation[8] reactions; the former being applied in the manufacture of adiponitrile, $NC(CH_2)_4CN$, used to produce Nylon 6,6, and the latter being a route to produce aromatic isocyanates and possibly diisocyanates for use in the manufacture of polyurethanes. The isolation and identification of intermediates from the decomposition of methylamine on the close-packed Ru(001) surface will assist in clarifying the mechanistic details of these commercial processes. In particular the dehydrogenated surface species characterized here may play crucial roles in the disproportionation reactions observed to occur during the production of long chain, aliphatic amines.[2,3,9] The findings of this study should be of wide interest and use to researchers in commercially applied catalysis.

Previous studies of monomethylamine on Pt(111),[10,11] Rh(111),[11,12] Mo(100),[13] W(100), and carbon- and oxygen-modified W(100),[14] Cr(111) and Cr(100),[15] Ni(111),[15,16] Ni(100)[15,17] and Pt(100)[18] surfaces have been conducted with a variety of surface sensitive techniques. Dehydrogenation of methylamine occurs on all surfaces between approximately 300 and 500 K, and the desorption of reversibly adsorbed molecular methylamine ceases near 400 K. The reactivity of each surface towards activating C–N bond cleavage varies dramatically, as determined by the gas phase products other than H_2 formed from CH_3NH_2 decomposition. On Pt(111) methylamine undergoes no CN bond dissociation with only HCN and cyanogen produced, while on Rh(111), Pt(100) and Mo(100), it experiences partial dissociation as evidenced by cyanogen, HCN, N_2 and surface carbon production. On Ni(111), Ni(100) and W(100) surfaces it is completely dissociated, with only N_2 and surface carbon formed.

II. Experimental Details

The high-resolution EEL spectrometer used in these studies as well as the ultrahigh vacuum chamber in which it is contained have been described in detail elsewhere.[19] Briefly, the stainless steel UHV chamber is pumped by both a 220 l– s^{-1} noble ion pump and a titanium sublimation pump which reduce the base pressure to below 10^{-10} Torr. The home-built HREEL spectrometer is of the Kuyatt-Simpson type, with 180° hemispherical deflectors serving as the energy dispersing elements in both the monochromator and the analyzer. The monochromator is spatially fixed, but the analyzer is rotatable to allow off-specular spectra to be measured. On- and off-specular spectra were collected during these experiments, but all spectra presented in this paper were collected in the on-specular direction. The impact energy of the incident electron beam was between 4 and 6 eV in all cases, and the beam was incident on the Ru(001) crystal at an angle of 60° with respect to

the surface normal. The instrumental energy resolution in these studies, defined as the full width at half maximum of the elastically scattered beam, varied between 60 and 80 cm^{-1}, while maintaining count rates in the elastic peak between 1.5 and 3.5 x 10^5 counts per second, cps.

The Ru(001) crystal was cooled to 80 K with liquid nitrogen and was heated resistively with the temperature monitored by a W–5%Re/W–26%Re thermocouple spotwelded to the back of the crystal. The crystal was cleaned by using periodic ion sputtering and routine annealing to 1000 K in 1 x 10^{-7} Torr of O_2, followed by annealing to 1625 K *in vacuo*. Surface cleanliness was determined by both HREELS and H_2 thermal desorption mass spectrometry.

A second UHV chamber was used to conduct the thermal desorption mass spectrometry and low-energy electron diffraction measurements.[20] This chamber also has a base pressure below 10^{-10} Torr using similar pumping techniques. Liquid nitrogen cooling and resistive heating of the Ru(001) crystal were similarly employed. It contains a UTI–100C quadrupole mass spectrometer enclosed in a glass envelope for selective sampling of gases that desorb only from the well-oriented front face of the single crystal. Low-energy electron diffraction optics and a rotatable Faraday cup are available for the display of LEED patterns and the measurement of LEED beam profiles. No ordered LEED structures other than the (1 x 1) pattern of the unreconstructed substrate were observed following the adsorption of various coverages of methylamine and annealing to higher temperatures. Hence, no LEED results are discussed here. A single-pass cylindrical mirror electron energy analyzer with an integral electron gun is available for Auger electron spectroscopy. The Ru(001) crystal mounted in this chamber was cleaned as described above, and cleanliness was determined both by AES and H_2 thermal desorption mass spectrometry.

Methylamine, CH_3NH_2 (98.0% min.) was obtained from Matheson, and N, N-dideuteromethylamine (99.1% min., 98% CH_3ND_2) was obtained from MSD Isotopes. Perdeuteromethylamine (98% min., 95% CD_3ND_2) was obtained from Protech. All three isotopes of methylamine were further purified by several freeze-pump-thaw cycles prior to use. The purity of all gases was verified by mass spectrometry in both chambers. Gas exposures are reported in units of Langmuirs, where 1 Langmuir = 1 L = 1 x 10^{-6} Torr-s. The quoted exposures have not been corrected for the relative ionization probabilities of methylamine and nitrogen.

III. Results

A. Thermal Desorption Mass Spectrometry

Thermal desorption spectra measured after the adsorption of CH_3NH_2 and CH_3ND_2 on Ru(001) at temperatures below 100 K and subsequently ramped with heating rates, β, of 15 K-s^{-1} are shown in Figs. 1 and 2. Only molecular methylamine, hydrogen, nitrogen and ammonia desorb from these overlayers with surface carbon also deposited as a result of the reaction. In particular, cyanogen, hydrogen cyanide and methane are not observed. In Fig. 1(a), molecular methylamine desorbs in a peak at 330 K for low initial coverages of between 0.2 L and 1 L, and this peak downshifts and broadens with increasing coverage. Assuming a preexponential factor of the desorption rate coefficient of 10^{13} to 10^{14} s^{-1}, the activation energy of desorption of methylamine at low coverages is estimated by the Redhead method[21] to be 23 ± 2 kcal – mol^{-1}. At intermediate exposures a second peak appears at 240–250 K, which saturates for exposures of 3 to 4 L. Finally, at high exposures a peak at 130 K, which does not saturate with increasing exposures, appears and is due to desorption from multilayer methylamine.

In addition to reversibly adsorbed CH_3NH_2, the observed desorption of H_2, N_2 and NH_3 indicates that irreversible, dissociative adsorption of methylamine occurs. From Fig. 1(b), it is seen that with increasing exposures the peak desorption temperature of H_2 shifts from 395 K to 375 K. From a saturated monolayer of methylamine, a low-temperature shoulder at approximately 350 K appears. For the heating rate of 15 K-s^{-1} employed in these thermal desorption experiments, all of the H_2 is seen to desorb from the surface by 450–460 K.

Ammonia produced from the decompositon of methylamine desorbs over the temperature range of 300 to 400 K with a peak desorption temperature of 365 – 370 K independent of the initial coverage of methylamine, cf., Figs. 1(c). This desorption behavior differs from that of similarly low coverages of ammonia on clean Ru(001) where desorption is complete by approximately 360 K and the peak temperature is 315 K.[22,23] Thermal desorption spectra of N_2 (not shown) indicate that the desorption peak temperature shifts from 950 to 875 K with increasing methylamine coverage. This coverage dependence and the high desorption temperatures indicate that desorption results from the second-order recombination of nitrogen adatoms. The desorption of N_2 from the decomposition of ammonia on Ru(001)[24] exhibits a similar coverage dependence although the desorption temperature is approximately 100 K lower. The presence of carbon adatoms causes the recombinative desorption of dinitrogen to occur at higher temperatures by either increasing the ruthenium-nitrogen bond energy, hindering nitrogen adatom surface diffusion via a site blocking mechanism, or a combination of both effects.

Figure 2 shows the thermal desorption spectra of masses 2, 3 and 4 amu (panel a) and masses 17, 18, 19 and 20 amu (panel b) that result from annealing a 5 L exposure of N,N-dideuteromethylamine adsorbed at 95 K. The hydrogen isotopes are all desorbed by 460 K with the peak desorption temperatures being 360, 395 and 415 K, respectively, for H_2, HD and D_2. Thermal desorption of isotopically pure, saturated H and D coverages on

clean Ru(001)[25] give virtually identical desorption spectra with their peak desorption temperatures occurring at 370 K and a high temperature shoulder at 415-420 K.

Figure 2(b) shows the desorption spectra of ammonia isotopes and their fragments formed from CH_3ND_2. The two parent isotopes, ND_3^+ (20 amu) and ND_2H^+ (19 amu), are responsible for the signals at masses 17 and 18 amu. Cleavage of one N–D bond in ND_3 yields the fragment ND_2^+ as does cleavage of the N–H bond in ND_2H. Likewise, the cleavage of one of the two N–D bonds of ND_2H yields the fragment NDH^+ of mass 17 amu. Mass spectrometric and high resolution EEL spectroscopic verification of the purity of N–N–dideuteromethylamine eliminates the possibility of H–D exchange at the nitrogen atom in the parent molecule, and hence there is no possibility that these spectrometric fragment signals at 17 and 18 amu arise from ammonia molecules, NH_2D^+ and NH_3^+. Furthermore, as discussed in Section IVB hydrogenation of either surface nitrogen adatoms or deuterated imidogen, ND, to form NH_3 and NH_2D is not at all likely under these ultrahigh vacuum conditions.[24] The integrated areas under the desorption peaks reveal that $ND_3^+ > ND_2^+ > ND_2H^+ > NDH^+$, and that their relative areas, uncorrected for varying spectrometric sensitivities, are respectively 0.42: 0.35:0.17:0.06.

The high-resolution EELS data presented in the next section demonstrate that side-on bonded cyano, CN, is formed as the product of complete dehydrogenation of methylamine. The detection of ammonia in the thermal desorption experiments shows that C–N bond cleavage competes with complete dehydrogenation. Analysis of the NH_3 and H_2 thermal desorption spectra resulting from several experiments of saturated coverages of CH_3NH_2 yields the fractional coverages of ammonia and atomic hydrogen: $\Theta_{NH_3} = 0.02 \pm 0.01$ and $\Theta_H = 0.70 \pm 0.03$. These fractional coverages are obtained by comparing the areas of the products to those for saturated exposures of NH_3 and H_2 and applying the known saturated coverages:[22,26] $\Theta_{NH_3}^{sat'd} = 0.25$ and $\Theta_H^{sat'd} = 1.00$. Applying a hydrogen mass balance on these data yields a fractional coverage of irreversibly adsorbed

methylamine of $\Theta_{CH_3NH_2} = 0.15 \pm 0.01$. Quantification of the branching ratio between competing C-N bond cleavage and complete dehydrogenation reaction paths will be discussed in Section IV B.

B. High-Resolution Electron Energy Loss Spectroscopy

While the thermal desorption data suggest the overall course followed by the surface catalyzed decomposition of methylamine, it is the high resolution EELS results which allow a *direct* observation of the chemical changes that occur as the reaction proceeds. The production of ammonia indicates that C-N bond breaking takes place in some fraction of the adsorbed CH_3NH_2, and, as will be developed in this section, this path competes with complete dehydrogenation. Careful analysis of the HREEL spectra allows numerous surface intermediates to be identified and, in particular, that one which is present prior to the branching of the reaction and hence common to both competing pathways.

High-resolution EEL spectra were measured with two different types of experimental annealing treatments. In order to coincide with the temperature-dependent features of the thermal desorption spectra, flash annealing ($\beta \approx 20$ K-s^{-1}) of the crystal to the desired temperature was followed by rapid cooling to liquid nitrogen temperature. A second series of HREEL spectra to investigate the surface intermediates of the reaction required similarly rapid but careful annealing in order to control the extent of conversion. The spectra in this second set of data were typically measured at 10 degree increments, and upon observing significant change in a spectrum, a second and sometimes third spectrum was obtained at that annealing temperature. Numerous off-specular spectra (typically 5-10°) were measured, and, while none are shown here, the findings of these spectra are

embodied in the discussion in the text. During the course of the experiments, CO from the chamber background adsorbed on the crystal. Its surface concentration is always extremely low, and only because of the very large dynamic dipole moment for the CO stretching frequency is it observed in the spectra. Readsorption of methylamine was kept to a minimum by use of a cyropanel throughout the duration of the experiments.

The HREEL spectra following saturation exposures of either CH_3NH_2, CH_3ND_2 or CD_3ND_2 (typically between 4 and 6 L exposures adsorbed at 80-90 K) and subsequently annealed to the indicated temperatures are presented in Figs. 3-6. A spectrum characteristic of methylamine multilayers is shown in Fig. 3(a) when the crystal at a temperature of 80 K is exposed to greater than 6 L of methylamine. Annealing this multilayer coverage to 140 K induces the desorption of the multilayers [cf., Fig. 1(a)] and results in the spectrum of Fig. 3(b). This spectrum is that of second-layer methylamine, a designation supported by observed changes as the surface is further annealed to above 200 K. The librational mode, or frustrated rotation parallel to the surface plane, R_{xy}, at 365 cm^{-1}, is seen to attentuate upon annealing to 189 K, and its disappearance by 200-220 K coincides precisely with the second-layer desorption results of Fig. 1(a).

Upon the desorption of the second layer, the overlayer present on the surface is that of a saturated first layer of methylamine. Figures 3(d-f), represent the spectra for molecularly adsorbed, saturated first-layer coverages of CH_3NH_2, CH_3ND_2 and CD_3ND_2, respectively. Mode assignments for the first- and second-layer methylamine and vibrational gas and solid phase references[27,28] are listed in Table I. It is evident that no bonds have been broken, and, furthermore, the molecule is bonded to the surface through the nitrogen atom's donation of its lone pair of electrons. Evidence for this bonding interaction lies in the strong wagging and overlapping deformation modes of the methyl group, $\omega(CH_3)$ at 1180 cm^{-1} and $\delta_a(CH_3)$ and $\delta_s(CH_3)$ at 1425 cm^{-1}, and the hydrogenic stretching modes, $\nu(NH_2)$ at 3200–3300 cm^{-1} and $\nu(CH_3)$ at 2900-2950 cm^{-1}. The

nitrogen's coordination to the surface is borne out by the ν(Ru–N) stretching mode at 340 cm^{-1} to 350 cm^{-1} in the spectra of the three isotopes between 200 and 220 K, in excellent agreement with that observed for NH_3 on Ru(001).[23]

Annealing the saturated first layer above 220 K results in competitive molecular desorption and conversion, via C–H bond cleavage, to form chemisorbed methylene iminium, CH_2NH_2. From examination of the spectra, these two processes appear to act in consort with one another in that as one molecule desorbs an active site on the surface becomes available to catalyze the cleavage of a CH bond in a neighboring methylamine molecule. This reaction to form H_2CNH_2 occurs most rapidly over the temperature range of 280 to 300 K, as illustrated in Figs. 4(a-c) where the deformation modes of the methyl group at 1460 cm^{-1} are lost, while a strong loss feature at 555 cm^{-1} appears. The methylene iminium intermediate coordinates to the surface in a side-on bridging manner in which the carbon and nitrogen atoms bond to neighboring Ru atoms on the surface. This μ–η^2–H_2CNH_2 coordination gives rise to the broad intense loss features observed at 555 cm^{-1} for CH_2NH_2, 540 cm^{-1} for CH_2ND_2 and 510 cm^{-1} for CD_2ND_2 and assigned to the symmetric and antisymmetric stretching modes of the Ru–CN complex. The di–σ bonding configuration is further supported by the agreement of the CH_2 scissoring and wagging modes at 1430 and 1195 cm^{-1}, respectively, to those of di–σ bonded ethylene on clean Ru(001) which appear at 1450 and 1145 cm^{-1}.[29] If the CH_2NH_2 intermediate were π–bonded to the surface, this would require sp^2 hybridization for the carbon and nitrogen atoms, resulting in $\delta(CH_2)$ and $\omega(CH_2)$ frequencies closer to values of unperturbed gas-phase ethylene, i.e., 1444 and 949 cm^{-1}, respectively,[30] or of π–bonded ethylene in Zeise's salt, $K[PtCl_3(C_2H_4)]$,[31] in which $\delta(CH_2)$ = 1515 cm^{-1} and $\omega(CH_2)$ = 975 cm^{-1}. Organometallic analogues of the bridging CH_2NH_2 intermediate have been synthesized and crystallographically characterized by Adams, et al.[32] The bridging dimethylamino iminium ligand, μ–η^2–H_2CNMe_2, in the triosmium compound, $Os_3(CO)_{10}(\mu$–η^2-$H_2CNMe_2)(\mu$–

H) has a C–N bond distance of 1.53 Å and internal bond angles that indicate sp^3 hybridization of both the carbon and nitrogen atoms. The interpretation of the broad intense loss features at 555 cm^{-1} for CH_2NH_2 as the overlapping bridge-bonded symmetric and asymmetric stretching modes is supported by strong infrared absorption bands between 506 and 589 cm^{-1} for bidentate ethylenediamine in Pt, Pd, Cu and Ni organometallic complexes[33] and also by a very strong HREELS loss feature centered at 565 cm^{-1} for ethylenediamine adsorbed on Pd(111).[34] The complete mode assignments for μ–η^2–H_2CNH_2 and its isotopes present on the surface at 300 K are given in Table II.

Requiring comment beyond the mode assignments of Table II is the appearance of a loss feature at 1430 cm^{-1} in Fig. 4(e). While this feature is assigned as the symmetric deformation, or scissoring, mode of the CH_2 group in the spectra of H_2CNH_2 and H_2CND_2 in Figs. 4(c,d), respectively, the intermediate D_2CND_2 generates no loss feature assignable to that observed at 1430 cm^{-1}. The possibility of contamination by some hydrogen containing methylamine is discarded because the purity of these isotopes was verified by mass spectrometric characterization prior to their use. The appearance of this loss feature results from the reaction having progressed beyond pure D_2CND_2, and there being subsequent decomposition products on the surface as well as the deuterated methylene iminium, D_2CND_2. Additional evidence of the reaction having proceeded beyond pure D_2CND_2 is the comparatively weak ν(Ru–CN) stretching modes at 510 cm^{-1} relative to loss features at 540 and 555 cm^{-1} in the spectra of H_2CND_2 and H_2CNH_2, respectively. While the temperature indicated in Fig. 4(e) is 300 K, it is likely that in the operation of flash annealing the crystal, this temperature was actually overshot slightly, thereby inducing the decomposition reaction to proceed beyond pure CD_2ND_2, vide infra.

Careful annealing of the crystal between 300 and 330 K produces dramatic changes in the spectra as illustrated in Figs. 5(a-c). Three loss features assignable to bridging methylene iminium at 300 K are no longer present at 330 K: The strong Ru–CN stretching

modes at 555–565 cm^{-1}, the CN stretching mode at 1000 cm^{-1} and the CH_2 stretching modes at 2800–3000 cm^{-1}. In place of these loss features appear new peaks at 1070, 1220 and 730 cm^{-1}, accompanied by a noticeable sharpening of the amine scissoring mode at 1545 cm^{-1} with resolvable features at 1420 and 1640 cm^{-1}. The disappearance of the 1000 cm^{-1} peak assigned to the overlapping ν(CN) and $\omega(NH_2)$ modes of μ–η^2–H_2CNH_2 coincides with the loss of the ν(Ru–CN) stretching modes. The changes seen between 300 K and 330 K can be interpreted best by the decomposition of methylene iminium into several new surface products.

Cleavage of one CH bond occurs to form the secondary aminocarbene, $HCNH_2$, which is bound to the surface through the carbon atom only, possibly at an on-top site of a single Ru atom. This terminally bound coordination is represented as η^1–(C)–$HCNH_2$ in which both the carbon and nitrogen atoms are sp^2 hybridized with a partial double bond between them. Back donation from the surfrace to the anti-bonding π^* orbital of the planar $HCHN_2$ intermediate serves to yield a CN stretching frequency of 1420-1430 cm^{-1}. The assignment of this loss feature to the ν(CN) of η^1–(C)-$HCNH_2$ is supported by its presence in the spectra of the deuterated isotopes that have been annealed to 350 K in Figs. 5(f,g).

The precedence for this terminally bound secondary aminocarbene is obtained from organometallic cluster chemistry. Adams, et al.[35] in a very thorough series of studies of triosmium cluster compunds have demonstrated the stability of the terminally bound dimethylaminocarbene ligand, $HCNMe_2$. Its crystallographic characterization yields a CN bond distance of 1.27–1.29 Å, in excellent agreement with that of a CN double bond,[36] and a planar geometry with the carbon and nitrogen both having nearly ideal sp^2 hybridization. Infrared data on the dimethylaminocarbene ligand are not reported, but as a point of reference the CN stretching frequency in gas phase methyleneimine, $H_2C{=}NH$, is 1638 cm^{-1}.[37]

Cleavage of both CH bonds of the H_2CNH_2 intermediate produces the amino-carbyne intermediate, CNH_2, which has its CN bond axis perpendicular to the surface and bonds in a bridging fashion across a two-fold surface Ru site. This μ–CNH_2 product is characterized by a very strong scissoring deformation of the NH_2 group and a CN stretching mode of 1640 cm^{-1}. The aminocarbyne intermediate appears to be produced upon annealing the surface above 300 K and is stable to 360 K. Dimethylaminocarbyne ligands are found in organometallic cluster compounds, such as $Ru_3(CO)_{10}(\mu$–$CNMe_2)$ synthesized by Churchill[38] and in a variety of compounds synthesized by Adams et al.[32,35,39]

Both η^1–(C)–$HCNH_2$ and μ–CNH_2 have sp^2 valence hybridization and planar geometries. As a result of this rehybridization, the wagging and rocking modes of the amine group undergo significant shifts. A compilation of documented shifts in these and other modes of –CH_2 and –CH groups as the carbon-atom hybridization varies is provided by Ibach and Mills[40]. For both the secondary aminocarbene and the bridging aminocarbyne, the $\omega(NH_2)$ mode has a large red shift to 720-750 cm^{-1}, and the $\rho(NH_2)$ mode has a blue shift to 1070 cm^{-1}. As noted earlier, similar shifts in these fundamental modes of an sp^3 hybridized methylene group are seen for di–σ–bonded ethylene on Ru(001)[29] when compared to sp^2 hybridized methylene groups in gas-phase ethylene and π-coordinated ethylene in Zeise's salt.[30,31]

As will be discussed later in relation to the quantification of the branching ratio between the dehydrogenation and CN bond cleavage reaction pathways, the methylene iminium, H_2CNH_2, is the intermediate from which C–N bond cleavage leads to the production of ammonia. Upon annealing above 300 K and by 330 K the loss feature at 1185 cm^{-1} assigned to the $\omega(CH_2)$ mode of H_2CNH_2 is attenuated and shifts to a higher energy loss feature at 1215 cm^{-1}. This feature is from the symmetric deformation of the ammonia product, $\delta_s(NH_3)$, and is blue shifted in its frequency due to the presence of

electron withdrawing intermediates on the surface. On clean Ru(001) ammonia's symmetric deformation mode monotonically shifts from 1160 cm^{-1} at low coverages to 1070 cm^{-1} at saturation coverages.[23] In the presence of a p–(1x2) overlayer of oxygen on Ru(001), low coverages of ammonia exhibit $\delta_s(NH_3)$ at 1220 cm^{-1}.[41]

When the C–N bond cleaves, surface methylene and amido groups are formed. Neither CH_2 nor NH_2 are stable surface intermediates on Ru(001) under these conditions, the former dehydrogenating to methylidyne, CH, and hydrogen adatoms, and the latter either dehydrogenating to imidogen, NH, and hydrogen or being hydrogenated to produce adsorbed ammonia.[24,42] High-resolution EELS loss features of methylidyne and imidogen demonstrate CH and NH bending deformation modes at 800 and 1340 cm^{-1} respectively.[43,44] Methylidyne and imidogen bending modes are unresolved from overlapping loss features of the predominant η^1–(C)–$HCNH_2$ and μ–CNH_2 intermediates. Furthermore, there is such a low coverage of imidogen, methylidyne and ammonia that their respective loss features are just at or below the HREELS experimental detection limits, and this issue shall be dealt with later as the branching ratio is discussed in Section IV B. The complete mode assignments for the mixture of η^1–(C)–$HCNH_2$, μ–CNH_2, and NH_3 present on the surface at 330 K (and their deuterated isotopes) are given in Table II.

Over the temperature range 330–360 K, shown in Figs. 5(c-g) and 6(a), it is apparent that dehydrogenation at the amine group is occurring. Proof of this statement lies in the significant disappearance of the NH_2 scissoring deformation at 1545 cm^{-1}, which dominates the spectrum of η^1–(C)–$HCNH_2$ at 330 K in Fig. 5(c). The presence of a loss feature at 1590–1600 cm^{-1} at 350-360 K coupled with the observed frequency shift to 1255 cm^{-1} upon deuteration at the amine group in Figs. 5(f,g) indicates that an intermediate retaining the amine functional group still remains on the surface at 360 K. Coincident with changes in the NH_2 deformation, there appears a very broad and intense loss feature at 720-780 cm^{-1}. This feature was assigned at 330 K to the overlapping

$\delta(CH)$ and $\omega(NH_2)$ modes of η^1–(C)–$HCNH_2$ and μ–CNH_2, but with the dehydrogenation of most of the amine groups, this very strong feature at 720-780 cm^{-1} is comprised of predominantly a CH bending deformation. A similarly strong CH bending mode is observed at 765 cm^{-1} for molecularly chemisorbed acetylene on Ru(001)[43] in which the carbon atoms are nearly sp^3 hybridized. The loss feature at 1235-1240 cm^{-1} is seen in Figs. 5(d,e) and 6(a) to maintain its intensity, while that of the $\delta(NH_2)$ signal attenuates and is assignable to an NH deformation mode. The feature at 1440 cm^{-1} does not shift upon either selective or complete deuteration of the intermediate [cf., Figs. 5(f,g)] and is assigned to the CN stretching mode.

The interpretation consistent with these observed changes in the spectra between 330 and 360 K requires separately addressing the fates of the η^1–(C)-$HCNH_2$ and μ–CNH_2 intermediates. Organometallic studies[35(b,e),39] have demonstrated that the terminally bound, secondary dimethylaminocarbene ligand in $Os_3(CO)_9(HCNMe_2)(\mu\text{–}SPh)(\mu\text{–}H)$ readily converts to a bridging dimethylaminocarbyne ligand, μ–$CNMe_2$, upon either pyrolysis at 475K or photodecarbonylation of the starting compound. Thus, below 360 K the bridging aminocarbyne, μ– CNH_2, is stable, thereby giving rise to the weak, but observed, scissoring deformation of the amine group as well as the CN stretching mode at 1600 cm^{-1}, which is resolved upon deuteration of the methylamine [cf., Figs. 5(f,g)]. The marked attenuation of the $\delta(NH_2)$ feature at 360 K relative to 330 K indicates that the population of bridging aminocarbyne is quite low and that the surface at 330 K is populated predominantly by the terminally bound aminocarbene. While the aminocarbyne undergoes no reaction over this temperature range, η^1–(C)–$HCNH_2$ experiences N–H bond cleavage to yield chemisorbed formimidoyl, HCNH, which dominates the surface at 360 K.

On the Ru(001) surface the formimidoyl intermediate has both the carbon and nitrogen atoms bonded to adjacent Ru atoms with the molecular plane tilted across a surface threefold site allowing for coordination to a third surface atom either via π electron density

donation to the surface or by surface electron density backdonation to the adsorbate's π^* antibonding orbital. This triply bridging configuration involving bonding by both the carbon and nitrogen atoms is designated μ_3–η^2–HCNH. The justification for this tilted coordination comes from the CN stretching frequency lying between that for a single and double bond and the appearance of all four bending modes for the CH and NH in Fig. 6(a). Were the molecular plane of the intermediate parallel to the surface normal, the in-plane deformations, δ(CH) and δ(NH), at 770 and 1235 cm^{-1} would dominate the spectrum, and the out-of-plane deformations, π(CH) and π(NH), at 1015 and 1600 cm^{-1} would be detectable only through impact scattering interactions with the incident electron beam, and their vanishing dipolar derivatives in the direction of the surface normal would render their loss features very weak relative to the in-plane deformations. With the formimidoyl intermediate inclined across the threefold surface Ru site, both the in-plane and out-of-plane bending modes of the CH and NH groups are indoubitably assigned. The final mode assignment consistent with this coordination of HCNH is the CN stretching mode at 1440–1450 cm^{-1}. As noted earlier, the double bond CN stretching frequency is 1638 cm^{-1} in methyleneimine,[37] H_2C=NH, and its bond length is 1.273 Å.[36(b)] With π donation to or π^* backdonation from the surface, the CN bond stretching frequency appears at 1440–1450 cm^{-1}, only slightly shifted from the ν(CN) loss feature at 1420–1430 cm^{-1} of the preceding intermediate, η^1–(C)–$HCNH_2$.

A related organometallic analogue to chemisorbed HCNH is the acetimidoyl ligand in the triiron cluster compound, $HFe_3(CH_3C{=}NH)(CO)_9$.[45] The μ_3–η^2–CH_3C=NH ligand is triply bridging and has a CN bond length of 1.344 Å and a stretching frequency of 1353 cm^{-1}. This virtually planar ligand has the carbon and nitrogen atoms retaining nearly pure sp^2 hybridization, and, while each is coordinated to adjacent Fe atoms, the ligand tilts approximately 45° across the threefold site to allow coordination to the third Fe atom. Yin and Deeming[46] also report a triply bridging acetimidoyl ligand in $Os_3(\mu$–$H)(CO)_9(\mu_3$–η^2–

$CH_3C{=}NH$). On the W(100)–(1x5)–C surface, HCN is purported to undergo self hydrogenation upon annealing to 475 K to yield terminally coordinated formimidoyl, η^1–(C)–HCNH; HREELS[47] and NEXAFS[48] experiments have been conducted that indicate CN, CH and NH stretching modes at 1400, 2940 and 3360 cm^{-1}, yet neither CH nor NH deformation modes are reported. The planar HCNH product with sp^2 hybridization at both the carbon and nitrogen is believed to have its CN bond vector inclined at an angle of 58° ± 10° from the surface normal with only the carbon atom bonded to the surface and the molecular plane perpendicular to the surface.

From the preceding analysis it is known that at 350 K the conversion of the secondary aminocarbene, η^1–(C)–$HCNH_2$, to the bridging formimidoyl, μ_3–η^2–HCNH, is not yet complete and that bridging aminocarbyne, μ–CNH_2, is also present. When saturated coverages of CH_3ND_2 and CD_3ND_2 are annealed to 350 K, the spectra of Figs. 5(f,g) are obtained and must be interpreted as mixtures of their respective deuterated aminocarbyne, secondary aminocarbene and formimidoyl intermediates. Upon deuteration the $\delta(ND_2)$, $\rho(ND_2)$ and $\omega(ND_2)$ appear respectively at 1255, 755 and 580 cm^{-1}, while the δ(ND) and π(ND) modes appear at 1010 and 1255 cm^{-1}. The deformation δ(CD) and π(CD) modes appear at 585 and 715 cm^{-1}, and, of course, the CN bond frequency does not shift noticeably upon deuteration and appears at 1425–1435 cm^{-1}. The complete mode assignments for these chemisorbed species and their deuterated isotopes are provided in Table III.

Annealing between 370 and 390 K induces the changes in the spectra of Figs. 6(b–d), indicating that both intermediates present at 360 K, μ_3–η^2–HCNH and μ–CNH_2, have undergone dehydrogenation reactions. The very strong δ(CH) mode at 720–780 cm^{-1} is gone from the spectrum at 390 K, and, as it attenuates, a very intense feature at 595–605 cm^{-1} appears. The δ(NH) mode at 1260–1280 cm^{-1} retains its intensity, and by 380 K a resolvable feature at 1665 cm^{-1}, characteristic of a CN double bond, appears.

The feature at 1590–1600 cm^{-1}, assigned to the NH_2 scissoring deformation of the low-coverage intermediate, μ–CNH_2, is lost upon annealing to 370 K.

The surface intermediate formed by 380 K and appearing to be stable to 390 K is chemisorbed hydrogen isocyanide, HNC. There are two possible bonding configurations for HNC, and the analogous system of methylisocyanide, CH_3NC, adsorbed on Pt(111) has been thoroughly investigated by Avery and Matheson.[49] Terminal, linear bound CH_3NC revealed a very strong CN stretching frequency of 2240–2265 cm^{-1}, accompanied by a similary strong Pt-C stretch at 385 cm^{-1}. The terminally bound methylisocyanide coexisted at higher coverages with a bridge-bound imine-like configuration with a characteristic CN double bond stretching frequency that increased with coverage over the range of 1690–1770 cm^{-1}. Very strong Pt–C frustrated translation and skeletal deformation modes were observed at 265 and 530 cm^{-1} for this second bridge-bonded imine-like configuration.

With this information the hydrogen isocyanide intermediate present on the Ru(001) surface at 380–390 K is observed to exist as a mixture of terminally bound, η^1–(C)–CNH, and bridge-bound, μ–CNH. The mode assignments for the two configurations are given in Table III with the CN stretching frequencies at 2275-2295 cm^{-1} and 1660-1670 cm^{-1}, respectively, for the terminally bound and bridge bound HNC intermediates. The NH bending deformations are at 1090 cm^{-1} for η^1–(C)–CNH and at 1260-1280 cm^{-1} for μ–CNH. For comparison the NH bending deformation is at 1344 cm^{-1} for gas-phase methyleneimine[37]. The very strong loss feature at 595-605 cm^{-1} is assigned to the frustrated translation of the bridge bound hydrogen isocyanide, ν(Ru–C). The appearance of CO on the surface is evidenced by ν(CO) at 2000 cm^{-1}. The amount of CO is quite small, however. The loss feature at 2400-2450 cm^{-1} in Figs. 6(c,d) is puzzling. Its assignment as a combination band of ν(Ru–C) and ν(CO) for the background-adsorbed carbon monoxide is not reasonable since the feature at 2450 cm^{-1} is comparable in intensity

to the ν(CO) loss feature itself. The strongest feature is the 595-605 cm^{-1} frustrated translation of the bridging HNC intermediate, and the second strongest loss feature at 1260 cm^{-1} is the bending deformation, δ(NH), of this same intermediate. With both these modes having strong perpendicular dynamic dipole moments for the bridging imine-like configuration, the loss feature at 2400-2450 cm^{-1} is tentatively assigned as the combination of the first overtone of ν(Ru-C) with δ(NH).

Annealing the crystal to 400 K causes dehydrogenation of this remaining NH bond and the conversion to side-on bonded cyano, CN. Figs. 6(e–g) correspond to saturation exposures of CH_3NH_2, CH_3ND_2 and CD_3ND_2 adsorbed at 80 K and annealed to 400–425 K. All three isotopes yield identical spectra showing Ru–CN symmetric and asymmetric stretching modes at 340–350 and 585–595 cm^{-1}, and ν(CN) stretching modes at 1655–1665 cm^{-1}. The presence of CO present on the surface is noted by the loss features at 450 and 2000 cm^{-1}. Annealing above 425 K desorbs the small amount of CO present on the surface, removing the ν(CO) feature at 2000 cm^{-1} and attenuating that at 450 cm^{-1}. By 450 K thermal decomposition of side-on bonded cyano begins accompanied by an increase in the intensity of the loss feature at 585-595 cm^{-1}. At 600 K no cyano adspecies remains on the surface, as evidenced by the loss of ν(CN), and annealing above 800-900 K initiates recombinative desorption of dinitrogen, decreasing the intensity of the 585-595 cm^{-1} feature but never entirely eliminating it. Thus, the loss feature at 585-595 cm^{-1} present in HREEL spectra above 450 K is due to ν(Ru–C) and ν(Ru–N) of surface carbon and nitrogen adatoms overlapping with the asymmetric ν(Ru–CN) mode of surface cyano present between 400 K and 600 K.

Other surface HREELS studies have isolated chemisorbed CN on Pd(111) and Pd(100),[50] and on Cu(111) and O-predosed Cu(111).[51] On both Pd(111) and Pd(100) surfaces, ν(CN) is observed at 220–240 meV (1774–1935 cm^{-1}). On clean Cu(111) ν(CN) is at 2045 cm^{-1}, and on O-predosed Cu(111) it is blue shifted to 2140 cm^{-1}. On

Pd(111) and Pd(100) the cyano adspecies is proposed to be side-on bonded with the CN bond vector parallel to the surface. A NEXAFS study[52] of CN/Pd(111) revealed the CN bond axis to be tilted 14° above the plane of the surface, but the authors believe the cyano to be exactly parallel with the 14° tilt resulting from the experimental uncertainty inherent in the measurement. On the Cu(111) surfaces, CN is believed to exist in a side-on bonded configuration on the clean surface, but, when adsorbed onto an O-precovered surface, it reorients to a vertical, terminally bound configuration. This argument is used to explain the observed blue shift and intensification of the loss feature at 2140 cm^{-1} for CN/O–Cu(111) relative to the feature at 2045 cm^{-1} for CN/Cu(111). In our view, this increase in frequency for ν(CN) can more reasonably be explained as resulting from preadsorbed oxygen withdrawing electron density from the surface and thereby decreasing the extent of backdonation to the terminally coordinated CN. On the clean Cu(111) surface the ν(CN) loss feature at 2045 cm^{-1} is too high to be consistent with a side-on bonded configuration, but rather reflects a terminally coordinated cyano adspecies bound to the surface predominantly by backdonated electron density from the electron-rich, late-transition metallic Cu surface.

As expressed in an earlier publication,[53] the bonding configuration of CN on Ru(001) is best described as μ_3–η^2–CN. Both the carbon and nitrogen atoms interact with the surface: The carbon atom is σ–bonded to a single surface Ru atom while the CN bond vector is inclined across the center of a surface threefold site, thereby allowing either the bonding 1π orbitals to donate electron density to the surface or the antibonding 2π orbitals to receive backdonated density from the surface. The 4σ lone pair orbital on the nitrogen atom remains collinear with the CN bond vector and thus stays orthogonal to the bonding orbitals between the surface and the cyano adspecies. This μ_3–η^2–CN configuration affords the greatest degree of overlap of surface and adsorbate orbitals and hence is preferred over alternative configurations.

IV. Discussion

The data presented in the previous section allow several important statements to be made regarding the decomposition of methylamine on Ru(001). The demonstrated preference for cleavage of C–H bonds over N–H and C–N bonds is evident from both the thermal desorption and high resolution EEL spectra, and a comparison of this behavior to that observed for other surface reactions is now possible. Through careful accounting of the ammonia produced from the decomposition of CH_3ND_2, quantification of the branching ratio can be made for the competing dehydrogenation and C–N bond cleavage reaction pathways. Finally, the relevance of this study to commerical disproportionation reactions of aliphatic amines can be discussed.

A. Comparison of CH_3NH_2/Ru(001) to Related Surface Science Studies

The interaction of methylamine on Pt(111), Rh(111), Ni(111), W(100), W(100)–(1x5)–C and W(100)–(1x2)–O, Mo(100), Ni(100), Cr(100), Cr(111) and Pt(100) surfaces have been reported. On Pt(111)[10,11] temperature programmed desorption, TPD, and Auger electron spectroscopy, AES, indicate that no C–N bond cleavage occurs, and dehydrogenation is the only decomposition pathway available to CH_3NH_2. For room temperature exposures only H_2, HCN and C_2N_2 are observed as decomposition products, and for exposure at 100 K in addition to the above products molecular methylamine also is observed. On Rh(111)[11,12] the decomposition of CH_3NH_2 yields H_2, HCN and C_2N_2 as it did on Pt(111) except that at ~850K cyanogen desorption ceases and N_2 desorption is observed. Thus, on Rh(111) there is evidence of C–N bond cleavage seemingly well after

methylamine has been completely dehydrogenated to leave surface cyano, CN. High-resolution EELS experiments following the progress of the reaction would certainly help identify the occurrence of any low temperature cleavage of the C–N bond. In contrast, TPD and AES studies of methylamine adsorbed at 87 K on Ni(111)[16] indicate that molecular methylamine, H_2 and N_2 desorb as gas phase products with surface carbon deposited as all irreversibly adsorbed methylamine experiences complete dissociation of the C–N bond. By approximately 430 K all the H_2 has desorbed, and an Auger line shape analysis indicates that near 410 K carbidic and nitridic species are being formed from C–N bond cleavage of the surface cyano. By studying the H_2 and D_2 thermal desorption specta from the deuterated isotopes, CD_3NH_2 and CH_3ND_2, it was determined unequivocally that when adsorbed at 412 K, some, if not both, N–H bonds are retained while all the C–H bonds have been cleaved. On W(100) and the carbon and oxygen precovered W(100) surfaces,[14] CH_3NH_2 adsorbed at 120 K undergoes competing molecular desorption and complete decomposition to H_2, N_2 and surface carbon. The carbon precovered surface affected the reaction only by stabilizing the molecular methylamine to higher temperatures, and the oxygen precovered surface oxidized the surface carbon to yield gaseous CO as a product. On Mo(100),[13] thermal decomposition of monomethylamine following room temperature adsorption yields H_2, N_2, HCN and a small amount of CH_4. No intact molecular CH_3NH_2 is observed, and the HCN product desorbs between 400 and 500 K. High-resolution electron energy loss spectroscopy studies of CH_3NH_2 adsorbed at 300 K on the Ni(111), Ni(100), Cr(111) and Cr(100) surfaces[15] indicate that molecular CH_3NH_2 exists on all surfaces with bonding through the lone pair of electrons on the nitrogen atom. On the Cr surfaces a substantial amount of dissociation is purported to occur based upon the appearance of a very intense, sharp loss feature at 510 cm^{-1} on Cr(100) and an intense, but broad, feature also at 510 cm^{-1} on Cr(111). This loss feature correlates with the surface-adsorbate stretching modes observed here on Ru(001) for the intermediate

H_2CNH_2. Temperature programmed reaction spectrometry results of methylamine's decomposition on Ni(100)[17] are remarkably similar to those observed in this study. Molecular methylamine, hydrogen, nitrogen and ammonia are the observed gaseous products with surface carbon observed with post reaction Auger spectroscopy. The ammonia is seen to have a peak desorption temperature of 365 K, while hydrogen peaks at approximately 375 K. The decomposition of CH_3ND_2 was also examined and showed the ammonia product made up of primarily ND_2H and ND_3, and the H_2 and D_2 desorption spectra had peaks at 370 and 385 K respectively. On Pt(100)–(5x20) and Pt(100)–(1x1),[18] methylamine's interaction and decomposition were studied. The Pt(100)–(5x20) surface is a stable, pseudohexagonal surface similar to Pt(111), and thermal desorption and high resolution EELS data indicate that only reversible desorption occurs for methylamine. On metastable Pt(100)–(1x1), however, decomposition is evident from the gas-phase TDS detection of H_2 (T_{pk} ~ 380 K), HCN (550K), C_2N_2 (780K) and N_2 (810 K). The appearance of an HREELS loss feature at 1140 cm^{-1} upon annealing to 410 K is assigned to the C–C stretching mode of chemisorbed cyanogen implying completely dehydrogenated cyano, CN, adspecies have dimerized on the surface. Such an assignment must be considered tentative since the HREEL spectrum at 550 K contains evidence of a C–H stretching mode at 2980 cm^{-1}, implying that the 1140 cm^{-1} feature might also arise from a hydrogenic deformation mode of an incompletely dehydrogenated surface intermediate such as HCN.

In addition to the single crystalline studies, the reaction of CH_3NH_2 with H_2 has been examined on other kinds of transition metal surfaces. Kemball and Moss[54] have studied this reaction over polycrystalline Ni, Fe, Pd, Pt and W films, while Anderson and Clark[55] examined it over evaporated Pt, Pd, Ni, W, Co, V and Cu films. The cracking of CH_3NH_2 to CH_4 and NH_3 and disproportionation to di- and trimethylamines were the dominant reaction processes observed. Meitzner, et al.[56] studied the reaction over silica

supported Ru, Rh, Re, Pd, Os, Ir, Pt and Au catalysts and found that cracking to CH_4 and NH_3 occurred on all metals as did a significant amount of disproportionation to dimethylamine, except on Rh. Minor products were found to be produced from the various metals, and most notably Ru and Os converted one-third of the methylamine to acetonitrile. Orita, et al.[57] studied the decomposition of CH_3NH_2 at 393 K over Ru black in both the presence and absence of H_2. Of particular relevance is the fact that no higher amines were observed and small amounts of C_2–C_4 hydrocarbons were formed along with the CH_4 and NH_3 cracking products.

A comparison of the interactions of ammonia and methylamine with the Ru(001) surface is of pedagogic interest. The thermal desorption of reversibly adsorbed methylamine, as seen in Fig. 1(a), contains the same qualitative features as ammonia desorption from clean Ru(001). The desorption temperatures for methylamine are approximately 15 K greater than those of ammonia, and this observation is readily understandable based on the greater Lewis base character of methylamine and noting that both adsorbates bond to the Ru(001) surface via nitrogen lone pair donation. The formation of a second layer of ammonia on Ru(001) gives rise to a resolvable desorption feature at 140 K[22] and a strong librational loss feature at 360 cm^{-1} in HREEL spectra.[23] Methylamine thermal desorption spectra do not reveal a second-layer feature resolved from that of multilayer of CH_3NH_2. However, the strong librational mode associated with the second layer is readily observed after annealing off the multilayer [cf., Figs. 3(a–c)]. Thus, the bonding interactions of ammonia and molecular methylamine are predictably similar with the presence of the methyl group slightly modifying the strengths of the bond to the surface.

B. Branching Ratio: Competing Decomposition Pathways of CH_3NH_2

The majority decomposition pathway available to irreversibly adsorbed methylamine is complete dehydrogenation to chemisorbed cyano, CN. A smaller fraction of methylamine will follow the minority path of carbon-nitrogen bond cleavage, forming the ultimate products of carbon and nitrogen adatoms and ammonia. The production of ammonia occurs subsequent to this C–N bond cleavage step and provides the means for quantifying the branching ratio of the competing decomposition reactions.

The surface reaction that forms ammonia results from amido, NH_2, combining with surface hydrogen. This statement is made based on the observation that for the low coverages of surface hydrogen encountered in this reaction, it is not at all likely that nitrogen adatoms or even imidogen, NH, could be reduced to form ammonia.[24] Thus, the production of ammonia follows the cleavage of the carbon-nitrogen bond in a surface intermediate that has retained the integrity of the amine functional group.

The intermediate which precedes C–N bond cleavage is bridging methylene iminium, μ–η^2–H_2CNH_2, present and stable on the surface at 300 K. The CN bond lengths in two separate triosmium cluster compounds[32] were found to be 1.53Å and 1.50Å, which are elongated relative to the CN single bond length of 1.47Å.[36(a)] Heating one of these compounds, $Os_3(CO)_{10}(\mu$–η^2–$H_2CNMe_2)(\mu$–H), to 370 K induces cleavage of a C–H bond to yield a triply-bridging, secondary aminocarbene, μ_3–η^2–$HCNMe_2$, with a C–N bond length of 1.40 Å. The triple-bridging coordination of secondary dimethylaminocarbene is less favored than its terminally coordinated isomer, η^1–(C)–$HCNMe_2$, which is encountered in numerous other organometallic compounds.[35]

In the decomposition of methylamine on Ru(001), a definitive isolation and identification of μ_3–η^2–$HCNH_2$ has not been made. Mode assignments for such an intermediate would have to include the stretching modes of the Ru–CN framework, which presumably would lie between 500 and 600 cm^{-1}, together with a C–N single bond stretching mode near 1000 cm^{-1} and a C–H deformation mode near 750 cm^{-1}. Such assignments may be possible for the spectra between 310 and 320 K, but the preference of

$HCNH_2$ to be sp^2 hybridized and terminally coordinated has been demonstrated, and it is for this reason that triple-bridging secondary aminocarbene is not unambiguously isolated.

The competition between C–H and C–N bond cleavage in methylene iminium begins upon annealing above 300 K and appears to be completed by 320–330 K. The majority pathway continues, after C–H bond cleavage yields $HCNH_2$, and it follows the sequence presented earlier in the interpretation of the HREEL spectra. The minority pathway is initiated by C–N bond cleavage in μ–η^2–H_2CNH_2, leading to the formation of surface methylene, CH_2, and amido, NH_2. As noted previously, both of these intermediates are unstable under these conditions and will quickly convert to further products.

Quantification of the branching ratio is made dependent upon the extent to which the surface amido, NH_2, itself branches to form imidogen and surface hydrogen or is hydrogenated to form ammonia. The key input in addressing this issue lies in the ammonia thermal desorption data, and especially that of the mixed deuterated isotopes of ammonia formed from the decomposition of CH_3ND_2 [cf., Fig. 2(b)]. The hydrogenation reaction of surface amido involves the transfer of a hydrogen (or deuterium) atom from some surface state (not necessarily a ground state) to the short-lived amido intermediate before the amido itself decomposes. From the thermal desorption spectra of the deuterated ammonia product in Fig. 2(b), and assuming equal mass spectrometric sensitivities for the parent ND_3 and ND_2H molecules, the amount of ND_2H formed is 40% of that of ND_3, or 28% of the total ammonia, ND_3 + ND_2H. Together these two ammonia products account for the observed cracking fragments at masses 17 and 18. The production of ND_3 *must* occur from the deuteration of ND_2, where the deuterium adatom has been formed from the decomposition of a second deuterated amido. This surface deuterium is most likely in a highly mobile surface state where it possesses most of the energy from the decomposition

reaction of the unstable ND_2. Upon locating an intact, unstable, but newly formed ND_2, it deuterates this amido and yields the more stable ND_3 product.

The production of ND_2H obviously results from the reaction of ND_2 with the available surface hydrogen adatoms. It is interesting to note that despite the fact that there is significantly higher coverage of surface H than surface D, the fact remains that 72% of the ammonia product is ND_3 while only 28% is ND_2H. This experimental result is simply a manifestation of the difference in relative reaction rates of the deuterated amido, ND_2, with highly mobile D atoms versus thermally equilibrated, less mobile H atoms. The higher reactivity of similarly "hot" hydrogen adatoms has been observed recently in the decomposition of formates on the Ru(001) surface.[58]

The fate of the mobile surface deuterium is not exclusively to react with surface ND_2, but it might also combine with surface hydrogen adatoms and desorb as HD. As seen in Fig. 2(a), the beginning of HD desorption occurs near 320 K, while that of D_2 is not seen until near 365 K. The preponderance of both the HD and D_2 thermal desorption results from later decomposition of majority path intermediates: η^1–(C)–$HCND_2$, μ–η^2–HCND, μ–CND and η^1–(C)–CND. The low-temperature tail of the mass 3 amu signal, however, contains H recombination with D released from ND_2 decomposition from the minority path. Thus, a definitive determination of the branching ratio must include the ultimate products of all the surface amido formed when the C–N bonds are cleaved.

For each ND_3 molecule formed, two amido intermediates have to participate, since one of these must decompose in order to release the deuterium atom required to make ND_3. The total ammonia produced from a saturation exposure of CH_3NH_2 was given earlier as 0.02 ± 0.01 monolayer while that of irreversibly adsorbed methylamine was 0.15 ± 0.01 monolayer. With 72% of ammonia formed from CH_3ND_2 being ND_3 and 28% being ND_2H, the most efficient production of ammonia following C–N bond cleavage leads to an estimate of 0.034 monolayer for the fractional coverage of methylamine that follows the

minority reaction. In terms of the branching ratio, this result implies that 23%, or one in every four or five, of the irreversibly adsorbed methylamine molecules undergoes C–N bond scission.

As noted above, however, the low temperature tail, 320 K < T < 350 K, of the HD desorption spectrum arises from deuterium and hydrogen recombination, where the deuterium source is the decomposing amido, ND_2. The amount of HD present in the leading edge is estimated to be less than 25% of the total HD produced, and the total fractional coverages of HD and this atomic D in Fig. 2(a) are 0.25 and 0.06 monolayer, respectively, both relative to saturation coverages of atomic deuterium, $\Theta_D = 1.00$. The estimate of the maximum amount of amido decomposition that appears as HD is 0.031 monolayer. Combining this with the amount of hydrogenated amido that forms ND_3 yields an estimate of 0.065 for the maximum fractional coverage of methylamine experiencing C–N bond cleavage. In this case the distinction between minority and majority paths is virtually meaningless since 44%, or nearly one of each two molecules, completely dehydrogenates, while the other cleaves its CN bond.

It must be noted, however, that when the C–N bond of methylene iminium is broken, a methylidyne, CH, and hydrogen adatom will be formed upon the decomposition of surface methylene. Methylidyne is stable on Ru(001) to above 500 K and its bending deformation mode, δ(CH), at 800 cm^{-1} is a strong loss feature.[43] The fact that no such HREEL assignment can be made for methylidyne in the spectra from methylamine's decomposition implies that the fractional coverage of methylidyne must be below its detection limit by the HREEL spectrometer. Bearing this in mind, the extent of C–N bond cleavage along the minority pathway is most likely near the lower limits of the above estimates, i.e., between 0.04–0.05 monolayer, yielding a branching ratio between one of every three to four irreversibly adsorbed molecules. The following reaction scheme

incorporates the principal products of the sequence of elementary reaction steps along the majority and minority paths.

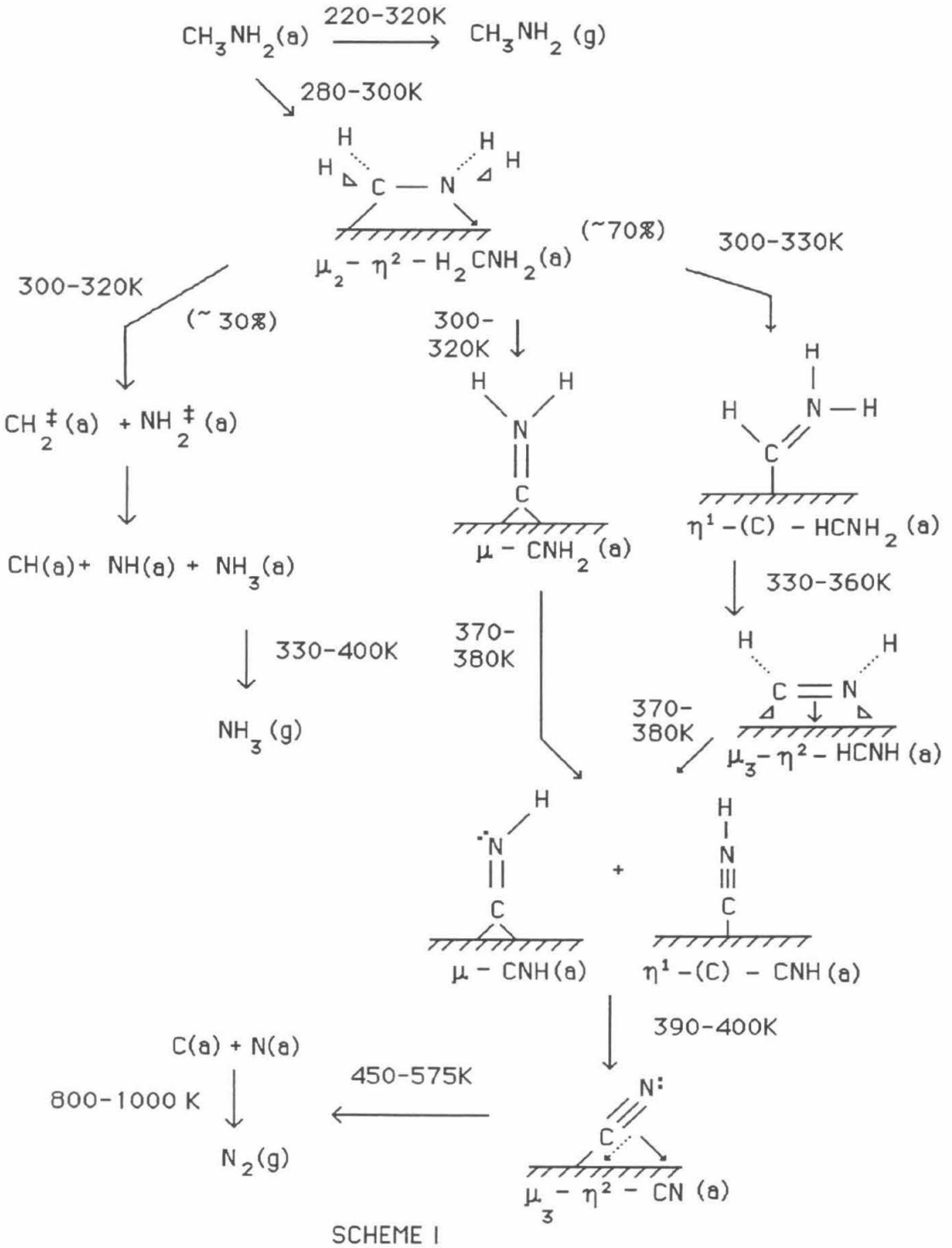

SCHEME I

C. η^1–(C)–$HCNH_2$ and the Disproportionation of Amines

Some of the intermediates identified in the decomposition of methylamine on Ru(001) are of general interest because they may play relevant roles in related catalytic processes. For example, the catalytic amination of aliphatic alcohols by Copper oxide produces aliphatic amines that are commercially used as corrosion inhibitors and as additives to textile products.[3] The process uses either dimethylamine or monomethylamine reacting with long chain primary alcohols to yield the desired amine product and water as in reaction (1):

$$RCH_2OH + (CH_3)_2NH \rightarrow RCH_2N(CH_3)_2 + H_2O \ . \qquad (1)$$

The mechanism has been studied by Baiker, et al.[2], and it is believed to involve the aldehyde of the reagent alcohol. The selectivity of the reaction is hampered however by disproportionation [(reactions (2)–(4)] of the reagent dimethyl- or monomethylamine.[55]

$$2CH_3NH_2 \rightarrow (CH_3)_2NH + NH_3 \qquad (2)$$

$$CH_3NH_2 + (CH_3)_2NH \rightarrow (CH_3)_3N + NH_3 \qquad (3)$$

$$2(CH_3)_2NH \rightarrow (CH_3)_3N + CH_3NH_2 \qquad (4)$$

At the temperature range of the amination process, 400–600 K, the equilibrium mixture consists predominantly of ammonia and trimethylamine. To improve the selectivity of the process, it was discovered that a hydrogen partial pressure of 15–80 kPa in the reaction stream inhibited disproportionation of the feed amine.

In the decomposition of methylamine on Ru(001), the identification of terminally bound, secondary aminocarbene has been made. This planar intermediate has a partial double bond between the carbon and nitrogen, in part due to the incomplete delocalization

of the nitrogen lone pair to the empty p_π orbital of the carbon atom. As a result, the carbenoid carbon of η^1–(C)–$HCNH_2$ is electron deficient and susceptible to nucleophilic attack, a chemical property common to metal-coordinated amino carbene ligands.[59] A mechanism for the transalkylation of tertiary amines has been proposed for the dimethylaminocarbene ligand in $Os_3(CO)_8$ (η^1–$HCNMe_2$) (μ–H)$_2$(μ_3–S) by Adams et al. which involves equilibration between two zwitterionic intermediates.[9] This mechanistic step is illustrated in Scheme II below to demonstrate the disproportionation of monomethylamine. The sequence begins with η^1–(C)–$HCNH_2$ experiencing nucleophilic attack at its carbenoid carbon by a second monomethylamine molecule. The cationic pair, (A) and (B), are formed by the intramolecular transfer of a proton between the two amine moieties. The new secondary methylaminocarbene then can be reduced by surface hydrogen to form dimethylamine, $(CH_3)_2NH$.

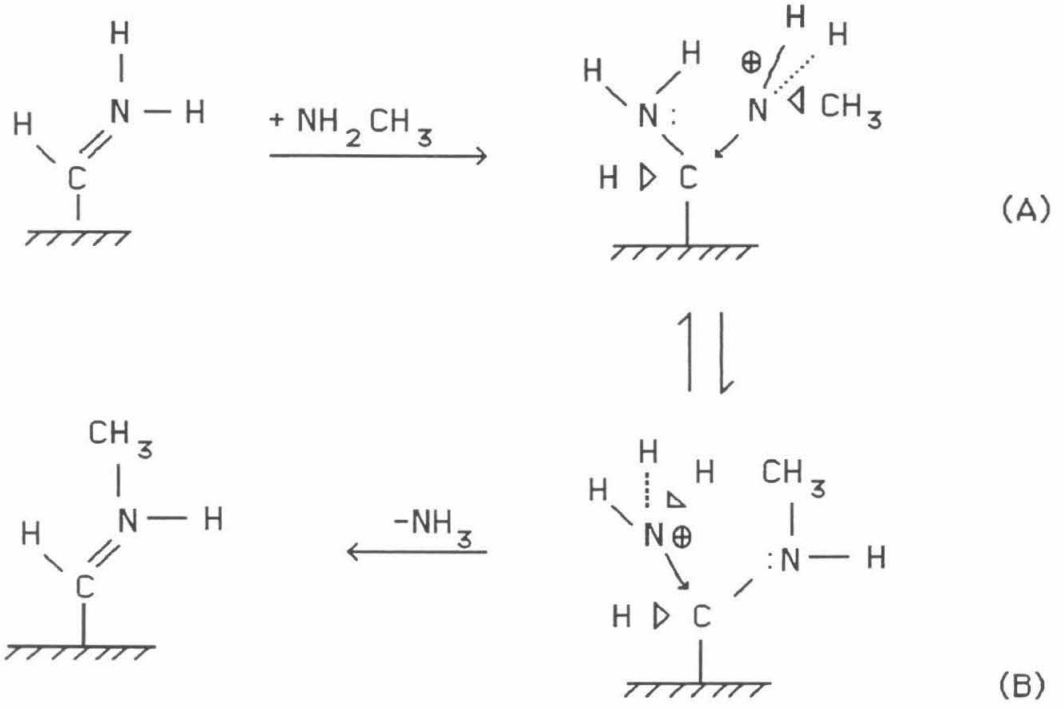

SCHEME II

Related to this reaction mechanism is the amination step of long chain aliphatic alcohols. When α–deuterium labeled alcohols, RCD_2OH, were aminated by dimethylamine, the product mixture contained 33% $RCDHN(CH_3)_2$ and 67% $RCH_2N(CH_3)_2$, but no $RCD_2N(CH_3)_2$.[22] These results indicate that at least one α–CD bond is cleaved during the amination reaction. A mechanism involving an intermediate analogous to η^1–(C)–$HCNH_2$ is proposed in Scheme III to account for the majority product. The aliphatic alcohol will undergo initial O–H bond cleavage on the surface followed by the cleavage of both of the α–CH bonds to yield an intermediate with an electron deficient carbonyl carbon. This carbon atom is then attacked by the nucleophilic amine, followed by a very rapid intramolecular proton transfer. Protonation from the surface produces the cationic pair, (C) and (D), with water ultimately released as a leaving group upon C–O bond cleavage. The resulting surface intermediate is the secondary dimethylamino carbene, which, when reduced by surface hydrogen, yields the desired aliphatic long-chain amine.

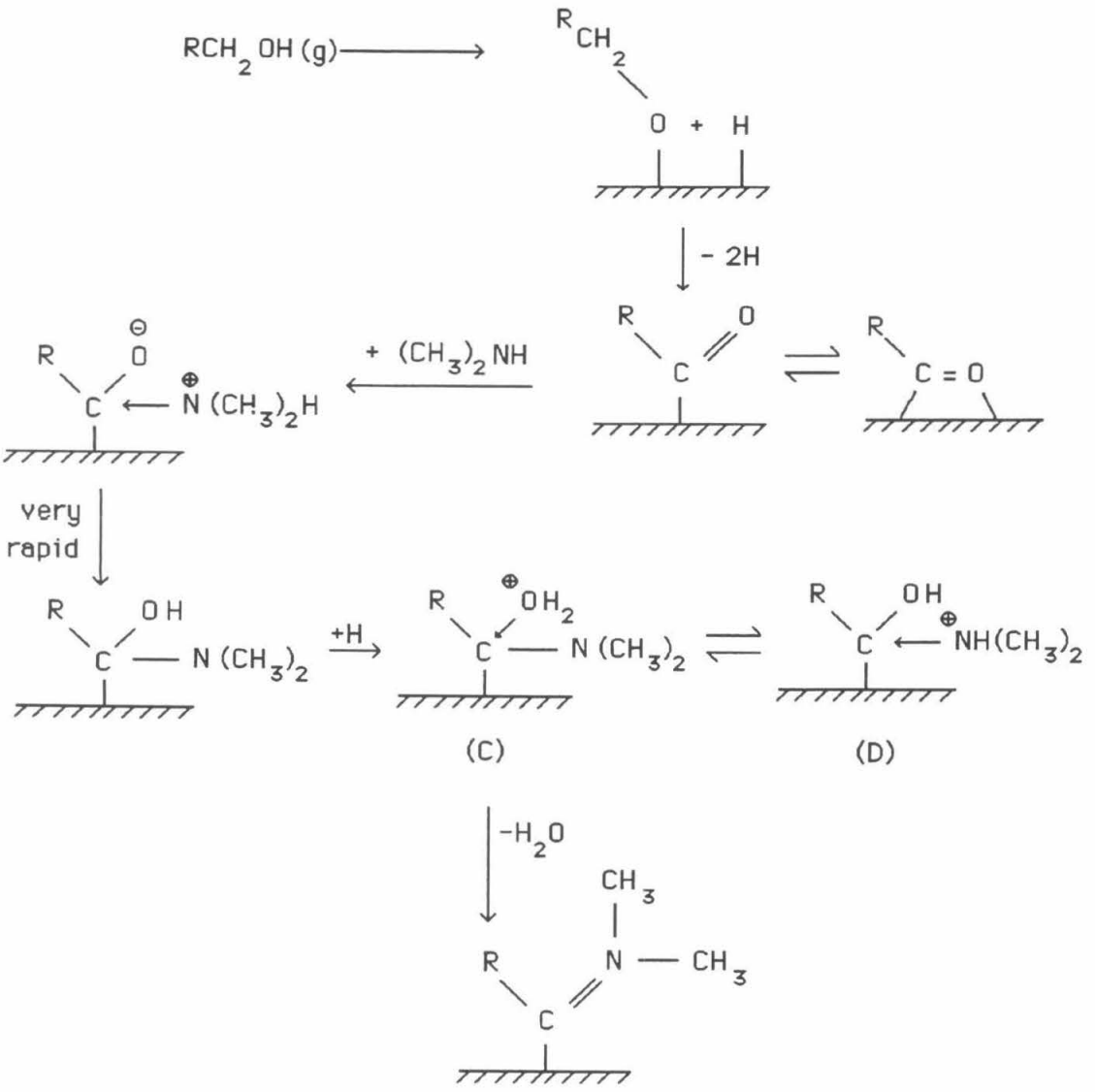
RCH2 OH (g)
R
CH2
O + H
- 2H
R
O
C
C = O
+ (CH3)2 NH
very
rapid
N (CH3)2H
OH
N (CH3)2
+H
OH2
(C)
NH(CH3)2
(D)
-H2O
CH3
N — CH3

SCHEME III

V. Summary

A high-resolution electron energy loss spectroscopy and thermal desorption mass spectrometry study of monomethylamine on the clean surface of Ru(001) has been performed, and the important findings are the following:

1. Molecular methylamine coordinates to this surface through lone pair donation of the nitrogen atom, and its interaction is of the same nature as that of ammonia with only a slightly stronger bond formed as a result of the substituent methyl group.

2. Preferential dehydrogenation is observed relative to C–N bond cleavage. Approximately ~70% of the irreverisbly adsorbed methylamine dehydrogenates completely to surface cyano, μ_3–η^2–CN , with ν(CN) = 1660 cm^{-1}.

3. Activation of C–H bonds is more facile than that of N–H bonds, as judged by the isolation of η^1–(C)–$HCNH_2$ and μ–CNH_2 intermediates.

4. No desorption products other than reversibly adsorbed methylamine are observed to retain the CN bond, and the surface cyano is stable to 450 K at which point it begins to decompose to carbon and nitrogen adatoms.

5. A mechanism for amine disproportionation and amination of aliphatic alcohols is proposed that involves the secondary aminocarbene, η^1–(C)–

$HCNH_2$, stable on this surface under these ultrahigh vacuum conditions between 300 and 330 K.

Acknowledgment. This work was supported by the National Science Foundation under Grant number CHE-90 03553. Additional support was provided by the Donors of the Petroleum Research Fund (Grant No. PRF23801-AC5-C).

References

(1) (a) Ryan, R.C.; Adams, C.T.; Washecheck, D.M. U.S. Patent 4 530 911, 1985; *Chem. Abstr.* **1985**, *103*, 382. (b) Laine, R.M. *Catal. Rev. Sci. Eng.* **1983**, *25*, 459-474.

(2) Baiker, A.; Caprez, W.; Holstein, W.L. *Ind. Eng. Chem. Prod. Res. Dev.* **1983**, *22*, 217-225.

(3) Baiker, A.; Richarz, W. *Ind. Eng. Chem. Prod. Res. Dev.* **1977**, *16*, 261-266.

(4) Volf, J.; Pasek, J. In *Catalytic Hydrogenation;* Cerveny, L., Ed.; Studies in Surface Science and Catalysis; Elsevier Science: Amsterdam, 1986; Vol. 27, Chapter 4.

(5) Endter, F. *Platinum Met. Rev.* **1962**, *6*, 9-10.

(6) Pirie, J.M. *Platinum Met. Rev.* **1958**, *2*, 7-11.

(7) Collman, J.P; Hegedus, L.S.; Norton, J.R.; Finke, R.G.; *Principles and Applications of Organotransition Metal Chemistry;* University Science: Mill Valley, CA, 1987; pp 568-571.

(8) *ibid;* pp. 643-644.

(9) Adams, R.D.; Kim. H.-S.; Wang, S. *J. Am. Chem. Soc.* **1985**, *107*, 6107-6108; and references therein.

(10) Hwang, S.Y.; Seebauer, E.G.; Schmidt, L.D. *Surf. Sci.* **1987**, *188*, 219-234.

(11) Cordonier, G.A.; Schüth, F.; Schmidt, L.D. *Vacuum* **1990**, *41*, 278-281.

(12) Hwang, S.Y.; Kong, A.C.F.; Schmidt, L.D. *J. Phys. Chem.* **1989**, *93*, 8327-8333.

(13) Walker, B.W.; Stair, P.C. *Surf. Sci.* **1981**, *103*, 315-337.

(14) Pearlstine, K.A.; Friend, C.M. *J. Am. Chem. Soc.* **1986**, *108*, 5842-5847.

(15) Baca, A.G.; Schulz, M.A.; Shirley, D.A. *J. Chem. Phys.* **1985**, *83*, 6001-6008.

(16) Chorkendorff, I.; Russell, Jr., J.N.; Yates, Jr., J.T. *J. Chem. Phys.* **1987**, *86*, 4692-4700.

(17) Schoofs, G. R.; Benziger, J. B. *J. Phys. Chem.* **1988**, *92*, 741-750.

(18) Thomas, P.A.; Masel, R.I. *J. Vac. Sci. Technol. A* **1987**, *5*, 1106-1108

(19) Thomas, G.E.; Weinberg, W.H. *Rev. Sci. Instrum.* **1979**, *50*, 497-501.

(20) Williams, E.D.; Weinberg, W.H. *Surf. Sci.* **1979**, *82*, 93-101.

(21) Redhead, P.A. *Vacuum,* **1962**, 203-211.

(22) Benndorf, C.; Madey, T.E. *Surf. Sci.* **1983**, *135,* 164-183.

(23) Parmeter, J.E.; Wang, Y.; Mullins, C.B.; Weinberg, W.H. *J. Chem. Phys.* **1988**, *88,* 5225-5236.

(24) Tsai, W.; Weinberg, W.H. *J. Phys. Chem.* **1987**, *91,* 5302-5307.

(25) Feulner, P; Pfnür, H.; Hofmann, P.; Menzel, D. *Surf. Sci.* **1987**, *184*, L411-L414.

(26) Sun, Y.-K.; Weinberg, W.H. *Surf. Sci.* **1989**, *214,* L246-L252.

(27) Gray, A.P.; Lord, R.C. *J. Chem. Phys.* **1957**, *26,* 690-705.

(28) Durig, J.R.; Bush, S.F.; Baglin, F.G. *J. Chem. Phys.* **1968**, *49,* 2106-2117.

(29) Hills, M.M.; Parmeter, J.E.; Mullins, C.B.; Weinberg, W.H. *J. Am. Chem. Soc.* **1986,** *108,* 3554-3562.

(30) Shimanouchi, T. *Tables of Molecular Vibrational Frequencies;* National Institute of Standards and Technology: Washington, DC, 1972; Consolidated Volume, NSRDS-NBS-39, p 74.

(31) Hiraishi, J. *Spectrochim. Acta, Part A* **1969**, *25A,* 749-760.

(32) (a) Adams, R.D.; Babin, J.E. *Organometallics* **1988**, *7,* 963-969. (b) Adams, R.D.; Babin, J.E.; Kim, H.-S. *Organometallics* **1987**, *6,* 749-754.

(33) (a) Adams, D.M. *Metal-Ligand and Related Vibrations;* Edward Arnold: London, 1967; p 309. (b) Powell, D.B.; Sheppard, N. *Spectrochim. Acta* **1961**, *17,* 68-76.

(34) Kordesch, M.E.; Stenzel, W.; Conrad, H. *Surf. Sci.* **1987**, *186,* 601-623.

(35) (a) Adams, R.D.; Babin, J.E.; Kim, H.-S; Tanner, J.T.; Wolfe, T.A. *J. Am. Chem. Soc.* **1990**, *112,* 3426-3435. (b) Adams, R.D.; Babin, J.E.; Kim, H.-S. *J. Am Chem. Soc.* **1987**, *109,* 1414-1424. (c) Adams, R.D.; Babin, J.E. *Organometallics* **1987**, *6,* 1364-1365. (d) Adams, R.D.; Babin, J.E.; Kim, H.-S. *Inorg. Chem.* **1986**, *25,* 4319-4320. (e) Adams, R.D.; Babin, J.E.; Kim. H.-S. *Organometallics* **1986**, *5,* 1924-1925.

(36) (a) *International Tables for X-ray Crystallography;* Kynoch Press: Birmingham, England, 1975; Vol. III, Table 4.2.4, p 276. (b) Pearson, R.; Lovas, F.J. *J. Chem. Phys.* **1977**, *66,* 4149-4156.

(37) Hamada, Y.; Hashiguchi, K.; Tsuboi, M. *J. Mol. Spectrosc.* **1984**, *105,* 70-80.

(38) Churchill, J.R.; DeBoer, B.G.; Rotella, F.J. *Inorg. Chem,* **1976**, *15,* 1843-1853.

(39) Adams, R.D.; Babin, J.E. *Organometallics* **1987**, *6*, 2236-2241.

(40) Ibach, H.; Mills, D.L. *Electron Energy Loss Spectroscopy and Surface Vibrations;* Academic: New York, 1982; pp 193-198.

(41) Wang, Y.; Weinberg, W.H. University of California, Santa Barbara, unpublished results.

(42) George, P.M.; Avery, N.R.; Weinberg, W. H.; Tebbe, F.N. *J. Am. Chem. Soc.* **1983**, *105*, 1393-1394.

(43) Parmeter, J.E.; Hills, M.M.; Weinberg, W.H. *J. Am. Chem. Soc.* **1986**, *108*, 3563-3569.

(44) Parmeter, J.E.; Schwalke, U.; Weinberg, W.H. *J. Am. Chem. Soc.* **1988**, *110*, 53-62.

(45) (a) Andrews, M.A.; Kaesz, H. D. *J. Am. Chem. Soc.* **1979**, *101*, 7238-7244. (b) Andrews, M.A.; van Buskirk, G.; Knobler, C.B.; Kaesz, H.D. *J. Am. Chem. Soc.* **1979**, *101*, 7245-7254.

(46) Yin, C.C.; Deeming, A.J. *J. Organomet. Chem.* **1977**, *133*, 123-138.

(47) Serafin, J.G.; Friend, C.M. *J. Phys. Chem.* **1988**, *92*, 6694-6700.

(48) Stevens, P.A.; Madix, R.J.; Friend, C.M. *Surf. Sci.* **1988**, *205*, 187-206.

(49) (a) Avery, N.R.; Matheson, T.W. *Surf. Sci.* **1984**, *143*, 110-124. (b) Avery, N.R.; Matheson, T.W.; Sexton, B. A. *Appl. Surf. Sci.* **1985**, *22/23*, 384-391.

(50) (a) Kordesch, M.E.; Stenzel, W.; Conrad H. *J. Electron Spectrosc. Relat. Phenom.* **1986**, *39*, 89-96. (b) Kordesch, M.E.; Stenzel, W.; Conrad, H. *Surf. Sci.* **1986**, *175*, L687-L692.

(51) (a) Kordesch, M.E.; Stenzel, W.; Conrad, H.; Weaver, M. *J. Am. Chem. Soc* **1987**, *109*, 1878-1879. (b) Kordesch M.E.; Feng, W.; Stenzel, W.; Weaver, M.; Conrad, H. *J. Electron Spectrosc. Relat. Phenom.* **1987**, *44*, 149-162. (c) Feng, W.; Stenzel, W.; Conrad, H.; Kordesch, M.E. *Surf. Sci.* **1989**, *211/212*, 1044-1052.

(52) Somers, J.; Kordesch, M. E.; Linder, Th.; Conrad, H.; Bradshaw, A. M.; Williams, G. P. *Surf. Sci.* **1987**, *188*, L693-L700.

(53) Weinberg, W.H.; Johnson, D.F.; Wang, Y.; Parmeter, J.E.; Hills, M.M. *Surf. Sci. Lett.* **1990**, *235*, L299-L302.

(54) Kemball, C.; Moss, R.C. *Proc. R. Soc. London A* **1957**, *238*, 107-116.

(55) Anderson, J.R.; Clark, N.J. *J. Catalysis* **1966**, *5*, 250-263.

(56) Meitzner, G.; Myktka, W.J.; Sinfelt, J.H. *J. Catalysis* **1986**, *98*, 513-521.

(57) Orita, H.; Naito, S.; Onishi, T.; Tamaru, K. *Bull. Chem. Soc. Jpn.* **1983**, *56*, 3390-3392.

(58) Sun, Y.-K.; Weinberg, W. H. *J. Chem. Phys.* **1991**, *94*, 4587-4599.

(59) (a) Connor, J.A.; Fischer, E.O. *J.Chem. Soc. A* **1969**, 578–584. (b) McCormick, F.B.; Angelici, R.J. *Inorg. Chem* **1981**, *20*, 1118-1123.

Table I. Vibrational Frequences (cm^{-1}) of 1st and 2nd layer methylamine and Spectroscopic reference data

Mode	2nd Layer	Sat'd 1st Layer, 200-220K			CH_3NH_2		CH_3ND_2		CD_3ND_2	
	140K	CH_3NH_2	CH_3ND_2	CD_3ND_2	Gas[a]	Solid[b]	Gas[a]	Solid[b]	Gas[a]	Solid[b]
$\nu_a(NH_2)$ or $\nu_a(ND_2)$	3240	3255			3427	3331	2556	2484	2556	2485
			2460	2450						
$\nu_s(NH_2)$ or $\nu_s(ND_2)$	3190	3200			3361	3260	2479	2443	2477	2445
$\nu_a(CH_3)$ or $\nu_a(CD_3)$					2985	2942	2985	2941	2238	2220
	2905	2920	2920	2200						
$\nu_a(CH_3)$ or $\nu_a(CD_3)$					2961	2887	2961	2863	2202	2190
$\nu_s(CH_3)$ or $\nu_s(CD_3)$	2840	2865	2895	2085	2820	2793	2817	2801	2073	2061
$\delta(NH_2)$ or $\delta(ND_2)$	1555	1560[c]	1210	n.r.	1623	1651	1234	1220	1227	1217
$\delta_a(CH_3)$ or $\delta_a(CD_3)$					1485	1492	1485	1470	1077	1121
	n.r.	n.r.	n.r.	n.r.						
$\delta_a(CH_3)$ or $\delta_a(CD_3)$					1473	1467	1468	1448	1065	1070
$\delta_s(CH_3)$ or $\delta_s(CD_3)$	1425	1425	1465	1055	1430	1441	1430	1421	1123	1050
$\tau(NH_2)$ or $\tau(ND_2)$	n.o	n.o.	n.o	n.o	1455	1353	1140	1130	1110	1070
$\omega_a(CH_3)$ or $\omega_a(CD_3)$					1195	1172	1187	1189	910	929
	1180	1190	1170	850						
$\omega_s(CH_3)$ or $\omega_s(CD_3)$					1130	1182	1117	1130	880	919

Table I. Vibrational Frequences (cm^{-1}) of 1st and 2nd layer methylamine and Spectroscopic reference data (continued)

Mode	2nd Layer	Sat'd 1st Layer, 200-220K			CH_3NH_2		CH_3ND_2		CD_3ND_2	
	140K	CH_3NH_2	CH_3ND_2	CD_3ND_2	Gas[a]	Solid[b]	Gas[a]	Solid[b]	Gas[a]	Solid[b]
ν(CN)	1000	1025[c]	995	975	1044	1048	997	1005	942	942
ω(NH_2) or ω(ND_2)	1000	980[c]	780	730	780	955	624	751	601	730
NH_2 or ND_2 torsion	n.o.	n.o.	n.o.	n.o.	264	498	229	360	201	365
ρ(NH_2) or ρ(ND_2)	775	780	n.o.	n.o						
R_{xy}	365									
ν(Ru–N)	n.r.	340	335[c]	n.r.						

(a) Ref. 27.
(b) Ref. 28.
(c) Resolved off-specular

n.r. = not resolved
n.o. = not observed

a = asymmetric
s = symmetric

Table II. Vibrational Frequencies (cm^{-1}) and Mode Assignments for side-on bonded methylene iminium, μ-η^2-H_2CNH_2, terminally bound secondary aminocarbene, η^1-(C)-$HCNH_2$, bridging aminocarbyne, μ-CNH_2, and ammonia, NH_3.[a]

Mode	Methylene iminium, 280-320K			Sec. Aminocarbene, 310-350K			Aminocarbyne, 310-360K		Ammonia, 310-370K	
	H_2CNH_2	H_2CND_2	D_2CND_2	$HCNH_2$	$HCND_2$	$DCND_2$	CNH_2	CND_2	NH_3	ND_3
$\nu_a(NH_2)$ or $\nu_a(ND_2)$	3340	2510	2510	3250	2450	2450	3250	2450		
$\nu_s(NH_2)$ or $\nu_s(ND_2)$	3300	2400	2450	3175	2325	2325	3175	2325		
$\nu_a(NH_3)$ or $\nu_a(ND_3)$									3250	2500
$\nu_s(NH_3)$ or $\nu_s(ND_3)$										
$\nu_a(CH_2)$ or $\nu_a(CD_2)$	2950	2950	2225							
$\nu_s(CH_2)$ or $\nu_s(CD_2)$	2900	2900	2150							
ν(CH) or ν(CD)				2920	2920	2200				
$\delta(NH_2)$ or $\delta(ND_2)$	1545	1260	1250	1545	1260	1250	1545	1260		
$\delta(CH_2)$ or $\delta(CD_2)$	1430[b]	1425	1100							
$\delta_s(NH_3)$ or $\delta_s(ND_3)$									1215	1000
δ(CH) or δ(CD)				740	740	550				
π(CH) or π(CD)				980	980	720				
$\omega(CH_2)$ or $\omega(CD_2)$	1190	1180	900							
$\omega(NH_2)$ or $\omega(ND_2)$	980[b]	810	800	740	550	550	740	550		

Table II. Vibrational Frequencies (cm^{-1}) and Mode Assignments for side-on bonded methylene iminium, μ–η^2–H_2CNH_2, terminally secondary bound aminocarbene, η^1–(C)–$HCNH_2$, bridging aminocarbyne, μ–CNH_2, and ammonia,NH_3.[a] (continued)

Mode	Methylene iminium, 280-320K			Sec. Aminocarbene, 310-350K			Aminocarbyne, 310-360K		Ammonia, 310-370K	
	H_2CNH_2	H_2CND_2	D_2CND_2	$HCNH_2$	$HCND_2$	$DCND_2$	CNH_2	CND_2	NH_3	ND_3
ν(CN)	1005	1000	1000	1420	1430	1430	1620	1620		
$\rho(NH_2)$ or $\rho(ND_2)$	790[c]	n.r.	n.r.	1050	750	750	1050	750		
$\rho(CH_2)$ or $\rho(CD_2)$	680[b]	n.r.	n.r.							
ν_a(Ru–CN)										
	555	540	540							
ν_s(Ru–CN)										
ν(Ru–C)				n.r.	n.r.	n.r.	n.r.	n.r.		
ν(Ru–N)									n.r.	n.r.

(a) Indicated temperatures in the column headings correspond to the ranges in which each intermediate populates the surface and influences the high resolution EEL spectra; refer to text and figures.
(b) Resolved off-specular
(c) Reproducibly observed in other HREEL spectra
n.r. = not resolved, a = asymmetric, s=symmetric

Table III. Vibrational frequencies (cm^{-1}) and Mode Assignments of triply bridging formimidoyl, μ_3–η^2–HCNH, bridging and terminally bound hydrogen isocyano, μ–CNH and η^1–(C)–CNH, and triply bridging cyano, μ_3–η^2–CN.[a]

Mode	Formimidoyl, 335-370K			Hydrogen Isocyano, 370-390K[b]		Cyano, 400-450K
	HCNH	HCND	DCND	μ–CNH	η^1–CNH	μ^3–η^2–CN
ν(NH) or ν(ND)	3250	2450	2450			
ν(CH) or ν(CD)	2920	2920	2200			
ν(CN)	1450	1450	1450	1660	2280	1670
π(NH) or π(ND)	1450	1220	1220	1450		
δ(NH) or δ(ND)	1240	1000	1000	1280	1060	
π(CH) or π(CD)	950	950	720			
δ(CH) or δ(CD)	770	770	550			
ν_a(Ru–CN)						465
ν_s(Ru–CN)						355
ν(Ru–C)				600	350	

(a) Indicated temperatures in the column headings correspond to the ranges in which each intermediate populates the surface and influences the high resolution EEL spectra; refer to text and figures.

(b) The first overtone of the strong symmetric stretch, ν(Ru-C), combines with the bending deformation, δ(NH), of the bridge-bonded μ –CNH adsorbate to yield a loss feature at 2450 cm^{-1} in Figs. 6b-d.

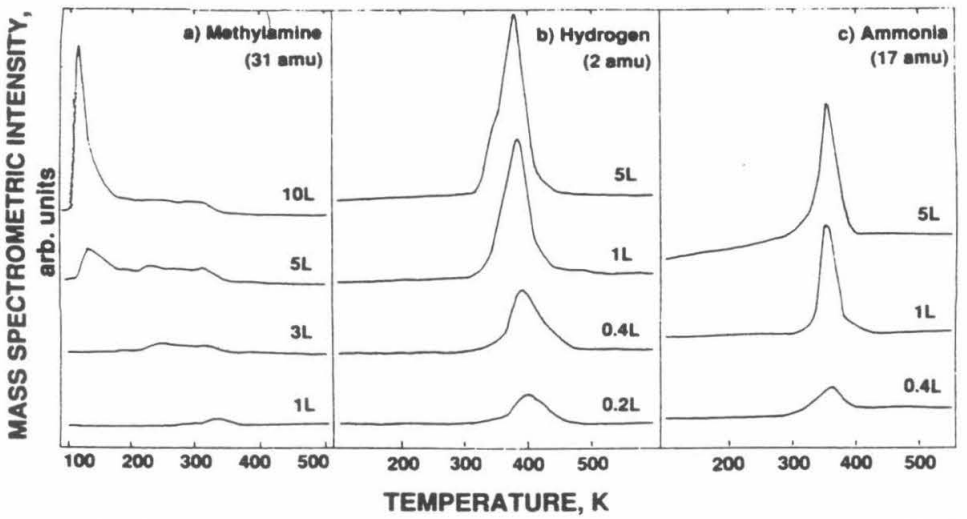

Figure 1. Thermal desorption mass spectra of (a) molecular methylamine, (b) hydrogen, and (c) ammonia following the indicated exposures of CH_3NH_2 on Ru(001) at 80 K and annealed with a heating rate, β, of $\sim$15 K s^{-1}.

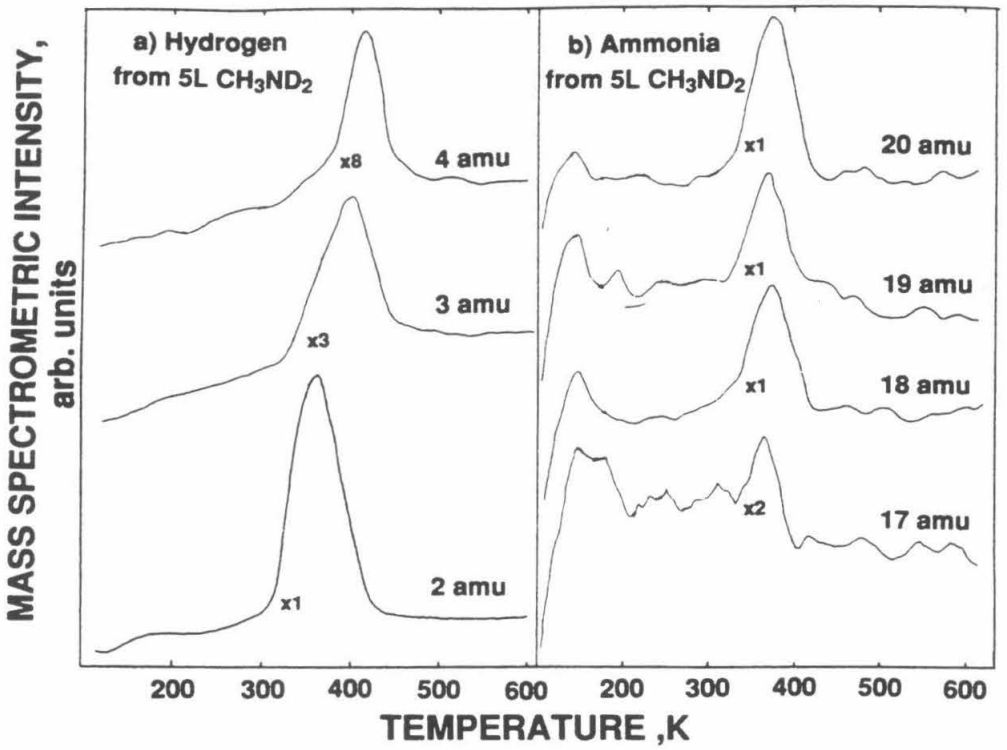

Figure 2. Thermal desorption mass spectra of (a) hydrogen and (b) ammonia following a 5-langmuir exposure of CH_3ND_2 on Ru(001) at 80 K and annealed with a heating rate, β, of $\sim$15 K s^{-1}.

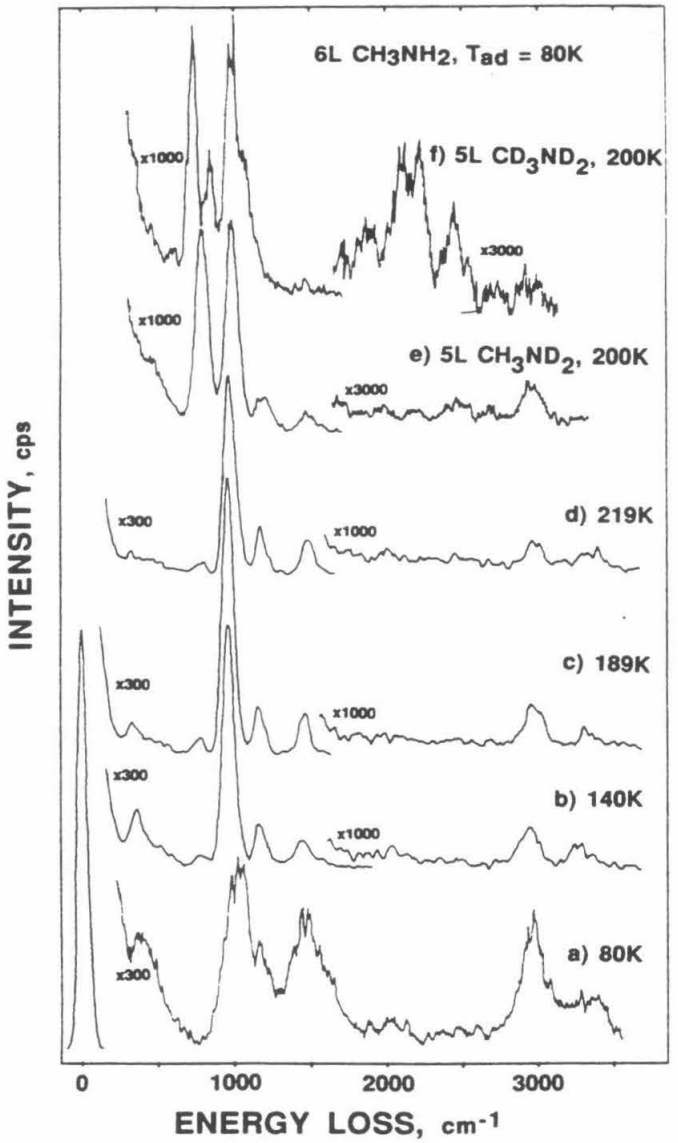

Figure 3. High-resolution EEL spectra resulting from saturation exposures of methylamine and its deuterated isotopes on the Ru(001) surface at 80 K and then annealed rapidly to the indicated temperatures: (a) 80 K, this spectrum is characteristic of partial multilayers of methylamine; (b) 140 K, this spectrum is characteristic of second-layer methylamine; (c) 189 K; (d) 219 K, this spectrum is characteristic of first-layer molecular methylamine; (e and f), 200 K, these spectra are characteristic of first-layer molecular CH_3ND_2 and CD_3ND_2, respectively. See text.

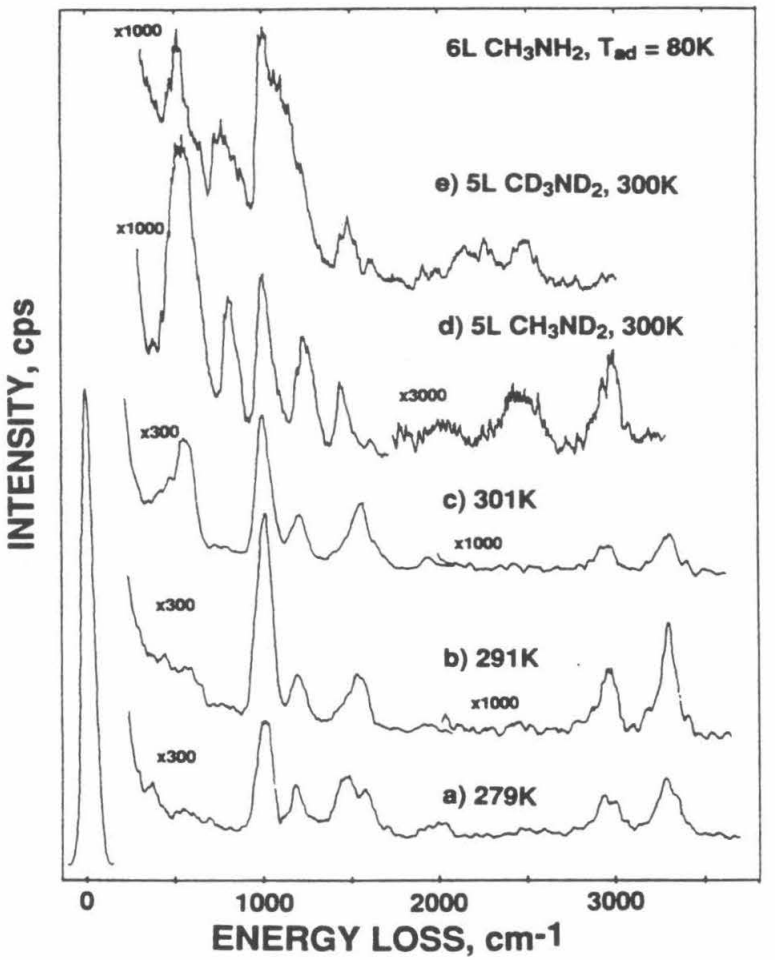

Figure 4. High-resolution EEL spectra resulting from saturation exposures of methylamine and its deuterated isotopes on the Ru(001) surface at 80 K and rapidly annealed to the indicated temperatures: (a and b) 279–291 K, these spectra illustrate the conversion of molecularly adsorbed methylamine to the bridging iminium intermediates; (c) 301 K, this spectrum is characteristic of μ-η^2-H_2CNH_2; (d and e) 300 K, these spectra are characteristic of the deuterated bridging iminium intermediates, μ-η^2-H_2CND_2 and μ-η^2-D_2CND_2, respectively. See text.

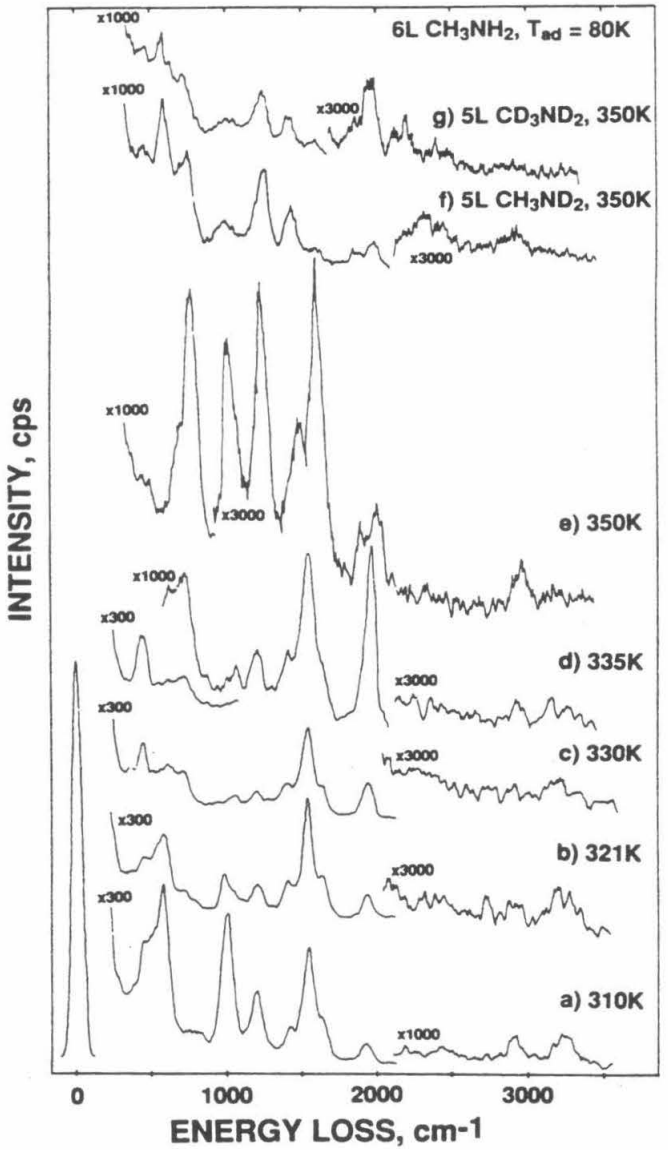

Figure 5. High-resolution EEL spectra resulting from saturation exp sures of methylamine and its deuterated isotopes on the Ru(001) surfa at 80 K and rapidly annealed to the indicated temperatures: (a and b 310–321 K, these spectra illustrate the conversion of bridging iminiu to the mixture of bridging aminocarbyne and secondary aminocarbe intermediates; (c) 330 K, this spectrum is characteristic of η^1-(C) $HCNH_2$ and μ-CNH_2; (d and e) 335–350 K, these spectra illustrate t conversion of secondary aminocarbene to formimidoyl; (f and g) 350 K these spectra are characteristic of mixtures of the deuterated isotopes the bridging carbyne, secondary aminocarbene, and formimidoyl inte mediates. See text.

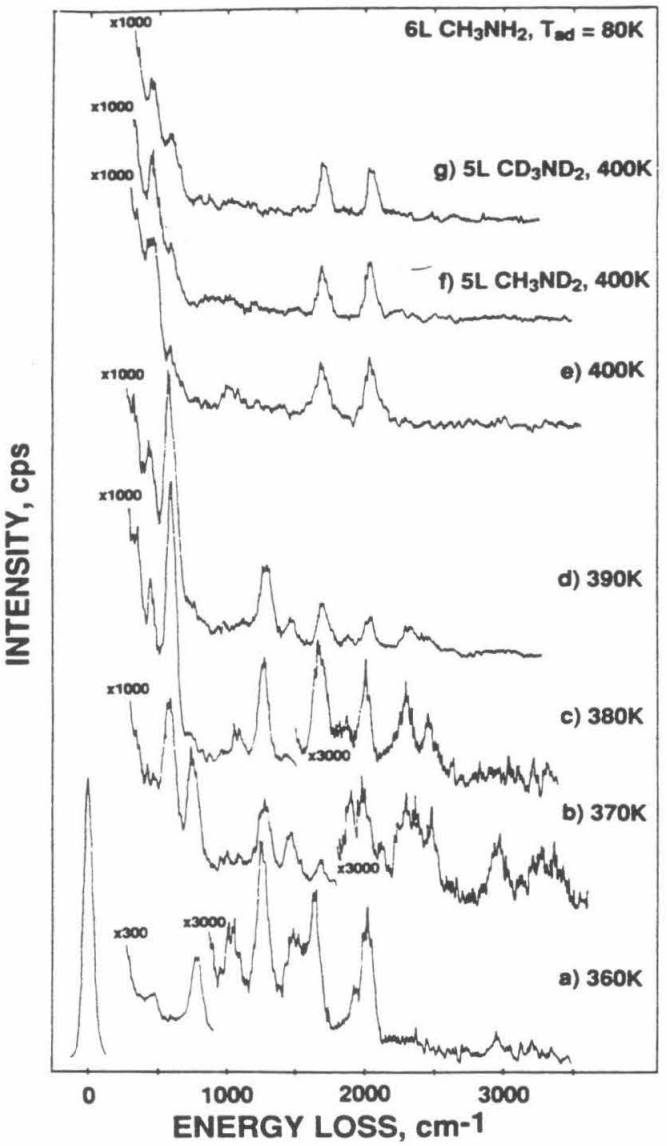

Figure 6. High-resolution EEL spectra resulting from saturation exposures of methylamine and its deuterated isotopes on the Ru(001) surface at 80 K and rapidly annealed to the indicated temperatures: (a) 360 K, this spectrum is characteristic of the mixture of μ-CNH_2 and μ_3-η^2-HCNH, (b and c) 370–380 K, these spectra illustrate the conversion of the overlayer present at 360 K to the mixture of terminally bound and bridge bound hydrogen isocyanide; (d) 390 K, this spectrum is characteristic of η^1-(C)-CNH and μ-CNH; (e–g) 400 K, these spectra are characteristic of μ_3-η^2-CN. See text.

CHAPTER 2

The Identification of μ_3–η^2-coordinated CN from the Dehydrogenation of Methylamine on the Ru(001) Surface

[The text of Chapter 2 consists of an article coauthored with W. H. Weinberg, Y. Wang, J. E. Parmeter, and M. M. Hills, which has appeared in *Surface Science Letters* **1990**, *235*, L299.]

Surface Science Letters

The identification of μ_3–η^2-coordinated CN from the dehydrogenation of methylamine on the Ru(001) surface

W.H. Weinberg, D.F. Johnson, Y.-Q. Wang

Department of Chemical Engineering, University of California, Santa Barbara, CA 93106, USA

J.E. Parmeter [1] and M.M. Hills [2]

Division of Chemistry and Chemical Engineering, California Institute of Technology, Pasadena, CA 91125, USA

Received 25 January 1990; accepted for publication 7 June 1990

Results of thermal desorption mass spectrometry and high-resolution electron energy loss spectroscopy (HREELS) indicate that the dehydrogenation of monomethylamine (CH_3NH_2) on the clean Ru(001) surface produces side-on bonded cyanide (CN) that engages in $\mu_3 - \eta^2$ coordination with the threefold site of the hexagonally closed packed surface, resulting in a bond order of two for the CN adsorbate.

Careful characterization of the bonding interactions of CN adsorbates with single crystalline surfaces is important for several reasons, of which three are delineated here. First, as an electrolyte in solution, the cyanide anion is observed to chemisorb on the surfaces of noble metal electrodes and to participate in oxidation/reduction reactions during cyclic voltammetry experiments [1–3]. Second the adsorption of cyanogen (C_2N_2) on single-crystalline surfaces has led to speculation that a two-dimensional surface polymer analogous to paracyanogen is responsible for the characteristic "β_1" and "β_2" C_2N_2 thermal desorption and semi-ordered LEED features observed for some platinum-group metals (vide infra). Third, and most important, a fundamental understanding of the selective activation of C–H, N–H and C–N bonds by transition metal surfaces must have as its foundation the results of careful decomposition studies of simple molecules containing these bonds.

The formation of CN on single crystalline surfaces has been observed from the decomposition of C_2N_2 on Pt(111) [4,5], Pt(110) [6,7], Pt(100) [8–10], Ag(110) [7], Cu(110) and oxygen-precovered Cu(110) [11], Cu(111) and oxygen-precovered Cu(111) [12], Rh(111) and oxygen-precovered Rh(111) [13], Ru(100) [14], Ni(111) [15], Pd(111) [16–18] and Pd(100) [17,19]; and from the dehydrogenation of CH_3NH_2 on Pt(111) [20] and Ni(111) [21]. There is tentative evidence that the adsorbed CN coordinates through both the carbon and nitrogen on a number of these clean surfaces. X-ray photoelectron spectroscopic (XPS) studies of C_2N_2 on Ru(100) show that upon annealing above 250 K, the N(1s) level shifts from 401.3 to 397.6 eV, indicative of a strong interaction between the nitrogen atom and the surface. Similarly, the absence of either an UV-photoemission feature or an electronic transition in EELS in the region near 5 eV, which is characteristic of metal–ligand charge transfer in terminally-coordinated platinum cyanide complexes [22], has led Wille et al. [8] and Conrad et al. [9], in independent studies of C_2N_2 on Pt(100), to conclude that adsorbed CN must involve significant interaction of the nitrogen atom with the surface.

[1] Current address: Chemistry Department, Texas A&M University, College Station, TX 77843-3255, USA.

[2] Current address: Aerospace Corp., P.O. Box 92957, Los Angeles, CA 90009, USA.

Other than the study reported here, the only other HREELS experiments conducted with CN on single crystalline surfaces are for Pd(111) and Pd(100) [17], and Cu(111) and oxygen-precovered Cu(111) [23]. Both Pd(111) and Pd(100) yield the same HREELS loss features associated with CN: 280 cm^{-1} for ν(Pd–CN) and 1895 cm^{-1} for ν(CN) stretching modes. The CN was interpreted by these authors as lying parallel to the surface with a $\sigma + \pi$ bonding interaction arising from metal to 5σ donation with some 1π to metal donation, partially counterbalancing the metal to adsorbate charge transfer. A near edge X-ray absorption fine structure (NEXAFS) study of CN on Pd(111) [18] suggested that the CN bond axis is tilted 14° above the plane of the surface. The authors prefer a parallel bonding orientation and state that "some other source of error associated with the NEXAFS experiment itself is responsible for the small deviation". The HREELS loss features of the ν(CN) stretching mode on Cu(111) and oxygen-precovered Cu(111) are at 2045 and 2140 cm^{-1}, respectively [23]. The authors interpret these results as the CN being oriented in a parallel $\sigma + \pi$ bonding configuration on the clean surface, but that in the presence of oxygen it reorientates to a terminal coordination through the carbon atom. This reorientation is purportedly driven by a competition for the available charge that the copper surface is able to transfer and an assumption that the 5σ orbital of CN is better able to withdraw electron density when directed at a copper surface atom. In our view, this interpretation for cyanide adsorbed on Cu(111) and oxygen-precovered Cu(111) is not credible. We believe that on both surfaces the cyanide adsorbs terminally via lone-pair donation to the metal surface from the 5σ orbital of the carbon atom. The ν(CN) stretching mode is at a higher frequency in the presence of the oxygen overlayer because the more highly electronegative oxygen adatoms withdraw electron density from the copper surface, thereby reducing the amount of charge which would otherwise be backdonated into the antibonding π^* orbitals of CN. The blue-shift of 95 cm^{-1} for the oxygen-precovered Cu(111) versus the clean Cu(111) surface is understood easily in light of these simple principles.

There are several organometallic complexes that exhibit $\sigma + \pi$ bonding interactions for bridging ligands containing CN triple bonds. Acetonitrile, CH_3CN, coordinates in a μ_3–η^2 fashion to the threefold site of $Fe_3(CH_3CN)(CO)_9$ with ν(CN) = 1610 cm^{-1} [24]. The *p*-tolylisonitrile ligand bridges the dimanganese complex (μ–*p*-$CH_3C_6H_5NC$)-$Mn_2(dppm)_2(CO)_4$, in a μ_2–η^2 fashion with ν(CN) = 1661 cm^{-1} [25a,25b]. Three isonitriles coordinate in a similar manner in the dimolybdenum complex $Cp_2Mo_2(CO)_4(\mu_2$–η^2-CNR) with ν(CN) = 1725 cm^{-1} for R = CH_3, 1666 cm^{-1} for R = phenyl, and 1690 cm^{-1} for R = *t*-butyl [26]. In $Ni_4[CNC(CH_3)_3]_7$, bridging isonitriles coordinate either across the edges or the faces of the tetrahedron generated by the four nickel atoms, yielding values of ν(CN) between 1605 and 1610 cm^{-1} [27].

Within organometallic clusters, bridging CN ligands are most often found to be di-σ bonded in a linear fashion between two metal atoms [28a–28c]. The corresponding values of ν(CN) range from approximately 2000 to 2150 cm^{-1}, indicating that the CN triple bond is retained. One exception, however, is the μ_2–η^2-CN ligand observed in the cationic di-rhodium complex $[Rh_2(\mu_2$–CN)(μ–CO)$(CO)_2(\mu$–dppm$)_2]^+$ in which ν(CN) = 2044 cm^{-1}, and X-ray crystallographic measurements show the CN to be inclined 55° above the plane containing the rhodium atoms and dppm ligands [29]. For comparison to these ν(CN) stretching frequencies, those of CH_3NC and methylene imine, H_2CNH, are 2166 and 1638 cm^{-1}, respectively [30,31].

Thermal desorption and HREELS experiments for the decomposition of CH_3NH_2 and its deuterated isotopes CH_3ND_2 and CD_2ND_2 [32] were conducted in two ultrahigh vacuum systems described elsewhere [33a,33b]. A combination of thermal desorption and Auger spectra shows that the decomposition products arising from a saturation coverage of CH_3NH_2 adsorbed on Ru(001) at 80 K are H_2, N_2, NH_3 and surface carbon. In particular, neither HCN nor C_2N_2 are observed. The HREELS measurements indicate that below 270 K molecular CH_3NH_2 adsorbs via electron lone pair donation from the nitrogen atom. The isolation and identification of adsorbed CH_2NH_2

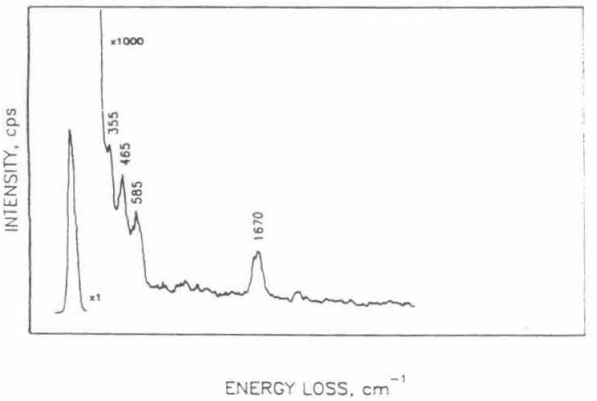

Fig. 1. High-resolution electron energy loss spectrum after adsorption of methylamine on the Ru(001) surface at 80 K, followed by annealing to 425 K. The modes at 1670, 465 and 355 cm^{-1} are due to ν(CN), ν_a(Ru–CN) and ν_s(Ru–CN) of adsorbed cyanide; and the peak at 585 cm^{-1} is due to the overlapping ν(RuC) and ν(RuN) modes.

and $CHNH_2$ are achieved after annealing to approximately 290 and 320 K, respectively. Competing reaction pathways open between 330 and 360 K leading to the formation of both NH_3 and further dehydrogenated adsorbates retaining C–N bonds. Thermal desorption measurements indicate that essentially all of the hydrogen-containing reaction products — H_2 and NH_3 — have desorbed by 425 K.

All three isotopes of methylamine produce identical EELS spectra after annealing to 425 K, and that of CH_3NH_2 is shown in fig. 1. There are four peaks observed at 355, 465, 585 and 1670 cm^{-1}. The 585 cm^{-1} peak increases in intensity after annealing to 500–550 K, and by 600 K, it is the only feature remaining. Between 800 and 1000 K, where recombinative desorption occurs, its intensity decreases but does not disappear entirely; hence, it is assigned to the overlapping ν(Ru–N) and ν(Ru–C) stretching modes. The remaining three peaks can only be attributed to a side-on bonded CN species. The 1670 cm^{-1} peak is assigned to the ν(CN) stretching mode, and the 355 and 465 cm^{-1} peaks are the symmetric and asymmetric ν(Ru–CN) stretching modes. Note that the CN bond is cleaved irreversibly on the Ru(001) surface at temperatures between 500 and 600 K.

The frequency of the CN stretching mode at 1670 cm^{-1} is typical of a CN adspecies with a bond order of two. Based on the observed value of ν(CN), X-ray crystallographic measurements of analogous organometallic complexes, and the electron-donating nature of the CN adsorbate, we think it is most plausible to describe the bonding as a $\sigma + 2\pi$ interaction resulting from μ_3–η^2 coordination of CN in a threefold surface site. In this picture, the carbon atom is σ-bonded to one ruthenium atom with the CN bond axis inclined across the center of the site. In this manner, the valence d-orbitals of the surface ruthenium atoms can overlap with both of the π systems of the CN triple bond, thereby allowing donation from the π systems and/or backdonation from the ruthenium surface atoms to the π^* antibonding orbitals.

In summary, we have characterized the side-on bonded CN adsorbate on Ru(001) which stands in sharp contrast to similar species on clean Pd(111) and Pd(100) surfaces. At first glance it might be thought that the bonding and catalytic behavior would be nearly the same in each case since each CN is described by similar $\sigma + \pi$ interactions. However, unlike the other surfaces where the CN adspecies is believed to exist as $CN^{\delta-}$ with δ approaching unity, strong electron donation to the ruthenium surface from the π systems of the CN adsorbate reduce significantly its bond order from three to two. This interaction and the concomitant d–π rehybridization explains the observed propensity of ruthenium surfaces toward activating the cleavage of the formidable CN triple bond.

This research was supported by the National Science Foundation under Grant number CHE-8617826. Additional support was provided by the Donors of the Petroleum Research Fund (Grant No. PRF 19819-AC5-C).

References

[1] R.E. Benner, K.U. von Raben, R. Dornhaus, R.K. Chang, B.L. Laube and F.A. Otter, Surf. Sci. 102 (1981) 7.
[2] R.E. Benner, R. Dornhaus, R.K. Chang and B.L. Laube, Surf. Sci. 101 (1980) 341.
[3] K. Kunimatsu, H. Seki, W.G. Golden, J.G. Gordon II and M.R. Philpott, Surf. Sci. 158 (1985) 596.

[4] J.R. Kingsley, D. Dahlgren and J.C. Hemminger, Surf. Sci. 139 (1984) 417.
[5] W. Hoffmann, E. Bertel and F.P. Netzer, J. Catal. 60 (1979) 316.
[6] M.E. Bridge and R.M. Lambert, Surf. Sci. 63 (1977) 315.
[7] M.E. Bridge, R.A. Marbrow and R.M. Lambert, Surf. Sci. 57 (1976) 415.
[8] R.A. Wille, F.P. Netzer and J.A.D. Matthews, Surf. Sci. 68 (1977) 259.
[9] H. Conrad, J. Küppers, F. Nitschke and F.P. Netzer, Chem. Phys. Lett. 46 (1977) 571.
[10] F.P. Netzer, Surf. Sci. 61 (1976) 343.
[11] D.A. Outka, S.W. Jorgensen, C.M. Friend and R.J. Madix, J. Mol. Catal. 21 (1983) 375.
[12] F. Solymosi and J. Kiss, Surf. Sci. 108 (1981) 368.
[13] F. Solymosi and L. Bugyi, Surf. Sci. 147 (1984) 685.
[14] N.J. Gudde and R.M. Lambert, Surf. Sci. 124 (1983) 372.
[15] J.C. Hemminger, E.L. Muetterties and G.A. Somorjai, J. Am. Chem. Soc. 101 (1979) 62.
[16] M.E. Kordesch, W. Stenzel and H. Conrad, J. Electron. Spectrosc. Relat. Phenom. 39 (1986) 89.
[17] M.E. Kordesch, W. Stenzel and H. Conrad, Surf. Sci. 186 (1987) 601.
[18] J. Somers, M.E. Kordesch, Th. Linder, H. Conrad, A.M. Bradshaw and G.P. Williams, Surf. Sci. 188 (1987) L693.
[19] K. Besenthal, G. Chiarello, M.E. Kordesch and H. Conrad, Surf. Sci. 178 (1986) 667.
[20] S.Y. Hwang, E.G. Seebauer and L.D. Schmidt, Surf. Sci. 188 (1987) 219.
[21] I. Chorkendorff, J.N. Russell, Jr. and J.T. Yates, Jr., J. Chem. Phys. 86 (1987) 4692.
[22] J.J. Alexander and H.B. Gray, J. Am. Chem. Soc. 90 (1968) 4260.
[23] M.E. Kordesch, W. Stenzel, H. Conrad and M.J. Weaver, J. Am. Chem. Soc. 109 (1987) 1878.
[24] M.A. Andrews and H.D. Kaesz, J. Am. Chem. Soc. 101 (1979) 7255.
[25] (a) A.L. Balch and L.S. Benner, J. Organomet. Chem. 135 (1977) 339;
(b) L.S. Benner, M.M. Olmstead and A.L. Balch, J. Organomet. Chem. 159 (1978) 289.
[26] R.D. Adams, D.A. Katahira and L.-W. Yang, Organometallics 1 (1982) 231.
[27] V.W. Day, R.O. Day, J.S. Kristoff, F.J. Hirsekorn and E.L. Muetterties, J. Am. Chem. Soc. 97 (1975) 2571.
[28] (a) G.A. Carriedo, M.C. Crespo, V. Riera, M.L. Valin, D. Moreiras and X. Solans, Inorg. Chim. Acta 121 (1986) 191;
(b) H.M. Dawes, M.B. Hursthouse, A.A. del Paggio, E.L. Muetterties and A.W. Parkins, Polyhedron 4 (1985) 379;
(c) J.K. Ruff, Inorg. Chem. 8 (1969) 86.
[29] S.P. Deraniyagala and K.P. Grundy, Inorg. Chim. Acta 84 (1984) 205.
[30] Y. Hase and O. Sala, An. Acad. Bras. Cienc. 45 (1973) 381.
[31] Y. Hamada, K. Hasiguchi and M. Tsuboi, J. Mol. Spectrosc. 105 (1984) 70.
[32] D.F. Johnson, J.E. Parmeter, M.M. Hills, Y.-Q. Wang and W.H. Weinberg, in preparation.
[33] (a) E.D. Williams and W.H. Weinberg, Surf. Sci. 82 (1979) 93;
(b) G.E. Thomas and W.H. Weinberg, Rev. Sci. Instrum. 50 (1979) 497.

CHAPTER 3

Quantification of the Influence of Surface Structure on C-H Bond Activation by Iridium and Platinum

[The text of Chapter 3 consists of an article coauthored with W. H. Weinberg, which has appeared in *Science* **1993**, *261*, 76.]

Abstract. The trapping-mediated dissociative chemisorption of ethane on the closest-packed Ir(111) surface has been investigated, and the activation energy and preexponential factor of the surface reaction rate coefficient have been measured. These results are compared to those of ethane activation on Pt(111), and on the missing-row reconstructed Ir(110)-(1x2) and Pt(110)-(1x2) surfaces, allowing a quantitative determination of the effect surface structure has on the catalytic activation of C-H bonds. In the order Pt(111), Pt(110)-(1x2), Ir(111) and Ir(110)-(1x2), the activation energies for ethane dissociative chemisorption are 16.6, 10.5, 10.3 and 5.5 kilocalories per mole, demonstrating that the electronic and geometric effects are of approximately equal importance for ethane activation on these catalysts.

The catalytic reforming of petroleum naphtha fractions by supported bimetallic platinum and iridium catalysts is a process of great commercial importance in the fuels industry. The objective of reforming is the selective conversion of saturated hydrocarbons into high-octane aromatic components for gasoline. The overall yield of the process, however, is hampered by the competing hydrogenolysis of the feed stream hydrocarbon reactants (*1*). Also of importance in this industry is the catalytic conversion of C_1 to C_4 alkanes in natural gas into value-added fuel and feed stock chemicals (*2*). The common technological challenge relevant to these processes is the activation of the strong alkane C-H bonds: 105 kcal/mol for methane, 98 kcal/mol for primary bonds, 95 kcal/mol for secondary bonds, and 93 kcal/mol for tertiary bonds (*3*).

On supported catalysts, the metallic component is dispersed as small, 10 to 100 Å, particles on high surface area substrates of alumina or silica, for example, in which a large fraction of the metal atoms may be

considered as surface atoms (*1, 4*). The distinct micro-structures of these crystallites induce steric and electronic differences among the catalytic sites, with those on the faceted surfaces having relatively lower reactivities than those at the edges and defects. In an effort to go beyond this qualitative description, we have undertaken a quantitative determination of the effect surface structure has on C-H bond activation.

Platinum and iridium both form face-centered cubic lattice structures, and the four surfaces of interest in this report are Pt(111), Ir(111), Pt(110)-(1x2), and Ir(110)-(1x2). The (111) surfaces are the most stable, closest-packed arrangements of surface metal atoms, while the (110) surfaces reconstruct into a (1x2) surface unit cell, often referred to as the "missing row" structure (*5*). A measure of the structure sensitivity of these four surfaces toward alkane activation is found in the results of ultrahigh vacuum (UHV) thermal desorption and low-energy electron diffraction studies (*6-8*). The threshold temperatures for the thermal activation of alkane C-H bonds was found to be 130 K for Ir(110)-(1x2) and 200 K for Pt(110)-(1x2). Under these UHV conditions, Ir(110)-(1x2) activates all alkanes except methane, Pt(110)-(1x2) activates only C_4 and higher alkanes, and Ir(111) and Pt(111) fail to activate saturated hydrocarbons up to C_7 and C_8, respectively.

Our understanding of the influence of surface geometric and electronic structure on catalysis has been extended considerably by recent studies of the apparent kinetic parameters of C-H bond activation on these four surfaces (*9-11*). We report here the results of experiments concerning the activation of ^{13}C-labeled ethane on Ir(111) which, when combined with recent studies of this reaction on Pt(111), Pt(110)-(1x2), and Ir(110)-(1x2) quantify the very significant influence exerted by surface structure on C-H

bond activation. As would be expected, the initial step in the activation of ethane is C-H (and not C-C) bond cleavage since a deuterium kinetic isotope effect was observed on all four surfaces.

The measurements on the Ir(111) surface were carried out in a 200 liter per second ion-pumped UHV microreactor which has a base pressure of 2×10^{-10} torr and a volume of 10 cm^3 (*10, 12*). For the dissociative chemisorption of ethane over the surface temperature range that was employed ($450 < T_S < 1200$ K), the system was operated in a continuous flow mode. With the crystal held at a constant temperature, an ethane pressure of 1.0×10^{-7} torr was maintained for a reaction time, τ. The gas temperature, T_g, was always equal to the wall temperature ($\sim$ 300 K) because the mean-free path of ethane at this pressure was much greater than the dimensions of the microreactor. The amount of dissociated ethane was determined by titrating the carbonaceous residue on the surface after reaction with excess oxygen, producing exclusively ^{13}C-labeled CO_2 (*13*). By counting mass spectrometrically the amount of $^{13}CO_2$ that was produced, we obtained the total number of ^{13}C-adatoms on the surface, N_C. The reaction conditions and times were such that the fractional coverage of ^{13}C-adatoms was between 5 and 10% of a monolayer of carbidic carbon. The lower limit ensures that the results are not dominated by reactivity at surface defects (*14*), whereas the upper limit ensures that the initial rate of the C-H activation reaction has been measured, that is, the rate is approximately characteristic of a clean Ir(111) surface. This enhanced reactivity at steps and defect sites on the surface that we have observed (*14*) verifies that we are actually measuring the (low) reactivity of ethane and not the (high) reactivity of a contaminant hydrocarbon present in the

vacuum chamber in low concentrations. At a given surface temperature, T_S, the probability of dissociative chemisorption, $P_r(T_S)$, is obtained from:

$$P_r(T_S) = \frac{N_c}{2A\tau F} \tag{1}$$

where A is the sample surface area, F is the impingement flux of reactant molecules, and the stoichiometric factor of 2 converts N_c into the number of dissociated ethane molecules.

The study of alkane activation by single-crystalline transition metal surfaces reveals that two fundamentally different reaction mechanisms may be operative: (i) direct dissociation (*11, 15*) and (ii) trapping-mediated, dissociative chemisorption (*16, 17*). Direct dissociation occurs on the time scale of a collision between the gas-phase molecule and the surface ($<10^{-12}$ s), and the rate of this reaction depends primarily on the translational and internal energies of the gas-phase molecule. In trapping-mediated, dissociative chemisorption, the gas-phase molecule is trapped in the potential field of the surface (that is, it is adsorbed molecularly in the case of ethane), and it accommodates to the temperature of the surface. The physically adsorbed molecule may then either desorb with a rate coefficient k_d or it may react (dissociate) with a rate coefficient k_r. The relative rates of these competing reactions are dependent on the surface temperature, provided the associated activation energies of desorption, E_d, and reaction, E_r, are not equal. The gas temperature is important only insofar as it affects the probability of trapping into the physically adsorbed state.

For the dissociative chemisorption of physically adsorbed ethane, the initial C-H bond cleavage is rate limiting (*6, 7, 18*). The resulting

chemisorbed ethyl undergoes further dehydrogenation and ultimately C-C bond cleavage at elevated surface temperatures. This reaction sequence may be written as:

$$C_2H_{6(g)} \underset{k_d}{\overset{\xi F}{\rightleftarrows}} C_2H_{6(p)} \xrightarrow{k_r} C_2H_{5(c)} + H_{(c)} \longrightarrow 2C_{(c)} + 3H_{2(g)},$$

where ξ is the trapping probability of ethane into the physically adsorbed well, g, p, and c denote gaseous, physically adsorbed and chemisorbed states, respectively, and k_d and k_r are the elementary rate coefficients for desorption and reaction and are of the Polanyi-Wigner form, namely:

$$k_i = k_i^{(0)} e^{-E_i/k_B T_s}. \tag{2}$$

If the surface temperature is sufficiently high that the fractional coverage of the physically adsorbed ethane is negligibly small, as is the case for the experiments reported here, then a pseudo-steady-state analysis yields the following expression for the probability of ethane activation, which is the ratio of the reaction rate to the impingment rate (*17*):

$$P_r = \frac{\xi k_r}{k_d + k_r} \tag{3}$$

In general, Eq. 3 implies that

$$\frac{\xi}{P_r} - 1 = \frac{k_d}{k_r} \tag{4}$$

and for the special case of $k_r << k_d$, both Eqs. 3 and 4 reduce to:

$$\frac{P_r}{\xi} = \frac{k_r}{k_d} \tag{5}$$

For ethane activation on Ir(111), we have found experimentally that $k_r << k_d$, and, consequently, a semilogarithmic plot of P_r as a function of reciprocal surface temperature yields the apparent kinetic parameters of the elementary C-H bond scission reaction. Figure 1 is such an Arrhenius plot for the dissociative chemisorption of C_2H_6 on Ir(111). Combining Eqs. 2 and 5 yields:

$$\frac{P_r}{\xi} = \frac{k_r^{(0)}}{k_d^{(0)}} e^{-(E_r - E_d)/k_B T_s} \tag{6}$$

from which it is apparent that the slope of the straight line in Fig. 1 is equal to $-(E_r - E_d)/k_B$, and the intercept is equal to $k_r^{(0)}/k_d^{(0)}$.

As on Ir(111), ethane activation on Pt(111) and Pt(110)-(1x2) proceeds with $k_r << k_d$, and the apparent kinetic parameters are obtained just as described above (*9, 10*). On Ir(110)-(1x2), however, the special case of $k_r << k_d$ is inapplicable, and the semilogarithmic plot of the quantity $\xi/P_r - 1$ as a function of reciprocal temperature must be used (*11*). By combining Eqs. 2 and 4, one concludes that the slope of this semilog plot is equal to $-(E_d - E_r)/k_B$, and the intercept is equal to $k_d^{(0)}/k_r^{(0)}$. Together, the linearity of these constructions and the observed variation of the reaction rate with surface temperature (at a constant gas temperature) confirm that the surface reaction obeys a trapping-mediated mechanism. In constructing Fig. 1 [as well as those in (*9-11*)], it was recognized that the trapping probability is

only a weak function of surface temperature (*19*), and it was reasonably assumed that the trapping probability is unity for a Maxwell-Boltzmann energy distribution of ethane at 300 K (*16*).

Table 1 provides the energy differences, $E_r - E_d$, and the ratios of preexponential factors, $k_d^{(0)}/k_r^{(0)}$, for the activation of C_2H_6 on all four surfaces. For the atomically flat surfaces of both metals and for the corrugated Pt surface, it should be noted that $E_r - E_d > 0$, implying that for each of these systems there is an activation barrier with respect to the gas-phase energy zero. For the corrugated Ir surface, however, $E_r - E_d < 0$, and this reactive system is unactivated with respect to this gas-phase zero. It is noteworthy that $k_d^{(0)}/k_r^{(0)} > 1$ for all four systems, as would be expected in view of the greater entropy associated with the transition state for desorption relative to the transition state for C-H bond cleavage (*18*). Because the activation energy and preexponential factor for desorption of physically adsorbed ethane are approximately 7.7 kcal/mol and 10^{13} s^{-1}, respectively (*7*), the activation energies, E_r, and preexponential factors, $k_r^{(0)}$, for dissociative chemisorption may be evaluated easily, and are also listed in Table 1.

From these results, the electronic and geometric effects on C-H bond activation of these four surfaces of Pt and Ir can be discussed quantitatively. The activation energies given in Table 1 provide the magnitudes by which the Ir surfaces of a given geometry are more active than the corresponding Pt surfaces, and by which the corrugated (110) surfaces of each metal are more reactive than their atomically flat (111) counterparts. The activation energy on iridium is, by comparing samples of the same crystallographic orientation, 5.0 to 6.3 kcal/mol lower than the case of platinum. For each metal, the corrugated (110)-(1x2) surfaces have activation energies that are

4.8 to 6.1 kcal/mol lower than the close-packed (111) surfaces. Consequently, the Pt(110)-(1x2) and Ir(111) surfaces have approximately equal activity toward ethane activation, demonstrating that the difference in geometric structure compensates for the intrinsic electronic difference between the two metals. It is known from photoemission and x-ray absorption studies that changes in surface structure induce subtle, and yet significant, changes in the electronic structure of the catalyst surface (*20*). Hence, at the core of the structure sensitivity issue is the profound influence microscopic surface geometry has on surface electronic structure, and the continued study of this important effect is of great interest in the heterogeneous activation of saturated hydrocarbons.

References and Notes

1. J. H. Sinfelt, *Bimetallic Catalysts: Discoveries, Concepts and Applications* (Wiley, New York, 1983), pp. 130-157.

2. A. E. Shilov, *Activation of Saturated Hydrocarbons by Transition Metal Complexes* (Reidel, Dordrecht, 1984); R. H. Crabtree, *Chem. Rev.* **85**, 245 (1985); B. Meunier and B. Chaudret, Eds., *Perspectives in the Selective Activation of C-H and C-C Bonds in Saturated Hydrocarbons*, vol. CXXX of the *NATO ASI Series* (Reidel, Dordrecht, 1987).

3. D. F. McMillen and D. M. Golden, *Annu. Rev. Phys. Chem.* **33**, 493 (1982).

4. J. C. Rasser, *Platinum-Iridium Reforming Catalysts* (Delft Univ. Press, Delft, 1977), pp. 156-193.

5. M. A. Van Hove, W. H. Weinberg, C.-M. Chan, *Low-Energy Electron Diffraction: Experiment, Theory and Surface Structure Determination* (Springer-Verlag, Heidelberg, 1986), pp. 265-272.

6. T. S. Wittrig, P. D. Szuromi, W. H. Weinberg, *J. Chem. Phys.* **76**, 3305 (1982); P. D. Szuromi, J. R. Engstrom, W. H. Weinberg, *J. Chem. Phys.* **80**, 508 (1984).

7. P. D. Szuromi, J. R. Engstrom, W. H. Weinberg, *J. Phys. Chem.* **89**, 2497 (1985).

8. L. E. Firment and G. A. Somorjai, *J. Chem. Phys.* **66**, 2901 (1977).

9. J. A. Rodriquez and D. W. Goodman, *J. Phys. Chem.* **94**, 5342 (1990).

10. Y.-K. Sun and W. H. Weinberg, *J. Vac. Sci. Technol. A* **8**, 2445 (1990).

11. C. B. Mullins and W. H. Weinberg, *J. Chem. Phys.* **92**, 4508 (1990).

12. J. J. Vajo, W. Tsai, W. H. Weinberg, *Rev. Sci. Instrum.* **56**, 1439 (1985). The Ir(111) crystal was cut, polished, and prepared with standard techniques. The crystal surface was cleaned between experiments by heating to 1000 K for 5 min in 5 x 10^{-8} torr of O_2 flowing through the microreactor, followed by annealing to 1625 K for one minute to desorb the surface oxygen. Thermal desorption spectra of CO, which were in complete agreement with previously published ones from the clean Ir(111) surface [C. M. Comrie and W. H. Weinberg, *J. Chem. Phys.* **64**, 250 (1976)], were measured frequently to verify the cleanliness of the surface. Furthermore, since kinetic data are known to be extremely sensitive to surface conditions, the high degree of reproducibility of the data presented here indicates the absence of surface contamination. The ^{13}C-labeled ethane (1,2-di-^{13}C-C_2H_6, 99 atom % ^{13}C) was obtained from Icon Services and was introduced into the microreactor from a gas handling manifold that was pumped by a diffusion pump to a base pressure below 10^{-7} torr.

13. Under these experimental conditions the dissociative chemisorption of ethane is irreversible, and no gas-phase carbon-containing products of a surface self-hydrogenolysis reaction are formed. The titration conditions and procedure were selected to ensure the complete oxidation of the surface carbon to $^{13}CO_2$.

14. The measurements of ethane activation at defect sites on our Ir(111) sample have been done separately and will be reported elsewhere [D. F. Johnson and W. H. Weinberg, in preparation].

15. C. T. Rettner, H. E. Pfnür, D. J. Auerbach, *Phys. Rev. Lett.* **54**, 2716 (1985); A. C. Luntz and D. S. Bethune, *J. Chem. Phys.* **90**, 1274 (1989); M. B. Lee, Q. Y. Yang, S. T. Ceyer, *ibid.* **87**, 2724 (1987).

16. W. H. Weinberg, in *Dynamics of Gas-Surface Collisions*, C. T. Rettner and M. N. R. Ashfold, Eds. (Royal Society of Chemistry, Cambridge, 1991), pp. 171-220; G. Ehrlich, in *Chemistry and Physics of Solid*

Surfaces VII, R. Vanselow and R. F. Howe, Eds., (Springer-Verlag, Heidelberg, 1989), pp. 1-64.

17. W. H. Weinberg, in *Kinetics of Interface Reactions*, H. J. Kreuzer and M. Grunze, Eds. (Springer-Verlag, Heidelberg, 1987), pp. 94-121; W. H. Weinberg, *Langmuir*, in press.

18. C. T. Campbell, Y.-K. Sun, W. H. Weinberg, *Chem. Phys. Lett.* **179**, 53 (1991).

19. C. T. Rettner, E. K. Schweizer, H. Stein, D. J. Auerbach, *Phys. Rev. Lett.* **61**, 986 (1988).

20. M. Cardona and L. Ley, Eds., *Photoemission in Solids I and II*, vols. XXVI and XXVII of *Topics in Applied Physics* (Springer-Verlag, Heidelberg, 1978); J. W. Gadzuk, in *Electronic Structure and Reactivity of Metal Surfaces*, vol. XVI of the *NATO ASI Series B*, E. G. Derouane and A. A. Lucas, Eds. (Plenum, New York, 1976) pp. 341-387; J. C. Fuggle and J. E. Inglesfield, Eds., *Unoccupied Electronic States: Fundamentals for XANES, EELS, IPS and BIS*, vol. LXIX of *Topics in Applied Physics* (Springer-Verlag, Heidelberg, 1992); J. H. Sinfelt and G. D. Meitzner, *Acc. Chem. Res.* **26**, 1 (1993).

21. The support of this work by the Department of Energy (grant DE-FG03-89ER14048), the Donors of the Petroleum Research Fund administered by the American Chemical Society (grant ACS-PRF-23801-AC5-C), and the Universitywide Energy Research Group of the University of California is gratefully acknowledged.

TABLE 1. Rate parameters for the dissociative chemisorption of ethane on Ir(111), Pt(111), Ir(110)-(1x2) and Pt(110)-(1x2). The separately measured value for the desorption rate coefficient was used in evaluating E_r and $k_r^{(0)}$. The quantity $E_r - E_d$ is the activation energy with respect to a gas-phase energy zero, *i. e.* the gas-phase ethane infinitely far from the surface and at rest, whereas E_r is the activation energy of the reaction with respect to the proper reference energy, namely the bottom of the physically adsorbed well.

Surface	$E_r - E_d$, kcal/mol	$k_d^{(0)}/k_r^{(0)}$	E_r, kcal/mol	$k_r^{(0)}$ s^{-1}	Reference
Ir(111)	2.6 ± 0.2	100	10.3	1×10^{11}	this work
Pt(111)	8.9 ± 0.8	1200	16.6	8×10^{9}	(9)
Pt(110)-(1x2)	2.8 ± 0.2	200	10.5	5×10^{10}	(10)
Ir(110)-(1x2)	-2.2 ± 0.2	400	5.5	3×10^{10}	(11)

Figure Caption

Fig. 1. Initial probability of trapping-mediated dissociative chemisorption of C_2H_6 on Ir(111) as a function of reciprocal surface temperature. The slope, $-(E_r - E_d)/k_B$, and intercept, $k_r^{(0)}/k_d^{(0)}$, are reported in Table 1. The error bars represent one standard deviation in the measured rate at each temperature.

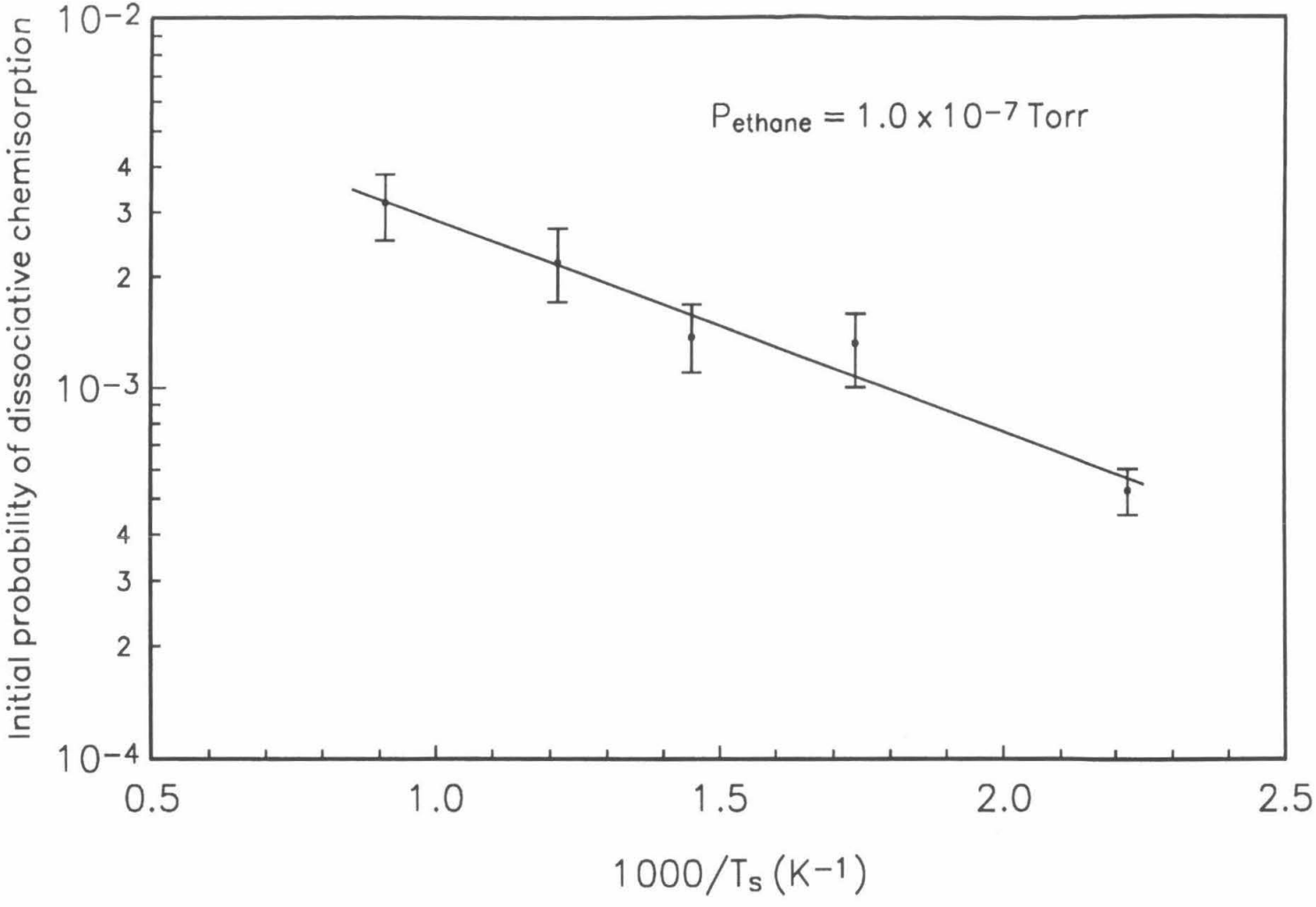
Initial probability of dissociative chemisorption
10^{-2}
4
3
2
10^{-3}
4
3
2
10^{-4}
$P_{ethane} = 1.0 \times 10^{-7}$ Torr
0.5
1.0
1.5
2.0
2.5
$1000/T_s\ (K^{-1})$

CHAPTER 4

Quantitative Determination of the Activity of Defect Sites on a Single-Crystalline Surface: C-H Bond Activation of Carbon-13 Labeled Ethane on Ir(111)

[The text of Chapter 4 consists of an article coauthored with W. H. Weinberg, which has been submitted to *The Journal of Chemical Physics*.]

Abstract. The C-H bond activation of carbon-13 labeled ethane, 1,2-di-^{13}C-C_2H_6, at defect sites on an Ir(111) single-crystalline surface, cut and polished to 0.70° ± 0.15° of the [111] direction, has been determined quantitatively. These results have been obtained from a kinetic model accounting for diffusion from sites on the less reactive terraces to step edges on the surface, combined with the appropriate trapping-mediated description of the overall rate processes operative at the defects. The activation energy for reaction at the defect sites was found to be 4500 ± 1500 cal/mol, which is ~6000 cal/mol less than the reaction barrier at the terrace sites. The preexponential factor of the reaction rate coefficient at the defect sites was found to lie between $5x10^{11}$ and 10^{12} s^{-1}, which is five to ten times greater than the preexponential factor of the reaction rate coefficient at the close-packed (111) terrace sites that dominate the surface. The net effect is that at room temperature the defect activity is approximately four and one-half orders of magnitude greater than that of the close-packed terrace sites.

I. INTRODUCTION

The use of single-crystalline transition metals as model catalysts in the study of heterogeneous catalysis has been extremely successful in identifying the specific mechanisms and quantifying the rate parameters of many reactions of technological importance. By examining the dependence of reactions as a function of the crystallographic orientation of the single-crystalline surface, important correlations have been obtained between the reactivity of a catalyst and its microscopic surface geometry.[1–3]

We present here results for the initial (low-coverage) reactivity of ethane at surface defect sites on a close-packed Ir(111) surface. The preparation of a perfectly cut and polished single-crystalline surface is not possible; on every such sample there are step edges. These edges are, in

general, uneven, and there is a distribution of terrace widths, i.e., an irregularity in the distances between step edges. Other types of defects within the three-dimensional single crystal arising from interstitial or substitutional point defects become exposed at the surface as upper layers are removed. With extreme care in sample handling and mounting, the extent of any induced damage of the surface can, and must, be minimized. The experimental measure of the precision in the crystallographic orientation of the sample is achieved by Laue X-ray diffraction methods.[4] The angle of misorientation is used to calculate the average distance between step edges under the assumption of a regular periodicity in terrace widths, and, ultimately, the concentration of defect sites on the otherwise atomically flat, ideally oriented surface. In this study, we extend the current knowledge of the relative reactivities of surfaces of different geometries to include the first detailed quantitative measurements of the reactivity of defect sites on an Ir(111) surface.

Motivated by this desire to obtain accurate kinetic data for the reactivity of defect sites for comparison with those of other surface geometries, we examined the initial probability of reaction of carbon-13 labeled ethane at the limit of detectable sensitivity of our microreactor system equipped with a quadrupole mass spectrometer. In this manner, we have regularly achieved the detection of carbonaceous residues of fractional coverages in the range $0.0010 < \theta_C < 0.0020$, and, on occasion, measured coverages between 0.0005 and 0.0010 monolayer. As will be discussed later, the method of detection involves quantitative mass spectrometric counting of the deposited carbon-13 as $^{13}CO_2$ after its titration with excess oxygen.

A. Trapping-Mediated Kinetics at Terrace Sites and Defect Sites

Before presenting and discussing the experimental data, the appropriate rate expression for the reaction probability at the surface defect sites will be derived. In order to quantify the difference between the reactivity at terrace and defect sites, it is critical to account for the role of surface diffusion in allowing molecular precursors, initially adsorbed at the terrace sites, to encounter surface defect sites. We assume the morphology of our surface to be such that the combined concentration of surface vacancies and substitutional defects is negligible in comparison to the defect site concentration associated with the step edges, which is to say, that all defects reside at step edges. This characterization of the surface is justified by the investigations of Poelsema et al. employing thermal energy atom scattering (TEAS) of He from oriented, and polished, Pt(111) surfaces.[5] In such studies, the amplitudes of the oscillations in the scattering intensity with incident angle, ϕ_i, are related to the surface step density.[6] By assuming a random distribution of terrace widths, application of the theory developed for atom scattering from structured surfaces by Lapujoulade[7] gave an estimate for the "average" terrace width of ~300 Å. Alternatively, assuming a uniform distribution of steps (as we do here with our Ir(111) sample), yielded a misalignment of 0.4-0.5° relative to the surface normal for this same sample. Further supporting the description that step edges dominate over all other types of defect sites are the results from scanning tunneling microscopy (STM) applied to a wide variety of metal surfaces.[8] In their investigations of the reconstructed Pt(100), Pt(110), and Au(111) surfaces, Behm et al. observed a stabilization of kink-free step edges.[9] The evidence from these surface-structure sensitive techniques indicates that step edges are indeed the predominant type of defect for low-index single-crystalline metal surfaces.

Thus, we model our surface by assuming a uniform distribution of terrace widths, all possessing the close-packed Ir(111) orientation, and that all of the surface defects are located at kink-free step edges. In our simplified picture, the Ir(111) surface can be illustrated by the analogy of a staircase in which the height of each adjacent stair step is only one atomic layer above the one below it. This step height, or separation of close-packed layers of Ir atoms, is calculated from the bulk lattice constant to be 2.22 Å. The uniform width of each stair step means that all of them have the same number of rows of surface atoms, N_r, lying across the terrace and parallel to the step edges themselves. The fractional coverage of step edges over the entire surface is *then just* the reciprocal of the total number of rows comprising the unit cell of the surface structure, $(N_r + 1)$. The balance of sites is comprised of identical sites of the close-packed (111) terraces, and their intrinsic reactivities are assumed to be independent of their proximity to the step edge.

B. Trapping-Mediated Kinetics at Uniformly Ordered Terrace Sites

The following derivation of the reactivity at a terrace site serves the purposes of (1) supporting our numerous studies of precursor-mediated kinetics and those of other investigators[10-13] and (2) illustrating clearly the distinct role that surface diffusion plays in the cases of reactivity at the dominant type of sites, (111) terrace sites, and the minority type of sites, step edge defect sites.

Adsorption from the gas phase, reaction at a surface site, and diffusion via single-site migration (or hopping) to adjacent nearest-neighbor sites are illustrated in Scheme I for an alkane molecule (ethane) at a terrace site on the (111) surface.[14]

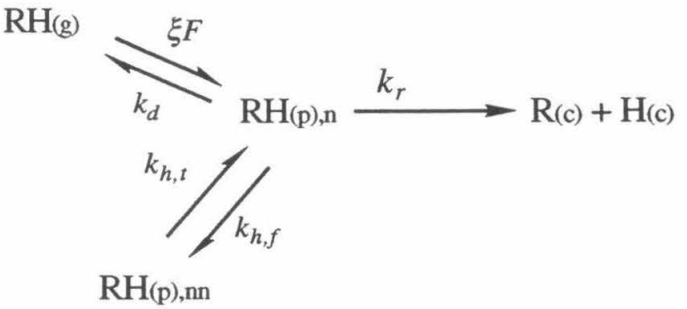

SCHEME I

The rate of trapping from the gas phase, RH(g), into the physically adsorbed state, RH(p), depends on the impingement rate, F (molecules site^{-1} s^{-1}), and the trapping probability, ξ, of the molecule into its physically adsorbed well. Trapping from the gas phase is dominated by the dissipative channels available to the incident molecule. These dissipative processes are not strongly surface-temperature sensitive in the temperature range examined here, but they are strongly gas-temperature sensitive.[15-17] Since the operating pressures are sufficiently low to ensure that the mean free path is greater than the dimensions of the microreactor, the gas temperature is equal to the wall temperature, which, in turn, is at room temperature in all cases.. In molecular beam measurements of the trapping probability of ethane on the reconstructed Ir(110) surface, ξ was found to be 0.97 ± 0.02 for the lowest beam energies, 1.2 kcal/mol or ~50 meV.[18] The kinetic energies of the ethane molecules in these 'bulb' experiments are characterized by a Boltzmann distribution with an average kinetic energy of ~25meV. Considering this fact, in conjunction with the invariance of the incident gas temperature, the value of ξ is taken to be unity and is approximately constant throughout these experiments. The rate coefficients for desorption from, reaction at, and single-site hopping from the selected *n*th terrace site are given by k_d, k_r, and $k_{h,f}$, respectively. The rate coefficient for hopping from a nearest-neighbor

(nn) site to the selected nth terrace site is given by $k_{h,t}$. All rate coefficients are assumed to be of the Polanyi-Wigner form, i.e.,

$$k_i = k_i^{(0)} e^{-E_i/k_B T_s},$$

with the relevant temperature being the surface temperature, T_S, since the adsorbed molecule has thermally accommodated to the temperature of the surface.[14,15]

The time rate of change of the concentration of adsorbed alkane at the nth site, expressed in terms of its time-averaged fractional coverage, θ_n, is

$$\frac{d\Theta_n}{dt} = \xi F + k_{h,t}\Theta_{nn} - k_d\Theta_n - k_r\Theta_n - k_{h,f}\Theta_n. \qquad (1)$$

The second and fifth terms on the right-hand side (rhs) of Eq. 1 embody the influence surface diffusion has in the overall material balance at a specific site on the (111) terrace. To relate the statistical configurations resulting from different site occupancies implied by the distinction between sites in Scheme I to the time-averaged fractional surface coverages, and, ultimately, to the macroscopically measured rate parameters, we must sum and weight the probabilities of the various statistical configurations (and thereby the probabilities of site occupancies) as a function of the surface lifetime of the adsorbed species. The ith local surface configuration, C_i, is accompanied by a probability of having the selected nth site occupied, P_i, and this probability of occupation is either one or zero. By summing the probabilities of occupancy over the fraction of time, $d\tau_i$, that the system is in the ith configuration, we obtain the weighted average of the occupancy of that site for the lifetime of the molecule on the surface. This weighted occupancy is, by definition, the fractional coverage, θ_n, i.e.,

$$\Theta_n = \frac{\sum_i P_i d\tau_i}{\sum_i d\tau_i}. \qquad (2)$$

At the atomic level, the respective probabilities for desorption, diffusion, and reaction for our selected site, n, and its nearest diffusive neighbor sites, nn, are microscopically identical. The equivalency of the sites and their pairwise reversible roles as diffusive sinks and sources for one another imply that on the scale of the entire surface, the lifetimes of occupying equivalent sites are exactly the same. The deduction, then, is that the site, n, and its neighboring sites, nn, are indistinguishable statistically, and the fractional coverage at the selected site, θ_n, is equal to that of its nearest neighbor, θ_{nn}. The second and fifth terms on the rhs of Eq. 1 exactly cancel one another yielding the familiar result employed heretofore in the pseudo-steady-state, trapping-mediated analyses of the kinetic data of model single-crystalline catalysts,[10-14] namely,

$$P_r = \frac{\xi k_r}{k_d + k_r}. \tag{3}$$

C. Trapping-Mediated Kinetics at Defect Sites

With the incorporation of defects (indicated below by asterisks) onto the otherwise ideally flat surface structure, we must modify the description of the kinetic processes of Scheme I. The dissimilarity between the defect sites and the neighboring atomically close-packed (111) sites yields a different result for the reaction probability than that given by Eq. 3. The localized interaction of the adsorbed molecule, RH(p), with the surface is derived from the induced polarization associated with dispersive London forces. In a similar manner, the diffusive motion of the molecule across the surface, when described as a series of single migratory hops, implies that at each stable adsorption site, the molecule reestablishes the same interaction with the surface. Alternatively, if the adsorbed molecule is nonlocalized, it is inappropriate to speak of a specific local minimum in the surface potential for

its adsorption site, but, nonetheless, as it diffuses across the surface, the molecule must maintain its physical bonding to the surface. Because of this dispersive nature of the bonding in the physically adsorbed state, the desorption rate coefficients of alkanes from a wide variety of different transition metal surfaces and surface geometries are found to be equal.[2,10-13,19] By extension, the diffusion rate coefficients for alkanes on most metal surfaces will be equal as well, most notably when comparing surfaces of the same geometry such as for the close-packed fcc-(111) and hcp-(001) surfaces, which collectively have smooth, i.e., only slightly corrugated, surface electronic structures. These observations imply that, when comparing the (111) terrace sites and the surface defect sites, the activation barriers to desorption and diffusion (migratory hopping) are equal. In the notation of this work, $E_d = E_d^*$ and $E_h = E_h^*$. The same, however, cannot be said of the energetic barriers to C-H bond activation for the physically adsorbed ethane molecule. For the bond-cleavage reaction, $E_r \neq E_r^*$, and it is by properly accounting for the influence of surface diffusion that we are successful in obtaining quantitative measurements of the barrier to reaction at the defect sites on the Ir(111) model catalyst.

Scheme II provides the overall description of the kinetic processes occurring at the defect sites. In this case, the equivalency between neighboring sites is lost because adjacent to the defect sites at the step edge are close-packed sites of the (111) terrace.

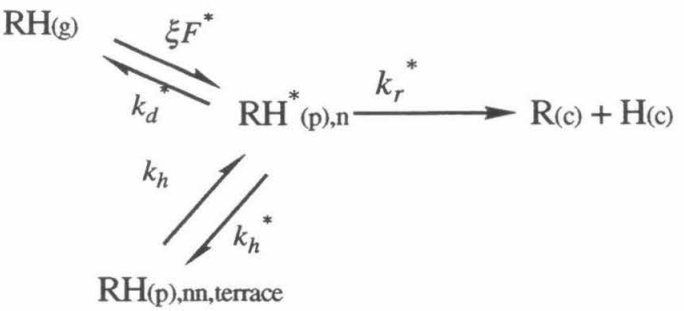

SCHEME II

Equation 4 gives the time rate of change of the fractional coverage of physically adsorbed ethane at the surface defect sites,

$$\frac{d\Theta^*}{dt} = \xi F^* + k_h\Theta_t - k_d^*\Theta^* - k_r^*\Theta^* - k_h^*\Theta^*, \qquad (4)$$

where F* is the impingement rate of gas-phase ethane directly at the defect sites, θ_t and θ^* represent the fractional coverages of the molecularly adsorbed ethane at the neighboring terrace sites and the defect site, respectively, and the rate coefficients are as defined in Scheme I. Migratory hopping between adjacent defect sites of the step edge are not included in the expression as their precise equivalency ($k^*_{d,nn} = k^*_{d,n}$; $k^*_{h,nn} = k^*_{h,n}$; and $k^*_{r,nn} = k^*_{r,n}$) leads to the same result as for the case of diffusion between equivalent terrace sites above, i.e., their exact cancellation.

Even though we assume that the rate coefficients of desorption and diffusion, k_d and k_h, are the same at terrace and surface defect sites, the difference in the reaction rate coefficients, k_r and k_r^*, causes the probability of reaction at the defect sites to be distinct from that at the terrace sites. Whereas in Eq. 1 the two terms accounting for diffusion into and out of a terrace site exactly cancel one another, the argument of precise equivalency between adjacent sites obviously no longer holds in the case of pairwise

exchange between terrace and defect sites. The two respective lifetimes are given by

$$\tau_t = \frac{1}{k_d + k_r + k_h} \text{ and } \tau^* = \frac{1}{k_d^* + k_r^* + k_h^*}, \tag{5}$$

and the difference in the reaction rate coefficients, k_r and k_r^*, will alter the respective lifetimes, τ_i and τ_i^*, used in computing the site-specific fractional coverages, θ_t and θ^*, via Eq. 2. The inequality between the reaction rate coefficients results in a difference in the characteristic lifetimes at the two types of sites, and, hence, in their relative average surface concentrations, θ_t and θ^*. Invoking the pseudo-steady-state approximation ($d\theta^*/dt \approx 0$) allows Eq. 4 to be solved for the fractional coverage of ethane adsorbed at defect sites, θ^*. The defining relation for the reaction probability at the defect sites is given by

$$P_r^* = \frac{R_r^*}{F_{total}^*} = \frac{k_r^* \Theta^*}{F^* + k_h \Theta_t}, \tag{6}$$

where the total impingement rate at the defect sites, F^*_{total}, is equal to the sum of the direct gas-phase impingement rate, F^*, at the defect sites and the surface-mediated impingement due to diffusion from the terrace sites, $k_h\theta_t$. Substituting for the expression for θ^* resulting from the pseudo-steady-state approximation of Eq. 4 yields

$$P_r^* = \frac{k_r^*}{k_d^* + k_h^* + k_r^*}\left(\frac{\xi F^* + k_h \Theta_t}{F^* + k_h \Theta_t}\right) \tag{7}$$

which, for the case of the trapping probability, ξ, assumed to be unity, reduces to

$$P_r^* = \frac{k_r^*}{k_d^* + k_h^* + k_r^*}. \tag{8}$$

The results of Eqs. 3, 7 and 8 illustrate the fundamental difference between the terrace and defect sites. Surface diffusion carries adsorbed

reactant molecules to sites on the terraces at the same rate at which they are carried away, and since reaction and desorption are identical at each terrace site, the dynamic equilibrium created by surface diffusion causes it to be of no *net* impact in the overall observed rate of reaction. Since the defect sites have a different reaction rate coefficient from the terrace sites, a neighboring pair of defect and terrace sites are distinguishable, and diffusion establishes a different dynamic equilibrium than before. The time-averaged concentration of molecules which are carried into the defect sites is not the microscopically reversibile concentration which is carried away from the site. All of this is due to the differing barriers to reaction and the effect that difference has on the relative lifetimes of the molecule at the defect and at the neighboring terrace sites.

II. EXPERIMENTAL METHODS

The measurements on the Ir(111) surface were carried out in a 200 l/s ion-pumped UHV microreactor which has a base pressure of 2×10^{-10} Torr and a volume of 10 cm^3.[11,20] The Ir(111) crystal was cut, polished, and prepared with standard techniques, and its crystallographic orientation was found to be 0.70° ± 0.15° by Laue X-ray diffraction methods,[4] which, assuming a δ-function distribution of terraces, yields a terrace width, w_t, of between 150 Å and 230 Å, with the misorientation at 0.7° corresponding to w_t = 182 Å. The crystal surface was cleaned between experiments by heating to 1000 K for 5 min at an O_2 pressure of 5×10^{-8} Torr flowing continuously through the reactor, followed by annealing to 1625 K for 1 min to desorb the surface oxygen. Thermal desorption spectra of CO, which were in complete agreement with previously published ones from the clean Ir(111) surface,[21] were measured frequently to verify the cleanliness of the surface. Since

kinetic data are known to be extremely sensitive to surface conditions, the high degree of reproducibility in the data presented here indicates the absence of surface contamination.

For the dissociative chemisorption of carbon-13 labeled ethane (di-^{13}C-C_2H_6) over the surface temperature range that was employed ($350 < T_S < 1250$ K), the system was operated in a continuous flow mode. With the crystal held at a constant temperature, ethane was introduced from our gas-handling manifold to the microreactor by effusing through a single glass capillary. The continuous flow of ethane at a pressure of 1.0×10^{-8} Torr was maintained for a reaction time, τ, of approximately one minute (depending on the surface temperature). The amount of dissociated ethane was determined by titrating the carbonaceous residue with excess oxygen at a temperature of 600-650 K, producing exclusively C-13 labeled carbon dioxide, $^{13}CO_2$. Under these experimental conditions the dissociative chemisorption of ethane is irreversible, and no gas-phase carbon-containing products of a surface self-hydrogenolysis reaction are formed. The titration conditions and procedure were optimized to ensure the rapid and complete oxidation of the surface carbon-13 to $^{13}CO_2$. In this way, a sharp rise in the mass spectrometric signal intensity was obtained, and we were able to operate our system at the limits of its sensitivity. The experiments were repeated a minimum of six times at each temperature, and one standard deviation in the statistical distribution is taken as the error in the measured probabilities.

The signal intensity of the UTI-100C quadrupole mass spectrometer was calibrated against a known mass flow rate of the $^{13}CO_2$ titration product after each individual experiment. From this calibration, the integrated signal of the product $^{13}CO_2$ was converted to the total number of ^{13}C-adatoms on the surface, $N_{C\text{-}13}$. The reaction conditions and times were such that the

fractional coverage, $\theta_{C\text{-}13}$, was just above the limits of detectability of our system, between 0.0010 and 0.0020 monolayer of carbidic C-13. On occasion we obtained measurements of 0.0005 monolayer, but these measurements were judged to be at the limit of the sensitivity of the system and were not used in the computations of the reported reaction probabilities. In a separate series of experiments, the adsorption of ^{13}CO from our gas-handling manifold onto the sample was compared to the published CO uptake curve of Ir(111).[21] This set of measurements yielded two important results. First, the flux of the impinging ^{13}CO at the crystal could be determined accurately, and after correcting for the mass effect on the effusion rates, we obtained accurate effusive fluxes for the impinging ethane. Second, these measurements verified our calibration procedure of the mass spectrometric signals, because from the integrated signals of ^{13}CO obtained after saturation exposures, we calculated the saturation coverage of CO on Ir(111) to be 0.63 ± 0.02, in excellent agreement with the published value of 0.59 ± 0.02 from low-energy electron diffraction (LEED) and thermal desorption studies,[21] and for the saturation coverages of CO on other close-packed surfaces.[22]

At a given surface temperature, T_S, the apparent dissociative chemisorption probability, $P_r(T_S)$, uncorrected for diffusion, is obtained from

$$P_{r,app}(T_s) = \frac{N_{C\text{-}13}}{2A\tau F_{gas}} \tag{9}$$

where A is the total sample surface area (2 cm^2), F_{gas} is the impingement flux of reactant ethane (molecules cm^{-2} s^{-1}), and the stoichiometric factor of 2 converts $N_{C\text{-}13}$ into the number of reacted ethane molecules. The direct application of this expression to the measured data does not discriminate between the respective contributions of the dissociation of ethane at defect

and terrace sites. The proper analysis of the measured data is presented in the following section.

All gases (ethane, O_2, ^{13}CO, and $^{13}CO_2$) were introduced into the microreactor from a gas-handling manifold that was pumped with a diffusion pump to a base pressure below 10^{-7} Torr. Carbon-13 labeled ethane (1,2-di-^{13}C-C_2H_6, 99 atom % ^{13}C) was obtained from Icon Services, and was used without further purification. The $^{13}C_2H_6$ mass spectrometric cracking pattern was in excellent agreement with published data.[23] The ^{13}CO and $^{13}CO_2$ (each 99.5 atom % C-13) were obtained from Icon Services, and they were thrice successively cycled through liquid nitrogen freeze-pump-thaw procedures prior to their use.

III. RESULTS AND DISCUSSION

A. Reaction Rate at Defect Sites, R_r^*

The series of calulational steps necessary to evaluate the reaction probability at defect sites, P_r^*, begins with a determination of the reaction rate at defect sites, R_r^*, from the analysis of the $^{13}CO_2$ titration data. For each experiment, the spectrometrically counted $^{13}CO_2$ titration product, $N_{C\text{-}13}$, is recognized to be the sum of that obtained from reaction at the defect sites and the close-packed terrace sites. Using the known reaction probability as a function of temperature for ethane on the atomically flat Ir(111) surface,[3]

$$P_{r,t} = 10^{-2} e^{-2600 cal/mol/k_B T_s}, \tag{10}$$

we are able to correct each individual experiment for the contribution from reaction at the terrace sites under the specific reaction conditions of surface temperature, ethane gas pressure, and exposure time. The net result is the fractional coverage of reacted carbon-13 at the defect sites, $\theta^*_{C\text{-}13}$, and by

dividing by the exposure time, τ, we obtain the initial reaction rate of ethane at the defect sites, R_r^*.

The next step is to obtain the total impingement rate, F^*_{total}, which, when applied in Eq. 6 with the above determined reaction rates, R_r^*, yields the reaction probability at defect sites, P_r^*. As shown in Scheme II, the total impingement rate at the defect sites is derived from two sources: the incident gas-phase impingement rate at the defect step edge, F^*, and the two-dimensional diffusive flux arriving at the step edge from the adjoining terraces. The probability of diffusing to the edge defect from the sites on the terrace, P^*_{D,T_S}, is computed from the model of the δ-function distribution of terrace widths and estimates of the tracer diffusion coefficient, D, and the surface lifetime, τ_S, of the adsorbed molecular ethane on the terrace sites. Taken together, these two quantities can be considered to be representative of the total effective pressure of the incident ethane gas at the defect sites of the step edge. Equipped with an accurate measure of this total impingement rate, we are able to compute the initial dissociative probability, P_r^*, at the defects.

B. Gas-Phase Impingement Rate at Defects, F^*

The first contribution to impingement at the defect sites is from those molecules which trap and accommodate directly at the defect sites. This term is expressed as ξF^* in Eq. 4, and the impingement rate is derived from the incident gas-phase flux, F_{gas}, the defect density, n_S^*, and the fractional coverage of defects, θ^*, on the surface. The defect density results from the spatial extent of the perturbation to the surface electronic wavefunction induced by the defect step edge,[9] and is most often estimated to encompass one complete atomic row. Imagining the depiction in Fig. 1a to provide a

meaningful length scale of the true defect edge, it is seen that those atoms adjacent to the step edge at the top and bottom terraces share electron density with (111) terrace atoms to either side of the step, and it is at the termination of the upper terrace relative to the lower terrace that the defect is geometrically defined. In a purely mathematical sense, the step edge is a discontinuity and possesses an infinitesmally small width, but in terms of the electronic structure of the surface at the step, it is subtly complex.

As stated above, the truest description of the defect is in terms of its impact on the electronic wavefunction of the surface. We assume that the spatial extent of the perturbation is localized within one atomic row (2.35 Å), and we will discuss refinements to the details of this description later. The assumed spatial extent of the defect is relevant to the estimation of the contribution to the total impingement at the defect edge due to the gas-phase term in Eq. 4, which, under conditions of diminishing surface diffusion, becomes the only term introducing reactant ethane to the defect sites. The contribution to the total impingement rate from gas-phase impingement directly at a defect site, F^*, is simply the gas-phase flux, F_{gas}, divided by the defect site density, n_s^*, multiplied by the fraction of the surface which can be associated with the defect step edges, i.e.,

$$F^* = \left(\frac{F_{gas}}{n_s^*}\right)\frac{w_d}{w_t + w_d} = F\left(\frac{n_s}{n_s^*}\right)\frac{w_d}{w_t + w_d} \tag{11}$$

where w_d is the width of a defect step edge (2.35 Å), w_t is the uniform width of a smooth (111) terrace (~180 Å), and F is, as before, the incident gas impingement rate and is derived from the incident flux, F_{gas}, divided by the surface site density, n_s, of iridium atoms on the close-packed surface, i.e., $F = F_{gas}/n_s$.

C. Diffusion-Mediated Impingement, $P^*_{D,Ts}$

The second contribution to the total impingement rate at the defect arises from surface diffusion of adsorbed molecules which initially have trapped and accommodated on the terraces and subsequently diffuse to the step edge. Because its contribution results from the migration of ethane molecules adsorbed on the terraces, it is calculated from the incident gas-phase impingement rate at the terrace sites, F, and the probability of diffusion to a step, P^*_{D,T_S}. This latter quantity is obtained by computing the probability of encountering the step edge at a given surface temperature, T_S, and surface diffusion coefficient, D. On the microscopic scale, the adsorption on and migration across a terrace for an individual molecule are random events, both from the point of view of the initial adsorption site and the subsequent random walk executed by the adsorbate.[24] What we require for our development of P^*_{D,T_S} is a means of statistically averaging these two events. This is possible via the macroscopic values of the incident gas flux and the rate coefficients of desorption, reaction, and diffusion, of which we have independent knowledge[2,10,14,19,25] as well as the capacity to adjust in order to optimize the overall description of the system.

In the treatment of a random walk in two dimensions,[24] the mean square displacement, $\langle \Delta r^2 \rangle$, is given by

$$\langle \Delta r^2 \rangle = 4\, D\, \tau_S, \tag{12}$$

and, furthermore, the lifetime of the adsorbed molecule on the (111) terraces, τ_S, is simply the reciprocal of the sum of the desorption and reaction rates for the terrace sites, i.e.,

$$\tau_s = \frac{1}{k_d + k_r}, \tag{13}$$

and differs from the *site* lifetime of ethane, τ_t, in that while τ_s represents the length of time that the ethane molecule exists on the terrace, τ_t represents the length of time it resides at a specific site of the (111) terrace. For each selected surface temperature and each set of assumed values of preexponential factors and activation energies of the rate coefficients, the mean square displacement may be calculated. This result gives a measure of the average distance from the initial point of adsorption the molecule diffuses during its lifetime on the surface by executing a random walk. It is understood that nothing is implied about either how direct or how meandering any actual path of a specific molecule may be, only that *on average* it diffuses a distance of $<\Delta r^2>^{1/2}$ from its point of origin.

Working with the root-mean-square displacement of the diffusing molecule allows us to compute the probability of encountering a step edge from any position on the terrace face. From the perspective of a statistically averaged value, the molecule may be considered to sample a circular area of radius, $r_D = <\Delta r^2>^{1/2}$, as depicted in Fig. 1b, with all *net vector* displacements to the perimeter of the circle being equally probable. The fraction of projections which intersects the edge defect constitutes the probability of diffusing to the edge from the point of impingement on the terrace. This site-specific probability is indicated as P(x) in our nomenclature and represents the diffusion probability from a perpendicular distance, x, from the step edge. By integrating over all the accessible distances to the step edge from the terrace, $0 \leq x \leq r_D$, the total probability of encountering the defect edge via surface diffusion is obtained.

At this point, a more detailed examination of the nature of the defect step edge is required. In this discussion, we relate our system to findings from studies of adatom self-diffusion and metal-on-metal epitaxial growth.

The important question addressed here relates to the treatment of the two distinct directions an ethane molecule might migrate to access a given step: is "stepping down" from the terrace above equal to "stepping up" from the terrace below? Figure 1a depicts two different types of defect sites present at a step edge, the "ascending" step site adjoining the edge at the lower terrace, and the "descending" step site adjacent to the edge at the upper terrace. Both types of sites comprise the defect step edge and are localized within the one-full row of the physical step.

These different sites have been identified in connection with crystal growth. In particular, the self-diffusion of individually deposited adatoms of Ir as well as Ir_x clusters (x = 2 to 13) on Ir(111) has been studied with field ion microscopy (FIM) by Wang and Ehrlich.[26] Of relevance here, they have studied the diffusion behavior in the vicinity of steps in the surface temperature range of 100 to 128 K.[27] Their findings indicate that the Ir adatom and Ir_x clusters are trapped with increased binding energies at the strip of adsorption sites directly adjacent to a step, the "descending" step indicated in Fig. 1a, and that for adatoms approaching the "ascending" step, there is a depleted zone, in which no Ir adatoms are observed, between the step and the extended (111) plane. A slightly reflective barrier is proposed at the boundary of this depleted zone and reduced barriers to diffusion are proposed to arise within it. In this way, once the approaching adatom has overcome the thermal barrier at the perimeter of the zone, it rapidly diffuses to the step edge where it is incorporated. The overall picture is that the binding energies for these adatoms and clusters are stronger in the vicinities of *both* sides of a step than on the smooth (111) plane. Furthermore, the authors estimate that the barriers to diffusion out of the "descending" and "ascending" sites are approximately 10% greater than the ~6 kcal/mol barrier

observed for the self-diffusion of Ir adatoms on the smooth Ir(111) terrace. By examining the temperature dependence of the relative populations in these two strongly binding "defect" sites, they further estimate that the difference in the activation barriers between the two sites is approximately 150 cal/mol.

In applying these results to the case of the interaction of ethane at a step edge, we will not discriminate between the "descending" and "ascending" sites of a given step edge to the extent indicated above. Yet, by the same token, we do explicitly include both types of sites in our model, i.e., we conclude that the defect site density, n_S^*, is twice that of the step density. Further, we assume that the two sites are equivalent with respect to the kinetic rate coefficients of all of the modeled kinetic processes for the interaction and reaction of ethane at the defect sites. The implication to our analysis is that ethane will be capable of accessing defect sites from its motion across a terrace in either of two directions. From the terrace above, the model will account for its interaction with the "desending" step defect site, while from the terrace below, the model will account for its interaction with the "ascending" step defect site. (The possibility of an ethane molecule diffusing over the edge onto the adjacent terrace, in either direction is also allowed, and is discussed in the following paragraph.)

In Figure 1a, the side-view of the terrace-step interface illustrates the two types of defect sites at a step edge, and the sketch of the potential for the ethane migrating across the step edge is depicted as well. This potential shows no variation in its structure at the defect step edge, because, as mentioned previously, the dispersive forces characterizing the *physical* bonding of ethane in these surface sites has been found to be insensitive to the type of metal surface and to its surface geometry. Thus, we consider the elementary rate parameters for desorption and diffusion to be the same for

the terrace sites and the defect sites. The observed increases in the binding energies of Ir atoms and clusters on Ir surfaces and the detailed structure of the potential interactions in the vicinity of the steps are attributed to significant realignment of surface atoms, and redistribution of electron density, resulting from the strong metallic bonding (desorption energies are ~120 kcal/mol) of the chemisorbed Ir adatoms.[27,28]

At elevated surface temperatures, the diffusion from one terrace to another appears to be possible. In TEAS studies of He scattering from epitaxial Pt films grown on a Pt(111) substrate,[29] a transition from 3D-dendritic deposition at T_S = 250 K to 2D-layer-by-layer growth at T_S = 630 K is observed. This result indicates that, at the higher temperature, surface diffusion from the upper terrace and over the "descending" step is occurring, leading to incorporation into the step edge and nearly uniform n –> n+1 growth dynamics. Thus, considering the temperature range employed in our measurements and the strength of the bonding interaction of ethane with the surface, we will include the possiblility of a molecule diffusing across the step edge in either direction (the equivalency of this motion "stepping up" or "stepping down" is a direct result of the equivalency of the diffusion barriers in our model, as shown in Fig. 1a). Accounting for this effect involves allowances for the molecule to access both types of sites in its passage across the edge. It is not appropriate to incorporate terms which provide for diffusion along the step edge, because, as was derived earlier in Eqs. 1 – 3, the effect of diffusion between equivalent sites exactly cancels in the rate expression. Furthermore, we note that our computations reveal that the ethane has a limited diffusive range and interacts only with those edges nearest to its initial point of trapping on the surface. We find that at elevated surface temperatures, the lifetime of the adsorbed ethane molecule is too

short, and its root-mean-square-displacement, $<\Delta r^2>^{1/2}$, too small, to enable it to access additional steps beyond those which border its original point of adsorption.

Summarizing these points, we consider *two* types of defect sites associated with *each* step edge: the "descending" step site and the "ascending" step site. Thus, the true fractional coverage of defects is, in fact, twice that of the fractional coverage of the step edges, i.e., $\theta_{steps} = w_d/(w_d + w_t)$, and $\theta^* = 2\ w_d/(w_t + w_d)$.[30] We assume that the two types of sites are equivalent with respect to the elementary rate parameters for desorption, diffusion, and reaction. The diffusion effects of migrating over a step edge onto the adjacent terrace are included in the model in light of the elevated surface temperatures employed in these experiments.

With the refined model for the defects at the step edge, we can continue with the development of the probability, $P^*_{D,Ts}$, of diffusing to the step edge from an adsorbed site on the terrace. Figure 1b provides the geometric relationships involved in this computation for the assumed uniform distribution of terrace widths. The assumed isotropic description of the diffusion yields a continuously decreasing probability of impinging at the step as the distance from the edge, x, increases. Were the diffusion described in terms of discrete migratory hops, a summation over the accessible sites for physical adsorption within the enclosed circle of radius r_D would be necessary. As may be seen in Fig. 1b, from a given point Q, with coordinates (x,0) on the terrace, the angle subtended by the projection to the step edge is simply twice

$$\alpha = \cos^{-1}\left(\frac{x}{r_D}\right), \tag{14}$$

and, over the complete circle, this represents a site-specific probability of encountering the step edge of $P(x) = \alpha/\pi$. The molecule may access a given step edge from terraces either above or below, and, by noting this symmetry, we are able to simplify our computation by doubling the result obtained for motion in one direction. The integral formally computes the total probability across the full terrace width, w_t, noting that for distances greater than r_D, the probability of reaching the step edge is zero. It must be remembered that the width of the step is taken to be one full row, or $w_d = 2.35$ Å, and since a molecule adsorbed at the step edge has unit probability of impinging on the step, the lower limit of our integral for $P^*_{D,Ts}$ reflects the relative boundary between the step and the terrace. The total weighted probability of diffusing to the step is then

$$P^*_{D,Ts} = \frac{\int_0^{w_t} P_{x,1} + \int_0^{w_t} P_{x,2}}{\int_0^{w_t} dx}, \qquad (15a)$$

where $P_{x,1}$ and $P_{x,2}$ are the respective probabilities of diffusing to the left (step 1, in Fig. 1b) and to the right (step 2, in Fig. 1b). Noting that for $x > r_D$ the probability of diffusing to the step is zero, and making use of the symmetry in the problem, we reduce the integral expression above, by simply doubling the probability of diffusing to one step only, to

$$P^*_{D,Ts} = \frac{2}{\pi w_t}\int_0^{r_D} \cos^{-1}\left(\frac{x}{r_D}\right)dx = \frac{2}{\pi}\frac{r_D}{w_t}. \qquad (15b)$$

The total impingement rate at the step edge, F_{total}^*, is computed from the following relation,

$$F^*_{total} = F\left(\frac{n_s}{n_s^*}\right)\left\{\frac{w_d}{w_t + w_d} + P^*_{D,Ts}\frac{w_t}{w_t + w_d}\right\}, \qquad (16)$$

where the ratio of the differing site densities, n_S/n_S^*, accounts for the modeling of two defect sites per metal atom at the step edge relative to only one adsorption site per surface atom on the terraces.

D. Evaluation of the Rate Parameters for Activation at Defects

The accuracy and reliability of this computation relies upon the propagated precision of several factors, all of which we have chosen based on our experience and the published work of many researchers.[2,10-15,18,19,25] Of utmost importance are the values we assume for the diffusion, desorption, and reaction rate coefficients at the terrace sites, and, among these, the rate parameters for the diffusion coefficient are arguably the most difficult to specify.[24,25] The activation energy of desorption for ethane on single-crystalline surfaces of transition metals is 7.7 ± 0.2 kcal/mol,[2] and the corrugation in the potential surface between the activation energies of diffusion and desorption is generally thought to range from 20% to 40%.[14,15] For the diffusion of normal alkanes on Ru(001), George et al. have found that the corrugation is 30% ± 3%, and for neopentane, the corrugation was found to be 26%.[25]

We have assumed a corrugation of 30% for ethane on the Ir(111) surface, and we have examined the effect of varying the preexponential factor of the diffusion coefficient over two orders of magnitude (from 10^{-2} to 10^{-4} $cm^2\ s^{-1}$). The effect on our computed diffusion probability, $P^*_{D,Ts}$ in Eq. (15) above, and ultimately the computed results of the reaction rate parameters at the defect sites have been quantified and provide a good measure of the sensitivity of the calculation and the model to these parameters. In addition, we have examined the influence of the width of the terrace, w_t, as correlated with the uncertainty in the Laue diffraction measurement. Computations

using the extremes of low diffusion with wide terraces and its opposite of high diffusion with narrow terraces provide a range for our derived defect reaction rate parameters.

Having obtained the initial reaction rate for labeled ethane at the defect sites, R_r^*, and the correct values for the total impingement rate at the defects, F^*_{total}, the initial probability of reaction, P_r^*, at the defects on the Ir(111) surface may be calculated. From Eq. (8), the probability of reaction is related to the trapping probability, and the rate coefficients of desorption, reaction, and diffusion at the defect site. Algebraically isolating the ratio between the reaction and diffusion rate coefficients yields

$$\frac{P_r^*}{(1-P_r^*)}\left(\frac{k_d^*}{k_h^*}+1\right)=\frac{k_r^*}{k_h^*}, \tag{17}$$

the semilogarithmic plot of which as a function of reciprocal surface temperature, $1/T_S$, will yield a straight line the slope of which is equal to $-(E_r^* - E_h^*)/k_B$ and the intercept of which is equal to $\left[\frac{k_r^{*(0)}}{k_h^{*(0)}}\right]$.

The measured results for the initial reactivity of carbon-13 labeled ethane at the defect sites of our Ir(111) catalyst, P_r^*, are provided in Table I. The most important quantities necessary in deriving these reaction probabilities are shown as well, namely, the radius of diffusion, r_D, the measured apparent and net reaction probabilities, $P_{r,app}$ and $P_{r,net}$, (uncorrected for the influence of diffusion), and the relevant quantities used in the calculation of the left-hand-side (lhs) of Eq. 17. By dividing the net probabilities of reaction, $P_{r,net}$, by the values in the fifth column of Table I, which embody the gas-phase and diffusion-mediated contributions to the impingement at the defect sites, we obtain the probabilities of the reaction at the defect sites, P_r^*, on the Ir(111) surface. The values of the rate

parameters of the rate coefficients of migratory hopping, desorption, and reaction employed in the construction of Table I are

$$k_d = k_d^{(0)} \exp[-E_d/k_B T_s] \qquad k_d^{(0)} = 10^{13}\ s^{-1},\ E_d = 7{,}700\ \text{cal/mol},$$

$$D = D_0 \exp[-E_D/k_B T_s] \qquad D_0 = 10^{-3}\ cm^2\ s^{-1},\ E_D = 2{,}310\ \text{cal/mol},$$

$$k_h = k_h^{(0)} \exp[-E_h/k_B T_s] \qquad k_h^{(0)} = n_s D_0 = 1.6 \times 10^{12}\ s^{-1},\ E_h = E_D,$$

$$k_r = k_r^{(0)} \exp[-E_r/k_B T_s] \qquad k_r^{(0)} = 10^{11}\ s^{-1},\ E_r = 10{,}300\ \text{cal/mol},$$

$$k_d^* = k_d \quad \text{and} \quad k_h^* = k_h.$$

The plots of the measured apparent probability of reaction, $P_{r,app}$, and the net probability of reaction, $P_{r,net}$, as a function of reciprocal temperature are displayed in Fig. 2. The latter probability has been derived by simply subtracting the known probability for the dissociation of ethane at the smooth (111) terrace sites (*vide supra*, Eq. 10). The observed decrease in the net reaction probability with increasing surface temperature indicates that the activation energy for the intial C-H bond cleavage reaction at the defect sites on Ir(111) lies *below* the activation energy of desorption for the ethane molecule from these sites. This same behavior has been observed for the activation of ethane on the reconstructed surface of Ir(110), for which the activation energy for ethane dissociation, E_r, was found to be 2.2 ± 0.2 kcal/mol less than the activation energy, E_d, for desorption.[12] While most analyses of trapping-mediated kinetics are able to invoke the expression for the reaction probability in Eq. 3, the conversion of extremely small amounts of ethane in this study must account for the reaction at defect sites and must employ the expression for the reaction probability in Eq. 17.

The Arrhenius plots of the reaction probability at the defect sites, P_r^*, and the lhs of Eq. 17 versus reciprocal temperature are given in Fig. 3, for the data presented in Table I. We observe an excellent fit to a straight line for

temperatures between 500 and 1250 K, but for temperatures below 500 K, there is a pronounced deviation from the linearity of the fit. At low surface temperatures, i.e., $T_S < 500$ K, the situation appears similar to that observed in the activation of methane on Pt(110)-(1x2).[11] In that study the Arrhenius analysis of the measured data in the low-temperature regime provided nearly perfect agreement with heat of adsorption of CO, which is 28 kcal/mol. Thus, the data revealed, in a quantitative way, that the adsorption of CO from the background in the microreactor was blocking sites for the dissociation of methane. We note that a similar analysis of our measured data in the low-temperature regime ($350 < T_S < 500$ K), yields an apparent energy barrier of ~6.3 kcal/mol. We draw the similarity to the study of the activation of methane on Pt(110)-(1x2), and we find it intriguing to speculate that this value represents the diffusion barrier for CO on the clean Ir(111) surface. This possibility is substantiated by the tendency of CO to adsorb initially at defect sites on a single-crystalline surface, as observed with Fourier-transform infrared reflection-absorption spectroscopy (FT–IRAS) for low coverages of CO on Pt(111).[31] By following the shift in absorption peak intensities for CO adsorbed at terrace and defect sites, Bradshaw et al. demonstrated that CO preferentially migrated to surface defect sites upon thermally annealing from 93 to 346 K. We take the apparent barrier of ~6.3 kcal/mol, implied by our measurements, as a measure of the activation barrier to diffusion for the chemisorbed CO on terraces of the Ir(111) surface. It is interesting to note that it is generally accepted that covalently bound species yield potential corrugations (ratios of the activation energies of migratory hopping to desorption, E_h/E_d) close to 10–20%.[14,15] Carbon monoxide desorbs from the Ir(111) surface with an activation energy of 31.7 kcal/mol.[21] Hence, we obtain a potential corrugation of ~19% for the

interaction of CO with Ir(111). Our result of 6.3 kcal/mol for the activation energy of migratory hopping compares very well with those determined for the diffusion of CO on other close-packed transition metal surfaces. For CO on Ni(111), E_h was found by Zhu et al. and by Gomer et al. in independant studies to be 6.8 kcal/mol.[32,33] For comparison, Schmidt et al. found the barrier to diffusion for CO on Rh(111) to be 7.0 kcal/mol,[34] while on alumina-supported Pt clusters having average diameters of 100Å, Sinfelt et al. found the barrier to be 6.5 ± 0.5 kcal/mol.[35]

In Fig. 3 we plot the lhs of Eq. 17 versus reciprocal surface temperature for the complete temperature range employed in these experiments. By analyzing the data between 500 and 1250 K, as an Arrhenius construction, we determine the ratio of the preexponential factors for the rate coefficients of reaction and migratory hopping at the defect sites, $k_r^{(0)*}/k_h^{(0)*}$, to be 0.4 and the difference between the activation energies for reaction and diffusion at the defect sites, $E_r^* - E_h^*$, to be 2.2 kcal/mol. Of note is the fact that the ratio of the preexponential factors is expected to be less than unity, based on arguments that the phase space sampled in the transition state for diffusion should be somewhat greater than that for reaction.[14,19] With the preexponential factor for migratory hopping, $k_h^{(0)*}$, having been assumed to be 1.6×10^{12} s^{-1} in this calculation, the implied value of the preexponential factor for reaction is ~6×10^{11} s^{-1}. On the smooth [111]-oriented terraces, the preexponential factor for reaction is 10^{11} s^{-1}.[3] The uncertainties associated with accurately determining individual preexponential factors is large,[14] whereas the determination of their ratios has proven to be somewhat more precise.[19] Thus, we take these two preexponential factors to indicate that there is a greater phase space sampled in the transition state for reaction at the defects than that for reaction at the

terrace sites, presumably due to the greater number of configurations which may lead to C-H bond cleavage at defect sites. The comparison of the activation barriers for the activation of ethane at defect and terrace sites is even more revealing. We measure here that the activation energy to reaction at the defect sites on the Ir(111) surface, E_r^*, is 4.5 kcal/mol, while on the close-packed (111) terrace sites of this surface, the activation energy, E_r, is 10.3 kcal/mol.[3] Relevant to this discussion is the observed activation energy for the dissociation of ethane on reconstructed Ir(110), E_r, which was found to be 5.5 kcal/mol.[12] These three energies are referenced with respect to the bottom of the physically adsorbed well, which lies 7.7 kcal/mol below the gas-phase energy zero of the ethane molecule infinitly removed from the surface and at rest. The reconstructed Ir(110) surface is highly corrugated and is characterized by (331) facets involving the top three atomic layers,[36] and it has been demonstrated in a number of studies to be highly reactive towards C-H bond activation.[2,12] Based on the agreement between the activation energies for ethane dissociation on reconstructed Ir(110) and at the defects on Ir(111), we conclude that the microscopic details of the reactive sites (their respective electronic and geometric structures, i.e., coordination numbers) must be nearly identical.

In order to estimate the error in the computed results of the activation of ethane at the defects on the Ir(111) surface, we have made a series of calculations to judge the sensitivity of our model. We have used the same value for the rate parameters of the desorption rate coefficient (E_d = 7.7 kcal/mol and $k_d^{(0)} = 10^{13}$ s^{-1}) throughout these tests. We have varied the rate parameters of the diffusion coefficient, D_0 and E_D, from 10^{-2} to 10^{-4} cm^2s^{-1} and 20% to 40% of the desorption barrier, E_d. Variations in these parameters affect both the radius of diffusion, r_D, (and, hence, the probability

of diffusing to the step edge, $P^*_{D,Ts}$) and the rate coefficient for migratory hopping at the defect sites, k_h^*. We also have examined the dependence of the results on the width of the terrace. The findings are summarized in Table II, where we have selected a few representative computations to illustrate the observed effects. In general, we find the model to be insensitive to the variation in terrace width, which we obtain from the uncertainty in the Laue measurements. It should be noted that the entries in the third row are derived from the set of rate parameters listed earlier, and it is they which give rise to the values in Table I and the plots in Figs. 2 and 3.

As mentioned previously, we expect the ratio of the preexponential factors, $k_r^{(0)*}/k_h^{(0)*}$, to be very near unity , if not below it. For this reason, we tend to lend less credence to the computed results for data sets in which the ratio of the preexponential factors (column 5 in Table II) is greater than unity. Such results are obtained in the cases of limited diffusion, e.g., when modeled with high barriers, E_D, or with low values of the diffusion coefficient, D_0. Using the ratio of the reaction and migratory hopping preexponential factors as a measure as to the reasonableness of the result, we conclude, from these sensitivity measurements, that the error in the activation energy, as determined by the model alone, is ± 1.5 kcal/mol and that the ratio of the preexponential factors for reaction and migratory hopping at the defect sites ranges from $5x10^{11}$ s^{-1} to 10^{12} s^{-1}. Despite the limitations imposed by our model, we have included the most important elements of the system, and we have been successful in deriving a good quantitative estimate of the elementary rate parameters for C-H bond activation at defect sites on the Ir(111) surface.

IV. CONCLUSIONS

A microreactor study of the kinetics of the initial dissociative chemisorption of carbon-13 labeled ethane at defect sites on the Ir(111) surface has been performed. By controling the amount of reacted ethane to between 0.0010 and 0.0020 monolayer, we have been able to quantify the separate kinetic rate parameters for C-H bond activation at the defect sites. We have derived the appropriate expression for the trapping-mediated intial probability of reaction in the case where diffusion must be treated explicitly to account properly for the total impingement of the molecular precusor at the defect sites. Our model of diffusion in this system assumes that the terraces are all of uniform width, and that there are two types of defect sites, located at the "ascending" and "descending" step edge.

We obtain an activation energy of 4.5 ± 1.5 kcal/mol for the reaction rate coefficient at the defect sites, and the preexponential factor for reaction is found to be between $5x10^{11}$ s^{-1} and 10^{12} s^{-1}. These results are compared with the corresponding results for the smooth Ir(111) and corrugated Ir(110) surfaces. It is seen that, while the difference in activation energies is ~6 kcal/mol between reaction at the defect sites and smooth (111) terrace sites, the activation energies for the dissociation of ethane on the reconstructed Ir(110) surface and defect sites on the Ir(111) surface are within experimental error. These findings strongly support the continued use of single-crystalline surfaces in studies of the surface chemistry operating on supported commercial catalysts.

Furthermore, we have demonstrated the broad applicability of the trapping-mediated description of suface kinetics in gas-solid heterogeneous catalysis. Our results support the fundamental distinction articulated in Sec.

I regarding the inequality of the defect and terrace sites manifesting itself through their respective local site lifetimes,

$$\tau_t = \frac{1}{k_d + k_r + k_h} \text{ and } \tau^* = \frac{1}{k_d^* + k_r^* + k_h^*}.$$

The local site lifetime at the terrace site is dictated by the diffusion rate coefficient, k_h, while at the defect site, the lifetime depends on both the reaction and the diffusion rate coefficients. These detailed quantitative results for the activation of C-H bonds at the defect sites of the Ir(111) surface illustrate the mechanism through which diffusion manifests its effect in such systems.

Acknowledgement: This work was supported by the Department of Energy under grant no. DE-FG03-89ER14048.

REFERENCES AND NOTES

[1]J. H. Sinfelt, Adv. Catal. **23**, 91 (1973); J. H. Sinfelt, Catal. Rev. **3**, 175 (1969); J. R. Engstrom, D. W. Goodman, and W. H. Weinberg, J. Am. Chem. Soc. **110**, 8305 (1988).

[2]T. S. Wittrig, P. D. Szuromi, and W. H. Weinberg, J. Chem. Phys. **76**, 716 (1982); P. D. Szuromi, J. R. Engstrom, and W. H. Weinberg, J. Phys. Chem. **89**, 2497 (1985); P. D. Szuromi, J. R. Engstrom, and W. H. Weinberg, J. Chem. Phys. **80**, 508 (1984); L. E. Firment, and G. A. Somorjai, J. Chem. Phys. **66**, 2901 (1977).

[3]D. F. Johnson and W. H. Weinberg, Science **261**, 76 (1993).

[4]U. Linke and B. Poelsema, J. Phys. E: Sci. Instrum. **18**, 26 (1985).

[5]B. Poelsema, R. L. Palmer, G. Mechtersheimer, and G. Comsa, Surf. Sci. **117**, 60 (1982).

[6]B. Poelsema and G. Comsa, *Scattering of Thermal Energy Atoms from Disordered Surfaces*; (Springer-Verlag, Heidelberg, 1989), *Springer Tracts in Modern Physics*;Vol. 115, Chapter 6.

[7]J. Lapujoulade, Surf. Sci. **108**, 526 (1981).

[8]Ph. Avouris and I.-W. Lyo Science **264**, 942 (1994); J. Wintterlin, J. Weichers, H. Brune, T. Gritsch, H. Hofer, and R. J. Behm, Phys. Rev. Lett. **62**, 59 (1989); T. Gritsch, D. Coulman, R. J. Behm, and G. Ertl, Appl. Phys. A **49**, 403 (1989); R. J. Behm, J. Phys: Condens. Matter **3**, S117 (1991).

[9]The degree of preference for kink-free steps was observed to be greater for Pt(100) and Pt(110) than for Au(111): [J. V. Barth, H. Brune, G. Ertl, and R. J. Behm, Phys. Rev. B **42**, 9307 (1990)].

[10]W. H. Weinberg, Langmuir **9**, 655 (1993); W. H. Weinberg J. Vac. Sci. Technol. A **10**, 2271 (1992).

[11]Y.-K. Sun and W. H. Weinberg, J. Vac. Sci. Technol. A **8**, 2445 (1990).

[12]C. B. Mullins and W. H. Weinberg, J. Chem. Phys. **92**, 3986 (1990).

[13]J. A. Rodriguez and D. W. Goodman, J. Phys. Chem. **94**, 5342 (1990).

[14]W. H. Weinberg, in *Kinetics of Interface Reactions*; edited by H. J. Kreuzer and M. Grunze (Springer-Verlag, Heidelberg, 1987) p. 94.

[15]W. H. Weinberg, in *Dynamics of Gas-Surface Collisions*; edited by C. T. Rettner and M. N. R. Ashfold (Royal Society of Chemistry, Cambridge, 1991) p. 171.

[16]G. Ehrlich, in *Chemistry and Physics of Solid Surfaces VII,* edited by R. Vanselow and R. F. Howe (Springer-Verlag, Heidelberg, 1989) p. 1.

[17]C. T. Rettner, E. K. Schweizer, H. Stein, and D. J. Auerbach, Phys. Rev. Lett. **61**, 986 (1988).

[18]C. B. Mullins and W. H. Weinberg, J. Chem. Phys. **92**, 4508 (1990).

[19]C. T. Campbell, Y.-K. Sun, and W. H. Weinberg, Chem. Phys. Lett. **179**, 53 (1991).

[20]J. J. Vajo, W. Tsai, and W. H. Weinberg, Rev. Sci. Instrum. **56,** 1439 (1985).

[21]C. M. Comrie and W. H. Weinberg, J. Chem. Phys. **64**, 250 (1976).

[22]M. A. Van Hove, W. H. Weinberg, and C.-M. Chan, *Low-Energy Electron Diffraction*; (Springer-Verlag, Heidelberg, 1986) p. 305.

[23]A. Cornu and R. Massot, *Compilation of Mass Spectral Data*; 2nd ed., (Heyden, London, 1975).

[24]R. Gomer, Rep. Prog. Phys. **53**, 917 (1990).

[25]J. L. Brand, M. V. Arena, A. A. Deckert, and S. M. George, J. Chem. Phys. **92**, 5136 (1990); E. D. Westre, M. V. Arena, A. A. Deckert, J. L. Brand, and S. M. George, Surf. Sci. **233**, 293 (1990).

[26]S. C. Wang and G. Ehrlich, Phys. Rev. Lett. **68**, 1160 (1992); S. C. Wang and G. Ehrlich, J. Chem. Phys. **94**, 4071 (1991); S. C. Wang and G. Ehrlich, *Surf. Sci.* **239**, 301 (1990).

[27]S. C. Wang and G. Ehrlich, Phys. Rev. Lett. **70**, 41 (1993); S. C. Wang and G. Ehrlich, Phys. Rev. Lett. **67**, 2509 (1991).

[28]J. S. Nelson and P. J. Feibelman, Phys. Rev. Lett. **68**, 2188 (1992); C. M. Gilmore, J. A. Sprague, J. M. Eridon, and V. Provenzano, Surf. Sci. **218**, 26 (1989).

[29]J. E. Parmeter, R. Kunkel, B. Poelsema, L. K. Verheij, and G. Comsa, Vacuum **41**, 467 (1990); M. Bott, Th. Michely, and G. Comsa, Surf. Sci. **272**, 161 (1992).

[30]This result is further supported by previous studies of the dissociative adsorption of H_2 on the defect sites of this same Ir(111) crystal, in which the fractional coverage of defects was found to be ~0.025 monolayer. [J. R. Engstrom, W. Tsai, and W. H. Weinberg, J. Chem. Phys. **87**, 3104 (1987).] In this work, the step density has been found to be 0.013 ± 0.003 monolayer as derived from the Laue X-ray diffraction data. Thus, the step density on this Ir(111) surface is one-half that of the defect site density.

[31]M. Tüshaus, E. Schweizer, P. Hollins, and A. M. Bradshaw, J. Electron Spectrosc. Relat. Phenom. **44**, 305 (1987).

[32]X. D. Zhu, Th. Rasing, and Y. R. Shen Phys. Rev. Lett. **61**, 2883 (1988).

[33]T.-S. Lin, H.-J. Lu, and R. Gomer, Surf. Sci. **234**, 251 (1990).

[34]E. G. Seebauer, A. C. F. Kong, and L. D. Schmidt, J. Chem. Phys. **88**, 6597 (1988).

[35]L. R. Becerra, C. A. Klug, C. P. Slichter, and J. H. Sinfelt, J. Phys. Chem. **97**, 12014 (1993).

[36]M. A. Van Hove, W. H. Weinberg, and C.-M. Chan, *op. cit.*, p. 265.

TABLE I. Computations for the evaluation of the initial reaction probabilities, P_r^*, of 1,2-di-^{13}C-C_2H_6 at defect sites of step edges on the Ir(111) surface[a]

T_S (K)	$P_{r,app}$ (x10^3)[b]	$P_{r,net}$ (x10^3)[b]	r_D (Å)[c]	$\frac{n_s}{n_s^*}\left(\frac{w_d}{w_t+w_d}+P_{D,Ts}^*\frac{w_t}{w_t+w_d}\right)$	P_r^* (x10^2)	$\frac{k_d^*}{k_h^*}$ (x10^2)[d]	$\frac{P_r^*}{(1-P_r^*)}\left(\frac{k_d^*}{k_h^*}+1\right)$ (x10^2)
350	1.313	1.098	96.33	0.175	0.627	0.2745	0.633
400	2.518	2.171	59.35	0.105	2.064	0.7231	2.123
483	3.523	2.903	33.13	0.0645	4.500	2.319	4.822
500	4.243	3.562	30.12	0.0593	5.923	2.807	6.473
528	4.398	3.613	26.08	0.0521	6.928	3.742	7.723
575	4.658	3.692	21.14	0.0447	8.256	5.695	9.512
625	4.551	3.386	17.49	0.0371	9.123	8.305	10.87
700	4.625	3.158	13.87	0.0308	10.26	13.22	12.95
750	4.627	2.960	12.18	0.0278	10.65	17.12	13.95
825	4.873	2.911	10.35	0.0246	11.84	23.78	16.62
950	4.962	2.531	8.324	0.0210	12.03	36.66	18.68
1100	5.237	2.289	6.842	0.0185	12.40	54.10	21.82
1250	5.086	1.672	5.902	0.0169	9.870	72.73	18.91

[a]Refer to the text for details of the diffusive and precursor-mediated models employed.

[b]The apparent and the net probabilities of reaction, $P_{r,\,app}$ and $P_{r,net}$, are provided here and in Fig. 2 without the inclusion of diffusive impingement at the step edges. $P_{r,net}$ is computed from $P_{r,\,app}$ with knowledge of the dissociative probability of ethane on the smooth Ir(111) surface.[3] See text for details.

[c]Derived from the mean-square-displacement for the ethane molecule executing a random walk with the diffusion rate parameters taken to be $E_D = 0.30\ E_d = 2.31$ kcal/mol, $D_0 = 10^{-3}$ cm s^{-2}.

[d]Derived from the following assumed values of the elementary rate parameters for the desorption and migratory hopping (diffusion) rate coefficents: $E_d = 7.7$ kcal/mol, $E_h = E_D = 2.31$ kcal/mol; $k_d^{(0)} = 10^{13}$ s^{-1}, and $k_h^{(0)} = n_S D_0 = 1.57 \times 10^{12}$ s^{-1}.

TABLE II. Sensitivity analyses for the dependence of the calculated reaction rate coefficient at the defect sites on Ir(111)[a]

$w_t, (\text{Å})$	$D_0, \left(\frac{cm^2}{s}\right)$	$k_h^{(0)}, s^{-1} (10^{-12})$	$E_D = E_h^*$ (cal/mol)	$\frac{k_r^{(0)*}}{k_h^{(0)*}}$	$k_r^{(0)*}, s^{-1} (10^{-11})$	$E_r^* - E_h^*$ (cal/mol)	E_r^* (cal/mol)
181.5	10^{-2}	15.7	2310	0.096	15.1	1920	4230
181.5	$10^{-2.5}$	4.97	2310	0.178	8.82	1960	4270
181.5	10^{-3}	1.57	2310	0.381	5.98	2140	4450
181.5	$10^{-3.5}$	0.497	2310	1.40	6.94	2850	5160
181.5	10^{-4}	0.157	2310	8.02	12.6	3900	6210
181.5	10^{-3}	1.57	3080	0.324	5.08	2200	5280
181.5	10^{-3}	1.57	1540	0.222	3.48	1890	3430
149.4	10^{-3}	1.57	2310	0.307	4.82	2130	4440
231.0	10^{-3}	1.57	2310	0.502	7.88	2170	4480
149.4	$10^{-3.5}$	0.497	2310	1.11	5.52	2830	5140
231.0	$10^{-3.5}$	0.497	2310	1.88	9.32	2890	5200

[a]Comparisons of the computed results from Equation (16) for selected sets of the rate coefficients as indicated. For all cases, $k_d^{(0)} = 10^{13}\ s^{-1}$, $k_r^{(0)} = 10^{11}\ s^{-1}$, $E_d = E_d^* = 7700$ cal/mol, and $E_r = 10{,}300$ cal/mol. The values of the activation energy for reaction at the surface defect site, E_r^*, are expressed with respect to the bottom of the physically adsorbed well at the defect site.

Figure Captions

Figure 1. (a) Top and side-on views of the step edge on the Ir(111) surface. The "descending" and "ascending" step defect sites are identified on the shaded and unshaded terraces, respectively. (b) Top and side-on views of the idealized terrace of width, w_t, with a molecule physically adsorbed at the point, Q, a distance, x, from the adjacent step. The side-on view also depicts the assumed potential for the migration of the physically adsorbed ethane across the step edge. The "ascending" and "descending" defect sites at the step edges are indicated.

Figure 2. The initial probabilities of dissociative chemisorption of C-13 labeled ethane obtained from low conversions of ethane and low coverages of deposited carbon. The apparent probability of reaction, $P_{r,app}$, (closed circles) is the measured probability without accounting for surface diffusion and includes contributions from reaction at terrace sites as well as from reaction at defect sites. The net probability, $P_{r,net}$, (open triangles) is the measured apparent probability of reaction at the defect sites.

Figure 3. Plot of the lhs of Eq. 17 (closed circles) for the values computed in Table 1. The straight line is a linear regression fit to the data from 500 to 1250 K. The corresponding data for the probability of reaction at the defect sites, P_r^*, (open circles) are shown and are not included in the regression analysis.

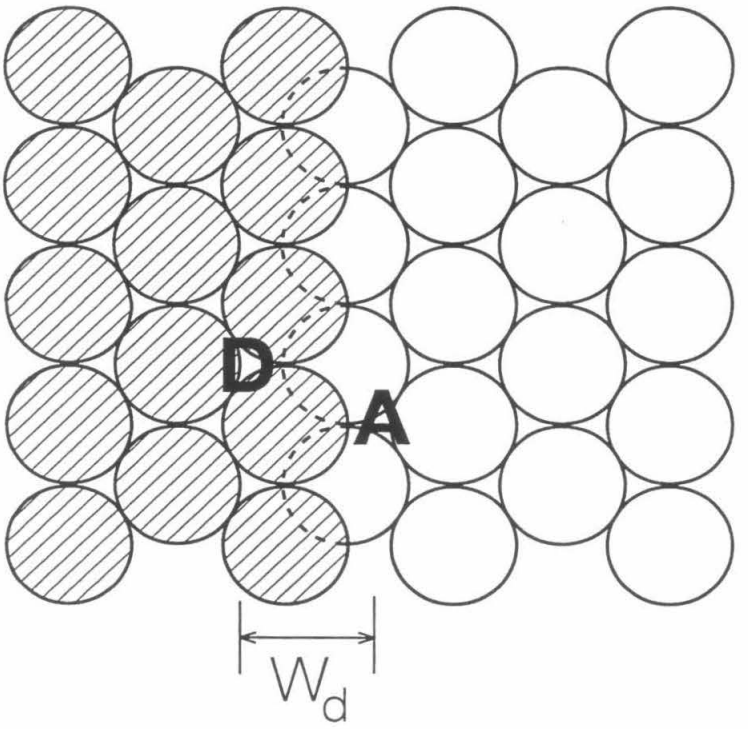

Top View

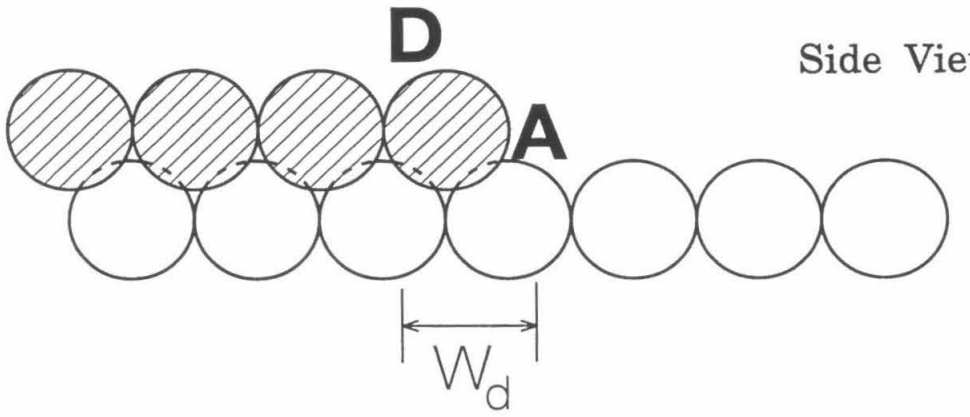

Side View

Figure 1a

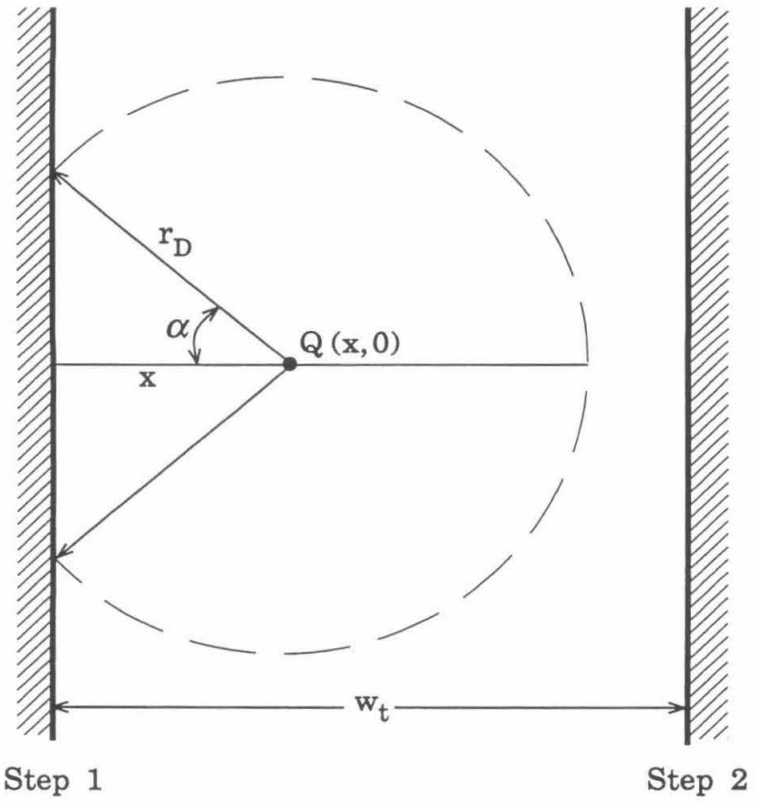

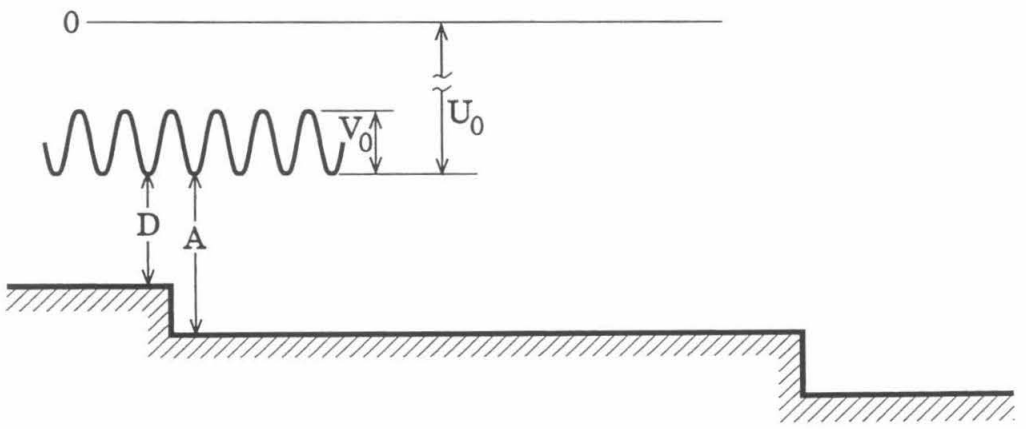

Figure 1b

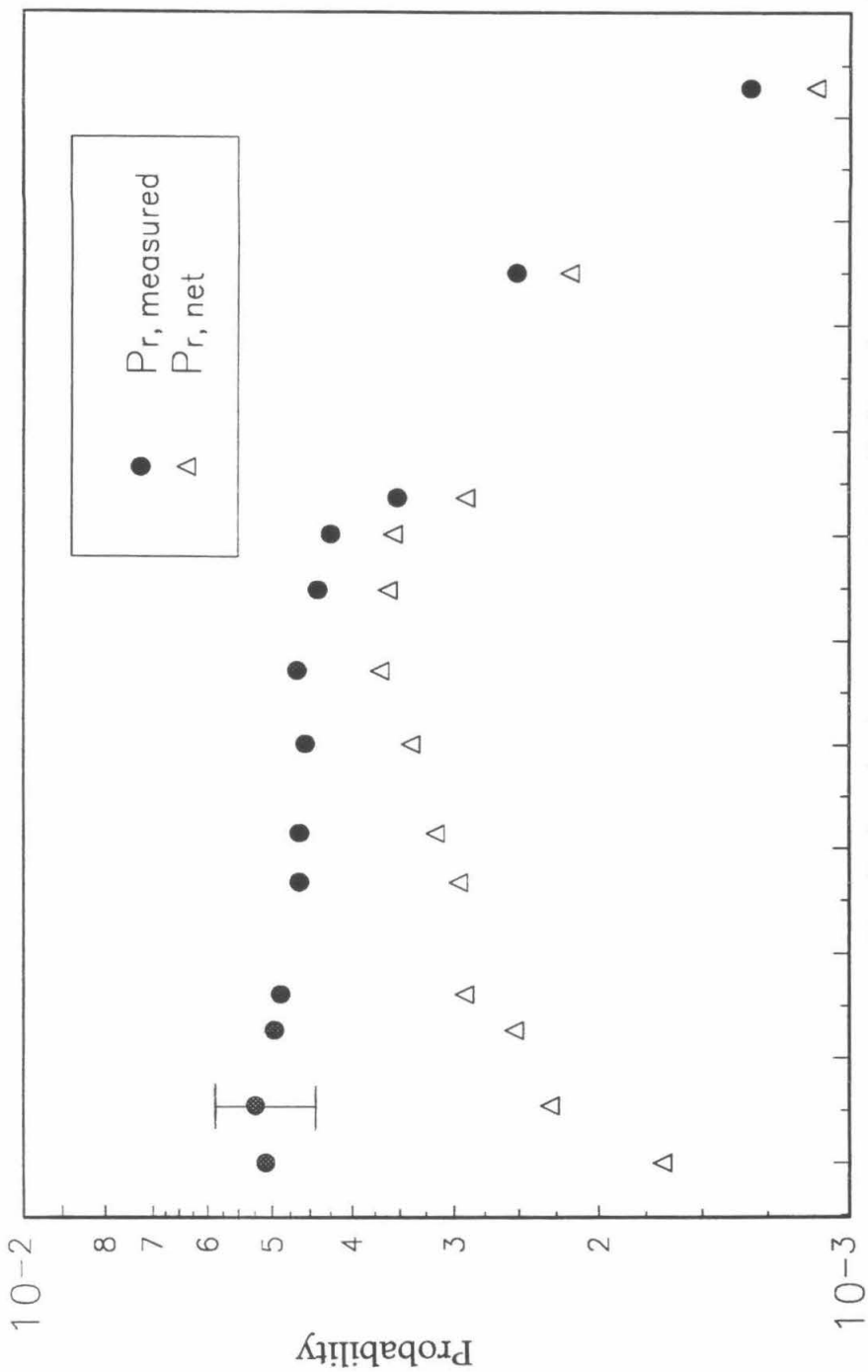
$^{13}C-C_2H_6$ Activation at Defects of Ir(111)
$P_{r,\ measured}$
$P_{r,\ net}$
Probability
10^{-2}
8
7
6
5
4
3
2
10^{-3}
0.8 1.0 1.2 1.4 1.6 1.8 2.0 2.2 2.4 2.6 2.8 3.0
$1000/T_s,\ (K^{-1})$

Figure 2

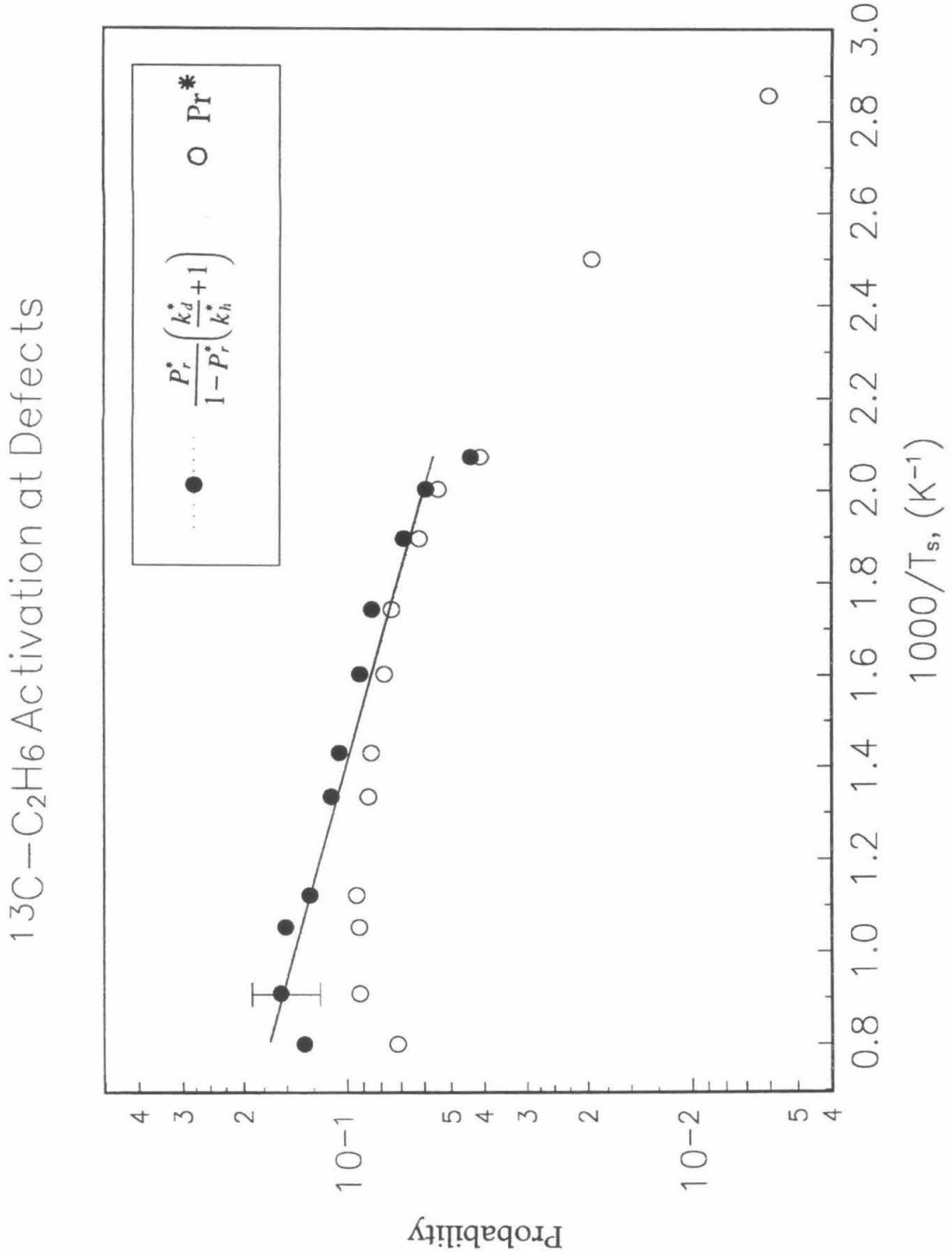
13C−C2H6 Activation at Defects
$\frac{P_r'}{1-P_r'}\left(\frac{k_d'}{k_h'}+1\right)$
Pr*
Probability
10−1
10−2
0.8 1.0 1.2 1.4 1.6 1.8 2.0 2.2 2.4 2.6 2.8 3.0
1000/Ts, (K−1)

Figure 3

CHAPTER 5

Quantification of the Selective Activation of C-H Bonds in Short Chain Alkanes: The Reactivity of Ethane, Propane, Isobutane, n-Butane, and Neopentane on Ir(111)

[The text of Chapter 5 consists of an article coauthored with W. H. Weinberg, which has been submitted to *Journal of the American Chemical Society*.]

Abstract: The initial probabilities of precursor-mediated, dissociative chemisorption of the saturated hydrocarbons ^{13}C-labeled ethane, propane, isobutane, n-butane, and neopentane on the close-packed Ir(111) surface have been measured. The selective activation of primary (1°), secondary (2°), and tertiary (3°) C-H bonds has been quantified by examining the reactivities of the selectively deuterated isotopomers of propane, C_3H_8, $CH_3CD_2CH_3$, and C_3D_8, and of isobutane, i-C_4H_{10}, $(CH_3)_3CD$, and $(CD_3)_3CH$ With respect to the bottom of the physically adsorbed well for each hydrocarbon, the apparent C-H bond activation energies have been found to be 10.4 ± 0.2 kcal/mol (ethane), 11.4 ± 0.2 kcal/mol (propane), 11.5 ± 0.2 kcal/mol (*n*-butane), 11.4 ± 0.2 kcal/mol (*i*-butane), and 11.5 ± 0.2 kcal/mol (neopentane). For all the alkanes examined, the ratios of the preexponential factors of the rate coefficients of reaction and desorption are $1x10^{-2}$. The C-D bond activation energies are higher than the corresponding C-H bond activation energies by 480 cal/mol (ethane), 630 cal/mol (propane), and 640 cal/mol (*i*-butane). By analyzing the primary kinetic isotope effects for the selectively deuterated isotopomers of propane and isobutane, the 2° C-H bond activation energy is found to be 310 cal/mol less than the 1° C-H bond activation energy on this surface, and, similarly, 3° C-H bond cleavage is 83 cal/mol less. The quantification of the branching ratios within the C-H bond activation channel for propane and isobutane on this surface shows that the formation of 1°-alkyl intermediates is, in general, favored over the formation of either 2°- or 3°-alkyl intermediates. This result is a direct consequence of the disproportionate number of 1° C-H bonds relative to the number of 2° and 3° C-H bonds in these alkanes. These results are compared to those for the reaction of these alkanes on the reconstructed Pt(110)-(1x2) surface, and the influence of surface structure on the selective activation of 1°, 2°, and 3° C-H bonds is discussed.

1. Introduction

The design of selective catalysts for the commercial reforming and isomerization of hydrocarbons is a critical, yet elusive, goal in the field of heterogeneous catalysis (**1**). The efficient conversion of natural gas into fuel and chemical feedstock compounds is another area of intense research, one requiring optimized catalysts of high activity and precise selectivity (**2**). The development of any catalyst for these applications will be achieved only by the complete characterization of its intrinsic reactivities for the selective activation of the bonds of interest. Reactions which compete and reduce the overall efficiency of the process, such as hydrogenolysis and catalyst coking, must be understood at their most fundamental levels in order to optimize the chosen catalytic system. To prove successful in these applications, the catalyst must selectively activate the strong C-H and C-C bonds in the alkanes used as process feed streams. Because of the strength of these alkane C-H and C-C bonds (**3**), the combination of high temperatures and pressures with active catalysts is generally required. Such extreme conditions, however, are counterproductive in effecting the desired chemical selectivity. The optimization of the selective conversion of these hydrocarbons may be achieved only with the knowledge afforded from the quantification of their elementary C-H and C-C bond activation reactions.

To this end, we have investigated the dissociative chemisorption of ethane, propane, isobutane, and their deuterated isotopomers on Ir(111). Our results enable us to quantify the selective activation of primary, secondary, and tertiary C-H bonds for these alkanes on this surface. In an extension of our examination of alkane activation on this surface, we have studied the dissociative chemisorption of perhydrido isotopomers of n-butane and neopentane. In addition to activating C-H bonds, the Ir(111) surface is

observed to catalyze the activation of C-C bonds, except for the case of ethane. The full analysis of the kinetic rate parameters of this competing C-C bond activation channel is reported in the manuscript following this article (**4**).

Precursor-Mediated Kinetic Model

The study of alkane activation by single crystalline transition metal surfaces reveals that two fundamentally different reaction mechanisms may be operative: (i) direct dissociation, and (ii) trapping-mediated, dissociative chemisorption (**5**, **6**). Direct dissociation occurs on the time scale of a collision between the gas-phase molecule and the surface ($<10^{-12}$ s), and the rate of this reaction depends primarily on the translational and internal energies of the gas-phase molecule. The trapping-mediated kinetic model, depicted in Scheme I, illustrates the elementary reactions leading to either C-C or C-H bond activation of an alkane molecule on the catalytic surface (**7**). To illustrate with a general example, we apply the model to an alkane, RH, (such as propane or isobutane) for which there are two C-H bond activation channels, characterized by the elementary rate coefficients for reaction, $k_{r1,CH}$ and $k_{r2,CH}$, and one C-C activation channel, characterized by the elemetary rate coefficient, $k_{r,CC}$.

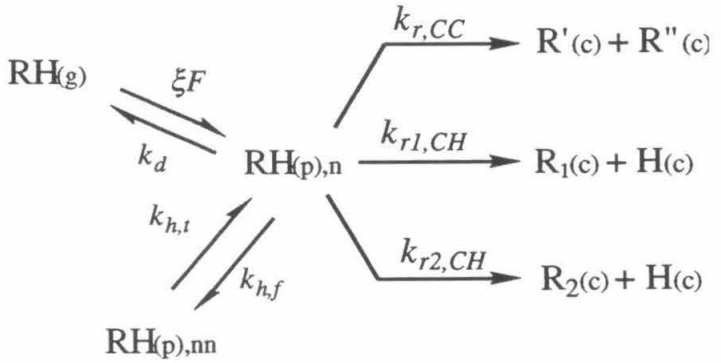

SCHEME I

The impinging gas-phase molecule, RH(g), is first trapped in the potential energy field of the catalyst surface, where it then thermally accommodates to the surface temperature, T_S, in a physically adsorbed state, RH(p), at the *n*th site of the surface. From this physically adsorbed state, the molecular precursor may execute one of the following elementary steps: (1) it diffuses via single-site hopping to one of its nearest neighbor, *nn*, sites with a rate coefficient $k_{h,f}$; (2) it reversibly desorbs to the gas phase with a rate coefficient of k_d; or (3) it reacts on the surface via one of the three available channels with the rate coeffiecients defined above. Migratory hopping into the *n*th site from its nearest neighboring sites may also occur with a rate coefficient $k_{h,t}$. The elementary rate coefficients for these surface reactions are of the Polanyi-Wigner form, namely,

$$k_i = k_i^{(0)} e^{-E_i/k_B T_s} \tag{1}$$

For the dissociative chemisorption of these alkanes, the initial C-H or C-C bond cleavage is irreversible and rate-limiting, and the resulting chemisorbed alkyl intermediates undergo further dehydrogenation, and ultimately complete decomposition, to form a carbonaceous residue. The relative rates of the two competing reactions are dependent on the surface temperature, provided the associated activation energy of desorption, E_d, and the relevant activation energy of reaction, E_r, are not equal. The gas temperature is important only insofar as it affects the probability of trapping, ξ, into the physically adsorbed state.

The time rate of change of the fractional coverage of the physically adsorbed alkane, θ_{RH}, derived from Scheme I, is

$$\frac{d\Theta_{RH}}{dt} = \xi F + k_{h,t}\Theta_{RH} - \left(k_d + k_{r1,CH} + k_{r2,CH} + k_{r,CC} + k_{h,f}\right)\Theta_{RH} \tag{2}$$

where the subscripts g, p, and c denote gaseous, physically adsorbed and chemisorbed states, respectively, and F is the impingement rate onto the surface from the gas-phase. This rate law may be expanded to include any number of additional surface kinetic events, such as including a second C-C bond scission channel for longer chain alkanes, such as n-butane. The simplification of this rate expression is possible by accounting properly for the effect of surface diffusion in the overall kinetic rate law, and by recognizing that under our experimental conditions, extremely low concentrations of the physically adsorbed precursors are always maintained.

The geometric structure of the Ir(111) surface is a mixture of two types of sites: the more abundant, but less reactive close-packed, terrace sites, and the more reactive, but less abundant, surface defect sites. The surface concentration of the terrace sites is about 70 to 100 times that of the concentration of the steps (**8**). As will be discussed in our Sect. 2, we ensure that the amount of converted alkane substantially exceeds the surface concentration of defect sites but is still sufficiently low enough to measure the kinetic rate characteristic of the clean close-packed, terrace sites. Furthermore, the microscopic reversibility of the surface diffusion resulting from the precise equivalency of neighboring terrace sites renders the fractional coverage of the adsorbed precursor the same for all terrace sites (**8**). As a result, the terms on the right hand side of Eq. 2 describing the rate of migratory hopping into the nth site, $k_{h,t}\,\theta_{RH}$, and the rate of migratory hopping from the nth terrace site, $k_{h,f}\,\theta_{RH}$, exactly cancel one another. However, in the evaluation of the kinetic rate processes at surface defect sites (achieved with purposefully low conversions of the alkane), the equivalency of neighboring sites is lost, and diffusion must be included explicitly in the precursor-mediated kinetic model (**8**).

If the surface temperature is sufficiently high that the fractional coverage of the physically adsorbed alkane is small, then a pseudo-steady-state analysis may be applied to Eq. 2 (**9**). This procedure yields the following set of expressions for the probabilities of alkane activation, $P_{r1,CH}$, $P_{r2,CH}$, and $P_{r,CC}$, which are each defined as the ratios of their respective reaction rates, $R_{r1,CH}$, $R_{r2,CH}$, and $R_{r,CC}$, to the gas-phase impingment rate , F:

$$P_r \equiv \frac{R_r}{F} \tag{3}$$

$$P_{r1,CH} = \frac{\xi k_{r1,CH}}{k_d + k_{r1,CH} + k_{r2,CH} + k_{r,CC}} \tag{4a}$$

$$P_{r2,CH} = \frac{\xi k_{r2,CH}}{k_d + k_{r1,CH} + k_{r2,CH} + k_{r,CC}} \tag{4b}$$

$$P_{r,CC} = \frac{\xi k_{r,CC}}{k_d + k_{r1,CH} + k_{r2,CH} + k_{r,CC}}. \tag{4c}$$

By definition, the reaction probabilities are all individually separable, and their sum is the total *measured* reaction probability, $P_{r,total}$. Because of the different temperature dependences of each reaction channel, these measurements for the total probability will not yield, in general, straight lines when cast as semilogarithmic plots in a standard Arrhenius construction (*vide infra*). The challenge is to extract kinetic information attributable to the individual elementary reactions from measurements of only the total probability. In general, Eq. 4 implies that

$$\frac{\xi}{P_{r1,CH}} - 1 = \frac{k_d}{k_{r1,CH}} + \frac{k_{r2,CH}}{k_{r1,CH}} + \frac{k_{r,CC}}{k_{r1,CH}} \tag{5a}$$

$$\frac{\xi}{P_{r2,CH}} - 1 = \frac{k_d}{k_{r2,CH}} + \frac{k_{r1,CH}}{k_{r2,CH}} + \frac{k_{r,CC}}{k_{r2,CH}} \tag{5b}$$

$$\frac{\xi}{P_{r,CC}} - 1 = \frac{k_d}{k_{r,CC}} + \frac{k_{r1,CH}}{k_{r,CC}} + \frac{k_{r2,CH}}{k_{r,CC}}. \tag{5c}$$

For the special case of $k_d >> k_{r1,CH} + k_{r2,CH} + k_{r,CC}$, Eq. 4 reduces to

$$P_{r1,CH} \cong \frac{\xi k_{r1,CH}}{k_d} \tag{6a}$$

$$P_{r2,CH} \cong \frac{\xi k_{r2,CH}}{k_d} \tag{6b}$$

$$P_{r,CC} \cong \frac{\xi k_{r,CC}}{k_d}. \tag{6c}$$

From our experimental observations of alkane activation on Ir(111), the contribution to the total probability by the C-C activation channel can be separated from those of the two C-H activation channels. At sufficiently low surface temperatures, conservatively, < ~400 K for these alkanes, the contribution from the C-C activation channel is observed to be negligible. On the other hand, over no temperature range in these experiments (for the activation of propane and isobutane) are the two competing C-H reaction channels separable from one another.

In order to determine the separate kinetics of the competing C-H bond activation reactions, we examine the deuterium kinetic isotope effects (KIE's) for selectively labeled isotopomers of propane and isobutane. In this way, each isotopomer yields an *apparent* Arrhenius dependence with temperature, in which the derived kinetic rate parameters, the activation energies, and the preexponential factors are actually combinations from the two competing C-H bond activation channels. Thus, it is more appropriate to write a single *apparent* rate coefficient for C-H bond activation, $k_{r,CH}$, in Eqs. 2 – 6 above than to continue to distinguish them explicitly as $k_{r1,CH}$ and $k_{r2,CH}$. We

shall adopt this nomenclature hereafter, but implicit in its use is its embodiment of two *independent* rate coefficients.

For the activation of all the alkanes examined here on Ir(111), we have found experimentally that $k_{r,CH} + k_{r,CC} << k_d$, and, combining Eqs. (1) and (6) yields

$$\frac{P_{r,CH}}{\xi} \cong \frac{k_{r,CH}^{(0)}}{k_d^{(0)}} e^{-(E_{r,CH}-E_d)/k_B T_s}, \tag{7a}$$

and

$$\frac{P_{r,CC}}{\xi} \cong \frac{k_{r,CC}^{(0)}}{k_d^{(0)}} e^{-(E_{r,CC}-E_d)/k_B T_s}. \tag{7b}$$

In the application of the trapping-mediated kinetic model to the selective activation of alkanes, Eq. 7a will apply to each type of C-H bond. We will quantify the rate coefficients of the intrinsic reactivities of the primary, secondary, and tertiary C-H bonds, each with their respective activation energies $E_{r,1}$, $E_{r,2}$, and $E_{r,3}$. We will subsequently use these results to determine the temperature dependence of the branching ratios of the dissociative chemisorption of propane and isobutane on Ir(111), and in this way, quantify the selective activation of these alkanes on this surface.

2. *Experimental Methods*

The measurements on the Ir(111) surface were carried out in a 200 l/s ion-pumped UHV microreactor which has a base pressure of 2×10^{-10} Torr and a volume of 10 cm^3 (**10**). The Ir(111) crystal was cut, polished, and prepared with standard techniques, and its crystallographic orientation was found to be 0.70° ± 0.15° by Laue X-ray diffraction methods. The crystal surface was cleaned between experiments by heating to 1000 K for 5 min at an O_2 pressure of 5×10^{-8} Torr flowing continuously through the reactor,

followed by annealing to 1625 K for 1 min to desorb the surface oxygen. Thermal desorption spectra of CO, which were in complete agreement with previously published ones from the clean Ir(111) surface (**11**), were measured frequently to verify the cleanliness of the surface. Furthermore, because kinetic data are known to be extremely sensitive to surface conditions, the high degree of reproducibility in the data presented here indicates the absence of surface contamination.

For the dissociative chemisorption of the alkanes over the surface temperature range that was employed ($310 < T_S < 1100$ K), the system was operated in a continuous flow mode. With the crystal held at a constant temperature, an alkane pressure of 1.0×10^{-7} Torr was maintained for a reaction time, τ. The amount of dissociated alkane was determined by titrating the carbonaceous residue with excess oxygen, producing exclusively carbon dioxide ($^{13}CO_2$ in the case of ^{13}C-labeled ethane). Under these experimental conditions the dissociative chemisorption of the alkane is irreversible, and no gas-phase carbon-containing products of a surface self-hydrogenolysis reaction are formed. The titration conditions and procedure were optimized to ensure the complete oxidation of the surface carbon to CO_2.

The integrated signal from a UTI-100C quadrupole mass spectrometer was combined with its calibrated sensitivity to the titration product, carbon dioxide, to obtain the total number of C-adatoms on the surface, N_C, The reaction conditions and times were such that the fractional coverage, θ_C, was between 5% and 10% of a monolayer of carbidic carbon. The lower limit ensures that the results are not dominated by reactivity at surface defects (**12**), whereas the upper limit ensures that the initial rate of the C-H activation reaction has been measured, *i. e.,* the rate is approximately

characteristic of a clean Ir(111) surface. At a given surface temperature, T_S, the total dissociative chemisorption probability, $P_{r,total}(T_S)$, is obtained from

$$P_{r,total}(T_s) = \frac{N_C}{nA\tau F_{gas}}, \tag{8}$$

where A is the sample surface area (cm^2), F_{gas} is the impingement flux of reactant alkane (molecules cm^{-2} s^{-1}), and the stoichiometric factor of n converts N_C into the number of reacted alkane molecules, e.g., n = 2 for ethane.

All gases were introduced into the microreactor from a gas-handling manifold that was pumped with a diffusion pump to a base pressure below 10^{-7} Torr. Carbon-13 labeled ethane (1,2-di-^{13}C-C_2H_6, 99 atom % ^{13}C) was obtained from Icon Services. The C_3H_8 (99.5%) was obtained from Matheson, and both the $CH_3CD_2CH_3$ (98 atom % D) and the C_3D_8 (99.5 atom % D) were obtained from MSD Isotopes. The i-C_4H_{10} (99.5%) was obtaind from Matheson, and both the i-$(CH_3)_3CD$ (97.5 atom % D) and the i-$(CD_3)_3CH$ (99 atom % D) were obtained from MSD Isotopes. The n-C_4H_{10} was obtained from Matheson (99.5%), and the $(CH_3)_4C$ was obtained from Phillips Chemical Company (~95%). The selectively deuterated gases were used without further purification, whereas the perhydrido samples were fractionally distilled from cryogenic hexane ice/liquid hexane baths. In this procedure, upon condensing the hydrocarbon at liquid hexane temperature (~180 K) and then allowing the sample mixture to warm slowly to room temperature, the low and high temperature boiling fractions were eliminated by the diffusion pumping of the gas-handling mainfold, while the center

fraction of the vaporizing condensate was collected in a clean, empty receiving flask.

3. Results

The measured initial probabilities of chemisorption of all alkanes studied in this work are plotted as functions of reciprocal surface temperature in Figs. 1a – 1d. The distinct non-Arrhenius behavior observed for propane, isobutane, n-butane, and neopentane were shown not to be artifactual by repeating the measurements for ^{13}C-labeled ethane. Ethane measurements made prior to the experiments with propane, isobutane, and n-butane, and published elsewhere (**13**), were reproduced well within experimental error after the propane, isobutane, and n-butane experiments had been run. The two independent ethane measurements yielded apparent activation barriers, $E_r - E_d$, that differed by only 90 cal/mol (2620 versus 2710 cal/mol), while the ratio of the desorption to reaction preexponential factors, $k_r^{(0)}/k_d^{(0)}$, were reproduced to within 3% (1.06×10^{-2} versus 1.03×10^{-2}). The combined data of the two independent sets of experiments for ethane activation on Ir(111) are displayed in Fig. 1a. Deviations from Arrhenius behavior are not uncommon (**14**), and in the present instance, Figs. 1b – 1d, are interpreted to arise from a second reaction channel, namely one with a stronger surface temperature dependence: initial C-C bond activation (**4**).

The analysis performed to extract and separate the kinetic information contained in the plots of Fig. 1 for the competing channels of C-C and C-H bond activation will be explained fully here. The discussion of the individual reaction channels, however, has been divided into a pair of consecutive papers in this journal: this paper addressing the selective activation of C-H

bonds, and the the next paper addressing the separate issue of the activation of C-C bonds (**4**).

The separation of the kinetic data for the C-H (and C-D) and C-C reaction channels in the plots of total reactivity of Fig. 1 is achieved by an iterative procedure. An initial value for the apparent rate parameters of C-H bond activation was derived from the data at low temperature, where the contribution from the competing channel of C-C bond activation is considered negligible. Extrapolating across the full temperature range provides initial estimates of the contribution to the total reaction probability from the C-H bond activation channel at each of the experimental surface temperatures. Subtracting these contributions from the total signal then yields the initial estimates of the competing C-C reaction channel. The computed apparent rate parameters for this second channel then provide, after extrapolation across the experimental temperature range, the correction to the C-H rate parameters to be applied in the second iteration of the calculation.

The final, extracted data sets from this process are plotted with their least squares regression fits in Figs. 2 – 5 for propane, isobutane, n-butane, and neopentane, respectively. The effect of selective deuteration on the kinetic rates of dissociative chemisorption via the C-H bond activation channel is seen clearly in Figs. 6 and 7, where the regression fits of the three isotopomers of propane (C_3H_8, $CH_3CD_2CH_3$, and C_3D_8) and of isobutane (i-C_4H_{10}, $(CH_3)_3CD$, and $(CD_3)_3CH$) are provided. The semilogarithmic plot of P_r as a function of reciprocal surface temperature yields the apparent kinetic parameters of the elementary C-H bond scission reactions. From Eq. 6, the slope of the straight lines in these Arrhenius constructions are equal to $-(E_r - E_d)/k_B$, and the intercepts are equal to $k_r^{(0)}/k_d^{(0)}$.

Table 1 provides the apparent activation energies, $E_{app} = E_r - E_d$, and the apparent preexponential ratios, $k_r^{(0)}/k_d^{(0)}$, for the C-H bond activation of these alkanes on the Ir(111) surface. Because the activation energies and preexponential factors for desorption, E_d and $k_d^{(0)}$, of the physically adsorbed alkanes have been determined in separate experiments (**15**), the apparent activation energies for reaction, E_r, and the apparent preexponential factors, $k_r^{(0)}$, can be calculated. The value of the preexponential factors of desorption for all the alkanes has been taken to be 10^{13} s^{-1} (**7**, **16**). The ratio of prefactors, $k_d^{(0)}/k_r^{(0)}$, is greater than unity for all the alkanes, a result which is expected in view of the greater entropy associated with the transition state for desorption relative to the transition state for C-H bond activation (**6**).

In analyzing the data for the probability of trapping-mediated dissociative chemisorption of alkanes on transition metal surfaces, we have used the knowledge that the trapping probability, ξ, is only a weak function of the surface temperature (**17**). The collisional dynamics between an impinging molecule and a solid surface dictate the magnitude of the trapping probability, and this topic has been examined theoretically and with molecular beam techniques by many research groups (**18**). The rapid, efficient dissipation of the normal component of the incident momentum of the molecule is what controls its ability to become trapped in the potential of the surface. Accommodating to the surface temperature requires that the molecule's excess internal energy and its incident momentum parallel to the surface be dissipated such that the entire system attains a state of thermal equilibrium. The low incident kinetic energies associated with an effusive beam at room temperature (~25 meV) coupled with the large vibrational manifold of these alkane molecules implies that it is eminently reasonable to assume that ξ is unity for these 'bulb' experiments. In fact, the molecular

beam experiments of Mullins, *et al.* of the trapping probability of ethane on the Ir(110)-(1x2) surface demonstrate that even for the lowest attainable beam energies possible in their system (> 50 meV), the molecular trapping probability approaches unity, 97± 2% (**19**).

It is noteworthy that as a group, the ratios of the preexponential factors, $k_d^{(0)}/k_r^{(0)}$, are all equal within experimental uncertainty, because this uniformity gives strong evidence that the same mechanism is operating to cleave the C-H bonds within all these alkanes. Were drastically different prefactors obtained for the different alkanes, or for the different isotopomers within a labeled group, then it would be possible to argue that different mechanisms for C-H bond activation were responsible for the results. However, with all of the hydrocarbons yielding the same value for the prefactors, it appears that the available phase space sampled by each reacting precursor is comparable. As distinct as each particular transition state for 1°, 2°, and 3° C-H bond activation may be, the corresponding transition state entropies of the molecules at the saddle point would appear to be indistinguishable.

In view of the fact that the plot of P_r as a function of reciprocal temperature for $CH_3CD_2CH_3$ in Fig. 6 lies on neither the perhydrido- nor on the perdeutero-propane data, it is obvious that both 1° and 2° C-H bond cleavage are occurring. If only 1° C-H bond activation were operative, then for the propane experiments, the results of C_3H_8 and $CH_3CD_2CH_3$ would be coincidental; whereas if only 2° C-H bond activation occurring, then the C_3D_8 and $CH_3CD_2CH_3$ results would coincide. Because neither of these two conditions is observed, it must be concluded that activation of both of the two available C-H bonds is operating for propane on this surface. As seen in Fig. 7, the similar separability of the rate data for the isotopomers of isobutane

indicates that both 1° and 3° C-H bond cleavage is occurring in this case. Thus, some fraction of each alkane is reacting via 1° C-H bond cleavage, and the remainder is reacting via 2° (or 3°) C-H bond cleavage. The apparent rate parameters derived from Figs. 6 and 7 are presented in Table 1, and each of them is a combination of the rate coefficients of the two respective competing dissociation channels. The evaluation of the independent rate parameters for the formation of primary, secondary, and tertiary propyl and isobutyl reaction products, as well as the intrinsic competition in the activation of 1°, 2°, and 3° C-H bonds is discussed below.

4. Discussion

The availability of two reaction channels for C-H bond activation implies that the branching between primary and secondary propyl intermediates, and between primary and tertiary isobutyl intermediates, must be included in the reaction rate processes depicted in Scheme II below.

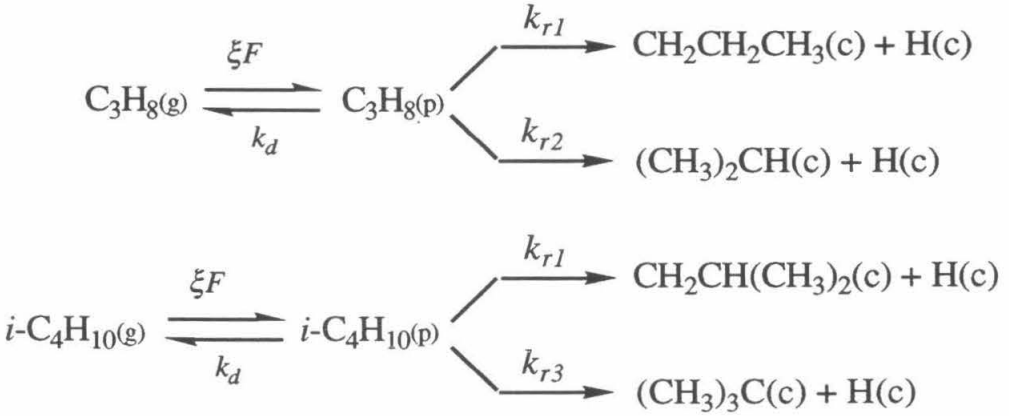

SCHEME II

The measured initial probabilities of dissociative chemisorption for these alkanes are the combined rates of the two reactive channels: for propane,

$$P_r = \frac{k_{r1} + k_{r2}}{k_{r1} + k_{r2} + k_d}, \tag{9}$$

and for isobutane,

$$P_r = \frac{k_{r1} + k_{r3}}{k_{r1} + k_{r3} + k_d}. \tag{10}$$

Our experiments have measured these combined probabilities of reaction, and the challenge to obtain the independent rate coefficients, k_{r1}, k_{r2}, and k_{r3}, is met by analyzing the kinetic isotope effects observed in the data of Figs. 6 and 7. The quantification of the rate coefficients for the selective activation of the 1°, 2°, and 3° C-H bonds begins with the definition of the conditional probabilities, $\tilde{P}_p$, $\tilde{P}_s$, and $\tilde{P}_t$, that primary, secondary, and tertiary *alkyl* intermediates are formed upon reaction of the precursor alkane molecule.

Propanes

We will demonstrate the methodology with the case of propane activation. Under the condition that the propane molecule reacts, $\tilde{P}_p$ is the conditional probability that a 1° Ir-propyl intermediate is formed, and $\tilde{P}_s$ is the conditional probability that a 2° Ir-propyl intermediate is formed. Thus, it is a precise definition to express the total measured probability of the dissociative chemisorption of C_3H_8 as

$$P_{r,C3H8} = \tilde{P}_p P_{r,C3H8} + \tilde{P}_s P_{r,C3H8}. \tag{11}$$

The rate coefficients for the selective activation of primary and secondary C-D bonds are obtained from the values derived for $\tilde{P}_p$ and $\tilde{P}_s$ and the experimentally measured difference in the activation energies for C-H and C-D bond cleavage. Defining $P_{r,i}$ as the experimentally measured probability of dissociation of the i^{th} isotopomer of propane, the measured reaction

probability of $CH_3CD_2CH_3$ can be expressed, in the absence of secondary kinetic isotope effects, as

$$P_{r,CH3CD2CH3} = \tilde{P}_p P_{r,C3H8} + \tilde{P}_s P_{r,C3D8}, \quad (12)$$

and, by definition of the conditional probabilities, cf., Eq. 11, we also have

$$\tilde{P}_p + \tilde{P}_s = 1. \quad (13)$$

After substituting the apparent rate parameters from Table 1 into Eq. 12, it and Eq. 13 may be solved simultaneously for the conditional probabilities, $\tilde{P}_p$ and $\tilde{P}_s$. These results are,

$$\tilde{P}_p = 0.62 \exp[-135 \text{ cal/mol}/k_B T_s] \quad (14)$$

$$\tilde{P}_s = 0.38 \exp[+175 \text{ cal/mol}/k_B T_s]. \quad (15)$$

These activation energies are relative to the same reference energy as the measured apparent activation energies, the gas-phase zero of the perhydridopropane molecule. As noted above in Eq. 11, the elementary rate coefficients for the formation of 1° and 2° Ir-propyl intermediates on this surface are defined by the expressions, $\tilde{P}_p P_{r,C3H8}$ and $\tilde{P}_s P_{r,C3H8}$. The observed difference in activation energies between perhydridopropane and perdeuteropropane, $E_r^{CD} - E_r^{CH}$, is equal to 630 cal/mol, i.e., 2340 – 1710, cf., Table 1. This result compares well with accepted differences in the zero-point energies (ΔZPE's) for C-H and C-D bonds (**20**), and it substantiates the assumption that only primary deuterium kinetic isotope effects (KIE's) operate in these systems. By applying this isotopic energy difference to *both* rate coefficients for the formation of the 1° and 2° Ir-propyl products via C-H bond activation, we obtain the corresponding rate coefficients for the formation of 1° and 2° Ir-propyl products via C-D bond activation. The derived rate parameters describing the dissociative chemisorption of the three isotopomers of propane examined here on Ir(111) are given in Table 2 along with the calculated rate coefficients for the dissociative chemisorption

of the fourth isotopomer, $CD_3CH_2CD_3$. It must be pointed out that the rate coefficients for the formation of the 1° and 2° perhydrido products are exact by the construction of Eq. 11. Hence, they give exact agreement with the experimentally measured reaction probability of perhydridopropane. In contrast, the derived rate parameters for the formation of the mixed 1° and 2° Ir-propyls products are not exact by design, and the fact that they reproduce the experimentally measured dissociation probabilities of C_3D_8 and $CH_3CD_2CH_3$ to within ± 2% attests to the validity of our assumption that the ΔZPE may be applied equally to the activation of both 1° and 2° C-H (C-D) bonds.

Isobutanes

The same methodology developed for propane is applied to obtain the conditional probabilities of forming the primary and tertiary Ir-isobutyl products from the initial dissociative chemisorption of isobutane on this surface. With the measured initial probabilities for the dissociation of $(CH_3)_3CH$, $(CH_3)_3CD$, and $(CD_3)_3CH$, we are able to solve for the probability of dissociation of the perdeuterated isotopomer, $(CD_3)_3CD$. This result, together with that of $(CH_3)_3CH$, then provides the isotopic energy difference for activating C-H and C-D bonds. The set of equations relating the measured apparent rate parameters in Table 1 to the conditional probablilities is

$$P_{r,(CH3)3CD} = \tilde{P}_p P_{r,i\text{-}C4H10} + \tilde{P}_t P_{r,i\text{-}C4D10} \tag{16}$$

$$P_{r,(CD3)3CH} = \tilde{P}_p P_{r,i\text{-}C4D10} + \tilde{P}_t P_{r,i\text{-}C4H10} \tag{17}$$

$$\tilde{P}_p + \tilde{P}_t = 1, \tag{18}$$

which, when solved simultaneously, yields

$$\tilde{P}_p = 0.68 \exp[-28 \text{ cal/mol}/k_B T_s] \quad (19)$$

$$\tilde{P}_t = 0.32 \exp[+55 \text{ cal/mol}/k_B T_s] \quad (20)$$

$$P_{r,i\text{-}C4D10} = 1x10^{-2} \exp[-1600 \text{ cal/mol}/k_B T_s]. \quad (21)$$

Thus, the difference between C-D and C-H bond activation energies, E_r^{CD} - E_r^{CH}, computed from the apparent activation energies of perhydrido and perdeutero isobutane, is equal to 640 cal/mol, i.e., 1600 – 960, cf., Table 2. Again, we obtain a value that is indicative of a primary KIE by interpreting this result as the ΔZPE of the molecular adsorbates. This value combines with the conditional probabilities for the formation of the hydrogenated 1° and 3° Ir-isobutyl adsorbates to yield the rate parameters for the formation of the deuterated 1° and 3° Ir-isobutyls, analogous to the discussion above for the propane system. These derived rate coefficients for the formation of the 1° and 3° Ir-isobutyl reaction products reproduce the experimentally measured dissociation probabilities to within ± 3%.

The success in predicting the measured data validates our computational method and the uniquenss of the elementary rate parameters reported in Table 2 for the dissociative chemisorption of these alkanes on Ir(111). These results imply, in particular, that we are correct in our assumption that the respective isotopic differences in the activation energies apply equally to both the 1° and 2° bonds in propane and to both the 1° and 3° bonds in isobutane. Following from this result, and our measurents of the differences in the isotopic activation energies (630 and 640 cal/mol), we conclude that there is a negligible secondary kinetic isotope effect operating for the activation of these alkanes on this surface.

Conditional Probabilities of Selective C-H Bond Cleavage

The elementary rate coefficients derived thus far, the rate parameters of which are given in Table 2, describe the probabilities of forming the 1° and 2° Ir-propyl and 1° and 3° Ir-isobutyl products from the inital C-H bond dissociation reaction. Implicit in the definitions of $\tilde{P}_p$, $\tilde{P}_s$, and $\tilde{P}_t$ is that we have statistically averaged, over their respective stoichiometric proportions in the molecular alkanes, the conditional probabilities of cleaving, specifically, a 1°, 2°, or 3° C-H bond. Under the condition that the molecule reacts, the bond-specific conditional probabilities, P_p, P_s, and P_t, account for the cleavage of *individual* 1°, 2°, and 3° C-H bonds, i.e., they describe the unbiased case (in a statistical sense) of reacting 1° versus 2° and 3° bonds. Being explicit in expressing the relationships between the probabilities, $\tilde{P}_i$ and P_i, we are able to derive the characteristic rate parameters for the activation of 1°, 2°, and 3° C-H bonds on this surface. For propane,

$$\tilde{P}_p = 6Pp/(6Pp + 2Ps) \quad \text{and} \quad \tilde{P}_s = Ps/(6Pp + 2Ps), \tag{22}$$

and

$$P_p + P_s = 1, \tag{23}$$

and for isobutane,

$$\tilde{P}_p = 9Pp/(9Pp + Pt) \quad \text{and} \quad \tilde{P}_t = Pt/(9Pp + Pt) \tag{24}$$

and

$$P_p + P_t = 1. \tag{25}$$

These sets of equations can each be solved simultaneously to yield the respective conditional probabilities, again expressed as ratios between reaction and desorption rate coefficients. The results of these calculations for the activation of C-H bonds are, for the case of propane,

$$P_p = 0.35 \exp[-215 \text{ cal/mol}/kBTs] \tag{26}$$

$$P_s = 0.65 \exp[+95 \text{ cal/mol}/kBTs], \tag{27}$$

and in the case of isobutane,

$$P_p = 0.19 \exp[-68 \text{ cal/mol}/kBTs] \tag{28}$$

$$P_t = 0.81 \exp[+15 \text{ cal/mol/kBTs}]. \quad (29)$$

The application of the respective ΔZPE's for propane and isobutane, 630 and 640 cal/mol, respectively, to the results of Eqs. 26 – 29 yields the corresponding conditional probabilities for the cleavage of individual C-D bonds in these alkanes.

For comparison with the results of the apparent activation energies and the apparent ratio of preexponential factors obtained from the data in Figs 6 and 7, the elementary rate parameters for the cleavage of primary, secondary, and tertiary C-H bonds are given in Table 3. The activation energies are all reported relative to the bottom of the physically adsorbed wells of the precursor molecules, with the values of the desorption energies, E_d, listed in Table 1. The activation energies for the 1° C-H bond cleavage reaction are 10.4 ± 0.2 kcal/mol for ethane and average 11.6 ± 0.2 kcal/mol for the higher alkanes. The activation energies for the 2° and 3° C-H bond cleavage reactions are each found to be 11.3 ± 0.2 kcal/mol. The difference in the gas-phase bond dissociation energies (BDE's) of primary and secondary C-H bonds, $D_{0C2H5CH2\text{-}H} - D_{0(CH3)2CH\text{-}H}$, is equal to 3 ± 1 kcal/mol in propane (**3**), and on the Ir(111) surface, we observe only a 310 cal/mol difference in the activation energies of cleavage of these bonds. The situation is even more dramatic in the case of isobutane. Whereas the difference in the gas-phase BDE's for primary and tertiary C-H bonds, $D_0((CH3)2CHCH2\text{-}H) - D_0((CH3)3C\text{-}H)$, is 5 ± 1 kcal/mol (**3**), on Ir(111), the difference in the 1° and 3° C-H bond activation energies is only 83 cal/mol. This apparent discrepancy arises because we are only examining half of the thermochemical issue by viewing the gas-phase values of the BDE's. Kinetic activation barriers result from the topography of the interaction potential between the reactants, which in our case, are the metal surface and the physically

adsorbed precursor alkane molecule. We present in the next section, an energetic origin to the apparent conundrum resulting from our kinetic measurements.

Thermochemistry of the Competing C-H Bond Dissociation Reactions

The small differences observed between the activation energies for primary, secondary, and tertiary C-H bonds originate from the thermochemical considerations of the complete reactive system for propane and isobutane depicted in Figs. 8 and 9, respectively. These figures illustrate the effective compensation of the difference in the gas-phase BDE's, which favor 2° C-H cleavage for propane and 3° C-H cleavage for isobutane, by the reduced bond strengths formed between the surface and these reaction products. The reference energies for the diagrams are the molecular gas-phase zeros of propane and isobutane, with the molecules taken infinitely far from the surface and at rest.

In the construction of these potential energy diagrams, we have estimated the bond strengths to the Ir surface for the product hydrogen and alkyl adsorbates from three sources: (1) thermal desorption experiments of hydrogen and deuterium from the close-packed Ir(111) surface, (2) experimentally measured and theoretically predicted bond energies for the first-row and second-row transition metal-methyls, metal-hydrides, and their respective positive ions, and (3) recent theoretical work which correlates the trend in metal-alkyl bond strengths with the coordination of the alkyl group via primary, secondary, and tertiary metal-carbon bonds. These estimates of the bond strengths of adsorbed hydrogen and alkyls on the surface of iridium is not only applicable here, but also in the following paper where we address the C-C bond cleavage of alkanes by Ir(111).

In thermal desorption experiments of hydrogen and deuterium from the Ir(111) surface, Engstrom et al. obtained a barrier of 19.1 kcal/mol for the second-order recombinative desorption of deuterium, in the limit of vanishingly small coverages of adsorbed hydrogen (**21**), which, of course, is the case here for the hydrogen coverages from the dissociation of alkanes. With D_0(D-D) = 104.9 kcal/mol, we estimate the bond strength for the surface Ir-D species to be 62.0 kcal/mol, and that of the Ir-H species to be 61.5 kcal/mol (**22**). This result is quite close to the range of experimental bond strengths of neutral and ionic transition-metal hydrides, which average from ~45 to 55 kcal/mol for the 3d transition metals and ~40 to 60 kcal/mol for the 4d and 5d metals (**23**). However, trends within the gas-phase transition metal hydride series are difficult to predict, as the ground and low lying electronic states of individual metal atoms and ions bear directly upon the nature of the bonding (**24**).

The thermal desorption result of the Ir-H bond srength may also be compared with theoretical and organometallic systems. The Ir-H bond strength compiled from organometallic compounds, such as Ir(Cl)(CO)$(PMe_3)_2$(I)(H,) is estimated to be 70 ± 4 kcal/mol (**23a**, **25**), and the calculated generalized valence bond (GVB) result of 65.8 kcal/mol (**26**), can be taken together to delimit the upper bound of our estimate. Recognizing the range of values and the degrees of uncertainties in their measure, we have used a value of 61.5 ± 1.0 kcal/mol as the bond dissociation energy of Ir-H in the construction of Figs. 8 and 9.

Values of the metal-alkyl bond strengths are less numerous than for either metal-H or metal-CH_3, but we will begin by examining the tabulated thermochemical results for organometallic complexes, and the comparison of experimental studies of metal-methyl molecules and ions with theoretical

calculations. Combining the observations of these related systems with the recent calculations of branched alkyls bonded to the Sc^+ ion, which will be discussed shortly, we are able to arrive at reasonable estimates of the desired Ir-alkyl bond strengths.

From Bauschlichter et al. (**23b**), within the first transition metal row, the neutral M-CH_3 molecules have bond strengths between ~35 and 45 kcal/mol, while the corresponding positive ions, M^+-CH_3, have bond strengths between ~45 and 55 kcal/mol. For the second row of transition metals, the formation of stable methyl neutral molecules is not observed, nor is the formation of the stable metal methyl positive ions except for Y, Ru, Rh, and Pd, which have M^+-CH_3 bond dissociation energies of ~50 to 60 kcal/mol. These values for first and second row gas-phase M-CH_3 and M^+-CH_3 molecules provide some measure of the corresponding bond strengths within the third row, even though the isolation of third row molecules and ions is not observed, due to the strong dehydrogenating activity of the second and third row transition metals (**27**). To illustrate this point, in the gas-phase reaction of methane with the third row transition metals (**28**), the oligomerization via carbene intermediates dominates the chemistry. The initial production of an M-(H)(CH_3) intermediate is believed to eliminate H_2 and form the M=CH_2 stable product. The estimated bond strengths of the resulting metal carbenes are approximately 100 to 110 kcal/mol.

Selected Ir-R bond strengths have been tabulated for organometallic compounds (**2 3 a**). In the saturated compounds, such as Ir(Cl)(CO)$(PMe_3)_2$(I)(R) with R = CH_3, C_2H_5, n-C_3H_7 and i-C_3H_7 and Ir(Cp*)(PMe_3)(H)(c-C_6H_{11}) (**25**, **29**), the Ir-R bond strengths are 47 ± 3, 44 ± 3, 44 ± 3, 40 ± 4, and 50 ± 5 kcal/mol, respectively. For comparison, the tabulated Pt-CH_3 bond dissociation energy in Pt(Cp)$(CH_3)_3$ is 40 ± 5 kcal/mol

(**23a**), and the average calculated GVB bond energy within $Pt(H)(CH_3)$ and $Pt(CH_3)_2$ has been found to be 50 ± 3 kcal/mol (**30**).

From these observed values, we have elected to use a value of 50 ± 5 kcal/mol for the Ir-CH_3 bond strength in the construction of the potential energy diagrams of Figs. 8 and 9. The decreasing trend in the bond strengths of Ir-ethyl, and Ir-propyl ligands (relative to Ir-CH_3) in the organometallic compounds above (**25**) can be compared with a similar result obtained from the calculation of Sc^+-alkyl bond strengths.

Perry and Goddard (**31**) have conducted *ab initio* calculations of the Sc^+-R bond energies for R = CH_3, C_2H_5, *n*-C_3H_7, *i*-C_3H_7, and *t*-C_4H_9 in support of research investigating the observed selectivity of primary over secondary Sc^+-propyl formation involved in gas-phase σ-bond metathesis (**32**). Their work reveals that the metal ion-alkyl bond strengths follow a general trend of methyl > primary > secondary > tertiary, which is in agreement with the trend in the organometallic bond strengths just presented. Using the modified coupled pair functional (MCPF) method, they obtain bond strengths of 45, 40, 45, 37, and 35 kcal/mol for the Sc^+-alkyl series listed above. While the absolute magnitudes of these calculated bond energies are believed to be systematically low by 10 to 12 kcal/mol (**23b**), it is the application of the *relative* bond strengths that successfully predicts the observed trend in the exothermicities (and hence, the selectivity) in the gas-phase metathesis reactions. With the Ir-CH_3 bond strength as reference, we have used this calculated trend, and the observed trend of the Ir organometallic complexes, to provide estimates for the surface-alkyl bond strengths for the construction of Figs. 8 and 9. The calculated differences from Perry and Goddard for the bond strengths of Sc-R^+ organometallic ions are,

$$\Delta D_{0,ref} = D_0(M^+\text{-}CH_3) \approx D_0(M^+\text{-}n\text{-}Pr), \quad (30)$$

$$\Delta D_{0,1\text{-}2} = D_0(M^+\text{-}n\text{-}Pr) - D_0(M^+\text{-}i\text{-}Pr) = 8 \text{ kcal/mol}, \quad (31)$$

$$\Delta D_{0,1\text{-}3} = D_0(M^+\text{-}n\text{-}Pr) - D_0(M^+\text{-}t\text{-}Butyl) = 10 \text{ kcal/mol}. \quad (32)$$

The ability of the n-propyl group to coordinate its terminal, or β-methyl, to the Sc^+ metal center results in the gauche conformer being the most stable configuration, with a bond strength within 0.5 kcal/mol of the Sc^+-CH_3 organometallic ion. Within the saturated organometallic complex, $Ir(Cl)(CO)(PMe_3)_2(n\text{-}C_3H_7)$, this configuration of the propyl ligand is not possible, and, hence, the organometallic propyl ligand experiences a decrease in bond strength relative to the methyl ligand of ~3 kcal/mol (**33**). Calculations for the bond strength of the Sc^+-$CH_2CH(CH_3)_2$ were not conducted, and in lieu of it, we have used the primary n-propyl bond strength, with a correction due to the additional stabilization from the second β-methyl interaction (**34**). Under our experimental conditions, the initial dissociative chemisorption leads to the formation of products on an extended, clean surface. The 1°-alkyl dissociation products (1°-propyl, 1°-butyl, and 1°-isobutyl) would be expected to adopt configurations that allow their terminal methyl groups to interact with the Ir(111) surface. The increased stabilization from the physical coordination of a second β-methyl is estimated to provide an additional 2 kcal/mol to the bond strength of the adsorbed 1°-isobutyl.

The thermochemical results for the competing C-H bond activation reactions illustrated in Figs. 8 and 9 explain the observed lack of a large difference in the activation energies between 1° and 2° C-H bond activation in propane and between 1° and 3° C-H bond activation in isobutane. Precisely the same effect that makes the activation of 2° and 3° bonds more facile than 1° bonds is what makes their bonds to the surface compensatorily more weak.

The net result is that the potential energy curves cross at some point in their descent from their respective gas-phase radical states to their chemically adsorbed states. Our measurements indicate that their point of intersection lies at, or near the top of the activation barrier for C-H bond scission from the physically adsorbed state for these alkanes on Ir(111).

Selectivity of Alkane Activation

To discuss the selectivity of propane and isobutane in this system, we recall that in their dissociative chemisorption on Ir(111), activation of the physically adsorbed precursor occurs via either initial C-H, or initial C-C, bond cleavage (cf., Scheme I). From the data presented in Figs. 2 and 3, we observe that for temperatures > ~500 K for propane, and > ~450 K for isobutane the contributions from the C-C activation channels become nonnegligible. The complete description of the selectivity of these alkanes on Ir(111) requires that the branching ratio between the competing C-C and C-H activation channels be quantified. This complete analysis may be found in the following paper (**4**).

Here, we quantify the selectivity *within the C-H bond activation channel* for the initial dissociation of propane and isobutane. Our results apply over the complete temperature range of these investigations, including measurements extending up to 1000 K. The precise separability of the contributions to the total reaction probability by the competing C-H and C-C activation channels ensures the exactness of this description. Thus, even at elevated temperatures where C-C bond activation is nonnegligible, we are still able to separate, and quantify in a detailed fashion, the selectivity exhibited by that fraction of the reacting alkane molecules which follow the C-H bond cleavage path.

We must critically compare the two sets of conditional probabilities, $\tilde{P}_i$ and P_i, developed in this work. The important distinction between them is best illustrated by examining their ratios. The information contained in each set of probabilities is unique and must not be inadvertently thought of as interchangable. The ratios of the alkyl formation probabilities, $\tilde{P}_i$'s, *are* the branching ratios, describing the overall selectivity of the reactive system, and the ratios of the bond cleavage probabilities, P_i's, quantify the intrinsic competition between the dissociation of individual C-H bonds.

The ratios obtained from the conditional probabilities to form the various alkyl intermediates, $\tilde{P}_p/\tilde{P}_s$ for propane and $\tilde{P}_p/\tilde{P}_t$ for isobutane, reflect the selectivity that is observed under the macroscopic conditions of laboratory experimentation. The ratios of the conditional probabilities to activate the individual types of C-H bonds, P_p/P_s and P_p/P_t, reflect the "head-to-head" competition that impacts the observed selectivity, but by the same token, is not synonymous with it. The ratios of the $\tilde{P}_i$'s are the results with which experimentalists would compare other reactive systems, since in these macroscopic measurements the statistical averaging that arises from the unequal proportions of the different types of C-H bonds cannot be controlled. On the other hand, the ratios of the P_i's are the results against which theorists would compare their bond-specific calculations of C-H bond activation at the molecular level. For the selectivities of propane,

$$\tilde{P}_p/\tilde{P}_s = 1.63 \exp[-310 \text{ cal/mol}/k_B T_s] \text{ and} \tag{33}$$

$$P_p/P_s = 0.54 \exp[-310 \text{ cal/mol}/k_B T_s], \tag{34}$$

and, for the selectivities in isobutane,

$$\tilde{P}_p/\tilde{P}_t = 2.13 \exp[-83 \text{ cal/mol}/k_B T_s] \tag{35}$$

$$Pp/Pt = 0.24 \exp[-83 \text{ cal/mol}/k_B T_s]. \tag{36}$$

Considering the probabilities of formation of the respective alkyl products, we focus our attention on the two branching ratios given by Eqs. 33 and 35. For propane, we observe immediately that the formation of 1° Ir-propyl is more probable than the formation of 2° Ir-propyl for surface temperatures exceeding 320 K. Similarly, the formation of 1° Ir-isobutyl is more probable than the formation of 3° Ir-isobutyl for the complete temperature range employed in this study, and moreover, the branching ratio increases with increasing surface temperature. In fact, were the activation possible at all temperatures, the favored selectivity of 1° over 3° would not invert until 55 K. These statements *do not imply*, however, that the activation of the primary bonds in these alkanes is favored over the activation of the secondary and tertiary bonds: they simply reflect the fact that there are more pimary C-H bonds in the two alkanes.

The ratios of the conditional probabilities of C-H bond activation (Eqs. 34 and 36) present the nonstatistically weighted, and, hence, unbiased perspective of the competion between C-H bond cleavage reactions on this surface. Within propane, both the energetics and the entropy favor the activation of the 2° C-H bond over the 1° C-H bond. Specifically, the difference in activation energies favors secondary bond cleavage by 310 cal/mol, and the entropic difference, manifested in the ratio of the preexponential factors, favors secondary bond cleavage by a factor of 1.8. The case for isobutane is similar: 3° bond cleavage is favored energetically by 83 cal/mol, and entropically by a factor of 4.2.

When the term "selectivity" is used in catalysis, it must be remembered that it refers to the branching of competing reactions, and, hence, the relevant quantities to be used are those which incorporate the statistical properties of the system. For this study of the activation of alkanes on the

smooth Ir(111) surface, this means that the $\tilde{P}_i$'s, the conditional probabilities for the formation of the alkyl products, yield the rate coefficients necessary to describe the overall kinetics of the surface reaction. The computed branching ratios for the dissociative chemisorption of propane and isobutane on Ir(111) demonstrate that, despite the thermodynamic preference for cleavage of 2° and 3° C-H bonds relative to 1° bonds, this system will still populate the catalytic surface with a preponderance of primary alkyl intermediates. This result is a direct manifestation of the statistical "stacking of the deck" afforded by the disproportionate numbers of primary relative to secondary and tertiary C-H bonds in the parent alkane molecules. The related rate parameters for activation of the individual C-H bonds are instructive in a chemically intuitive sense. In fact, in the potential energy diagrams of Figs 8 and 9, the two reaction channels are being compared on an "even" basis, and to depict their relative activation energies properly, we have applied the results from the ratios of the competitive bond cleavage probabilities, P_i's. Their direct application as the conditional probabilities of alkyl formation, however, is not correct without first statistically folding them into the proper alkyl formation probabilities.

Comparison with the Dissociative Chemisorption of Propane and Isobutane on Pt(110)-(1x2)

The influence of surface geometric and electronic structure upon the activation of alkanes is a subject of great interest in the characterization of catalyst performance and optimization. The activity and selectivity are both intimately related to the surface structure of the catalyst, and by employing single-crystalline samples with well-ordered surface orientations, systematic studies of the issue of structure sensitivity in support of heterogeneous catalysis have been made possible (**35**).

In the trapping-mediated dissociative chemisorption of ethane on the close-packed (111) and reconstructed (110)-(1x2) surfaces of iridium and platinum, surface electronic and geometric effects were found to be of comparable magnitude (**10a**, **13**, **36**). The observed catalytic activities followed the trend Ir(110) > Pt(110) ≈ Ir(111) > Pt(111), with the measured C-H bond activation energies (kcal/mol) varying across the above series: 5.5 < 10.5 ≈ 10.3 < 16.6. It is apparent that the corrugated (110)-(1x2) reconstructed surface geometry has an enhanced activity relative to the smooth (111) surface geometry, and that, intrinsically, the Ir metal is more active towards C-H bond activation than Pt. While the effect due to geometric structure yields differences in activation energies of 4.8 (between the two Ir surfaces) and 6.1 (between the two Pt surfaces), that due to electronic structure yields differences in energy of 5.0 (between the two (110) surfaces) and 6.3 (between the two (111) surfaces). Consequently, the smooth surface of Ir(111) and the corrugated surface of Pt(110)-(1x2) have the same activation energy, within experimental uncertainty, and these two surfaces exhibit virtually identical reactivities toward the dissociative chemisorption of ethane. To examine further the issue of structure sensitivity in alkane activation, the results presented here for the dissociative chemisorption of propane, isobutane and their selectively deuterated isotopomers on Ir(111) will be compared with previous results for the reactivity of these same molecules on the corrugated surface of Pt(110)-(1x2) (**37**). In this way, we will quantify the influence of surface structure on the *selective* activation of alkanes.

The methods, as well as the instrumentation, employed to obtain the results for the dissociative chemisorption of propane, isobutane, and their deuterated isotopomers on Pt(110)-(1x2) were precisely the same as those

reported here. In the experiments with Pt(110), however, data could not be easily obtained above approximately 700 K, as diffusion of surface deposited carbon into the bulk of the crystal occurred. This difficulty was overcome in studies of the dissociative chemisorption of CH_4 on Pt(110)-(1x2) by depositing a known amount of carbon at a lower surface temperature, then annealing to, and holding at, the higher temperature for the exact length of time of the higher temperature experiment (**10a**). This effort proved to be unneccessary for the dissociation of ethane, propane, and isobutane, for which linear Arrhenius behavior and reproducible kinetic measurements were obtained $330 < T_S < 650$ K. It is noteworthy that at no temperature in this range, nor for any alkane molecule examined, did there appear a nonlinear Arrhenius behavior such as we report here on Ir(111). This issue is addressed in detail in the following article of this journal (**4**).

The activation energies obtained from the cleavage of 1° and 2° C-H bonds in the dissociative chemisorption of propane on Pt(110)-(1x2) were 11.38 kcal/mol and 10.96 kcal/mol, respectively. The apparent preexponential factor, expressed as the ratio of reaction to desorption rate coefficients, was 6.1×10^{-3}. The isotopic difference in C-H and C-D bond cleavage was 870 cal/mol. On the Ir(111) surface, and displayed in Table 3, the 1° and 2° C-H bond activation energies are 11.63 and 11.32 kcal/mol, the ratio of the apparent preexponential factors is 9.3×10^{-3}, and the observed difference in C-H and C-D bond activation energies is 630 cal/mol.

For the dissociative chemisorption of isobutane on Pt(110)-(1x2), the activation energies for 1° and 3° C-H bond cleavage were 11.26 kcal/mol and 11.12 kcal/mol, respectively. The ratio of the preexponential factors was 3.2×10^{-3}, and the difference in the activation energies for C-H and C-D bonds was 890 cal/mol. From Table 3, the corresponding values on Ir(111) are 11.43

kcal/mol and 11.34 kcal/mol for the 1° and 3° C-H bond activation energies. The ratio of the apparent preexponential factors is 1.0×10^{-2}, and the difference in the C-H and C-D bond activation energies is 640 cal/mol.

The distinction between the dissociative chemisorption of these alkanes on these two surfaces is very small, with both surfaces indicating that C-H bond cleavage between the competing 1°, 2°, and 3° paths is characterized by only very small differences. In general, the cleavage of all of the C-H bonds occurs with activation energies between 11.0 and 11.6 kcal/mol on the two surfaces, with the activation energies sightly less for Pt(110)-(1x2) than for Ir(111). The comparison of the ratios of the preexponential factors favors the Ir surface over the Pt surface by factors of approximately 1.5 and 3.0 for the dissociative chemisorption of propane and isobutane, respectively. This difference might be interpreted to reflect a greater phase space, on Ir(111) versus Pt(110)-(1x2), that isobutane samples in its interaction with the reactive coordinates of the potential energy hypersurface. However, the values of the preexponential factors are essentially equal to one another within the uncertainties associated with their determination, and, furthermore, both results lie within the expected range of both theory and empirically accumulated results from comparable reactive systems (**7**, **38**).

To compare the selectivities of the two catalytic systems, we examine the ratios of the individual conditional probabilities derived separately elsewhere for Pt(110)-(1x2) (**37**). The conditional probabilities for the formation of Pt-propyl and Pt-isobutyl products were determined using the same methodology demonstrated here with Ir(111), and from these results, the conditional probabilities for the activation of individual C-H bonds were obtained. The results for the pair of conditional probabilities for the activation of propane on Pt(110)-(1x2) are

$$\tilde{P}_p/\tilde{P}_s = 1.56 \exp[-425 \text{ cal/mol}/k_B T_s] \quad (37)$$

$$P_p/P_s = 0.52 \exp[-425 \text{cal/mol}/k_B T_s]. \quad (38)$$

Likewise, the pair of conditional probabilities for isobutane are

$$\tilde{P}_p/\tilde{P}_t = 2.85 \exp[-137 \text{ cal/mol}/k_B T_s] \quad (39)$$

$$P_p/P_t = 0.32 \exp[-137 \text{cal/mol}/k_B T_s]. \quad (40)$$

Comparing these results with those in Eqs. 33 – 36 from the corresponding analysis with Ir(111) reveals that both surfaces yield very small differences between the activation energies. The comparison reveals that these energetic differences are 425 cal/mol on Pt(110)-(1x2) and 310 cal/mol on Ir(111), for the cleavage of 1° versus 2° bonds, and that they are 137 cal/mol for Pt(110)-(1x2) and 83 cal/mol for Ir(111) for the cleavage of 1° versus 3° bonds. The small energy differences for the Pt(110)-(1x2) case are explained by potential energy diagrams similar to those shown for the case of Ir(111) in Figs. 8 and 9. On Pt(110)-(1x2), as on Ir(111), the formation of weaker surface bonds by the branched alkyl products (relative to primary alkyl products) produces the same compensating effect on the energetics of the activation energies for competitive C-H bond cleavage.

The branching ratios, $\tilde{P}_p/\tilde{P}_t$, for the dissociative chemisorption of isobutane on Ir(111) and Pt(110)-(1x2) show that the formation of 1° Ir-isobutyl and 1° Pt-isobutyl products are favored over the complete temperature ranges employed in these experiments. For the dissociative chemisorption of propane, however, the branching ratios, $\tilde{P}_p/\tilde{P}_s$, demonstrate that the formation of 1° Ir-propyl and 1° Pt-propyl products are only favored above surface temperatures of 320 and 480 K, respectively.

From our comparative study with ethane (**13**), and from these results with propane and isobutane, it has been demonstrated that the Ir(111) and

Pt(110)-(1x2) surfaces possess essentially equal *activities* toward alkane activation. Yet, the quantification of the activity of a catalyst is not sufficient to characterize fully its chemical behavior. Without the *selectivity* of the catalyst, such a description remains incomplete. As was achieved earlier in the examination of the dissociative chemisorption of propane and isobutane on Pt(110)-(1x2), we have characterized, in a detailed way, the selectivity exhibited by Ir(111) in the C-H bond activation of alkanes. The derived temperature dependence of the branching ratios for the dissociation of propane and isobutane on these two surfaces has allowed us to quantify their relative selectivities. Our results indicate that while these two catalytic surfaces are quantitatively similar, the Pt(110)-(1x2) surface distinguishes itself by favoring the formation of secondary propyl intermediates up to temperatures of 480 K, in contrast to only 320 K for the Ir(111) surface. This distinction between the two model catalytic surfaces quantifies, for the first time, the relative selectivities of these two important components to commercial catalytic systems.

5. Conclusions

An ultrahigh vacuum-microreactor study of the initial probability of trapping-mediated dissociative chemisorption of ethane, propane, *i*-butane, *n*-butane, and neopentane on Ir(111) over the temperature range $310 < T < 1100$ K has been performed. Two competing reaction channels are found to be available to the C_3 and higher alkanes on this surface. Initial dissociative chemisorption of these alkanes results in either irreversible C-H or C-C bond cleavage, while ethane reacts only via the C-H bond activation channel. The complete kinetic description is resolvable into the two distinct channels, and in this paper, we have presented the analysis of the kinetics of the C-H bond

activation channel. The analysis of the kinetic measurements for initial C-C bond cleavage is presented in an accompanying paper (**4**).

From the trapping-mediated kinetic rate expressions, we calculated the elementary rate parameters expressed as ratios between the reaction and desorption rate coefficients relative to the physically adsorbed state of the trapped molecule. By employing selectively deuterated isotopomers of propane and isobuane, we have quantified the rate parameters for the formation of 1°, 2°, and 3° Ir-alkyl initial reaction products. We have used these results to calculate the rate parameters of 1°, 2°, and 3° C-H bond cleavage on this surface. We found that the activation energy for 1° C-H bond cleavage in ethane is 10.4 ± 0.2 kcal/mol, and the average value for the higher alkanes is 11.4 ± 0.2 kcal/mol. A primary deuterium kinetic isotope effect is observed for the initial C-H bond cleavage reaction. The isotopic differences in the activation energies for the cleavage of C-H and C-D bonds were found to be 480 cal/mol in ethane, 630 cal/mol in propane, and 640 cal/mol in isobutane. The activation energies for the cleavage of 2° and 3° C-H bonds were both found to be 11.3 ± 0.2 kcal/mol. This small difference between cleavage of primary, secondary, and tertiary C-H bonds is accounted for by considering the relative energetics of these systems, and, in particular, the bond strengths of the alkyl products chemically adsorbed to the Ir surface.

We calculated the branching ratios for the dissociative chemisorption of propane and isobutane on Ir(111), and we compared our results to those obtained for the dissociative chemisorption of these alkanes on Pt(110)-(1x2). We found that these two single crystalline surfaces have the same activity toward the cleavage of C-H bonds. The Pt (110)-(1x2) surface is more selective in the activation of propane, since the branching ratio favors the formation of 2° Pt-propyl over 1° Pt-propyl products up to 480 K. The Ir(111)

surface favors 2° Ir-propyl formation up to only 320 K. In contrast, the branching ratios of the dissociative chemisorption of isobutane on both surfaces favors the formation of 1°-isobutyl products over 3°-isobutyl products for the full temperature range of these experiments.

Acknowledgement: This work was supported by the Department of Energy under Grant No. DE-FG03-89ER14048.

References and Notes

(1) (a) Sinfelt, J. H. *Bimetallic Catalysts: Discoveries, Concepts, and Applications;* Wiley: New York, 1983; pp. 130-157. (b) Rasser, J. C. *Platinum-Iridium Reforming Catalysts;* Delft Univ. Press.: Delft, Netherlands, 1977; pp. 156-193.

(2) (a) Shilov, A. E. *Activation of Saturated Hydrocarbons by Transition Metal Complexes*; Reidel: Dordrecht, Netherlands, 1984. (b) Meunier, B., Chaudret, B. Eds.; *Perspectivies in the Selective Activation of C-H and C-C Bonds in Saturated Hydrocarbons*, Vol. CXXX of the *NATO Advanced Study Institutes Series*; Reidel: Dordrecht, Netherlands, 1987.

(3) The bond dissociation energies at 298 K, $D_{0,298K}$, are 104.7 ± 0.2 kcal/mol for methane, 98 ± 1 kcal/mol for primary C-H bonds, 95 ± 1 kcal/mol for secondary C-H bonds, and 93 ± 2 kcal/mol for tertiary C-H bonds. The bond dissociation energies for C-C bonds are, on average, 10 kcal/mol lower. (a) McMillen, D. F.; Golden, D. M. *Annu. Rev. Phys. Chem.* **1982**, *33*, 493. (b) Berkowitz, J.; Ellison, G.B.; Gutman. D. *Ann. Rev. Phys. Chem.*, in press.

(4) Johnson, D. F.; Weinberg, W.H., *J. Am. Chem, Soc.*, this issue.

(5) (a) Rettner, C. T.; Pfnur, H. E.; Auerbach, D. J. *Phys. Rev. Lett.* **1985** *54*, 2716. (b) Luntz, A. C.; Bethune, D. S. *J. Chem. Phys.* **1989**,*90*, 1274. (c) Lee, M. B.; Yang, Q. Y.; Ceyer, S. T. *ibid* **1987**, *87*, 2724.

(6) (a) Weinberg, W. H. In *Dynamics of Gas-Surface Collisions*; Rettner, C. T., Ashfold, M. N. R., Eds.; Royal Society of Chemistry: Cambridge, 1991, pp. 171-220. (b) Ehrlich, G. In *Chemistry and Physics of Solid Surfaces*; Vanselow, R., Howe, R. F., Eds.; Springer-Verlag: Heidelberg, 1989; Vol. VII, pp. 1-64.

(7) (a) Weinberg, W. H. In *Kinetics of Interface Reactions*; Kreuzer, H. J., Grunze, M., Eds.; Springer-Verlag: Heidelberg, 1987; pp. 94-121. (b)

Weinberg, W. H. *Langmuir* **1993**, *9*. 655. (c) Weinberg, W. H. *J. Vac. Sci. Technol.* **1992**,*A10*, 2271.

(8) Johnson, D. F.; Weinberg. W. H. *J. Chem. Phys.*, submitted.

(9) The desorption temperatures of these alkanes from the physically adsorbed state on Ir(111) are all below 250 K,[15a,b] which is important in ensuring that there is a very small accumulation of the alkane precursor on the surface. The accumulation of physically adsorbed alkane under our conditions of surface temperature and impinging gas flux is infinitesimally low, $\theta_{RH} < 10^{-7}$ monolayer.

(10) (a) Sun, Y.- K.; Weinberg, W. H. J. *Vac. Sci. Technol.* **1990**,*A8*, 2445. (b) Vajo, J. J.; Tsai, W.; Weinberg, W. H. *Rev. Sci. Instrum.* **1985**,*56*, 1439.

(11) Comrie, C. M.; Weinberg, W. H. *J. Chem. Phys.* **1976**,*64*, 250.

(12) Laue diffraction methods werre used to determine that our sample was polished to within 0.70° ± 0.15° of the [111] normal direction of the surface. This corresponds to terrace widths, assuming that they are uniform, of between 63 and 98 atomic rows. Thus, the surface defect density is 0.013 ± 0.003 fractional monolayer.

(13) Johnson, D. F.; Weinberg, W. H. *Science*, **1993**,*261*, 76.

(14) Curvature in the temperature dependence of the reaction rate is observed in kinetic systems exhibiting concurrent reactions. (a) Laidler, K. J. *Chemical Kinetics*, 3rd ed.; Harper & Row: New York, 1987. (b) Hammes, G. G. *Principles of Chemical Kinetics*; Academic Press: New York, 1978. (c) Compton, R. G., Ed. *Kinetic Models of Catalytic Reactions: Chemical Kinetics*; Elsevier: New York, 1991; Vol. 32.

(15) (a) Szuromi, P. D.; Engstrom, J. R.; Weinberg, W. H. *J. Chem. Phys.* **1984**,*80*, 508. (b) Wittrig, T. S.; Szuromi, P. D.; Weinberg, W. H. *J.*

Chem. Phys. **1982**, *76*, 3305. (c) Westre, E. D.; Arena, M. V.; Deckert, A. A.; Brand, J. L.; George, S. M. Surf. Sci. **1990,** *233*, 293.

(16) Campbell, C. T.; Sun, Y.-K.; Weinberg, W. H. *Chem. Phys. Lett.* **1991**, *179*, 53.

(17) Rettner, C. T.; Schweizer, E. K.; Stein, H.; Auerbach, D. J. *Phys. Rev. Lett.* **1988**, *61*, 986.

(18) (a) Rettner, C. T. ; Auerbach, D. J. In *Kinetics of Interface Reactions*; Kreuzer, H. J., Grunze, M., Eds.; Springer-Verlag: Heidelberg, 1987, p. 145. (b) Andersson, S.; Persson, M. *Phys. Rev. Lett.* **1993**, *70*, 202. (c) Ceyer, S. T. *Annu. Rev. Phys. Chem.* **1988**, *39*, 479. (d) McMaster, M. C.; Schroeder, S. L. M.; Madix, R. J. *Surf. Sci.* **1993**, *297*, 253. (e) McMaster, M. C.; Madix, R. J. *Surf. Sci.* **1993**, *294*, 420.

(19) (a) Mullins, C. B.; Weinberg, W. H. *J. Chem. Phys.* **1990**, *92*, 3986. (b) Mullins, C. B.; Weinberg, W. H. *J. Vac. Sci. Technol.* **1990**, *A8*, 2458.

(20) The difference in ground state zero point energies, ΔZPE(CH-CD), is approximately 1100 cal/mol, and may be approximated from the asymmetric stretching frequencies of the C-H (C-D) bonds within a methyl group, approximately 3200 cm^{-1} and 2400 cm^{-1}, respectively.

(21) Engstrom, J. R.; Tsai, W.; Weinberg, W. H. *J. Chem. Phys.* **1987**, *87*, 3104.

(22) The difference in ground state zero point energies, ΔZPE[(Ru-D)–(Ru-H)], is 415 cal/mol, as may be calculated from the symmetric stretching frequencies of the Ru-H (Ru-D) bonds of chemisorbed hydrogen and deuterium on Ru(001), 1120 cm^{-1} and 830 cm^{-1}, respectively. [Barteau, M. A.; Broughton, J. Q.; Menzel, D. *Surf. Sci.* **1983**, *133*, 443]. Pettersson, et al.[23b] report the bond energy of Ru^{+}–H is 38 kcal/mol, while the experimental result is 40 ± 3 kcal/mol [Elkind, J. L.; Armentrout, P. B. *Inorg. Chem.* **1986**, *25*, 1080]. Thus, in comparison to

the Ir–H bond strength of 61.5 kcal/mol, we estimate the ΔZPE[(Ir-D) – (Ir-H)] to be between 500 and 600 cal/mol.

(23) (a) Simoes, J. A. M.; Beauchamp, J. L. *Chem. Rev.* **1990**, *90*, 629. (b) Pettersson, L. G. M.; Bauschlicher, C. W., Jr.; Langhoff, S. R. *J. Chem Phys.* **1987**, *87*, 481. (c) Bauschlicher, C. W., Jr.; Langhoff, S. R.; Partridge, H.; Barnes, L. A. *J. Chem. Phys.* **1989**, *91*, 2399.

(24) Better size match of the valence s and d orbitals for the second and the third row transition metals compared to the first row enables the former to employ greater d character in their bonding, and this manifests itself in the increased reactivities, as well their participation in catalytic mechanisms that require greater directionality of the metal orbitals. (a) Schilling, J. B.; Goddard, W. A., III; Beauchamp, J. L. *J. Am. Chem. Soc.* **1987**, *109*, 5573. (b) Armentrout, P. B.; Georgiadis, R. *Polyhedron*, **1988**, *7*, 1573.

(25) (a) Yoneda, G.; Blake, D. M. *J. Organoment. Chem.* **1980**, *190*, 71. (b) Yoneda, G. Blake, D. M. *Inorg. Chem.* **1981**, *20*. 67.

(26) Ohanessian, G.; Goddard, W. A., III *Acc. Chem. Res.* **1990**, *23*, 386.

(27) The bonds formed by third row transition metals are generally significantly stronger than those of metals in the first and second rows, because of the lanthanide contraction and relativistic effects. As a result, all of the second and third row transition metals are highly active in deydrogenation reactions, and they do not form stable metal methyl molecules except as noted in the text. (a) Pyykko, P. *Chem. Rev.* **1988**, *88*, 563. (b) Ziegler, T.; Snijders, J. G.; Baerends, E. J. In *The Challenge of d and f Electrons*, ACS Symposium Series 394, Salahub, D. R.; Zerner, M. C., Eds.; American Chemical Society: Washington, D. C., 1989, Chapter 23.

(28) Irikura, K. K.; Beauchamp, J. L. *J. Phys. Chem.* **1991**, *95*, 8344.

(29) (a) Buchanan, J. M.; Stryken, J. M.; Bergman, R. G. *J. Am. Chem. Soc.* **1986**, *108*, 1537. (b) *Ibid.* **1986**, *108*, 8119.

(30) Low, J. J.; Goddard, W. A., III *Organometallics* **1986**, *5*, 609.

(31) Perry, J. K.; Goddard, W. A., III *J. Am. Chem. Soc.*, in press.

(32) Crellin, K. C.; Geribaldi, S.; Beauchamp, J. L. *Organometallics*, submitted.

(33) Within the Sc^+ organometallic ions modeled by Perry and Goddard,[31] the bond strengths of the Sc^+-$CH_2CH(CH_3)_3$ and the Sc^+-$CH_2CH_2CH_3$ should be very nearly equal, because the spatial constrictions would preclude both β-methyls of the 1° Sc^+-isobutyl from coordinating simultaneously to the Sc^+ metal center.

(34) Interestingly, the eclipsed and trans conformers of the Sc^+-(n-propyl) molecular ions, respectively, yield bond energies that are 1 and 3 kcal/mol lower than Sc^+-methyl, in excellent agreement with the trend seen in the Ir-organometallic compounds.[25]

(35) (a) Jones, W. D. In *Selective Hydrocarbon Activation: Principles and Progress;* Davies, J. A., Watson, P. L., Greenburg, A., Liebman, J. F., Eds.; VCH Publishers: New York, 1990; pp. 113-148. (b) Armentrout, P. B. *ibid.* pp. 467-534. (c) Engstrom, J. R.; Goodman, D. W.; Weinberg, W. H. *J. Am. Chem. Soc.* **1988**, *110*, 8305.

(36) (a) Rodriguez, J. A.; Goodman, D. W. *J. Phys. Chem.* **1990**, *94*, 5342. (b) Mullins C. B.; Weinberg, W. H. *J. Chem. Phys.* **1990**, *92*, 4508.

(37) (a) Weinberg, W. H.; Sun, Y.-K. *Science* **1991**, *253*, 542. (b) Weinberg, W. H.; Sun Y.-K. *Surf. Sci. Lett.* **1992**, *277*, L39.

(38) Values between 10^{-2} and 10^{-3} for the ratios of the preexponential factors of the reaction and desorption rate coefficients for the activation of C-H bonds are expected.[6a,16]

Table 1. Apparent Rate Parameters for the Dissociative Chemisorption of Ethane, Propane, Isobutane, n-Butane, and Neopentane on Ir(111) [a]

Reactant	E_{app} (cal/mol)	$\frac{k_r^{(0)}}{k_d^{(0)}}$	E_d (cal/mol)	$E_{r,\,app}$ (cal/mol)	$k_r^{(0)}$, app (s^{-1}, $x10^{-11}$)
di-^{13}C-C_2H_6	2,670	1.1×10^{-2}	7,700	10,370	1.1
C_2D_6	3,150	1.1×10^{-2}	7,700	10,850	1.1
C_3H_8	1,710	9.3×10^{-3}	9,700	11,410	0.93
$CH_3CD_2CH_3$	1,950	9.3×10^{-3}	9,700	11,650	0.93
C_3D_8	2,340	9.3×10^{-3}	9,700	12,040	0.93
n-C_4H_{10}	780	9.9×10^{-3}	10,700	11,480	0.99
$(CH_3)_3CH$	960	1.0×10^{-2}	10,400	11,360	1.0
$(CH_3)_3CD$	1,120	1.0×10^{-2}	10,400	11,520	1.0
$(CD_3)_3CH$	1,300	1.0×10^{-2}	10,400	11,700	1.0
$(CH_3)_4C$	600	9.7×10^{-3}	10,700	11,300	0.97

[a]The separately measured values for the desorption rate coefficient were used in evaluating E_r and $k_r^{(0)}$. The quantity Eapp is the apparent activation energy with respect to a gas-phase energy zero, *i.e.*, the gas-phase alkane molecule infinitely far from the surface and at rest. By comparison, Er is the apparent activation energy of the reaction with respect to the proper reference energy, the bottom of the physically adsorbed well. The preexponential factor for desorption, $k_d^{(0)}$, has been assumed to be equal to 10^{13} s^{-1} for all of the alkanes.

Table 2. Rate parameters for the dissociative chemisorption of propane and isobutane on Ir(111) [a]

Reactant	E_{app} (cal/mol)	$\left[\frac{k_r^{(0)}}{k_d^{(0)}}\right]_{1°}$	E_{r1}-E_d (cal/mol)	$\left[\frac{k_r^{(0)}}{k_d^{(0)}}\right]_{2°}$	E_{r2}-E_d (cal/mol)	$\left[\frac{k_r^{(0)}}{k_d^{(0)}}\right]_{3°}$	E_{r3}- E_d (cal/mol)
C_3H_8	1,710	5.8x10-3	1845	3.5x10-3	1535		
$CH_3CD_2CH_3$	1,950	5.8x10-3	1845	3.5x10-3	2165		
$CD_3CH_2CD_3$[b]	1,930	5.8x10-3	2475	3.5x10-3	1535		
C_3D_8	2,340	5.8x10-3	2475	3.5x10-3	2165		
$(CH_3)_3CH$	960	6.8x10-3	988			3.2x10-3	905
$(CH_3)_3CD$	1,120	6.8x10-3	988			3.2x10-3	1545
$(CD_3)_3CH$	1,300	6.8x10-3	1628			3.2x10-3	905
$(CD_3)_3CD$[b]	1,600	6.8x10-3	1628			3.2x10-3	1545

[a]The measured energies, $E_{app} = E_r - E_d$, from the data in Figs. 7 and 8 are the apparent activation energies for the dissociative chemisorption of the indicated isotopomers of propane and isobutane relative to the gas-phase energy zero. The quantities, $E_{r1} - E_d$, $E_{r2} - E_d$, and $E_{r3} - E_d$, are the activation energies for the formation of 1°, 2°, and 3° Ir-propyl and Ir-isobutyl intermediates, and are derived from the conditional probabilities in Eqs. 14 and 15 (for propane) and Eqs. 19 and 20 (for isobutane) and the apparent probabilities of reaction $P_{r,app}$. The measured apparent and actual ratios of preexponential factors of the dissociative chemisorption and desorption rate coefficients of the physically adsorbed alkane are also provided.

[b]Calculated values.

Table 3. Elementary Rate Parameters for 1°, 2°, and 3° C-H and C-D Bond Activation in Ethane, Propane, Isobutane, n-Butane, and Neopentane on Ir(111)[a]

Reactant	$E_{r,app}$ (kcal/mol)	$E_{r,1°}$ (kcal/mol)	$k_r^{(0)},1°$ (s^{-1}, x10^{-11})	$E_{r,2°}$ (kcal/mol)	$k_r^{(0)},2°$ (s^{-1}, x10^{-11})	$E_{r,3°}$ (kcal/mol)	$k_r^{(0)},3°$ (s^{-1}, x10^{-11})
di-^{13}C-C_2H_6	10.37	10.37	1.1×10^{-2}				
C_2D_6	10.85	10.85	1.1×10^{-2}				
C_3H_8	11.41	11.63	3.3×10^{-3}	11.32	6.0×10^{-3}		
$CH_3CD_2CH_3$	11.65	11.63	3.3×10^{-3}	11.95	6.0×10^{-3}		
$CD_3CH_2CD_3$[b]	11.63	12.26	3.3×10^{-3}	11.32	6.0×10^{-3}		
C_3D_8	12.04	12.26	3.3×10^{-3}	11.95	6.0×10^{-3}		
n-C_4H_{10}	11.48						
$(CH_3)_3CH$	11.36	11.43	1.9×10^{-2}			11.34	8.1×10^{-3}
$(CH_3)_3CD$	11.52	11.43	1.9×10^{-2}			11.98	8.1×10^{-3}
$(CD_3)_3CH$	11.70	12.07	1.9×10^{-2}			11.34	8.1×10^{-3}
$(CD_3)_3CD$[b]	12.00	12.07	1.9×10^{-2}			11.98	8.1×10^{-3}
$(CH_3)_4C$	11.50	11.50	9.7×10^{-3}				

[a]The separately measured values for the desorption rate coefficient were used in evaluating the activation energies, Er, and the preexponential factors for the reaction rate coefficients, $k_r^{(0)}$. The quantities $E_{r,1°}$, $E_{r,2°}$, and $E_{r,3°}$ are the activation energies for the primary, secondary, and tertiary C-H (C-D) elementary bond cleavage with respect to the bottom of the physically adsorbed well. In comparison, $E_{r,app}$, taken from Table 1, is the apparent activation energy of the dissociative chemisorption of the indicated alkane.

[b]Calculated values.

Figure Captions

Figure 1. Initial probabilities of trapping-mediated dissociative chemisorption on Ir(111) as a function of reciprocal surface temperature for (a) di-^{13}C-C_2H_6 and C_2D_6, (b) C_3H_8, $CH_3CD_2CH_3$, and C_3D_8, (c) i-C_4H_{10}, $(CH_3)_3CD$, and $(CD_3)_3CH$, and (d) n-C_4H_{10} and $(CH_3)_4C$. The nonlinearity of these constructions for all but the ethane isotopomers arises from more than one reactive channel contributing to the total measured reaction probabilities. This text addresses the first of these two reaction channels, C-H bond activation, while the accompanying paper in this journal addresses the second channel, C-C bond activation (**4**).

Figure 2. Initial probabilities of the two competing channels for trapping-mediated dissociative chemisorption as a function of reciprocal surface temperature for C_3H_8, $CH_3CD_2CH_3$, and C_3D_8 on Ir(111). The probabilities associated with each reaction channel have been separated by the iterative procedure described in the text.

Figure 3. Initial probabilities of the two competing channels for trapping-mediated dissociative chemisorption as a function of reciprocal surface temperature for i-C_4H_{10}, $(CH_3)_3CD$, and $(CD_3)_3CH$ on Ir(111). The probabilities associated with each reaction channel have been separated by the iterative procedure described in the text.

Figure 4. Initial probabilities of the two competing channels for trapping-mediated dissociative chemisorption as a function of reciprocal surface temperature for n-C_4H_{10} on Ir(111). The probabilities associated with each reaction channel have been separated by the iterative procedure described in the text.

Figure 5. Initial probabilities of the two competing channels for trapping-mediated dissociative chemisorption as a function of reciprocal surface temperature for $(CH_3)_4C$ on Ir(111). The probabilities associated with each reaction channel have been separated by the iterative procedure described in the text.

Figure 6. Initial probabilities for the trapping-mediated dissociative chemisorption of C_3H_8, $CH_3CD_2CH_3$, and C_3D_8 on Ir(111) as a function of reciprocal surface temperature. The apparent activation energies, $E_r - E_d$, and the preexponential factors, $k_d^{(0)}/k_r^{(0)}$, for the activation of these alkanes are derived from the least-squares fits to these straight lines and are listed in Table 1.

Figure 7. Initial probabilities of the trapping-mediated dissociative chemisorption of i-C_4H_{10}, $(CH_3)_3CD$, and $(CD_3)_3CH$ on Ir(111) as a function of reciprocal surface temperature. The apparent activation energies, $E_r - E_d$, and the preexponential factors, $k_d^{(0)}/k_r^{(0)}$, for the activation of these alkanes are derived from the least-squares fits to these straight lines and are listed in Table 1.

Figure 8. The schematic reaction coordinate diagrams comparing the difference between the initial dissociative 1° and 2° C-H bond reaction steps of $CH_3CH_2CH_3$ on Ir(111). The gas-phase zero reference energy is the propane infinitely far from the surface and at rest. The gas-phase bond dissociation energies, $BDE^{(1°)}$ and $BDE^{(2°)}$, are depicted (**3**), as well as the different chemisorption bond energies for the selective dissociated products, *n*-C3H7(a) + H(a), and *i*-C3H7(a) + H(a). See text.

Figure 9. The schematic reaction coordinate diagrams comparing the difference between the initial dissociative 1° and 3° C-H bond reaction steps of $(CH_3)_3CH$ on Ir(111). The gas-phase zero reference energy is the isobutane infinitely far from the surface and at rest. The gas-phase bond dissociation energies, $BDE^{(1°)}$ and $BDE^{(2°)}$, are depicted (**3**), as well as the different chemisorption bond energies for the selective dissociated products, $(CH_3)_2CHCH_2(a) + H(a)$, and $(CH_3)_3C(a) + H(a)$. See text.

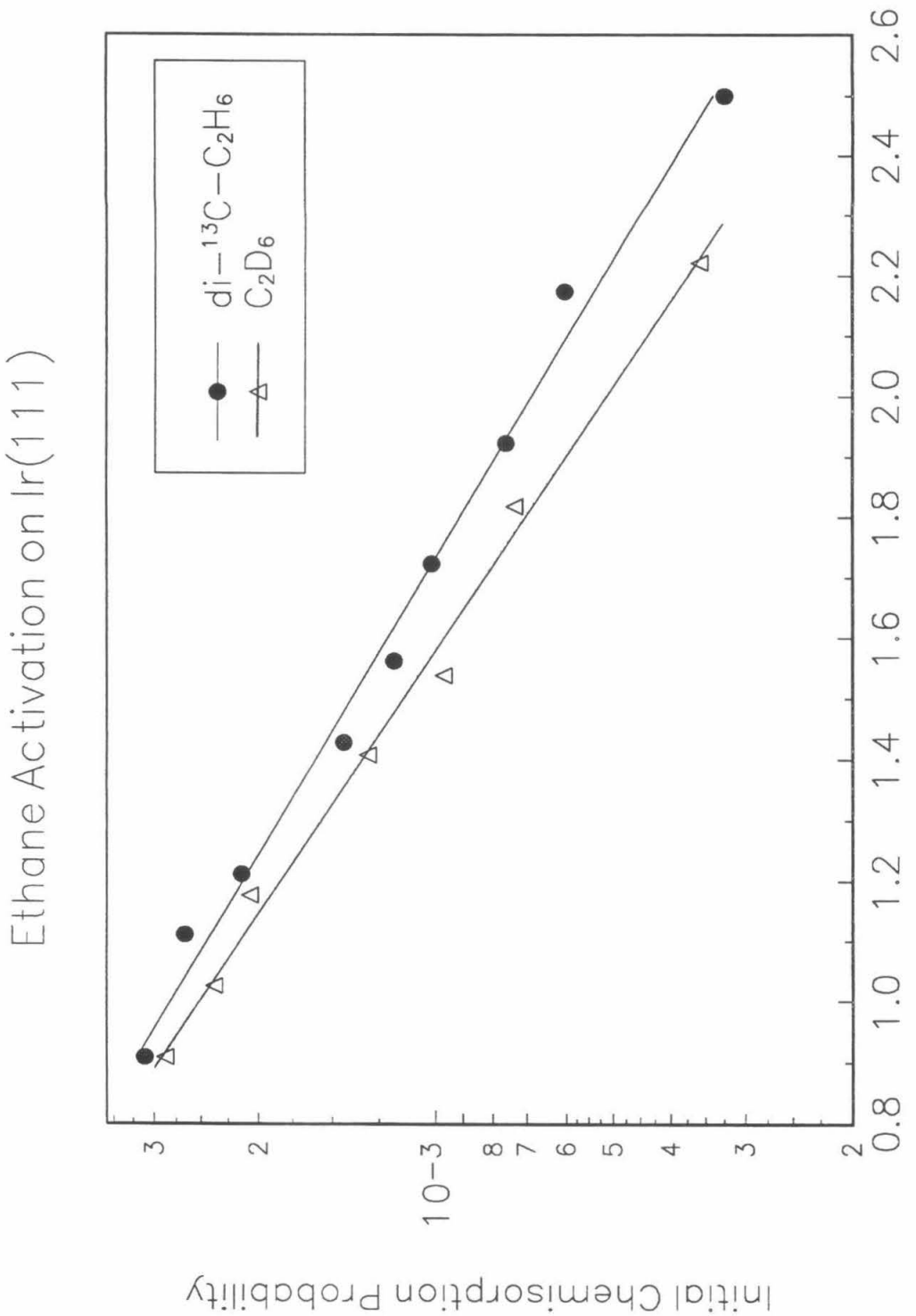
Ethane Activation on Ir(111)
Initial Chemisorption Probability
10−3
3
2
8
7
6
5
4
3
2
0.8
1.0
1.2
1.4
1.6
1.8
2.0
2.2
2.4
2.6
1000/Ts, (K−1)
di−13C−C2H6
C2D6

Figure 1a

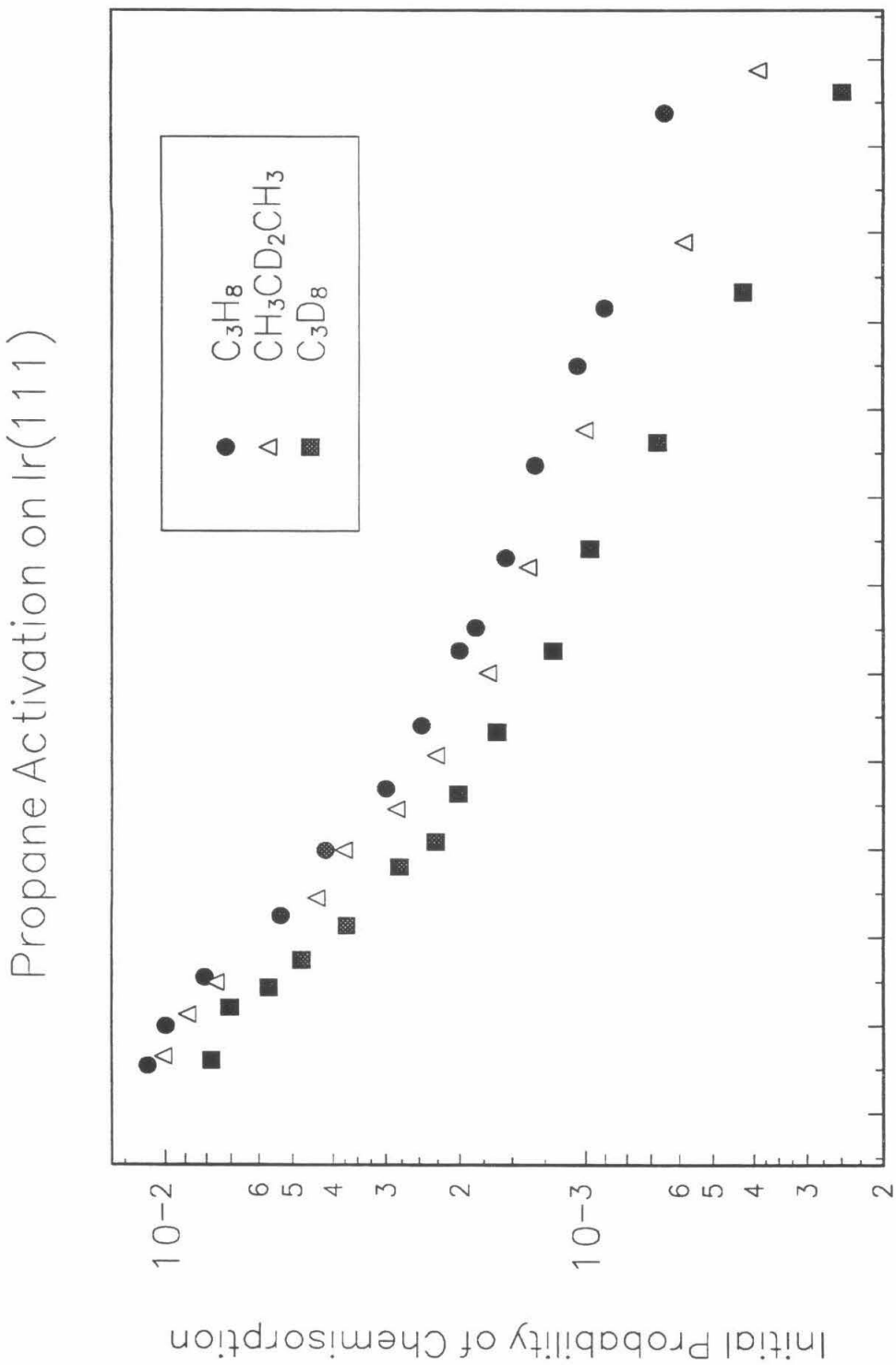
Propane Activation on Ir(111)
Initial Probability of Chemisorption
1000/Ts, (K-1)
C3H8
CH3CD2CH3
C3D8
10-2
10-3
0.8 1.0 1.2 1.4 1.6 1.8 2.0 2.2 2.4 2.6 2.8 3.0 3.2

Figure 1b

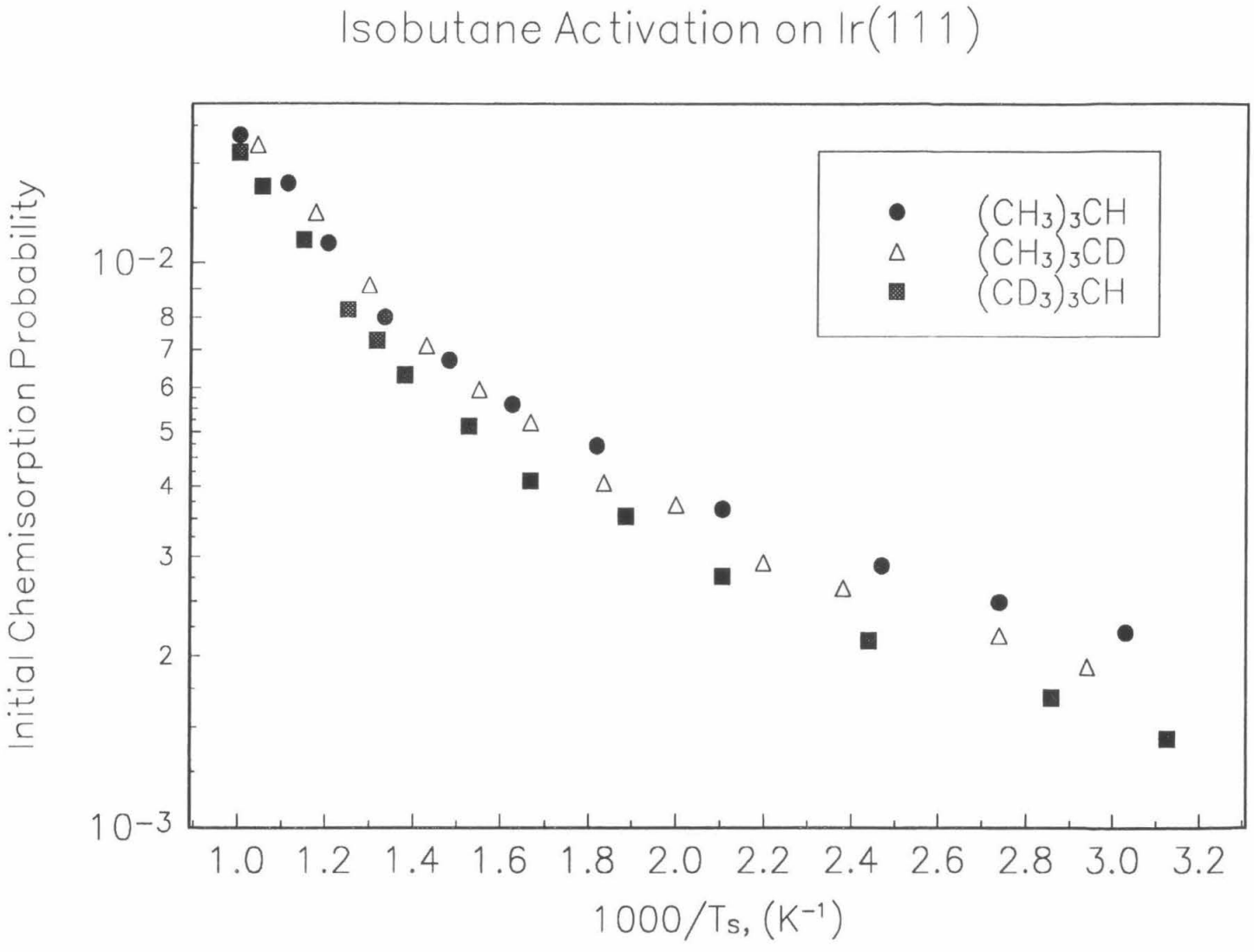
Isobutane Activation on Ir(111)
Initial Chemisorption Probability
10−2
8
7
6
5
4
3
2
10−3
1.0
1.2
1.4
1.6
1.8
2.0
2.2
2.4
2.6
2.8
3.0
3.2
1000/Ts, (K−1)
(CH3)3CH
(CH3)3CD
(CD3)3CH

Figure 1c

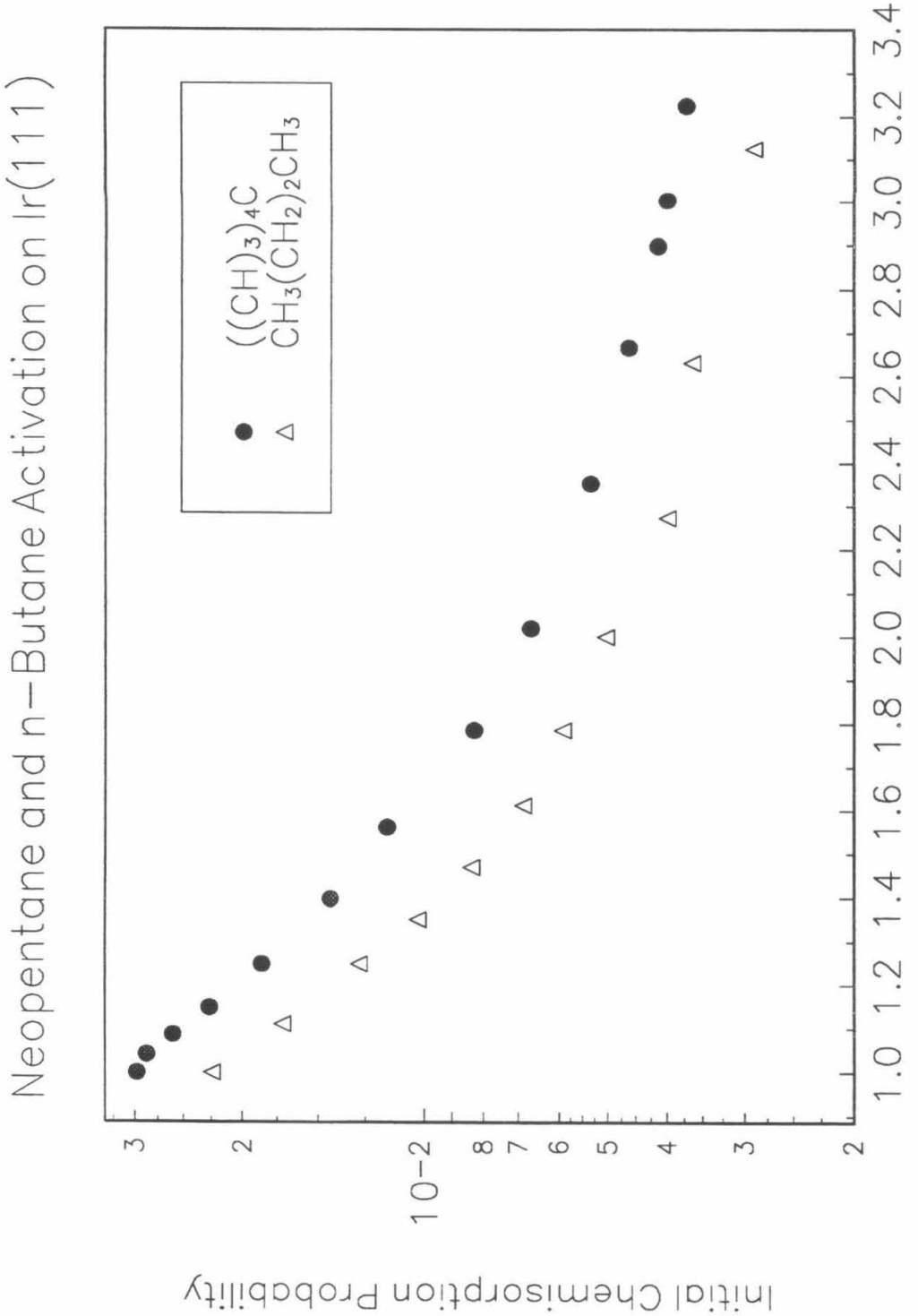
Neopentane and n–Butane Activation on Ir(111)
Initial Chemisorption Probability
10–2
3
2
8
7
6
5
4
3
2
1.0 1.2 1.4 1.6 1.8 2.0 2.2 2.4 2.6 2.8 3.0 3.2 3.4
1000/Ts, (K–1)
((CH3)3)4C
CH3(CH2)2CH3

Figure 1d

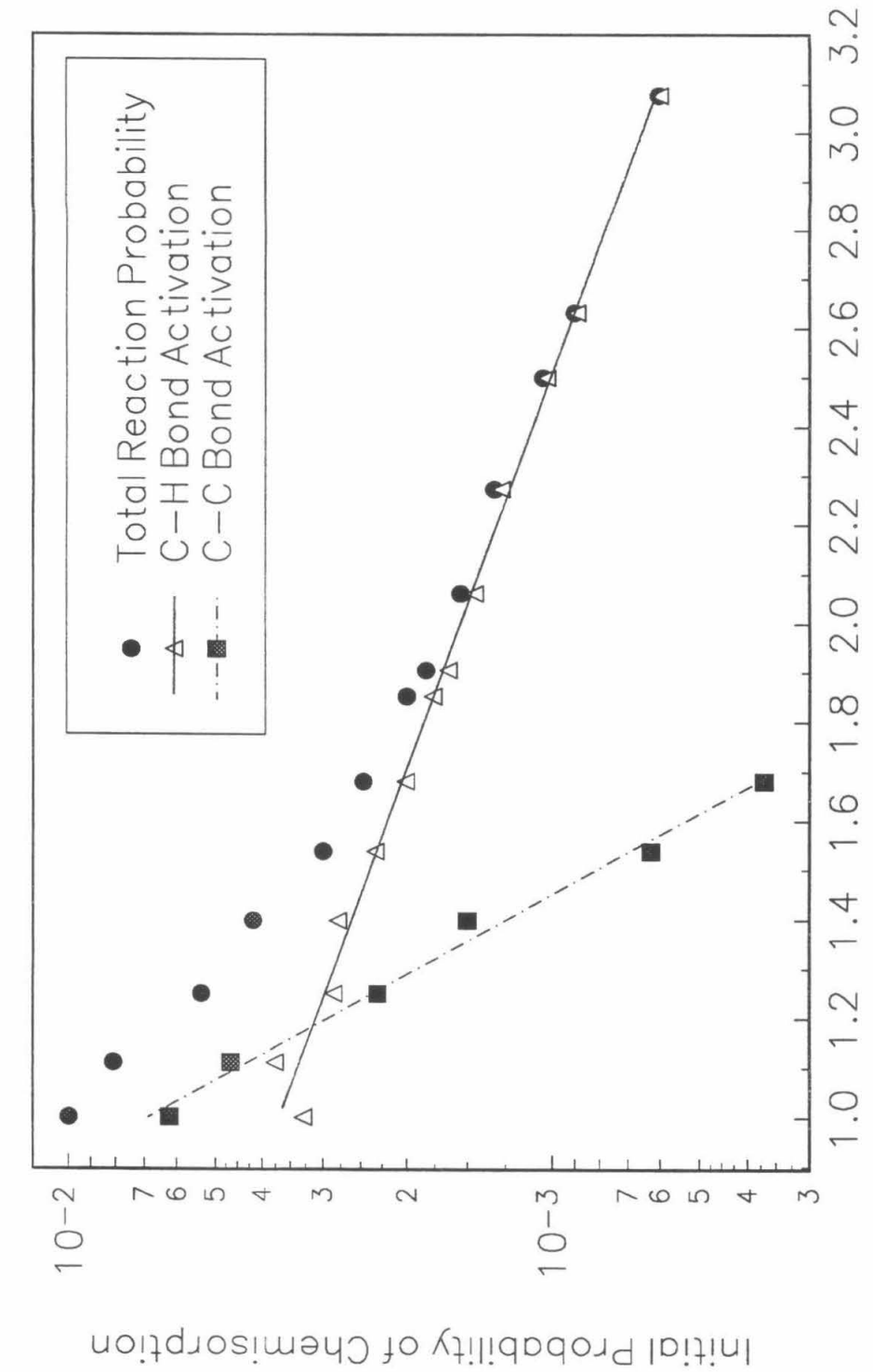
C3H8 Activation on Ir(111)
Total Reaction Probability
C–H Bond Activation
C–C Bond Activation
Initial Probability of Chemisorption
10–2
7
6
5
4
3
2
10–3
7
6
5
4
3
1.0 1.2 1.4 1.6 1.8 2.0 2.2 2.4 2.6 2.8 3.0 3.2
1000/Ts, (K–1)

Figure 2a

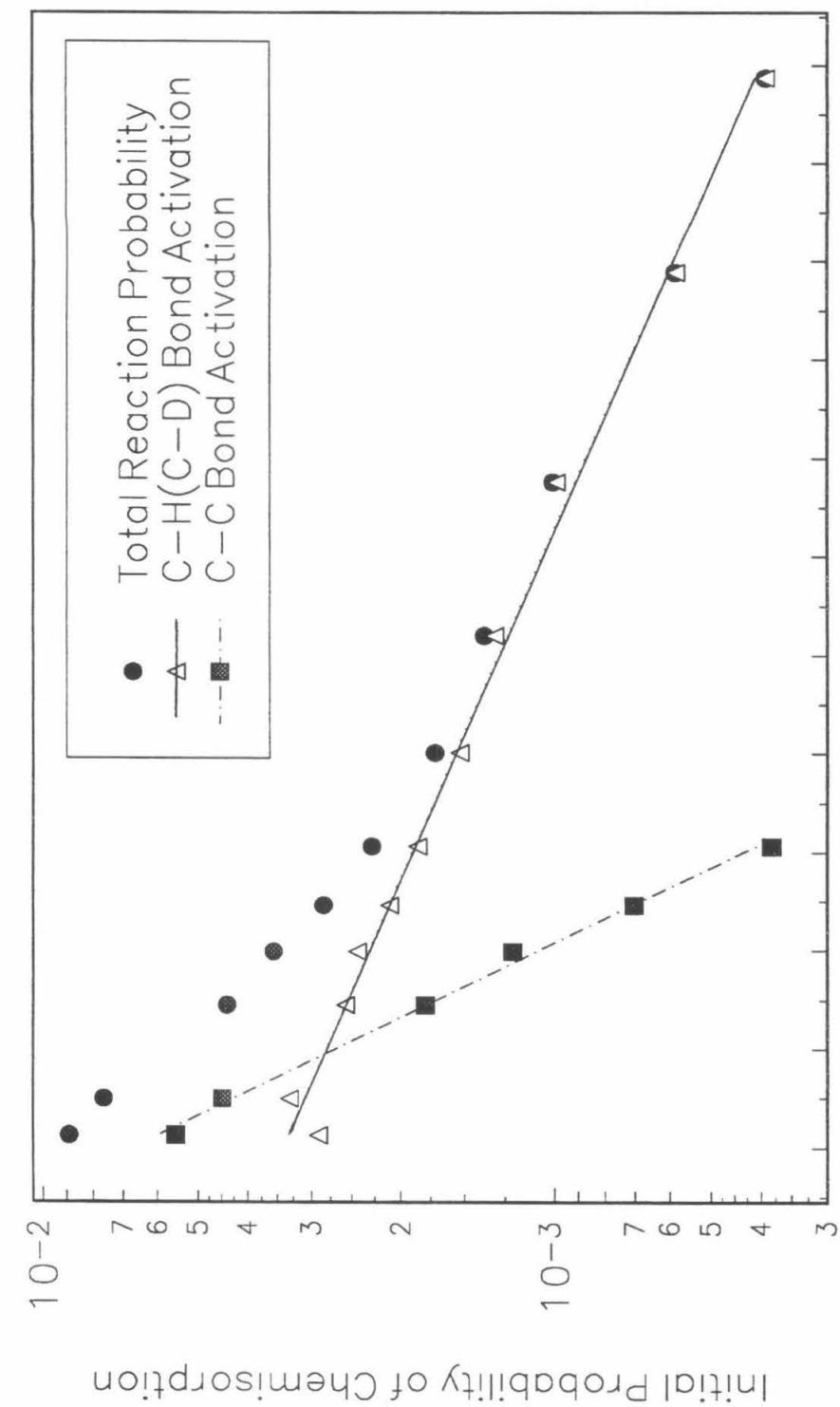
CH3CD2CH3 Activation on Ir(111)
Total Reaction Probability
C–H(C–D) Bond Activation
C–C Bond Activation
Initial Probability of Chemisorption
10–2
7
6
5
4
3
2
10–3
7
6
5
4
3
1.0 1.2 1.4 1.6 1.8 2.0 2.2 2.4 2.6 2.8 3.0 3.2
1000/Ts, (K–1)

Figure 2b

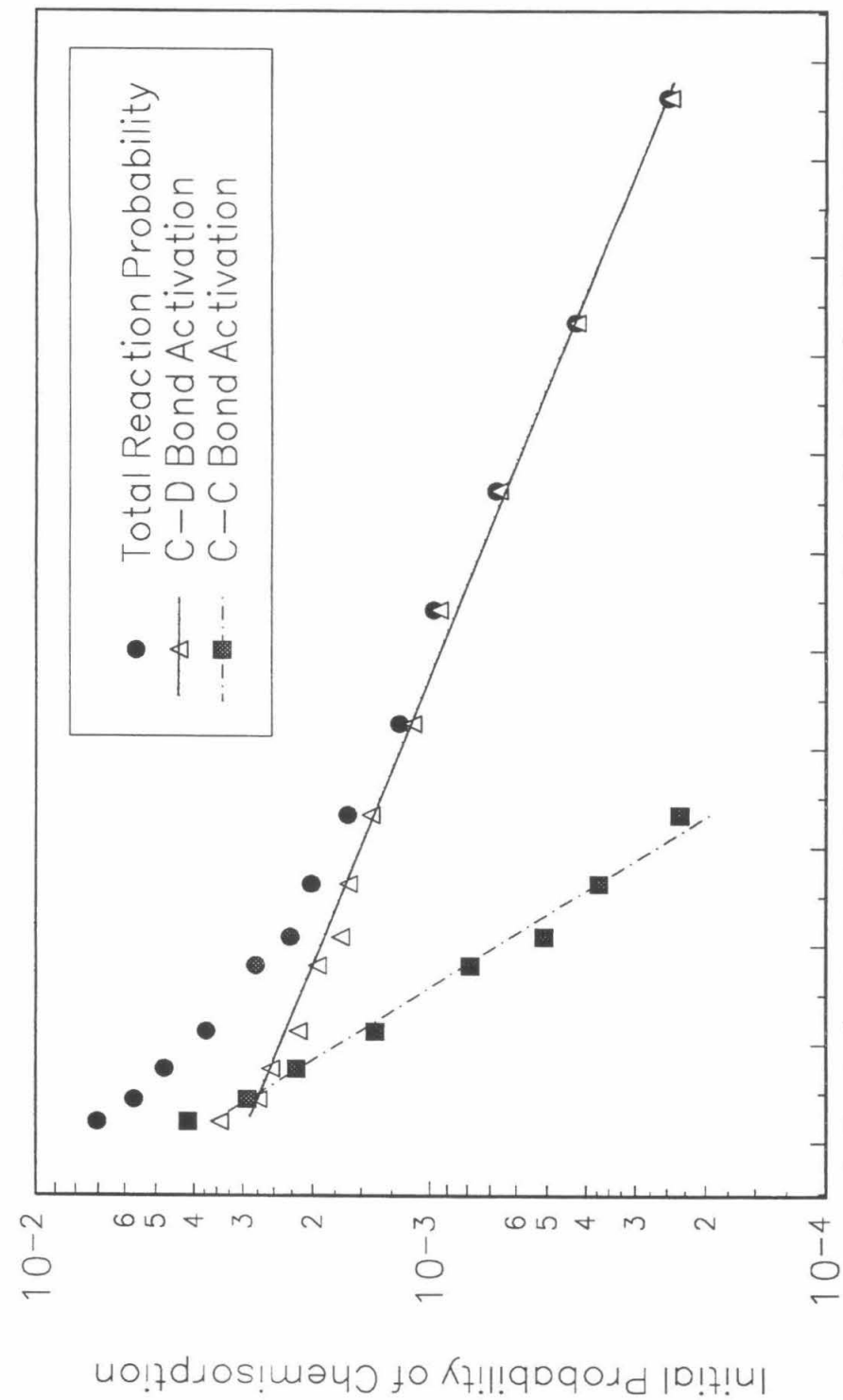
C3D8 Activation on Ir(111)
Total Reaction Probability
C—D Bond Activation
C—C Bond Activation
Initial Probability of Chemisorption
10−2
6
5
4
3
2
10−3
6
5
4
3
2
10−4
1.0 1.2 1.4 1.6 1.8 2.0 2.2 2.4 2.6 2.8 3.0 3.2
1000/Ts, (K−1)

Figure 2c

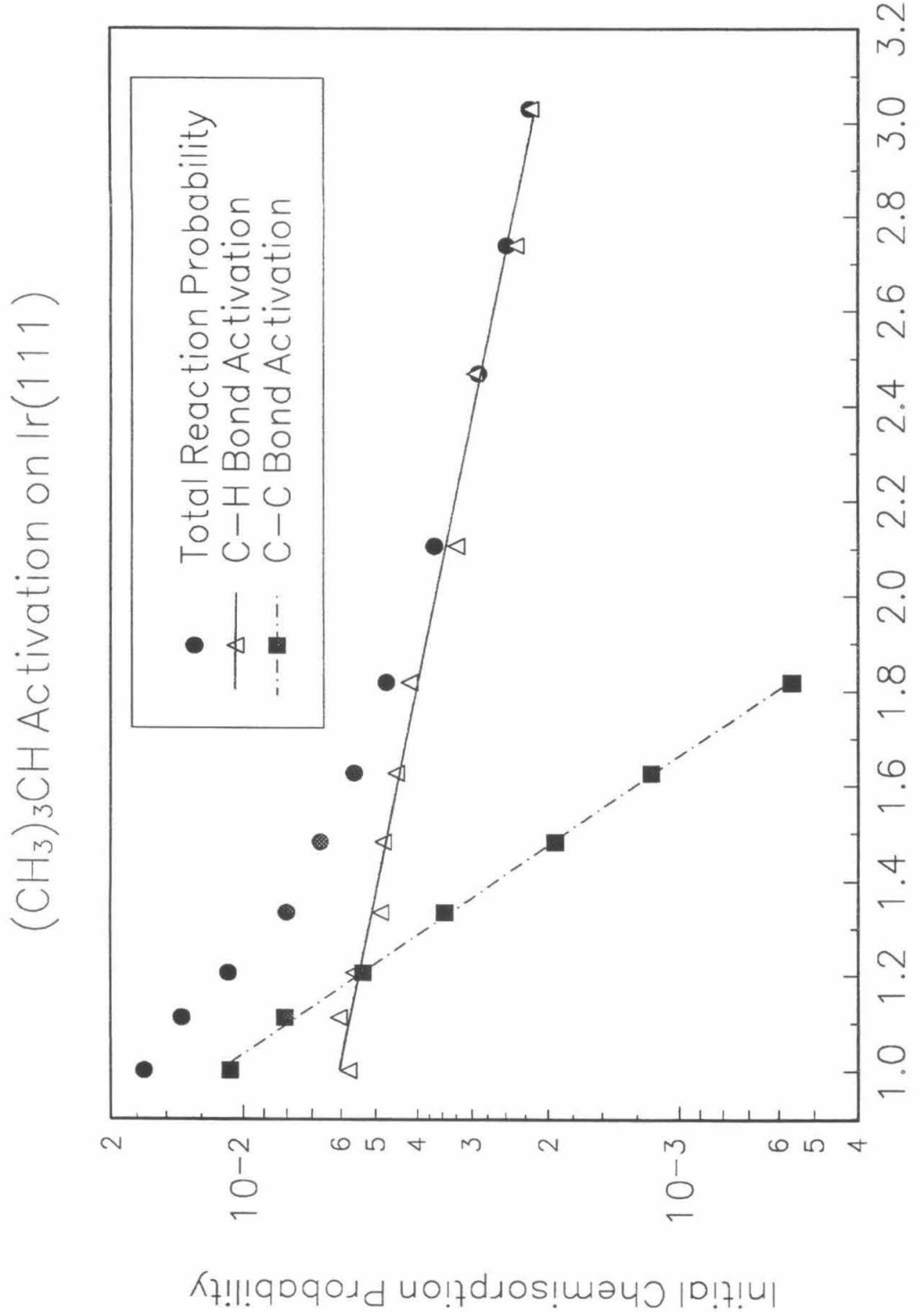
(CH3)3CH Activation on Ir(111)
Total Reaction Probability
C–H Bond Activation
C–C Bond Activation
Initial Chemisorption Probability
10–2
10–3
2
6
5
4
3
2
6
5
4
1.0 1.2 1.4 1.6 1.8 2.0 2.2 2.4 2.6 2.8 3.0 3.2
1000/Ts, (K–1)

Figure 3a

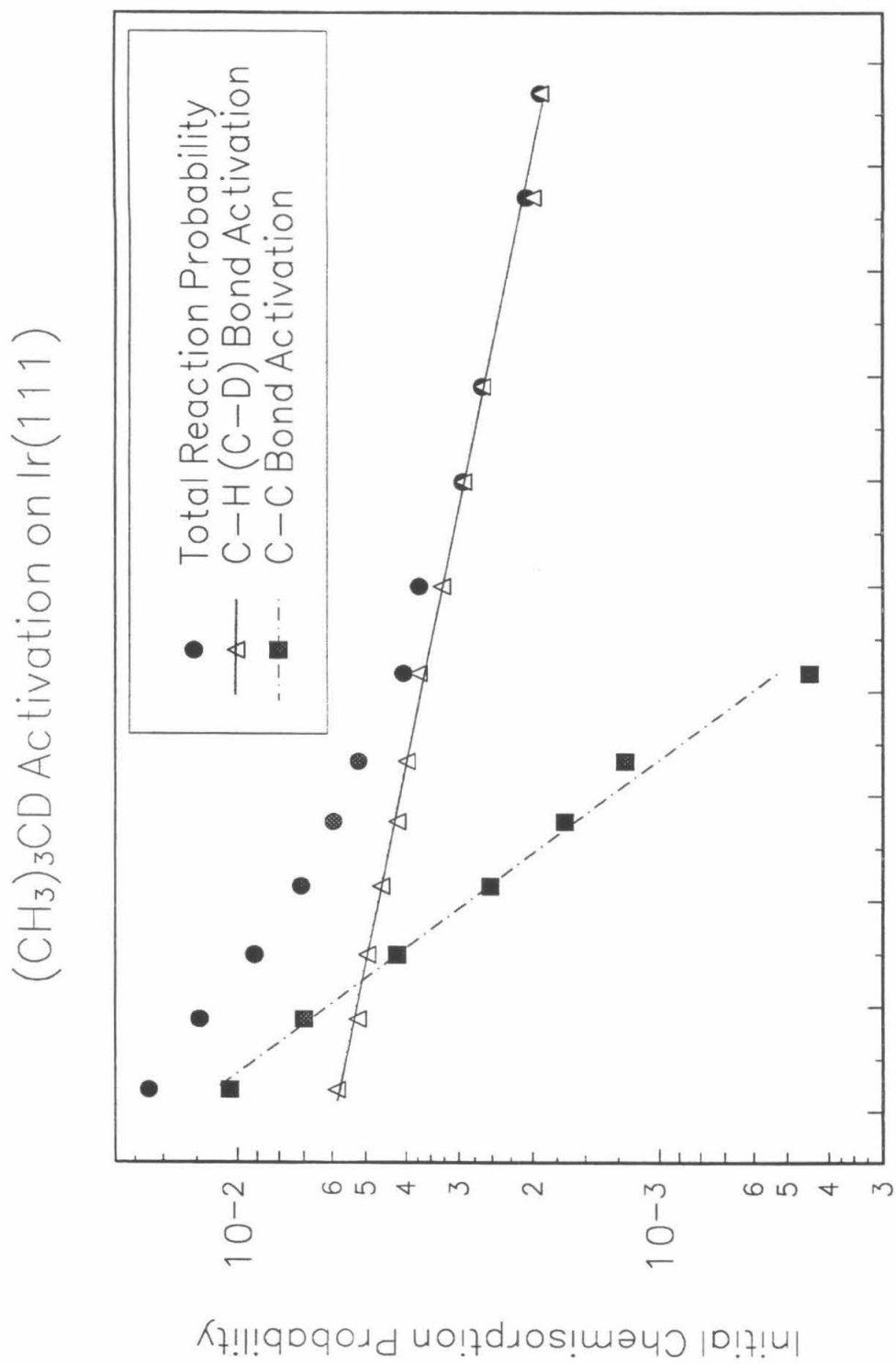
(CH3)3CD Activation on Ir(111)
Total Reaction Probability
C–H (C–D) Bond Activation
C–C Bond Activation
Initial Chemisorption Probability
10–2
10–3
1.0 1.2 1.4 1.6 1.8 2.0 2.2 2.4 2.6 2.8 3.0
1000/Ts, (K–1)

Figure 3b

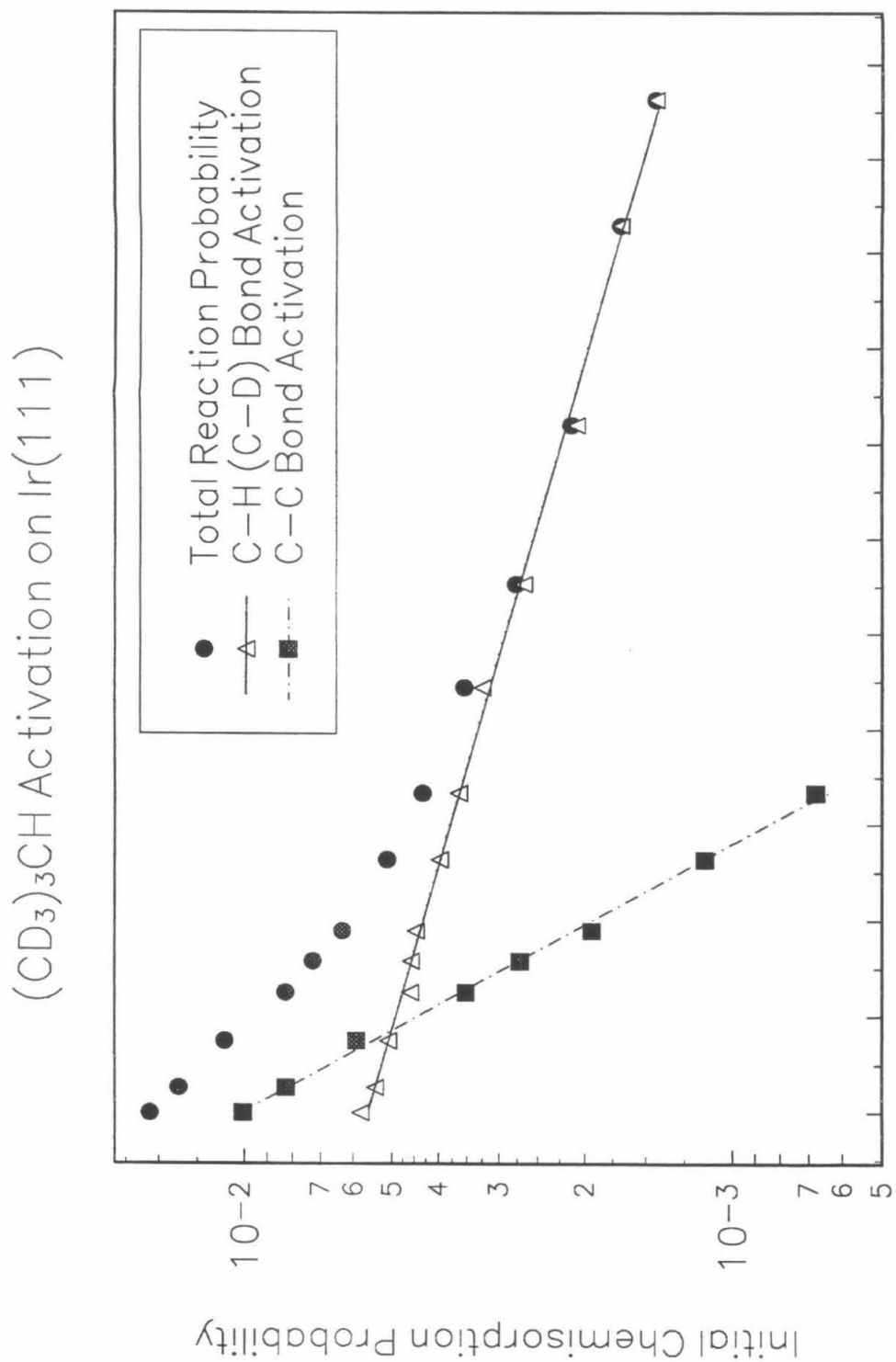
(CD3)3CH Activation on Ir(111)
Total Reaction Probability
C–H (C–D) Bond Activation
C–C Bond Activation
Initial Chemisorption Probability
10–2
10–3
1000/Ts, (K–1)
1.0 1.2 1.4 1.6 1.8 2.0 2.2 2.4 2.6 2.8 3.0 3.2

Figure 3c

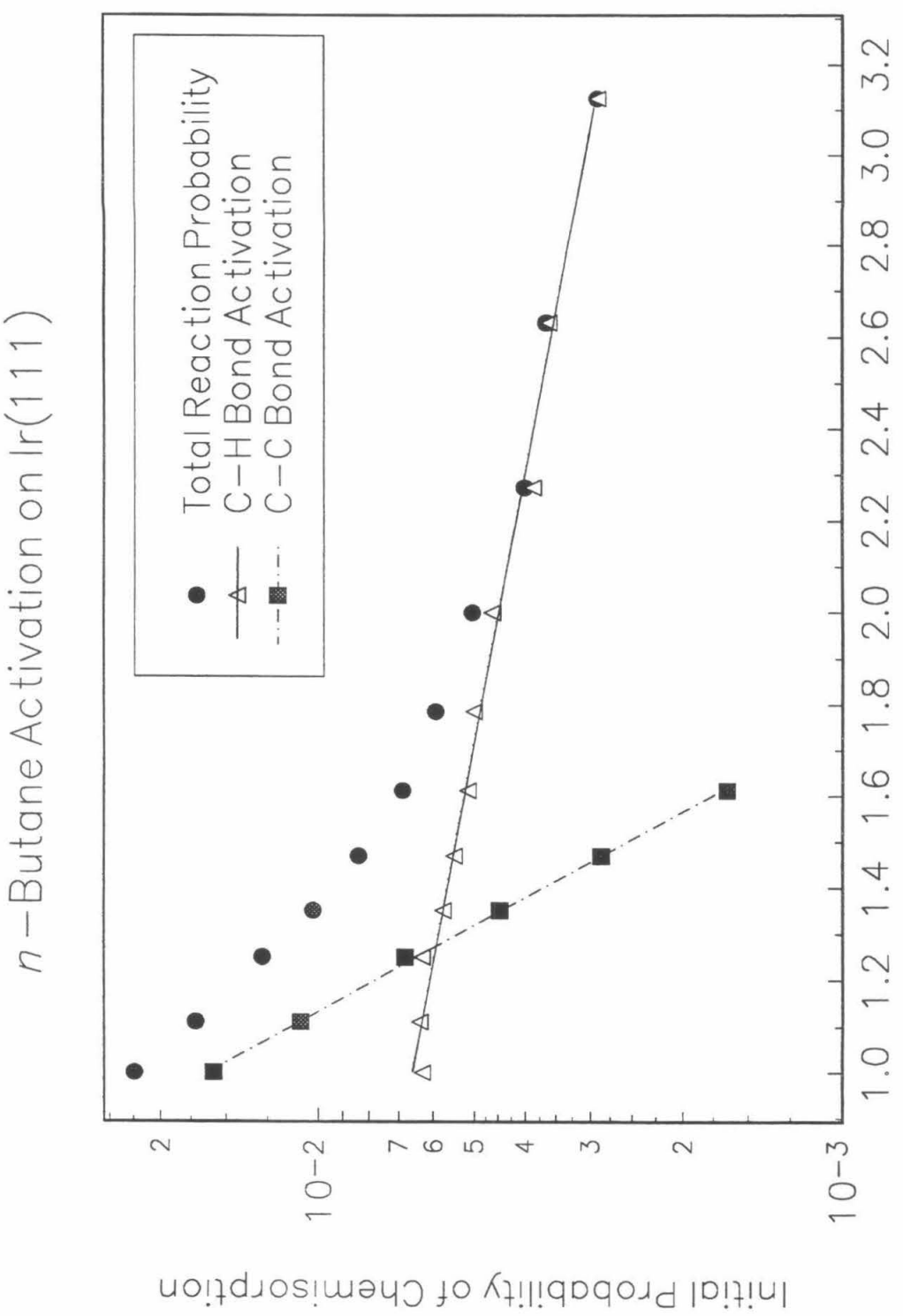
n-Butane Activation on Ir(111)
Total Reaction Probability
C-H Bond Activation
C-C Bond Activation
Initial Probability of Chemisorption
10-2
7
6
5
4
3
2
10-3
1.0 1.2 1.4 1.6 1.8 2.0 2.2 2.4 2.6 2.8 3.0 3.2
1000/Ts, (K-1)

Figure 4

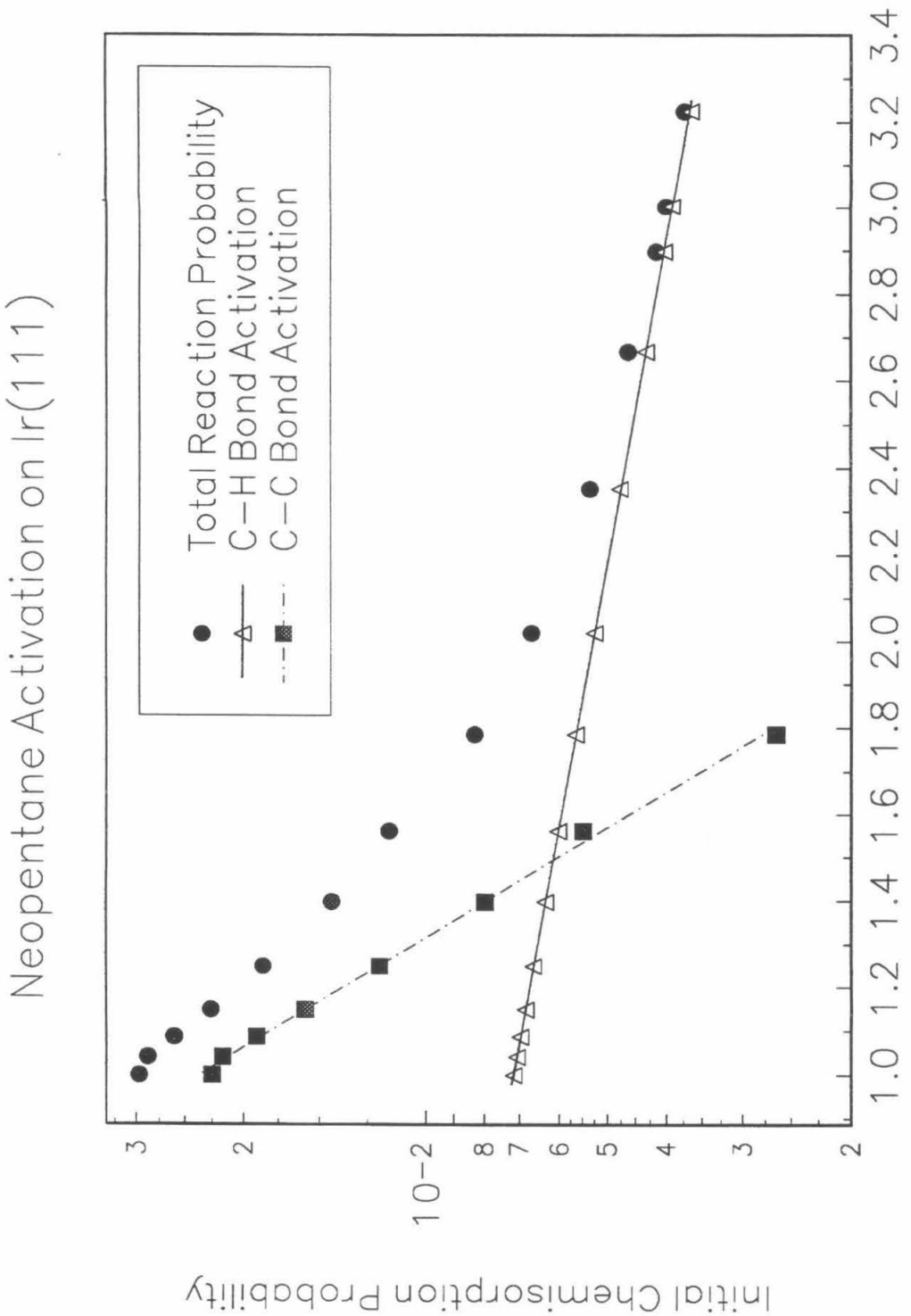
Neopentane Activation on Ir(111)
Total Reaction Probability
C–H Bond Activation
C–C Bond Activation
Initial Chemisorption Probability
10–2
1000/Ts, (K–1)
1.0 1.2 1.4 1.6 1.8 2.0 2.2 2.4 2.6 2.8 3.0 3.2 3.4

Figure 5

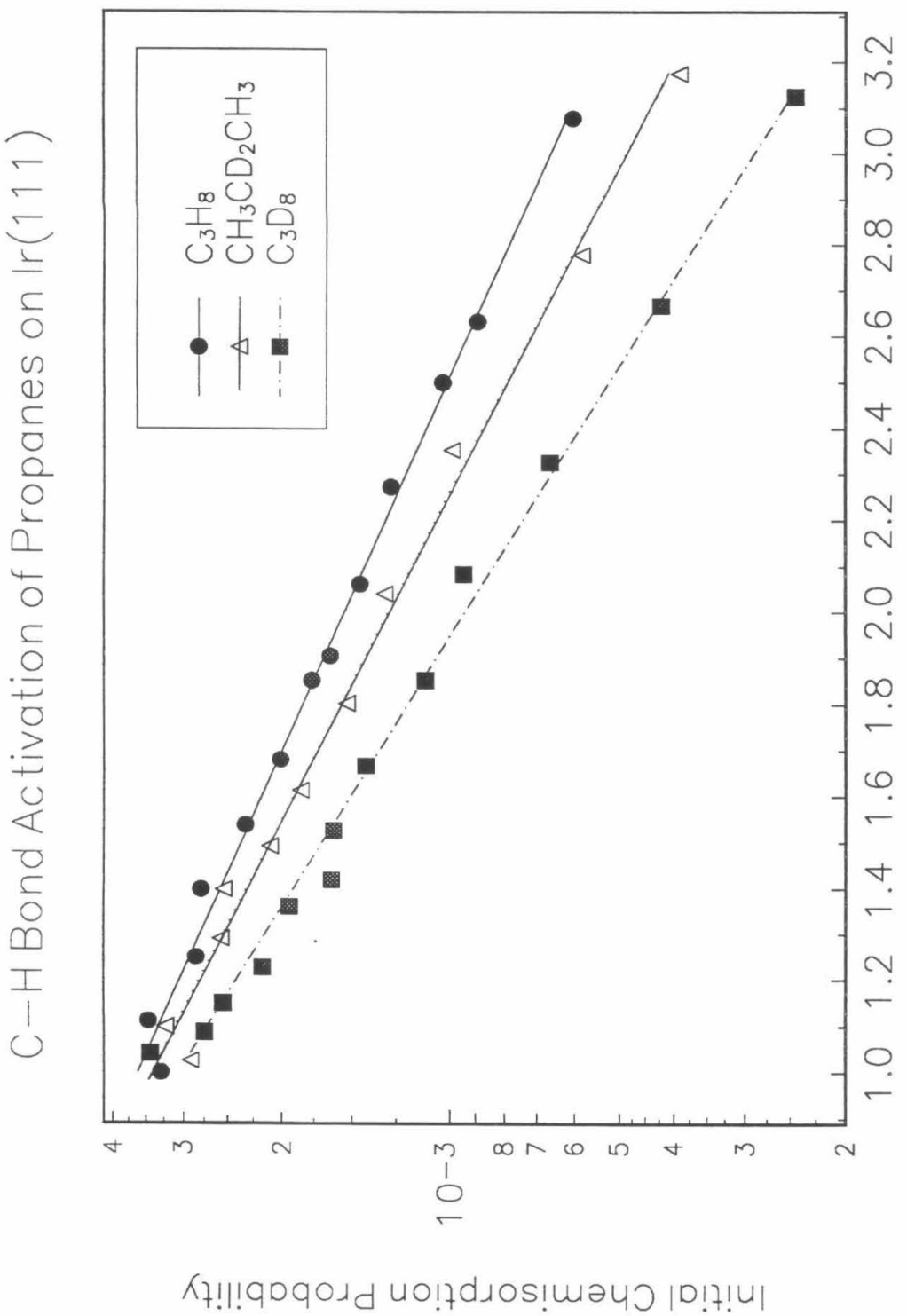
C–H Bond Activation of Propanes on Ir(111)
Initial Chemisorption Probability
10–3
4
3
2
8
7
6
5
4
3
2
1.0 1.2 1.4 1.6 1.8 2.0 2.2 2.4 2.6 2.8 3.0 3.2
1000/Ts, (K–1)
C3H8
CH3CD2CH3
C3D8

Figure 6

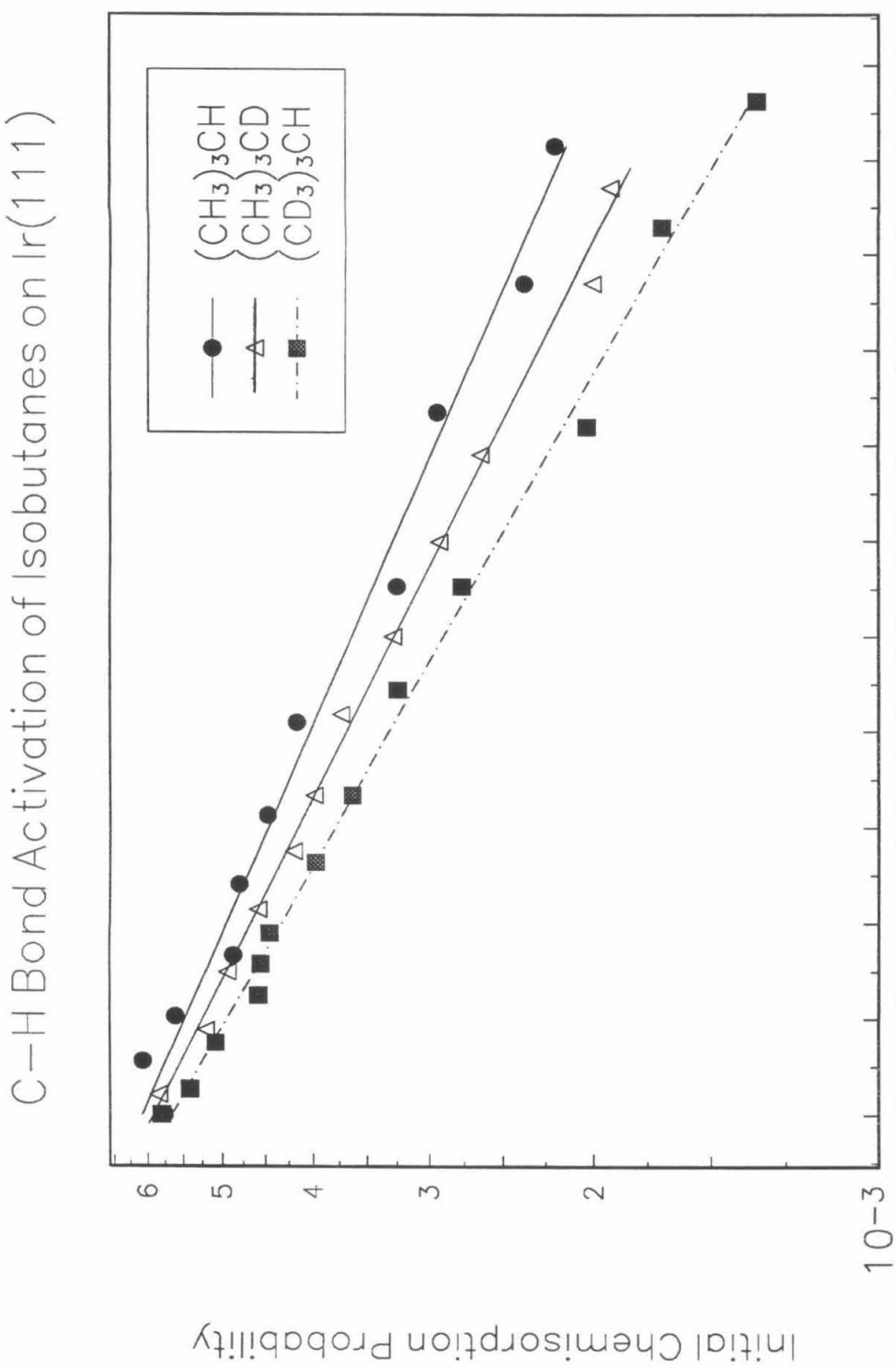
C–H Bond Activation of Isobutanes on Ir(111)
Initial Chemisorption Probability
1000/Ts, (K-1)
(CH3)3CH
(CH3)3CD
(CD3)3CH
10-3
6
5
4
3
2
1.0
1.2
1.4
1.6
1.8
2.0
2.2
2.4
2.6
2.8
3.0
3.2

Figure 7

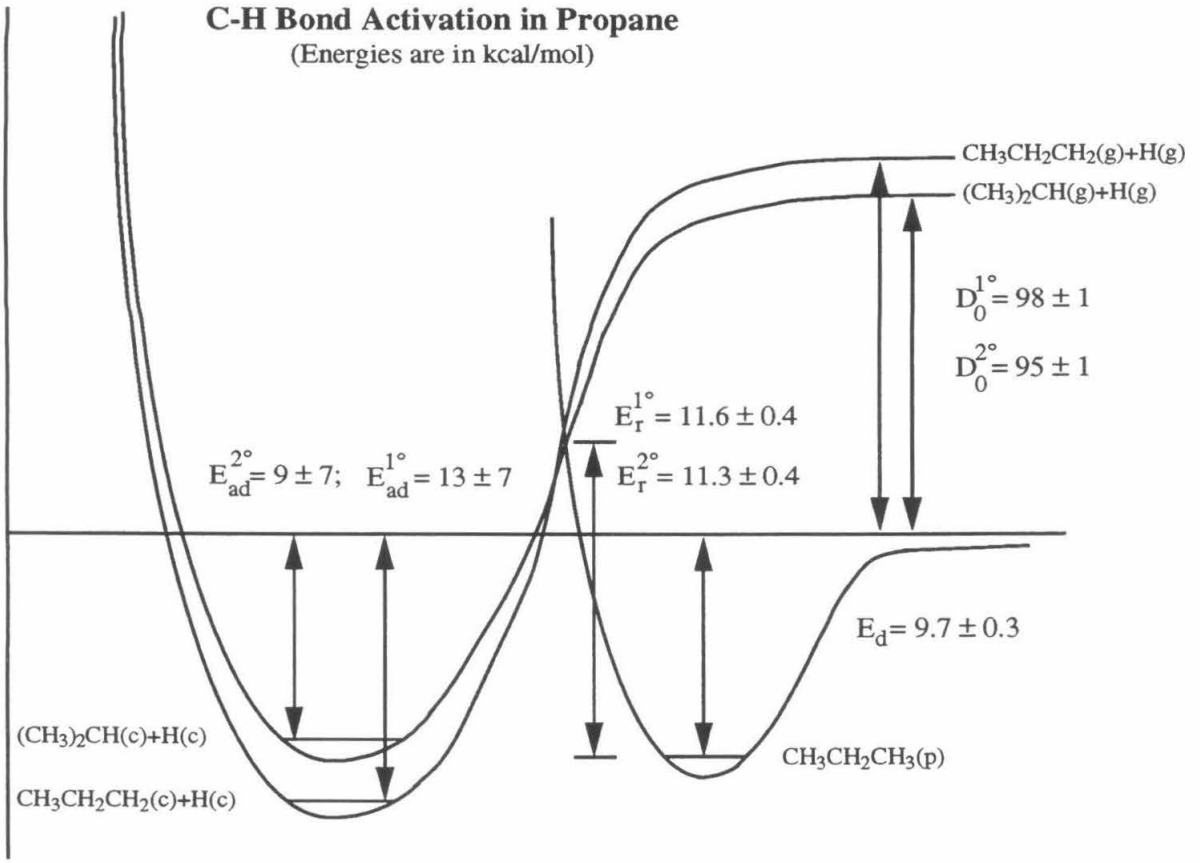
C-H Bond Activation in Propane
(Energies are in kcal/mol)
CH3CH2CH2(g)+H(g)
(CH3)2CH(g)+H(g)
D1° 0 = 98 ± 1
D2° 0 = 95 ± 1
E1° r = 11.6 ± 0.4
E2° r = 11.3 ± 0.4
E2° ad = 9 ± 7; E1° ad = 13 ± 7
Ed = 9.7 ± 0.3
(CH3)2CH(c)+H(c)
CH3CH2CH2(c)+H(c)
CH3CH2CH3(p)

Figure 8

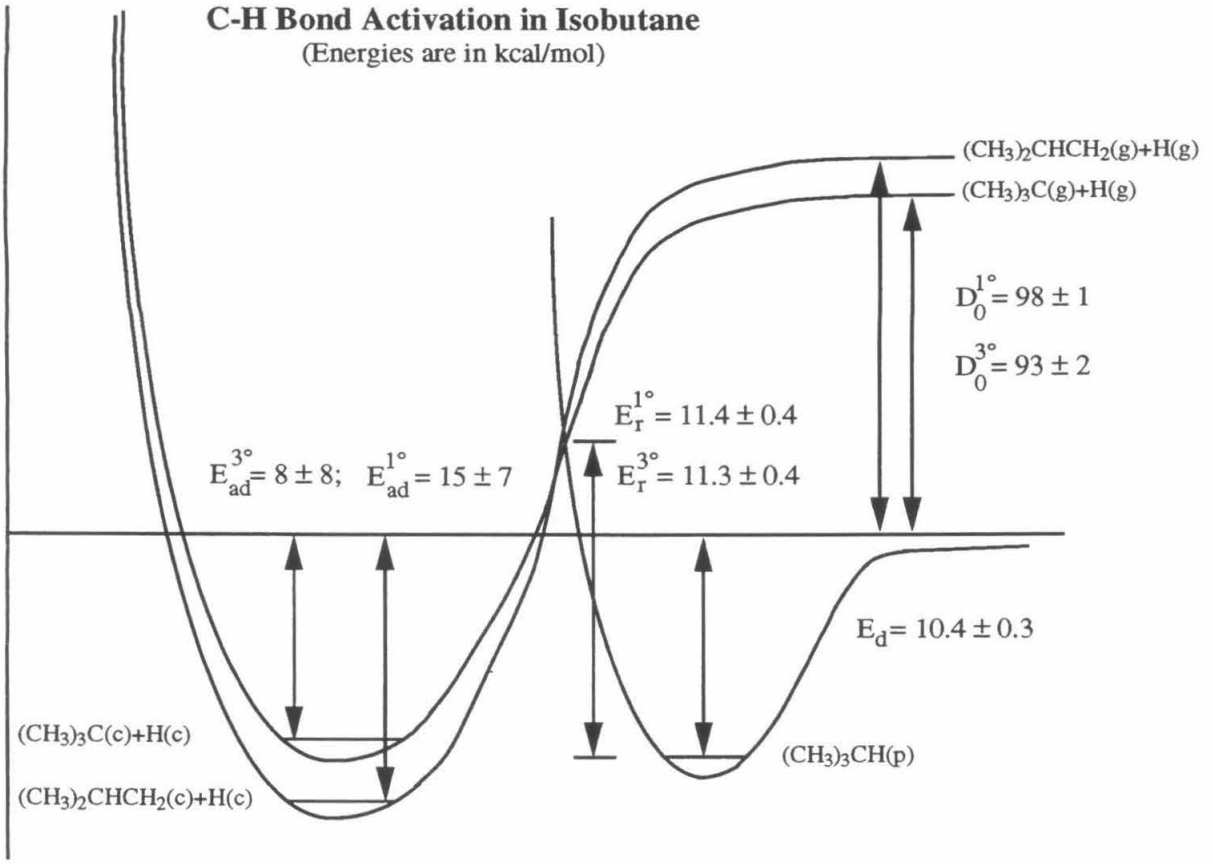
C-H Bond Activation in Isobutane
(Energies are in kcal/mol)
(CH3)2CHCH2(g)+H(g)
(CH3)3C(g)+H(g)
D1°0 = 98 ± 1
D3°0 = 93 ± 2
E1°r = 11.4 ± 0.4
E3°r = 11.3 ± 0.4
E3°ad = 8 ± 8; E1°ad = 15 ± 7
Ed = 10.4 ± 0.3
(CH3)3C(c)+H(c)
(CH3)2CHCH2(c)+H(c)
(CH3)3CH(p)

Figure 9

CHAPTER 6

Quantification of the Selective Activation of C-C Bonds in Short Chain Alkanes: The Reactivity of Ethane, Propane, Isobutane, n-Butane, and Neopentane on Ir(111)

[The text of Chapter 6 consists of an article coauthored with W. H. Weinberg, which has been submitted to *Journal of the American Chemical Society*.]

Abstract: The initial probabilities of trapping-mediated, dissociative chemisorption of the saturated hydrocarbons ^{13}C-labeled ethane, propane, isobutane, n-butane, and neopentane on the close-packed Ir(111) surface have been investigated. The activation of both C-C and C-H bonds has been observed in all alkanes examined, except for ethane, for which only C-H bond activation was observed. After separating the contribution to the total reaction probability from the competing C-H bond activation channel, the selective activation of C-C bonds in these alkanes has been quantified. A secondary deuterium kinetic isotope effect has been observed for the activation of C-C bonds upon deuteration of the terminal methyl groups of propane and isobutane. With respect to the bottom of the physically adsorbed well for each hydrocarbon, the apparent C-C bond activation energies (kcal/mol) have been determined to be 18.4 [C_3H_8 and $CH_3CD_2CH_3$] and 19.0 [C_3D_8], 17.7 [i-C_4H_{10} and $(CH_3)_3CD$] and 18.2 [$(CD_3)_3CH$], 17.9 [n-C_4H_{10}], and 16.1 [$(CH_3)_4C$]. The implications of the observed secondary kinetic isotope defect are discussed in terms of the deformation of the terminal methyl groups which accompanies the cleavage of the C-C bonds.

1. Introduction

The activation of C-C bonds in alkanes by transition metals is a reaction that is generally observed to occur subsequent to the initial activation of a C-H bond and formation of an alkyl intermediate. For example, C-C bond activation, in the reaction between 1,1-dimethylcyclopentane and an iridium complex, was observed to occur by an indirect mechanism in which a dehydrogenation step preceded the C-C bond scission reaction (**1**). In gas-phase reactions between metal ions and propane, products resulting from the cleavage of C-C bonds are observed, however, at low collisional energies, the mechanism is believed to follow the indirect path via initial dehydrogenation of the metal-alkane adduct (**2–4**). By collisionally

activating the thermalized cationic iron-propane complex, $Fe^{+}(C_3H_8)$, Schultz and Armentrout (**5**) determined that C-H bond activation occurred at 11 ± 3 kcal/mol. Furthermore, they demonstrated that this initial C-H bond scission reaction was responsible for the production of both dihydrogen (monitored via $FeC_3H_6^{+}$) and methane (monitored via $FeC_2H_4^{+}$) at collisional activation energies below ~1 eV. Above this energy, however, the production of $FeC_2H_4^{+}$ increased due to the initiation of a higher energy path, namely, direct, rather than indirect, C-C bond activation. They estimated the activation energy of this direct C-C bond cleavage to be only slightly less than the bond dissociation energy of the parent complex, $Fe^{+}(C_3H_8)$, which was found to be 19 ± 2 kcal/mol (**5**).

The differences in the bond dissociation energies for C-C and C-H bonds in alkanes favors the initial cleavage of C-C bonds, e.g., in kcal/mol, $D_0(H_3C–CH_3)$ = 90.4 ± 0.3, $D_0(H_5C_2–CH_3)$ = 87 ± 1, $D_0(H_7C_3–CH_3)$ = 87 ± 1, $D_0[(CH_3)_2C(H)–CH_3]$ = 86 ± 1, $D_0[(CH_3)_3C–CH_3]$ = 85 ± 1, and $D_0(H_5C_2–C_2H_5)$ = 84 ± 1, while the corresponding C-H bond dissociation energies are ~10 kcal/mol higher (**6**). However, it is well known that the directional nature of the sp^3-hybridized orbitals of the C-C bond prevents an easy transition from reactants to products (**7**), while, the stronger C-H bonds have lower activation energies because their isotropic spatial character allows for effective overlap in the formation of new bonds as the existing ones are breaking. Thus, to date, quantitative measurements of the activation of alkanes have characterized the more facile of the two reaction channels, C-H bond cleavage. This statement includes our accompanying manuscript, which presents results for the activation of C-H bonds in small chain alkanes on Ir(111) (**8**). We report here quantitative analyses of the competing reaction

channel of initial C-C bond cleavage which has, more often than not, eluded investigators in their studies of alkane activation.

Trapping-Mediated Kinetic Model

As discussed previously (**8**), the study of alkane activation by single-crystalline transition metal surfaces reveals that two fundamentally different reaction mechanisms may be operative: (1) direct dissociation, and (2) trapping-mediated, dissociative chemisorption (**9, 10**). Direct dissociation occurs on the time scale of a collision between the gas-phase molecule and the surface ($<10^{-12}$ s), and the rate of this reaction depends primarily on the translational and internal energies of the gas-phase molecule. The trapping-mediated kinetic model, depicted in Scheme I, illustrates the elementary competing reactions of C-C and C-H bond activation, characterized by the elementary rate coefficients for reaction, $k_{r,CH}$ and $k_{r,CC}$, available to an alkane molecule, RH, on the catalytic surface (**11**).

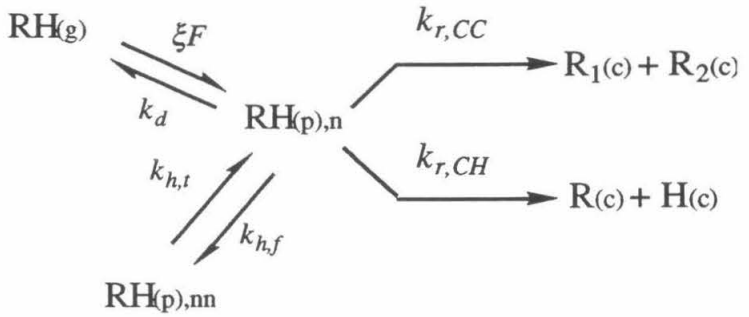

SCHEME I

After trapping from the gas phase with probability, ξ, the alkane molecule accommodates to the surface temperature, T_S, in a physically adsorbed state, RH(p). From this physically adsorbed state, it either diffuses with a rate coefficient, $k_{h,f}$, or it reversibly desorbs with a rate coefficient, k_d; or it reacts on the surface via one of the two available channels, with the

associated rate coefficients defined above. Migratory hopping to the nth site from a nearest-neighboring site may also occur with a rate coefficient $k_{h,t}$. The elementary rate coefficients are of the Polanyi-Wigner form, namely,

$$k_i = k_i^{(0)} e^{-E_i/k_B T_s} \tag{1}$$

For the dissociative chemisorption of these alkanes, the initial C-H or C-C bond cleavage is irreversible and rate-limiting, and the resulting chemisorbed alkyl products undergo further dehydrogenation, and ultimately complete decomposition, to form a carbonaceous residue. The relative rates of the two competing initial reactions are dependent on the surface temperature, provided the associated activation energy of desorption, E_d, and the relevant activation energy of reaction, E_r, are not equal. The gas temperature is important only insofar as it affects the probability of trapping, ξ, into the physically adsorbed state.

The time rate of change of the fractional coverage of the physically adsorbed alkane, θ_{RH}, derived from Scheme I, is

$$\frac{d\Theta_{RH}}{dt} = \xi F + k_{h,t}\Theta_{RH} - \left(k_d + k_{r,CH} + k_{r,CC} + k_{h,f}\right)\Theta_{RH}, \tag{2}$$

where the subscripts g, p, and c denote gaseous, physically adsorbed, and chemisorbed states, respectively, and F is the impingement rate onto the surface from the gas phase. This rate law may be expanded to include additional surface reactions, such as the competing 1° and 2° C-H bond cleavage channels and a second C-C bond scission channel for n-butane. The simplification of Eq. 2 is achieved by accounting properly for the effect of surface diffusion and by applying the pseudo-steady-state approximation, which is justified by the extremely low precursor concentrations, θ_{RH}, maintained under these experimental conditions. The two diffusion terms,

$k_{h,t}\,\theta_{RH,nn}$ and $k_{h,f}\,\theta_{RH,n}$, on the right-hand-side (rhs) of Eq. 2 exactly cancel one another for equivalent sites, an issue which has been addressed in detail elsewhere (**8, 12**).

Application of the pseudo-steady-state approximation yields the following set of expressions for the probabilities of alkane activation, $P_{r,CH}$ and $P_{r,CC}$, which are defined as the ratios of their respective reaction rates, $R_{r,CH}$ and $R_{r,CC}$, to the gas-phase impingment rate , F:

$$P_r \equiv \frac{R_r}{F} \tag{3}$$

$$P_{r,CH} = \frac{\xi\, k_{r,CH}}{k_d + k_{r,CH} + k_{r,CC}}, \tag{4a}$$

$$P_{r,CC} = \frac{\xi\, k_{r,CC}}{k_d + k_{r,CH} + k_{r,CC}}. \tag{4b}$$

By definition, the reaction probabilities are individually separable, and their sum is the total *measured* reaction probability, $P_{r,total}$. Because of the different temperature dependences of each reaction channel, these measurements for the total probability will not yield straight lines when cast as semilogarithmic plots in a standard Arrhenius construction, as presented earlier (**8**), and provided here again in Figs. 1a – 1d. By extracting the contribution attributable to the C-H bond activation channel, we were able to quantify the kinetic rate parameters for that reaction channel for these alkanes on Ir(111). We are to do likewise for the contribution from the C-C bond activation channel after examining further the relevant kinetic expressions, and reviewing the method employed to separate the contributions from the two competing reaction channels. In general, Eq. 4 implies that

$$\frac{\xi}{P_{r,CH}} - 1 = \frac{k_d}{k_{r,CH}} + \frac{k_{r,CC}}{k_{r,CH}}, \tag{5a}$$

$$\frac{\xi}{P_{r,CC}} - 1 = \frac{k_d}{k_{r,CC}} + \frac{k_{r,CH}}{k_{r,CC}}. \tag{5b}$$

For the special case of $k_d >> k_{r,CH} + k_{r,CC}$, Eq. 4 reduces to

$$P_{r,CH} \cong \frac{\xi k_{r,CH}}{k_d}, \tag{6a}$$

$$P_{r,CC} \cong \frac{\xi k_{r,CC}}{k_d}. \tag{6b}$$

From our experimental observations of alkane activation on Ir(111), the total measured probabilities, $P_{r,total}$, are sufficiently low to justify the assumption that the two rate coefficients of reaction, $k_{r,CC}$ and $k_{r,CH}$, are negligible in comparison to the rate coefficient of desorption, k_d. Thus, substitution of Eq. 1 into Eq. 6 yields

$$\frac{P_{r,CH}}{\xi} \cong \frac{k_{r,CH}^{(0)}}{k_d^{(0)}} e^{-(E_{r,CH}-E_d)/k_B T_s}, \tag{7a}$$

$$\frac{P_{r,CC}}{\xi} \cong \frac{k_{r,CC}^{(0)}}{k_d^{(0)}} e^{-(E_{r,CC}-E_d)/k_B T_s}. \tag{7b}$$

Furthermore, the relatively strong temperature dependence of the C-C bond activation channel enables us to separate its contribution to the total reaction probability from that of the C-H bond activation channel. The iterative procedure used to extract the kinetic data for the two competing channels is fully explained, and performed, in the preceding paper (**8**).

Reviewing the method briefly, from Fig. 1, we observe that for surface temperatures < 400 K, the contribution from the C-C activation channel is negligible for the dissociative chemisorption of all the alkanes examined. (Indeed, no C-C bond activation is observed in the case of ethane at any

temperature.) Thus, the data at low temperature is used to obtain, via Eq. 6a, the initial values of the apparent rate parameters (activation energy and ratio of preexponential factors) of the C-H bond activation channels for each alkane. By extrapolating the probability of C-H bond activation to high temperatures, we obtain, by subtraction from the total probability, the probability of C-C bond activation. These data allow the calculation of the inital values for the rate parameters of the C-C bond activation channel, which is then used in the susequent step of the iteration (**13**).

In the application of the trapping-mediated kinetic model to the selective activation of C-C bonds, we will employ Eq. 7b in the analysis of each alkane in this study. We will determine the rate coefficients of the initial C-C bond dissociation reaction in each case on the Ir(111) surface, and we will demonstrate the utility of these results in quantifying the temperature dependence of the branching ratio in the C-C and C-H bond activation channels.

2. Experimental Methods

The measurements on the Ir(111) surface were carried out in a 200 l/s ion-pumped UHV microreactor which has a base pressure of 2×10^{-10} Torr and a volume of 10 cm^3, which has been described in detail elsewhere (**8, 14**). The Ir(111) crystal was cleaned between experiments by heating to 1000 K for 5 min at an O_2 pressure of 5×10^{-8} Torr flowing continuously through the reactor, followed by annealing to 1625 K for 1 min to desorb the surface oxygen. Surface cleanliness was routinely monitored by obtaining thermal desorption spectra of CO, which were in complete agreement with previously published ones from the clean Ir(111) surface (**15**), and, since kinetic data are known to be extremely sensitive to surface conditions, the high degree of

reproducibility in the data presented here indicates the absence of surface contamination.

For the dissociative chemisorption of the alkanes over the surface temperature range that was employed ($310 < T_S < 1100$ K), the system was operated in a continuous flow mode. With the crystal held at a constant temperature, an alkane pressure of 1.0×10^{-7} Torr was maintained for a reaction time, τ. The amount of dissociated alkane was determined by titrating the carbonaceous residue with excess oxygen, producing exclusively carbon dioxide ($^{13}CO_2$ in the case of ^{13}C-labeled ethane). Under these experimental conditions the dissociative chemisorption of the alkanes is irreversible, and no gas-phase carbon-containing products of a surface self-hydrogenolysis reaction are formed. The titration conditions and procedure were optimized to ensure the complete oxidation of the surface carbon to CO_2.

The amount of carbon dioxide produced in the titration was counted mass spectrometrically to obtain the total number of carbon adatoms on the surface, N_C. The reaction conditions and times were such that the fractional coverage, θ_C, was between 5% and 10% of a monolayer of carbidic carbon. The lower limit ensures that the results are not dominated by reactivity at surface defects (**16**), whereas the upper limit ensures that the initial rate of the C-H activation reaction has been measured, i.e., the rate is approximately characteristic of a clean Ir(111) surface. At a given surface temperature, T_S, the total dissociative chemisorption probability, $P_{r,total}(T_S)$, is obtained from

$$P_{r,total}(T_s) = \frac{N_C}{nA\tau F_{gas}} \tag{8}$$

where A is the sample surface area (cm^2), F_{gas} is the impingement flux of reactant alkane (molecules cm^{-2} s^{-1}), and the stoichiometric factor of n converts N_c into the number of reacted alkane molecules.

All gases were introduced into the microreactor from a gas-handling manifold that was pumped with a diffusion pump to a base pressure below 10^{-7} Torr. Carbon-13 labeled ethane (1,2-di-^{13}C-C_2H_6, 99 atom % ^{13}C) was obtained from Icon Services. The C_3H_8 (99.5%) was obtained from Matheson, and both the $CH_3CD_2CH_3$ (98 atom % D) and the C_3D_8 (99.5 atom % D) were obtained from MSD Isotopes. The i-C_4H_{10} (99.5%) was obtained from Matheson, and both the i-$(CH_3)_3CD$ (97.5 atom % D) and the i-$(CD_3)_3CH$ (99 atom % D) were obtained from MSD Isotopes. The n-C_4H_{10} was obtained from Matheson (99.5%), and the $(CH_3)_4C$ was obtained from Phillips Chemical Company (95%). The selectively deuterated gases were used without further purification, whereas the perhydrido samples were fractionally distilled from cryogenic hexane ice/liquid hexane baths. In this procedure, upon condensing the hydrocarbon at liquid hexane temperature (~180 K) and then allowing the sample mixture to warm slowly to room temperature, the low and high temperature boiling fractions were eliminated by diffusion pumping of the gas-handling manifold, while the center fraction of the vaporizing condensate was collected in a clean, empty receiving flask.

3. Results

The measured initial probabilities of dissociative chemisorption for all alkanes studied are plotted against reciprocal surface temperature in Fig. 1a – 1d. As previously mentioned, the iterative technique used to separate the distinct channels of C-C and C-H bond activation has been performed elsewhere (**8**). In Figs. 2 – 4 these extracted probabilities of initial C-C bond

dissociation for propane, isobutane, n-butane, and neopentane are plotted as functions of reciprocal surface temperature.

These semilogarithmic plots in Figs. 2 – 4 yield the apparent kinetic rate parameters of the elementary C-C bond scission reactions. From Eq. 7b, the slope of the straight lines in these Arrhenius constructions are equal to $-(E_{r,CC} - E_d)/k_B$, and the intercepts are equal to $k_{r,CC}^{(0)}/k_d^{(0)}$. In Figs. 2 and 3, we have plotted the data of the three isotopomers examined for propane and for isobutane, respectively. It is apparent from these data that, for both alkanes, those molecules possessing terminal hydridomethyl groups have higher reactivities, and lower activation barriers, than those isotopomers containing terminal deuteromethyl groups. Relative to the gas-phase energy zero, the least squares fit to the data of the two hydridomethyl isotopomers of propane yields a difference in the activation energies of reaction and desorption, $E_{r,CC} - E_d$, of 8.7 ± 0.3 kcal/mol, while a similar fit for the two hydridomethyl isotopomers of isobutane yields a difference in the activation energies of 7.3 ± 0.3 kcal/ mol. For the deuteromethyl isotopomers of propane and isobutane, $E_{r,CC} - E_d$ = 9.3 ± 0.3 kcal/mol, and 7.8 ± 0.3 kcal/mol, respectively. Thus, the differences in the activation energies for C-C bond cleavage between the deuteromethyl and hydridomethyl isotopomers (9.3 - 8.7 = 0.6 kcal/mol, and 7.8 - 7.3 = 0.5 kcal/mol) are at the limit of the cumulative errors of these measurements, i.e., ± 600 cal/mol. With proper regard for this quantitative error in the results, the collinearity of the data for the pairs of isotopomers with hydridomethyl groups invites discussion regarding its implication to the mechanism of C-C bond activation on Ir(111). We will provide this discussion in Sect. 4. In Fig. 4, we have plotted the data of the C-C bond activation channel for n-butane and neopentane. The

measured activation energies, $E_{r,CC} - E_d$, are 7.2 ± 0.3 and 5.4 ± 0.3 kcal/mol, respectively.

Table 1 lists the apparent activation energies, $E_{app} = E_{r,CC} - E_d$, and the apparent preexponential factor ratios, $k_{r,CC}^{(0)}/k_d^{(0)}$, for the C-C bond activation of these alkanes on the Ir(111) surface. The rate coefficients of desorption of the physically adsorbed alkanes have been determined in separate experiments (**11**,**17**). From these values for the activation energies for desorption, E_d, the activation energies for C-C bond cleavage, $E_{r,CC}$, referenced to the bottom of the physically adsorbed well, can be determined. The value of the ratios of the reaction and desorption preexponential factors is seen to be approximately 0.5 and 0.6, a result that contrasts sharply with the corresponding values (between 10^{-2} and 10^{-3}) for the activation of C-H bonds (**8**, **11**,**18**).

In analyzing the data for the reactive probability of alkanes on transition metal surfaces, we have used the knowledge that the trapping probability, ξ, is only a weak function of the surface temperature, but that it does depend on the temperature of the impinging gas (**19, 20**). Our gas pressures are sufficiently low to ensure that the mean free path lengths are sufficiently long to allow the gas to equilibrate to the wall temperature, and not to the surface temperature. With the wall temperature equal to 300 K throughout all experiments for all the alkanes, we assume a constant value for the trapping probability. The average incident kinetic energy (~25 meV) of the Boltzmann distribution from the effusive source used in these 'bulb' experiments, is less than the lowest energy (~1.2 kcal/mol, or ~50meV) employed in a molecular beam study of the trapping probability of ethane on the reconstructed Ir(110) surface (**21**). At such low incident kinetic energies, Mullins and Weinberg found that the molecular trapping probability

approached unity, 97 ± 2%. Thus, we have assumed the trapping probability to be unity in these calculations .

4. Discussion

Table 1 and Figs. 2 – 4 present the results of the C-C bond activation channel for the initial dissociative chemisorption of small chain alkanes on the close-packed surface of Ir(111). On average, we observe that the cleavage of C-C bonds is between 6 and 7 kcal/mol greater than that of C-H bond cleavage. The results for neopentane reveal a difference of approximately 5 kcal/mol. These results are in remarkable agreement with the estimated difference in C-C and C-H activation energies (~19 – 11 = ~8 kcal/mol) for the collisionally induced gas-phase reaction of the cationic iron-propane complex, $Fe•(C_3H_8)^+$ (**5**).

Hydrogenolysis of Alkanes by Iridium

The high activity of single-crystalline and supported iridium catalysts in hydrogenolysis reactions of alkanes is evidence of its propensity to react with saturated, inert hydrocarbons. Hydrogenolysis, or the hydrogen-induced cleavage of hydrocarbon chains, is an important reaction necessary to the conversion of heavy hydrocarbon feed streams to value-added fuel products, such as in the reforming of naphtha streams over Pt-Ir and Pt-Re supported catalysts (**22**).

In the laboratory (**23, 24**), kinetics experiments of the hydrogenolysis reaction are conducted by introducing hydrocarbon and hydrogen gas mixtures (in P_{H2} : P_{alkane} ratios of between 10:1 to 100:1) to a preheated catalyst, and allowing the system to attain steady state. In studies on silica-supported metal catalysts, Ir was observed to be one of the most active

metals, third behind only Os and Ru in it hydrogenolysis of ethane at 475 K (**23**).

On the single-crystalline surface of Ir(111), the hydrogenolysis reactions of ethane, propane, and neopentane result in a product distribution characterized by the cleavage of a single C-C bond, resulting in the "demethylization" of the parent hydrocarbon (**24**). With n-butane, the two terminal C-C bonds were observed to be cleaved. With decreasing pressure of H_2 (at T = 500 K and 1.0 Torr of alkane), complete conversion of the parent alkane to methane occurred with a corresponding increase in the specific reaction rate from 10^{-2} to 1 molecule site^{-1} sec^{-1} (as P_{H_2} changed from 1000 to 20 Torr). It must be remembered that in these hydrogenolysis reaction mechanisms, like the majority of gas-phase ion-induced reactions of larger alkanes, C-C bond cleavage is generally preceded by the initial cleavage of a C-H bond. This initially formed, partially dehydrogenated, alkyl intermediate experiences intramolecular C-C bond cleavage, such as via β-methyl elimination reactions to produce shorter chain alkenes (**25**). Nonetheless, the high activity of iridium catalysts in hydrogenolysis reactions of alkanes is indicative of their intrinsic ability to activate saturated hydrocarbons via, presumably, both C-C and C-H bond cleavage reactions.

Secondary Kinetic Isotope Effect: Methyl Deformation in the Cleavage of the C-C Bond

The results presented in Figs. 2 and 3 for the activation of propane and isobutane, and their selectively deuterated isotopomers, indicate that there is a resolvable isotope effect in the activation of the C-C bond upon substitution of the hydridomethyl groups by deuteromethyl groups. Because the substitution occurs at a bond other than the one being activated, the effect is a secondary deuterium kinetic isotope effect (**26**). The measured differences

in the activation energies between the groups of isotopomers are 600 cal/mol for the case of propane, and 500 cal/mol for the case of isobutane. Their proportionate effect on the ratio, k_H/k_D, is rather small (a factor of ~1.5 at 700 K for each molecule), by virtue of the high temperatures associated with the bond cleavage reaction. The agreement between the two independent measurements for the isotopomers with hydridomethyl groups in each alkane, C_3H_8 and $CH_3CD_2CH_3$ for propane and i-C_4H_{10} and $(CH_3)_3CD$ for isobutane, is an intriguing experimental result, and one which we believe gives support for a mechanism involving significant deformation of the terminal methyl groups.

Secondary kinetic isotope effects are due largely to the induced changes in the vibrational frequencies of the reactants and transition states (represented below by a dagger, ‡). As an illustration, the change from sp^3 to sp^2 hybridization for the methyl group in CH_3X during a unimolecular substitution (S_N1) reaction,

$$H_3C\text{–}X \longrightarrow [\,H_3C\text{---}X]^{\ddagger} \longrightarrow CH_3^+ + X^-,$$

is accompanied by a decrease in the fundamental frequencies of the methyl bending modes (with the frequencies lower in the sp^2 product than for the sp^3 reactant). In the transition state, the hybridization is intermediate between sp^3 and sp^2, and, thus, there is a decrease in the frequencies of the molecule's bending modes as the transition state forms. When hydrogen is substituted by deuterium in the methyl group, the zero point energies for the methyl group are lowered (whether sp^3, sp^2, or intermediate between these two extremes). However, this lowering is greater in the reactant than in the transition state because of the closer spacings of the vibrational levels at the lower frequencies associated with the transition state. Thus, a small positive

kinetic isotope effect is observed, $k_H/k_D \approx 1.3$ to 1.4, in comparison to values of 4 – 6 for primary deuterium kinetic isotope effects (**26**).

For the activation of C-C bonds on the close-packed Ir(111) surface, the deuterium kinetic isotope effect we observe may be interpreted in terms which are similar to the above example. In theoretical investigations of the C-C bond activation of ethane by single atoms of the first and second rows of the transition metals, Siegbahn and Blomberg (**27**) and Low and Goddard (**28**) calculated fully optimized geometries of the reactive transition states. They found that the two methyl groups of the ethane molecule were (1) in an eclipsed configuration, and (2) bent back toward one another, in order to expose the "underside" of the ethane molecule to the metal center. We propose that the two asymmetric deformation modes, or a combination of asymmetric deformation and stretching modes, of the terminal methyl group are intimately involved in the coordinate space on the potential energy surface that results in C-C bond scission. Typical vibrational frequencies (gas-phase) for the two asymmetric deformation and the two stretching modes of hydridomethyl groups are (**29**)

$$\nu_a(CH_3) = 2985\ cm^{-1}, \qquad \nu_a(CH_3) = 2960\ cm^{-1},$$

$$\delta_a(CH_3) = 1485\ cm^{-1}, \qquad \delta_a(CH_3) = 1470\ cm^{-1}.$$

Likewise, for deuteromethyl groups, these vibrational modes shift to

$$\nu_a(CD_3) = 2240\ cm^{-1}, \qquad \nu_a(CD_3) = 2200\ cm^{-1},$$

$$\delta_a(CD_3) = 1075\ cm^{-1}, \qquad \delta_a(CD_3) = 1065\ cm^{-1}.$$

The calculated differences in zero point energies (ΔZPE) for these stretching and deformation modes, for the unperturbed reactant methyl group, are ~1.1 and ~0.6 kcal/mol, respectively. The differences in the zero point energies, ΔZPE, in these modes at the transition state for C-C bond cleavage cannot be estimated with certainty, given the degree of distension of the methyl group

in the transition state geometry (**30**). Nonetheless, it is reasonable to expect a concomitant change in the frequencies of the relevant modes, and we have measured a positive deuterium isotope effect with an associated zero point energy difference between the reactant and transition state methyl groups, $\Delta(\Delta ZPE)$, of between 500 and 600 cal/mol. Our results imply that a 15 – 20% softening of each of these four modes (i.e., the vibrational frequencies at the transition state are 80 – 85% of the frequencies of the reactant methyl group) will yield the observed difference in the reactant and transition state ΔZPE's, provided each mode is assumed to contribute equally.

Why C-C Bond Activation is not Observed for Ethane: Surface Coordination of β-Methyl Groups

We discuss next possible explanations for why the activation of the C-C bond in ethane is not observed (cf., Fig. 1a). The low polarizability of the neutral ethane molecule is often invoked as the reason behind why C-C bond cleavage is not observed. This line of reasoning (**2, 4**) argues that the ethane molecule is not sufficiently polarized in its interaction with a metal center to generate an induced electrostatic attraction that is sufficiently strong to enable it to overcome the intrinsic activation barrier to C-C bond cleavage. The polarizability volumes of ethane and propane are 4.4 $Å^3$ and 6.2 $Å^3$, respectively (**31**), and this difference does correlate with the observed bond strengths of the physically adsorbed alkanes on transition metal surfaces, 7.7 and 9.7 kcal/mol (**11**,**17**, **18**). The fact remains, however, that the activation energies for C-H bonds and C-C bonds are greater than these well depths of both physically adsorbed alkanes. The extention of the argument, then, is that neither ethane nor propane should be activated by the transition metal

surfaces. This simply is not the case, and we offer an alternative interpretation for why ethane is not observed to undergo C-C bond activation.

Common to all of the alkanes which are capable of dissociating via initial C-C bond cleavage is that they contain more than two carbon bonds. Thus, in the dissociation reaction of one of the C-C bonds, the alkyl groups in the "remote" end of the molecule may remain interacting with the surface as the C-C bond cleavage reaction at the other end of the molecule occurs. As a direct result of this independent behavior, these unperturbed alkyl groups of the saturated hydrocarbon chain serve the important role of "anchoring" the precursor molecule in a configuration which favors C-C bond activation.

For propane, isobutane, and neopentane, these unperturbed groups are all methyl groups; while for n-butane there may be two terminal methyl groups, when focusing our attention on the central C-C bond, or, alternatively, an ethyl group when the either terminal carbon-carbon bond is being activated. We will illustrate our nomenclature using propane as an example. The two carbon atoms participating in the C-C bond cleavage reaction are designated to be at the α and α' positions with the terminal carbon atom in the chain being in the α' position, and the more central carbon atom in the α position. Thus, for C-C bond activation in propane, the remaining carbon atom (and its associated methyl functionality) is in the β position. For the case of n-butane, the cleavage of one of the two terminal C-C bonds yields an ethyl group in the β position, whereas central C-C bond yields two methyl groups at the equivalent β and β' positions.

For C-C bond activation in propane, isobutane, neopentane, and n-butane, by virtue of the retention of their physical bonding interactions, these β alkyl groups are abetting the surface in its attack at the $C_\alpha - C_{\alpha'}$ bond. From our description, it follows that ethane, in lacking any alkyl groups at

the β positions, does not gain the additional stabilization of the configuration necessary for C-C bond activation. Given the strongly repulsive nature of the deformation of the terminal methyl group (**7**, **27**, **28**), the ethane molecule elects either to desorb or to migrate away from such a reactive site for C-C bond activation on the surface. The other alkane molecules are apparently coerced to stay for the necessary length of time in the configuration leading to C-C bond cleavage.

As an aside, our description proposes that this sort of anchoring interaction by the β-alkyl groups assists in locking the position of the reacting C-C bond as the molecule enters the transition state in its trajectory along the reaction coordinate. Once beyond the transition state for C-C bond activation, the system passes into the chemisorption well associated with the formation of the new metal-alkyl bonds. Taken together, these bonds are stronger than the C-C bond that has just been activated (**32**), and the exothermicity of the reaction is carried into the entire system, including the two newly formed surface alkyl intermediates. Thus, we further speculate that these anchoring groups, which had participated by retaining their interaction to the surface, now locally detach from the surface as the metal-alkyl locates its equilibrium geometry and carry with them some fraction of the released energy of the bond dissociation reaction. It is the transition of these groups from their physically adsorbed interaction to their final state of induced local detachment which we postulate gives rise to the large ratios of the preexponential factors for C-C bond activation (relative to those of C-H bond activation) reported in Table 1.

Selectivity of Alkane Activation: Branching Ratios for C-C and C-H Reaction Channels

The measured probabilities of reaction via C-C bond activation may be compared to the corresponding probabilities of reaction via C-H bond activation to obtain the branching ratios for these alkanes as functions of the surface temperature. This comparison requires the results from our previous analysis of the C-H bond activation channel. For that fraction which follows the C-H bond cleavage path, the earlier derived branching ratios (**8**) between 1° and 2° Ir-propyl formation from propane, and 1° and 3° Ir-isobutyl formation from isobutane, may be applied to quantify the overall selectivity of the system.

We select the results for the dissociative chemisorption of propane to illustrate the quantification of the selectivity of propane activation by the Ir(111) surface. From the apparent rate parameters of the reaction probability of propane via the C-H channel [1.7 kcal/mol and 10^{-2}, cf., Table 1 of Ref. (**8**)] and the apparent rate parameters of the reaction probability of propane via the C-C channel (8.7 kcal/mol and 0.5, cf., Table 1 of this work), the branching ratio between the C-C and C-H reaction channels is simply

$$P_{CC}/P_{CH} = 50 \exp[-7000/k_B T_S]. \quad (9)$$

This ratio implies that the reaction rates the two channels are equal to one another at 895 K. Referring to Fig. 2 of Ref. (**8**), we see that it is indeed at this temperature (± 40 K, due to the round off errors in the reported quantities) that the two reaction channels provide the same probabilities of reaction, i.e., their curves intersect. Thus, at a temperature of 600 K, for which the deviation from the linear Arrhenius fit to the C-H reaction channel is certain (cf., Fig. 1b), the above branching ratio indicates that 12.4% of the propane molecules have reacted via C-C bond activation with the remaining

87.6% undergoing C-H bond activation. From our previous work, we computed [Eq. 33 of Ref. (**8**)] the branching ratio for the formation of 1° versus 2° Ir-proyl products:

$$\tilde{P}_p/\tilde{P}_s = 1.63 \exp[-310 \text{ cal/mol}/k_B T_s]. \quad (10)$$

Thus, of the 87.6% of the propane molecules that experience C-H bond activation at 600 K, the branching ratio in Eq. 10 shows that the formation of 1° Ir-propyl is favored over the formation of 2° Ir-propyl by a factor of 1.26. Thus, the product distribution for the initial dissociative chemisorption of propane at 600 K on Ir(111) is: 12.4% activation via C-C bond cleavage to yield chemisorbed methyl and ethyl groups, 38.9% activation via secondary C-H bond cleavage to form 2° Ir-propyl intermediates, and 48.9% activation via primary C-H bond cleavage to form 1° Ir-propyl products. In a similar fashion, the selectivities in the dissociative chemisorption of all the alkanes investigated here on Ir(111) may be quantified.

The formulation of the overall branching ratios from the measured probabilities of each dissociation channel available to these alkanes quantifies the selectivities of these reactive systems. Furthermore, it explicitly includes the temperature dependence of the branching ratio, and, hence, the selectivity, in the description. This degree of precision in quantifying the selectivity of a catalytic reaction has long been sought (**22**, **23**) , and we anticipate that the methodology developed here, and in our preceding paper, may be extended to characterize other catalytic reactions.

5. *Summary*

Studies of the initial probabilities of the dissociative chemisorption of ethane, propane, isobutane, n-butane, and neopentane on the close-packed Ir(111) surface have been performed. Activation via both C-H and C-C bond

cleavage is observed and has been quantified. In our accompanying manuscript (**8**), the activation of these alkanes in the C-H reaction channel has been analyzed, and, in this work, the analysis of the C-C reaction channel has been carried out.

The activation energies for C-C bond cleavage average between 17 and 18 kcal/mol for propane, isobutane, and n-butane, and is 16 kcal/mol for neopentane, following the trend of the intrinsic bond dissociation energies, D_0(C-C), in these alkanes. Carbon-carbon bond activation in ethane is not observed, and we propose that this is a direct consequence of its chain length. Other larger alkanes (> C_2) possess β alkyl groups within the molecule which participate in the C_α – $C_{\alpha'}$ bond scission reaction by maintaining their physical coordination to the iridium surface while the C-C bond cleavage occurs.

Our measured probabilities of the initial dissociative chemisorption in both the C-C and C-H bond cleavage channels allows us to quantify the overall selectivity of the dissociation of these alkanes on Ir(111). Because 1° C-H bonds outnumber the 2° and 3° C-H bonds in propane and isobutane, we have determined that within the C-H activation channel, the preference for the formation of primary propyl dominates over that of secondary propyl formation for T_S > 320 K, and primary isobutyl formation dominates over tertiary isobutyl formation for all T_S. Furthermore, on the Ir(111) surface, the activation of these alkanes via initial C-C bond cleavage becomes the major reaction channel at surface temperatures of 850 – 900 K.

Acknowledgment: This work was supported by the Department of Energy under Grant No. DE–FG03–89ER14048.

References and Notes

(1) Crabtree, R. H.; Dion, R. P. *J. Chem. Soc., Chem. Commun.* **1984**, 1260.

(2) (a) Armentrout, P. B. In *Selective Hydrocarbon Activation: Principles and Progress*; Davies, J. A., Watson, P. L., Greenberg, A., Liebman, J. F., Eds.; VCH Publishers: New York, 1990; Chapter 14. (b) Armentrout, P. B.; Beauchamp, J. L. *Acc. Chem. Res.* **1989**, *22*, 315.

(3) (a) Schultz, R. H. ; Armentrout, P. B. *J. Phys. Chem.* **1987**, *91*, 4433. (b) Halle, L. F.; Armentrout, P. B.; Beauchamp, J. L. *Organometallics* **1982**, *1*, 963. (c) Houriet, R.; Halle, L. F.; Beauchamp, J. L. *Organometallics* **1983**, *2*, 1818.

(4) (a) van Koppen, P. A. M.; Brodbelt-Lustig, J.; Bowers, M. T.; Deardon, D. V.; Beauchamp, J. L.; Fisher, E. R.; Armentrout, P. B. *J. Am. Chem. Soc.* **1991**, *113*, 2369. (b) van Koppen, P. A. M.; Kemper, P. R.; Bowers, M. T. *J. Am. Chem. Soc.* **1992**, *114*, 10941.

(5) Schultz, R. H.; Armentrout, P. B. *J. Am. Chem. Soc.* **1991**, *113*, 729.

(6) For C-H bonds, the bond dissociation energies at 298 K, $D_{0,298K}$, are 104.7 ± 0.2 kcal/mol for methane, 98 ± 1 kcal/mol for primary C-H bonds, 95 ± 1 kcal/mol for secondary C-H bonds, and 93 ± 2 kcal/mol for tertiary C-H bonds. Hence, as provided in the text, the bond dissociation energies for C-C bonds are, on average, 10 kcal/mol lower. [(a) McMillen, D. F.; Golden, D. M. *Annu. Rev. Phys. Chem.* **1982**, *33*, 493. (b) Berkowitz, J.; Ellison, G.B.; Gutman. D. *Ann. Rev. Phys. Chem.*, in press.] To obtain the bond dissociation energies cited in the text for the C-C bonds, reaction enthalpies have been calculated from available thermochemical data. [Pedley, J. B.; Naylor, R. D.; Kirby, S. P. *Thermochemical Data of Organic Compounds*; 2nd ed.; Chapman Hall: London, 1986; p. 87.]

(7) (a) Low, J. J.; Goodard, W. A., III; *J. Am. Chem. Soc.* **1984**, *106*, 6928. (b) Low, J. J.; Goodard, W. A., III *Organometallics*, **1986**, *5*, 609.

(8) Johnson, D. F.; Weinberg, W. H. *J. Am. Chem. Soc.* this issue.

(9) (a) Rettner, C. T.; Pfnur, H. E.; Auerbach, D. J. *Phys. Rev. Lett.* **1985** *54*, 2716. (b) Luntz, A. C.; Bethune, D. S. *J. Chem. Phys.* **1989**, *90*, 1274. (c) Lee, M. B.; Yang, Q. Y.; Ceyer, S. T. *ibid.* **1987**, *87*, 2724.

(10) (a) Weinberg, W. H. In *Dynamics of Gas-Surface Collisions*; Rettner, C. T., Ashfold, M. N. R., Eds.; Royal Society of Chemistry: Cambridge, 1991, pp. 171-220. (b) Ehrlich, G. In *Chemistry and Physics of Solid Surfaces*; Vanselow, R., Howe, R. F., Eds.; Springer-Verlag: Heidelberg, 1989; Vol. VII, pp. 1-64.

(11) (a) Weinberg, W. H. In *Kinetics of Interface Reactions*; Kreuzer, H. J., Grunze, M., Eds.; Springer-Verlag: Heidelberg, 1987; pp. 94-121. (b) Weinberg, W. H. *Langmuir* **1993**, *9*, 655. (c) Weinberg, W. H. *J. Vac. Sci. Technol.* **1992**, *A10*, 2271.

(12) Johnson, D. F.; Weinberg. W. H. *J. Chem. Phys.*, submitted.

(13) After three or four iterations, the results reported in Table 1 and presented in Figs. 2 – 5 of Ref. (8) are obtained. The exponential functions with the weaker temperature dependence, i.e., less steep slopes, in these figures are associated with the C-H activation channel; the exponential functions with the stronger temperature dependence, i.e., steeper slopes, are associated with the C-C activation channel. It is these latter data which are plotted in Figs. 2 – 4 of this work.

(14) (a) Sun, Y.- K.; Weinberg, W. H. J. *Vac. Sci. Technol.* **1990**, *A8*, 2445. (b) Vajo, J. J.; Tsai, W.; Weinberg, W. H. *Rev. Sci. Instrum.* **1985**, *56*, 1439.

(15) Comrie, C. M.; Weinberg, W. H. *J. Chem. Phys.* **1976**, *64*, 250.

(16) Laue diffraction methods werre used to determine that our sample was polished to within 0.70° ± 0.15° of the [111] normal direction of the surface. This corresponds to terrace widths, assuming that they are uniform, of between 63 and 98 atomic rows. Thus, the step density on the surface is 0.013 ± 0.003 fractional monolayer. There are two types of defect sites associated with each step edge, the "ascending" and "descending" defect sites. Thus, the defect density (assumed to be represented only by such sites at step edges), is 0.026 ± 0.006.[12]

(17) (a) Szuromi, P. D.; Engstrom, J. R.; Weinberg, W. H. *J. Chem. Phys.* **1984**, *80*, 508. (b) Wittrig, T. S.; Szuromi, P. D.; Weinberg, W. H. *J. Chem. Phys.* **1982**, *76*, 3305. (c) Westre, E. D.; Arena, M. V.; Deckert, A. A.; Brand, J. L.; George, S. M. *Surf. Sci.* **1990**, *233*, 293.

(18) Campbell, C. T.; Sun, Y.-K.; Weinberg, W. H. *Chem. Phys. Lett.* **1991**, *179*, 53.

(19) Rettner, C. T.; Schweizer, E. K.; Stein, H.; Auerbach, D. J. *Phys. Rev. Lett.* **1988**, *61*, 986.

(20) (a) Rettner, C. T. ; Auerbach, D. J. In *Kinetics of Interface Reactions*; Kreuzer, H. J., Grunze, M., Eds.; Springer-Verlag: Heidelberg, 1987, p. 145. (b) Andersson, S.; Persson, M. *Phys. Rev. Lett.* **1993**, *70*, 202. (c) Ceyer, S. T. *Annu. Rev. Phys. Chem.* **1988**, *39*, 479. (d) McMaster, M. C.; Schroeder, S. L. M.; Madix, R. J. *Surf. Sci.* **1993**, *297*, 253. (e) McMaster, M. C.; Madix, R. J. *Surf. Sci.* **1993**, *294*, 420.

(21) (a) Mullins, C. B.; Weinberg, W. H. *J. Chem. Phys.* **1990**, *92*, 3986. (b) Mullins, C. B.; Weinberg, W. H. *J. Vac. Sci. Technol.* **1990**, *A8*, 2458.

(22) (a) Sinfelt, J. H. *Bimetallic Catalysts: Discoveries, Concepts, and Applications;* Wiley: New York, 1983; pp. 130-157. (b) Rasser, J. C. *Platinum-Iridium Reforming Catalysts;* Delft Univ. Press.: Delft, Netherlands, 1977; pp. 156-193.

(23) (a) Sinfelt, J. H. *Adv. Catal.* **1973**, *23*, 91. (b) Sinfelt, J. H. *Catal. Rev.* **1969**, *3*, 175. (c) Sinfelt, J. H.; Yates, D. J. C.; Taylor, W. F. *J. Phys. Chem.* **1965**, *69*, 1877. (d) Sinfelt, J. H.; Yates, D. J. C. *J. Catal.* **1967**, *8*, 82. (e) Sinfelt, J. H.; Yates, D. J. C. *J. Catal.* **1968**, *10*, 362. (f) Yates, D. J. C.; Sinfelt, J. H. *J. Catal.* **1969**, *14*, 182.

(24) Engstrom, J. R.; Goodman, D. W.; Weinberg, W. H. *J. Am. Chem. Soc.* **1988**, *110*, 8305.

(25) See for example: Watson, P. L. In *Selective Hydrocarbon Activation: Principles and Progress*; Davies, J. A., Watson, P. L., Greenberg, A., Liebman, J. F., Eds.; VCH Publishers: New York, 1990; Chapter 4.

(26) Laidler, K. J. *Chemical Kinetics*, 3rd ed.; Harper & Row: New York, 1987; Chapter 11.

(27) (a) Siegbahn, P. E. M.; Blomberg, M. R. A. *J. Am. Chem. Soc.* **1992**, *114*, 10548. (b) Blomberg, M. R. A.; Siegbahn, P. E. M.; Nagashima, U.; Wennerberg, J. *J. Am. Chem. Soc.* **1991**, *113*, 424.

(28) (a) Low, J. J.; Goddard, W. A., III *J. Am. Chem. Soc.* **1984**, *106*, 8321. (b) Low, J. J.; Goddard, W. A., III *J. Am. Chem. Soc.* **1986**, *108*, 6115.

(29) Shimanouchi, T. *Tables of Molecular Vibrational Frequencies*: National Institute of Standards and Technology: Washington, DC, 1972; Consolidated Volume, NSRDS-NBS-39.

(30) Seigbahn and Blomberg[27] computed the geometries, as noted, and the associated energies of the configurations, but not the vibrational frequencies of the deformed methyl groups .

(31) Rothe, E. W.; Bernstein, R. B. *J. Chem. Phys.* **1959**, *31*, 1619.

(32) In the case of propane, the bond dissociation energy of the C-C bond is 87 ± 1 kcal/mol (see text), and we estimate the bond strengths of the Ir-CH_3 and Ir-C_2H_5 dissociation products to be 50 ± 5 and 45 ± 5 kcal/mol, respectively.[8] Thus, the exothermicity for C-C bond activation for propane is calculated to be 8 ± 11 kcal/mol.

Table 1. Apparent Rate Parameters for the C-C Bond Activation Channel in the Dissociative Chemisorption of Ethane, Propane, Isobutane, n-Butane, and Neopentane on Ir(111) [a]

Reactant	$E_{r,CC} - E_d$ (cal/mol)[b]	$\frac{k_{r,CC}^{(0)}}{k_d^{(0)}}$	E_d (cal/mol)[b]	$E_{r,CC}$ (cal/mol)[b]
di-^{13}C-C_2H_6	n.o.			
C_2D_6	n.o.			
C_3H_8	8 700	0.5	9 700	18 400
$CH_3CD_2CH_3$	8 700	0.5	9 700	18 400
C_3D_8	9 300	0.5	9 700	19 000
n-C_4H_{10}	7 200	0.6	10 700	17 900
i-C_4H_{10}	7 300	0.5	10 400	17 700
$(CH_3)_3CD$	7 300	0.5	10 400	17 700
$(CD_3)_3CH$	7 800	0.5	10 400	18 200
$(CH_3)_4C$	5 400	0.6	10 700	16 100

[a]The separately measured values for the desorption rate coefficient were used in evaluating $E_{r,CC}$. The quantity $E_{r,CC} - E_d$ is the activation energy with respect to the gas-phase energy zero, *i.e.*, the gas-phase alkane molecule infinitely far from the surface and at rest. In comparison, $E_{r,CC}$ is the activation energy of the reaction with respect to the proper reference energy, namely, the bottom of the physically adsorbed well. For the case of n-C_4H_{10}, this energy is an apparent activation energy, because competitive activation of the terminal and central C-C bonds is occurring.

[b]The errors in the *measured* differences between the activation energies of reaction and desorption, $E_{r,CC} - E_d$, are ± 0.3 kcal/mol. The errors associated with the activation energies of desorption, E_d, are ± 0.25 kcal/mol. Thus, the reported errors in the apparent activation energies for reaction, $E_{r,CC}$, are taken to be ± 0.6 kcal/mol.

Figure Captions

Figure 1. Initial probabilities of trapping-mediated dissociative chemisorption on Ir(111) as a function of reciprocal surface temperature for (a) di-^{13}C-C_2H_6 and C_2D_6, (b) C_3H_8, $CH_3CD_2CH_3$, and C_3D_8, (c) i-C_4H_{10}, $(CH_3)_3CD$, and $(CD_3)_3CH$, and (d) n-C_4H_{10} and $(CH_3)_4C$. The nonlinearity of the total reaction probability for all but the ethane isotopomers arises from more than one reactive channel contributing to the total measured reaction probabilities. This text addresses the one of these two reaction channels, C-C bond activation, while the accompanying paper in this journal addresses the other channel, C-H bond activation (**8**).

Figure 2. Initial probabilities for the trapping-mediated activation of C-C bonds in the dissociative chemisorption of C_3H_8, $CH_3CD_2CH_3$, and C_3D_8 on Ir(111) as a function of reciprocal surface temperature.

Figure 3. Initial probabilities for the trapping-mediated activation of C-C bonds in the dissociative chemisorption of i-C_4H_{10}, $(CH_3)_3CD$, and $(CD_3)_3CH$ on Ir(111) as a function of reciprocal surface temperature.

Figure 4. Initial probabilities for the trapping-mediated activation of C-C bonds in the dissociative chemisorption of n-C_4H_{10} and $(CH_3)_4C$ on Ir(111) as a function of reciprocal surface temperature.

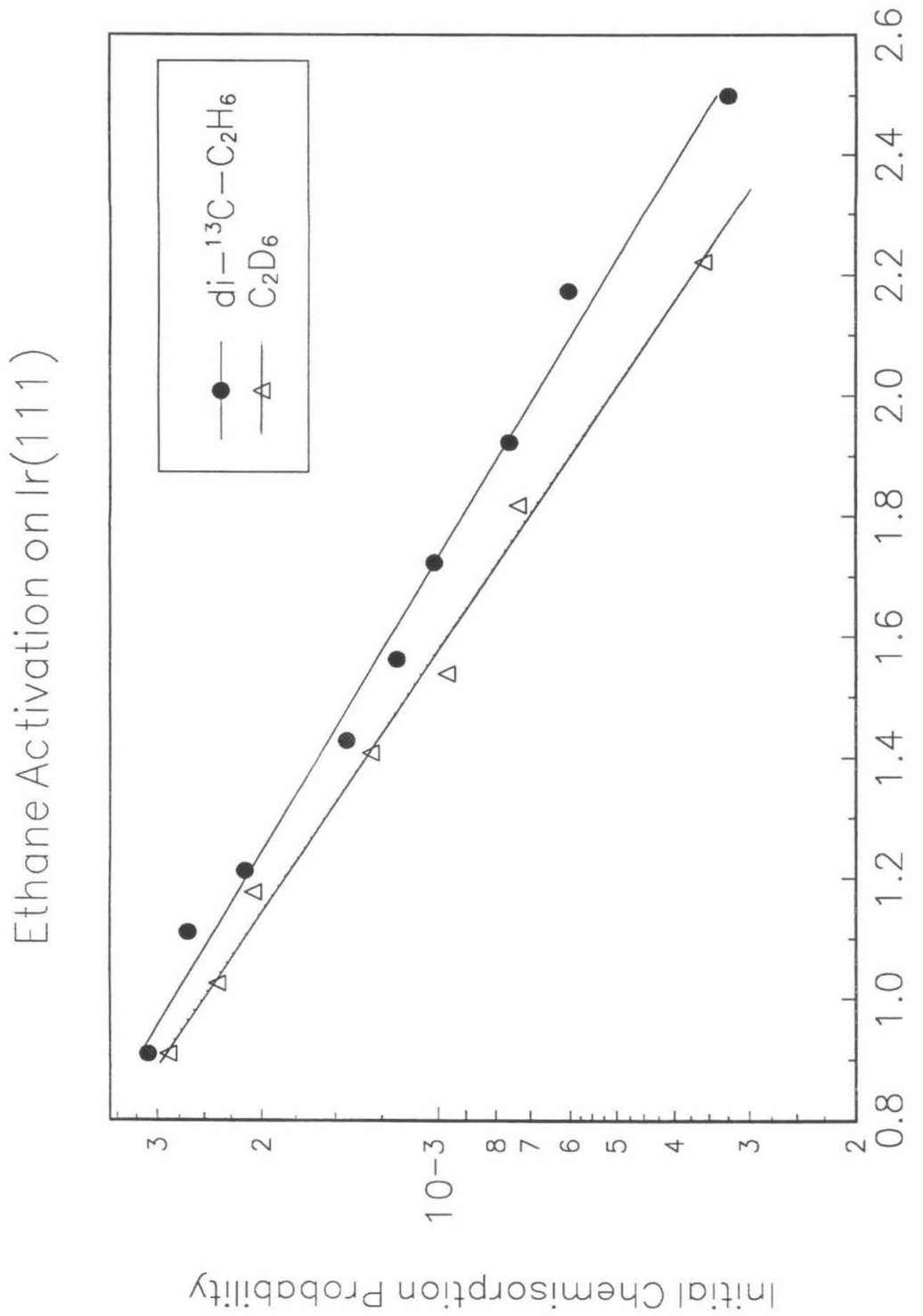
Ethane Activation on Ir(1 1 1)
di−13C−C2H6
C2D6
Initial Chemisorption Probability
10−3
3
2
8
7
6
5
4
3
2
0.8
1.0
1.2
1.4
1.6
1.8
2.0
2.2
2.4
2.6
1000/Ts, (K−1)

Figure 1a

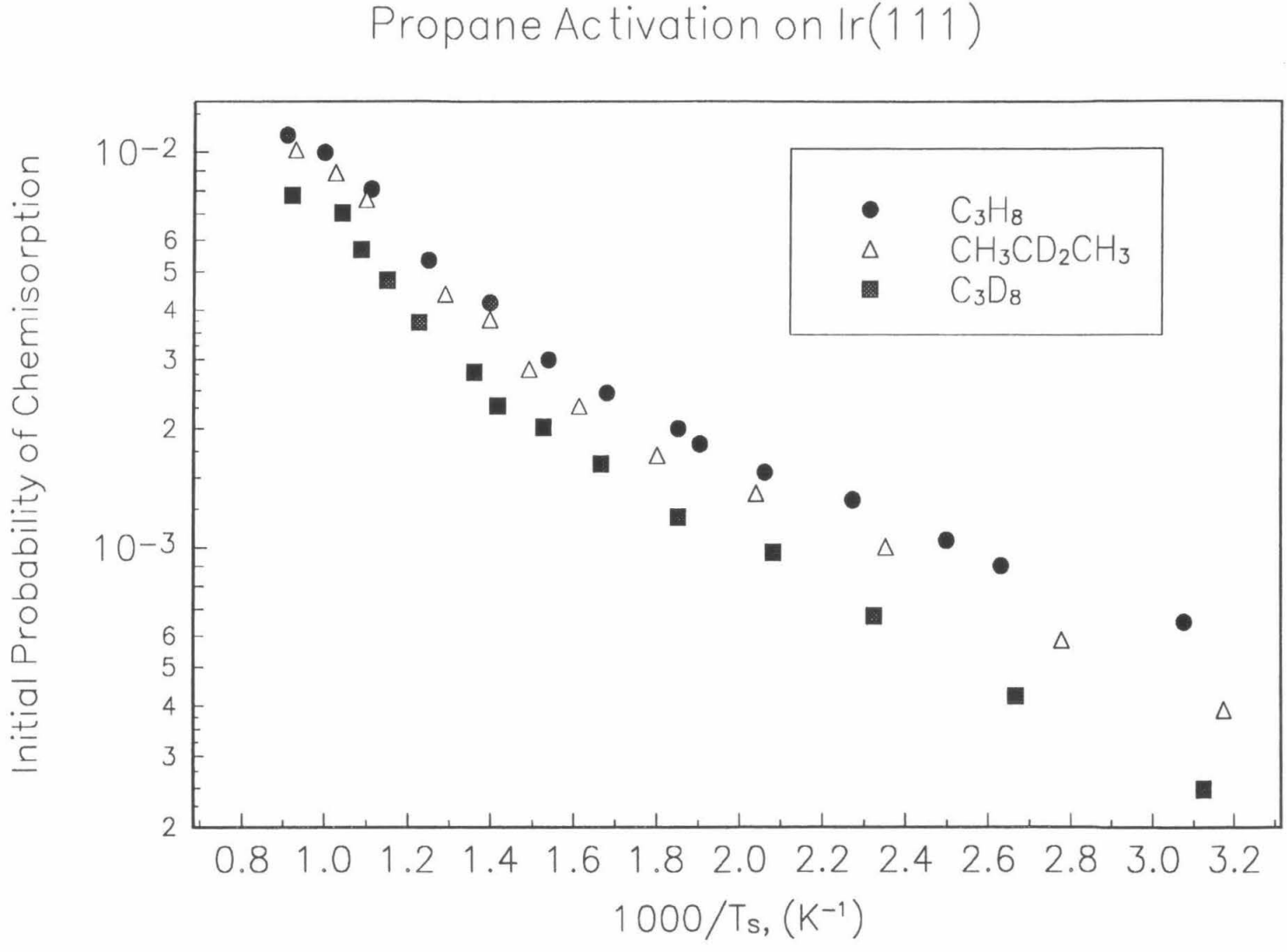
Propane Activation on Ir(111)
Initial Probability of Chemisorption
10−2
6
5
4
3
2
10−3
6
5
4
3
2
0.8 1.0 1.2 1.4 1.6 1.8 2.0 2.2 2.4 2.6 2.8 3.0 3.2
1000/Ts, (K−1)
C3H8
CH3CD2CH3
C3D8

Figure 1b

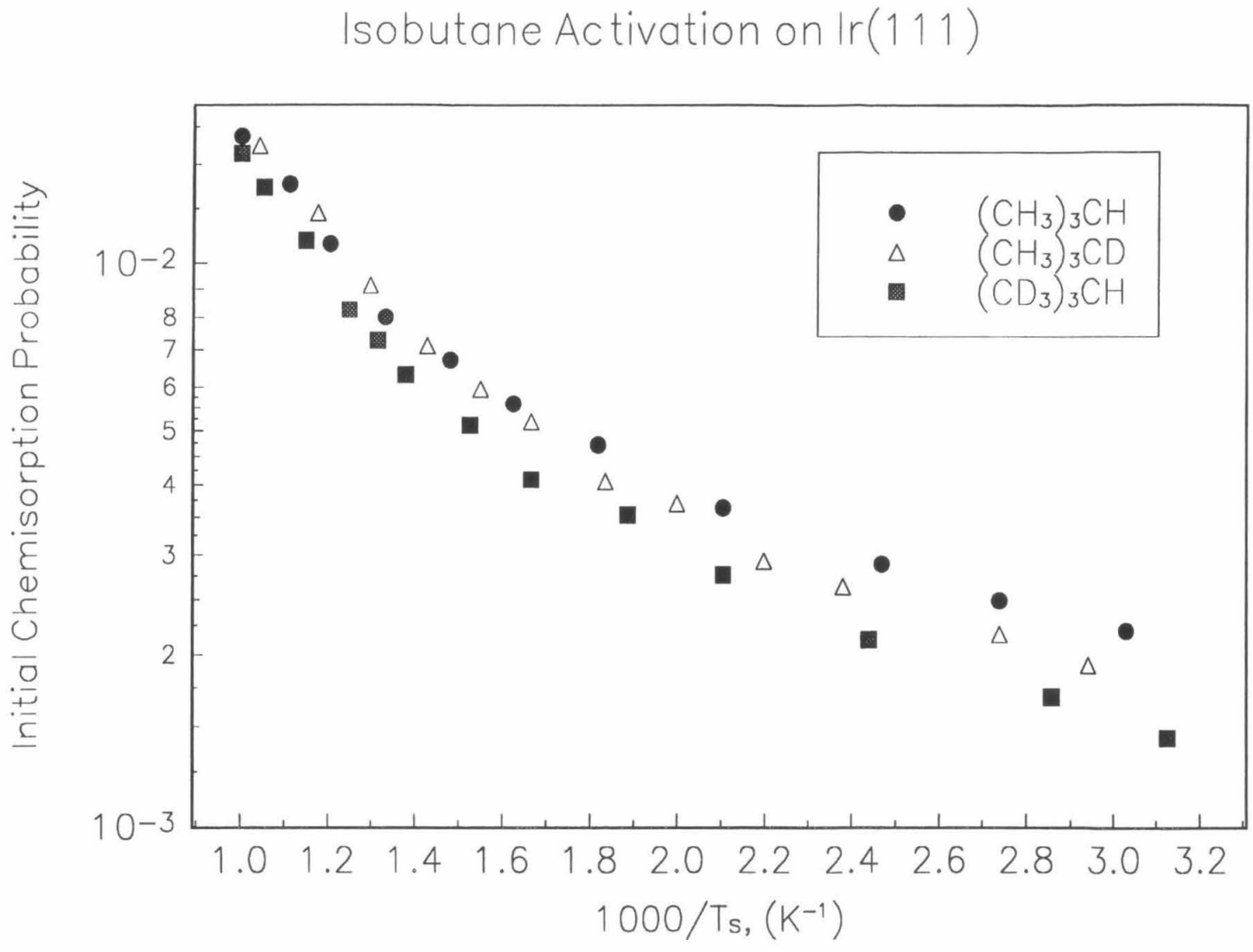
Isobutane Activation on Ir(111)
Initial Chemisorption Probability
10−2
8
7
6
5
4
3
2
10−3
1.0
1.2
1.4
1.6
1.8
2.0
2.2
2.4
2.6
2.8
3.0
3.2
1000/Ts, (K−1)
(CH3)3CH
(CH3)3CD
(CD3)3CH

Figure 1c

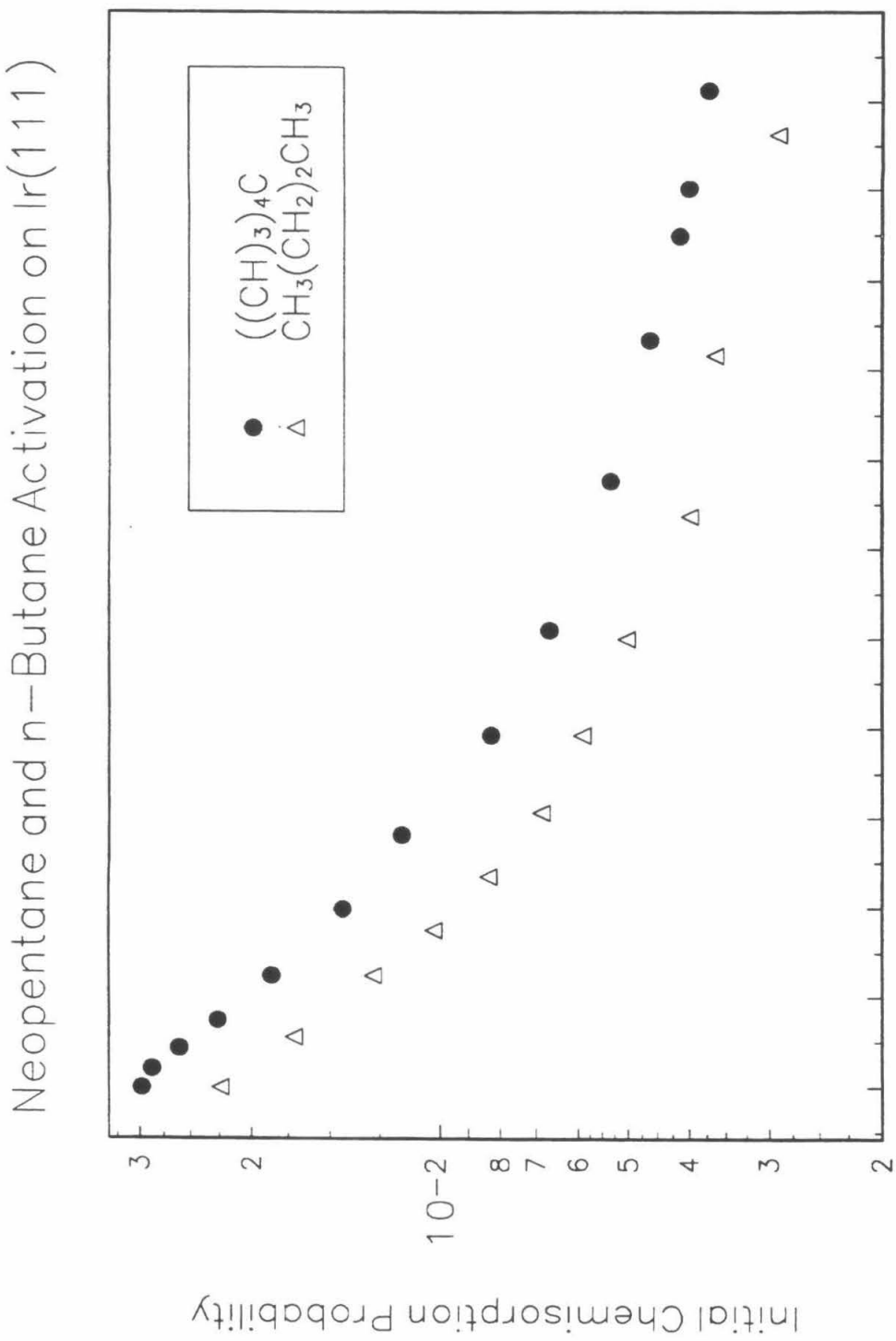
Neopentane and n-Butane Activation on Ir(111)
Initial Chemisorption Probability
10-2
3
2
8
7
6
5
4
3
2
1.0 1.2 1.4 1.6 1.8 2.0 2.2 2.4 2.6 2.8 3.0 3.2 3.4
1000/Ts, (K-1)
((CH)3)4C
CH3(CH2)2CH3

Figure 1d

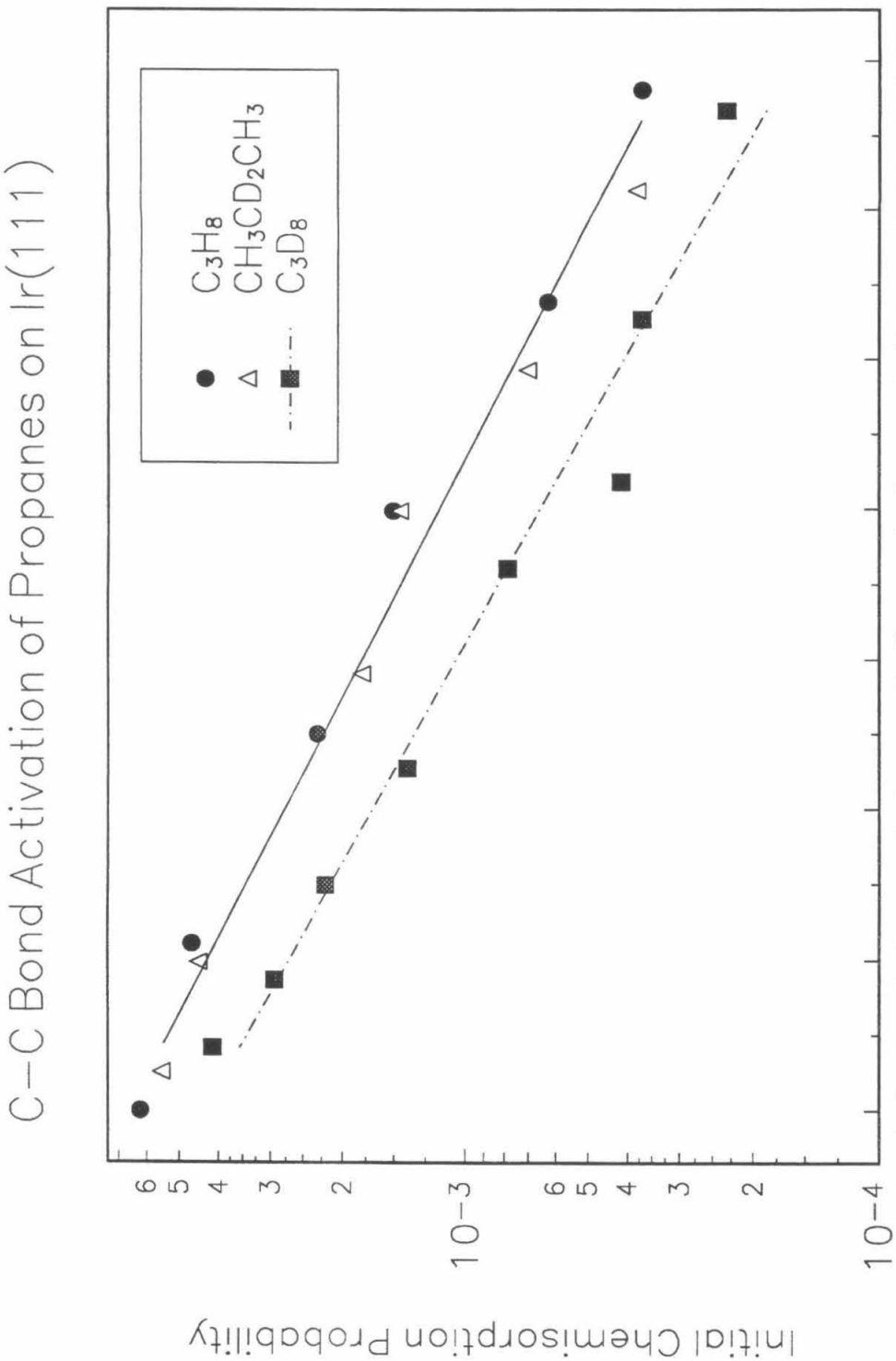
C–C Bond Activation of Propanes on Ir(111)
Initial Chemisorption Probability
1000/Ts, (K-1)
C3H8
CH3CD2CH3
C3D8
10-3
10-4
1.0
1.1
1.2
1.3
1.4
1.5
1.6
1.7

Figure 2

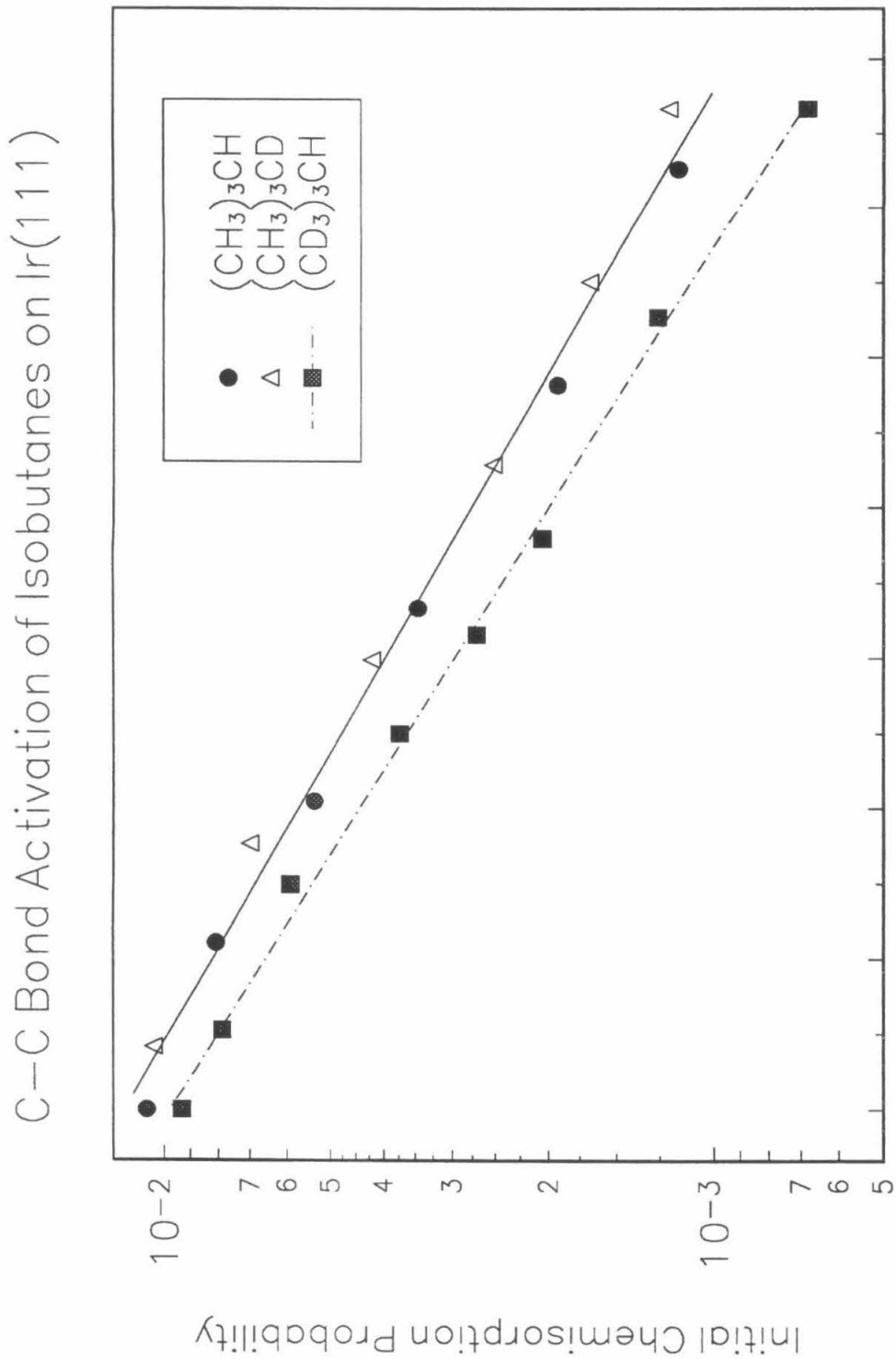
C–C Bond Activation of Isobutanes on Ir(111)
Initial Chemisorption Probability
10–2
7
6
5
4
3
2
10–3
7
6
5
1.0
1.1
1.2
1.3
1.4
1.5
1.6
1.7
1000/Ts, (K–1)
(CH3)3CH
(CH3)3CD
(CD3)3CH

Figure 3

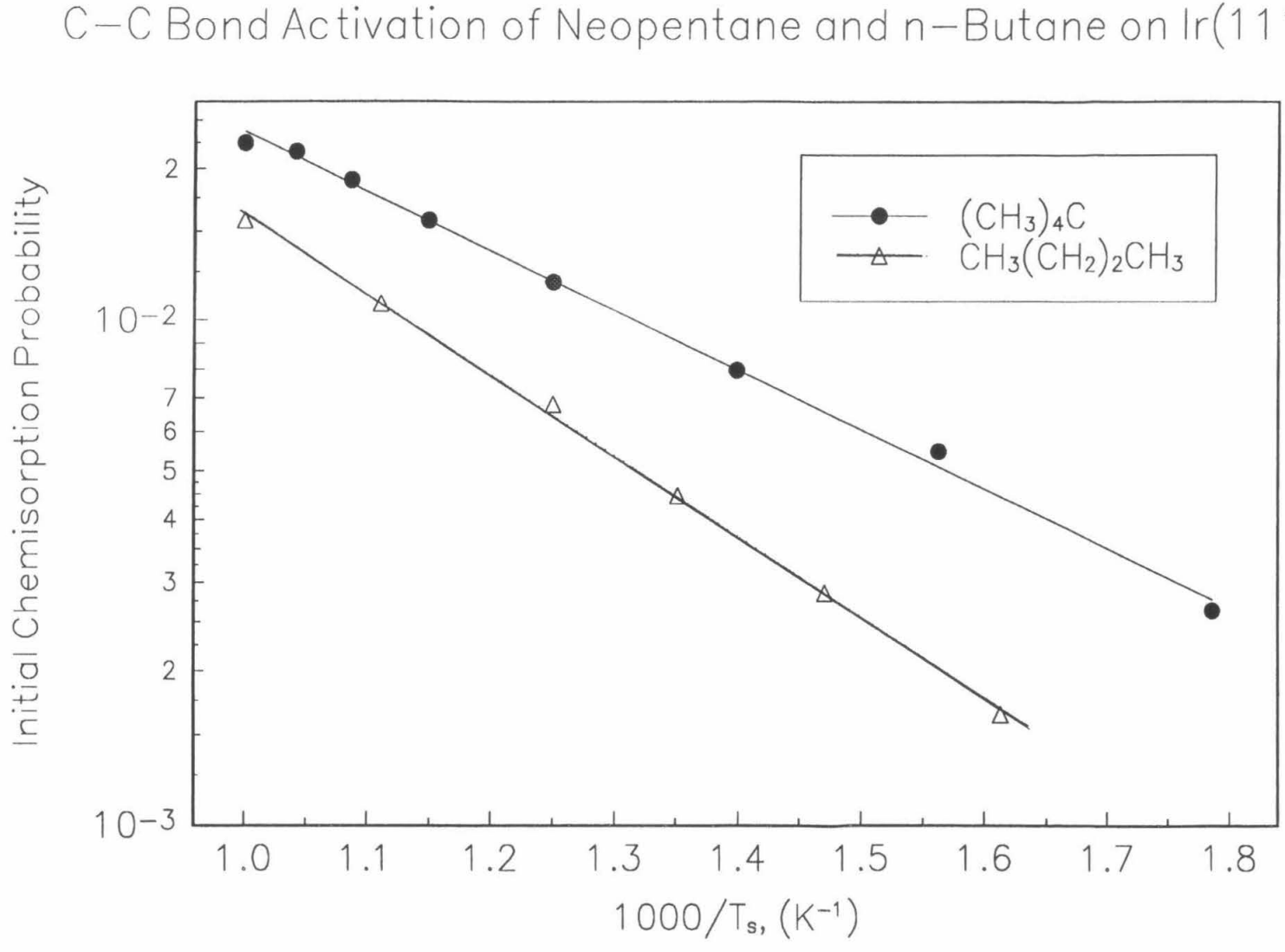
C–C Bond Activation of Neopentane and n–Butane on Ir(111)
Initial Chemisorption Probability
2
10−2
7
6
5
4
3
2
10−3
1.0
1.1
1.2
1.3
1.4
1.5
1.6
1.7
1.8
1000/Ts, (K−1)
(CH3)4C
CH3(CH2)2CH3

Figure 4

CONCLUSIONS

In Chapters 1 and 2, the interaction and thermal decomposition of CH_3NH_2, CH_3ND_2, and CD_3ND_2 were examined to elucidate the mechanism of reaction for the selective activation of N-H, C-H, and C-N bonds on the close-packed Ru(001) surface. Preferential activation of C-H bonds was observed, with sequential removal of the methyl carbon-hydrogen bonds yielding a secondary aminocarbene species, η^1-(C)-$HCNH_2$, which we implicate in the disproportionation reactions that plague the commercial amination of long-chain aliphatic alcohols. The behavior of this intermediate is believed to parallel that of coordinated acyl ligands, η^1-(C)-RCO, in organometallic chemistry, which are known to be particulary susceptible to nucleophilic attack at the carbenoid carbon atom. Continued dehydrogenation along the major path (~70%) for decomposition leads to the formation of μ_3-η^2–CN. This surface species is proposed to coordinate through a σ-bond at the carbon atom with both π electron systems interacting with the surface, presumably through the antibonding orbitals of the adsorbate. The observed stretching frequency of 1660 cm^{-1} indicates that this species has either significantly delocalized its π electron density to the surface, or it has received backdonated electron density. The minority path (~30%) for decomposition leads to C-N bond cleavage at approximately 280 K to 300 K, before significant dehydrogenation has occurred. Desorption limited production of ammonia is observed at 365 K, a temperature higher than on the clean surface and, hence, indicative of the presence of electron-withdrawing groups, such as η^1-(C)–$HCNH_2$, on the surface. The isotopically labeled product ammonias, ND_3 and ND_2H, from the reaction of CH_3ND_2 on the surface were used along with the product species, H_2, HD, and D_2, to derive the branching ratio of between 2:1 and 3:1.

In Chapters 3 and 4, the dissociative chemisorption of 1,2-di-^{13}C-C_2H_6 on the close-packed surface of Ir(111) was studied. From the proper precursor-mediated analysis of this reacting system, the probability of reaction for C-H bond activation in ethane was found to have an activation energy of 2.6 ± 0.2 kcal/mol, relative to the gas-phase reference energy, and a ratio of preexponential factors for the reaction and desorption rate coefficients of 10^{-2}. In comparison to the close-packed surface of Pt(111), the activation energy is 6.3 kcal/mol lower for ethane dissociation on Ir(111), and in comparison to the corrugated Ir(110)-(1x2) surface, it is 5.0 kcal/mol higher. As a result, when compared relative to the probability of ethane dissociation on the corrugated surface of Pt(110)-(1x2), the intrinsic difference in activities between these two metals is compensated by the modification to the surface electronic structure induced by the change in the surface geometric structures. The quantitative determination of the reaction probability at the defect sites on the Ir(111) surface was achieved experimentally by controlling the amount of converted ethane to between 0.0010 and 0.0020 monolayer. In this system, the two-dimensional transport of ethane molecules, via surface diffusion, from the less active terrace sites to the more reactive defect sites, located at the step edges, was explicitly included in the precursor-mediated kinetic model. The probability of reaction of ethane at the defects was determined to be approximatly three to four orders of magnitude greater, depending on the surface temperature, than at the sites of the close-packed terraces. The activation energy, relative to the bottom of the physically adsorbed well, was found to be 4.5 ± 1.5 kcal/mol, which is comparable to the measured activation energy of 5.5 ± 0.2 kcal/mol for the dissociation of ethane on the corrugated Ir(110)-(1x2) surface.

In Chapters 5 and 6, the quantification of the selective activation of C-C bonds and 1°, 2°, and 3° C-H bonds, in ethane, propane, isobutane, n-butane, and neopentane by the close-packed Ir(111) surface was made. The Ir(111) surface was observed not to distinguish strongly between the various C-H bonds, despite their intrinsic differences in their gas-phase bond dissociation energies. Within the C-H bond cleavage channel available to these alkanes, the results show that, for surface temperatures above 320 K, the formation of primary alkyl reaction intermediates dominates over secondary and tertiary intermediates, because of the disproportionate number of primary versus secondary and tertiary C-H bonds. The intrinsic activation of individual C-H bonds, however, results in the activation 2° C-H bonds being favored by 310 cal/mol over 1° C-H bonds in propane. In isobutane, 3° C-H bond activation is favored by 85 cal/mol over 1° C-H bond activation on this surface. Similar indiscriminate activation of C-H bonds was observed for the dissociative chemisorption of these alkanes on Pt(110)-(1x2), and it is proposed that this effect arises by the compensatorily weak bonds formed to the surface by secondary and tertiary alkyl reaction products. The same cause of their lower bond dissociation energies in the gas-phase relative to primary C-H bonds makes their Ir-alkyl bonds comparatively less strong. With respect to the bottom of the physically adsorbed well, the average activation energy for C-H bond scission by Ir(111) was found to be 11.5 ± 0.5 kcal/mol for these alkanes taken as a group (with that of ethane being 10.4 ± 0.2 kcal/mol). The corresponding activation energies for the cleavage of C-C bonds were found to be 18 ± 1 kcal/mol (with that of neopentane being 16 ± 1 kcal/mol).

A deuterium secondary kinetic isotope effect for the cleavage of the C-C bonds was discovered resulting from the substitution of deuterium for hydrogen in the terminal methyl groups. In the activation of the selectively deuterated isotopomers of propane and isobutane, C_3H_8 and $CH_3CD_2CH_3$ were found to yield activation energies for C-C bond scission that were 600 cal/mol lower than for C_3D_8. The comparable effect with isobutane was quantified to be 500cal/mol. This secondary kinetic isotope effect is accounted for by the excessive deformation of the terminal methyl group as the C-C bond cleavage reaction occurs, and, hence, from the accompanying changes in the frequencies of the fundamental asymmetric stretching and deformation modes of the methyl groups. Ethane is not observed to experience C-C bond activation. It is proposed that the presence, and participation, of remote β-alkyl groups of the molecule are necessary to effect C-C bond cleavage. By anchoring the alkane molecule in a given configuration, via their physical bonding to the surface, the dissociation of the relatively inaccessible C-C bond is allowed.